Early Excited State Dynamics of Selected Transition Metal Complexes

Elspeth Lindsay

A Thesis

in

The Department

of

Chemistry and Biochemistry

Presented in Partial Fufillment of the Requirements
for the Degree of Doctor of Philosphy at
Concordia University
Montreal, Quebec, Canada

June, 1993

ISBN 0-315-87274-8

Abstract

Early Excited State Dynamics of Selected Transition Metal Complexes

Elspeth Lindsay, Ph.D.
Concordia University, 1993

Primary photoprocesses of selected organometallic and coordination compounds ($[M(mnt)_2]^{2-}$ (M = Ni, Pt; mnt = $S_2C_2(CN)_2$); $W(CO)_4(phen)$; $W(CO)_5(4\text{-}X\text{-}Py)$ (X = CN, Formyl); $L_nM\text{-}Re(CO)_3(bpy')$ (L_nM = Ph_3Sn-, $(CO)_5Re$-)) were studied by a combination of picosecond time resolved absorption spectroscopy and quantum yield measurements in different solvents. Near UV excitation of $[M(mnt)_2]^{2-}$ in $CHCl_3$-CH_3CN mixtures promotes a sub-picosecond electron transfer from M to $CHCl_3$. The quantum yield of photooxidation is dependent upon both the excitation wavelength and the solvent. The quantum yield is higher for higher energy excitation and increases with increasing amounts of $CHCl_3$ up to a limiting value at high $CHCl_3$ concentrations. The wavelength dependence is independent of the solvent dependence. The reaction is controlled primarily by electronic factors, in particular, by the extent of mixing between the excited state which is formed initially and another of CTTS character.

$W(CO)_4(phen)$ undergoes photochemical replacement of a CO molecule by solvent or a phosphine ligand under both LF and MLCT excitation. The quantum yield of photosubstitution increases with increasing ligand concentration under LF excitation. LF excitation leads to the substitution of a CO molecule via two pathways: a major dissociative pathway which is accompanied by a smaller contribution from an associative

pathway. The quantum yield increases with decreasing excitation energy across the MLCT band envelope in halogenated solvents, but varies marginally in toluene and pyridine. The wavelength and solvent dependencies are coupled. Transient absorption spectroscopy reveals that identical excited states (MLCT) are produced within 20 ps under LF and MLCT excitation: a short lived MLCT state and another MLCT excited state that is longer lived. These undergo rapid equilibration ($\tau \sim 1$ ns). One state represents the distortion of the molecule leading to a conformational rearrangement which makes the molecule more susceptible to nucleophilic attack. The reactivity can be explained using Hollebone's octupole selection rule.

Transient absorption spectroscopy reveals a solvent dependent intersystem crossing which populates the ^{3}MLCT excited states involved in the photoreactivity of $W(CO)_5$(4-X-Py). It follows biphasic kinetics. The dominant ultrafast component is assigned to crossing from the vibrationally unrelaxed ^{1}LF state to the ^{3}MLCT state and occurs at a rate of approximately $6x10^{11}$ s^{-1} in methylcyclohexane. The minor component due to ^{1}MLCT --> ^{3}MLCT intersystem crossing occurs at a rate of $2x10^{10}$ and $3x10^{10}$ s^{-1} for $W(CO)_5$(4-NC-Py) and $W(CO)_5$(4-Formyl-Py) in toluene, respectively.

Excitation into the MLCT bands of $(CO)_5Re$-$Re(CO)_3$(bpy') and $(Ph)_3Sn$-$Re(CO)_3$(bpy') yields homolysis of the M-Re bond, an efficient process ($\Phi = 0.23$) which is independent of the excitation wavelength across both MLCT band envelopes. The high quantum yield and wavelength independence is attributed to reaction from a reactive excited state which is populated indirectly from a higher lying state. Picosecond spectroscopy reveals that identical excited states are produced under excitation into either

MLCT band envelope. In the case of $(CO)_5Re\text{-}Re(CO)_3(bpy')$, vibrational relaxation in the higher energy MLCT excited state is observed in addition to two longer lived excited states associated with the lower energy MLCT band envelope: ^{1}MLCT (decays within 2.5 ns) and ^{3}MLCT ($\tau > 10$ ns). Only the long lived ^{3}MLCT state is observed in $(Ph)_3Sn\text{-}Re(CO)_3(bpy')$.

Acknowledgements

I would like to thank the many people who have helped and supported me throughout this entire project:

My supervisor, Dr. Cooper H. Langford, for his continued guidance, encouragement, and generous contribution of his time throughout this project;

Dr. Tony Vlček, Jr. for his friendship and numerous valuable discussions;

Prof. Derk Stufkens for his generous hospitality while I visited the University of Amsterdam and his aid with both the nanosecond experiments and synthesis of the Re carbonyl complexes;

Dr. D.K. Sharma and Mr. R. Danesh for their technical assistance with the picosecond flash photolysis experiments;

Dr. A.Y.S. Malkhasian for his assistance in the measurement of the quantum yields of $Pt(mnt)_2^{2-}$;

Prof. A.J. Lees for generous donation of $W(CO)_5$(4-NC-Py);

Dr. F. Hartl for the spectroelectrochemical measurements;

The technical support staff for providing the chemicals and equipment necessary to complete this project;

The secretaries in the Chemistry Department for administrative assistance;

My father for his assistance with computer problems, my husband David, my mother, sister, and brother for believing in me;

My friends and colleagues at Concordia University who shared the experience and supported me from 1989 to 1993;

And finally, the Natural Sciences and Engineering Research Council of Canada for financial support.

To my Family

Table of Contents

List of Figures

Chapter 1

Chapter 2

Chapter 3

Chapter 4

Chapter 5

Chapter 6

List of Tables

Chapter 1

Chapter 2

Chapter 3

Chapter 4

Chapter 6

List of Abbreviations

bpy' . . . . . 4,4'-Dimethyl-2,2'-dipyridyl

CTTS . . . . . Charge Transfer to Solvent

ESA . . . . . Excited State Absorption

fs . . . . . Femtosecond

GS . . . . . Ground State

ISC . . . . . Intersystem Crossing

LF . . . . . Ligand Field

LMCT . . . . . Ligand to Metal Charge Transfer

MLCT . . . . . Metal to Ligand Charge Transfer

mnt . . . . . Maleonitriledithiolate ($C_2S_2(CN)_2$)

OTTLE cell . . . . . Optically Transparent Thin-Layer Electrochemical cell

PE . . . . . Potential Energy

phen 1,10-Phenanthroline

ps . . . . . Picosecond

1. Introduction

1.1. Preface

Over the last few years it has become increasingly clear that there is a large class of photochemical reactions in which the product is determined by events which occur on the timescale of vibrational relaxation or less. Femtosecond time-resolved spectroscopy can reveal this directly[1,2]. For example, dissociation of CO following ligand field, LF, excitation commonly occurs promptly with time constants of the order of a vibration period[3-5] in $M(CO)_6$ complexes (M = Cr, W). Joly and Nelson used 65 fs (1 fs = 10^{-15} s) pulses at 308 nm to excite into the LF transition of $Cr(CO)_6$ in a methanol (MeOH) solution[6]. This transition places electron density in a Cr - CO σ^* orbital and reduces π backbonding resulting in labilization of the Cr - CO bond. The spectrum acquired with the probe pulse set at 480 nm (the maximum absorption of the solvated complex, $Cr(CO)_5(MeOH)$), is shown in Figure 1.1. The data show 3 unique regions: (1) a "pulse duration limited rise" which corresponds to the initially excited state; (2) a rapid (<500 fs) non-exponential decay which corresponds to photodissociation of CO; and (3) a slower (1.6 ps; 1 ps = 10^{-12} s) exponential rise. This time is similar to the solvent coordination time obtained by Simon and Xie[6c], hence can be assigned as the time required for formation of $Cr(CO)_5(MeOH)$ (i.e. solvent complexation). Figure 1.1 thus clearly shows that the "naked" $Cr(CO)_5$ complex is formed in about 300 fs and requires 1.6 ps to complex to a solvent molecule. Upon examination of the excited state spectrum over a longer period of time (50 ps), Joly and Nelson observed a blue shift[6a,b]. They attributed this to vibrational relaxation of $Cr(CO)_5(MeOH)$. Separate experiments on

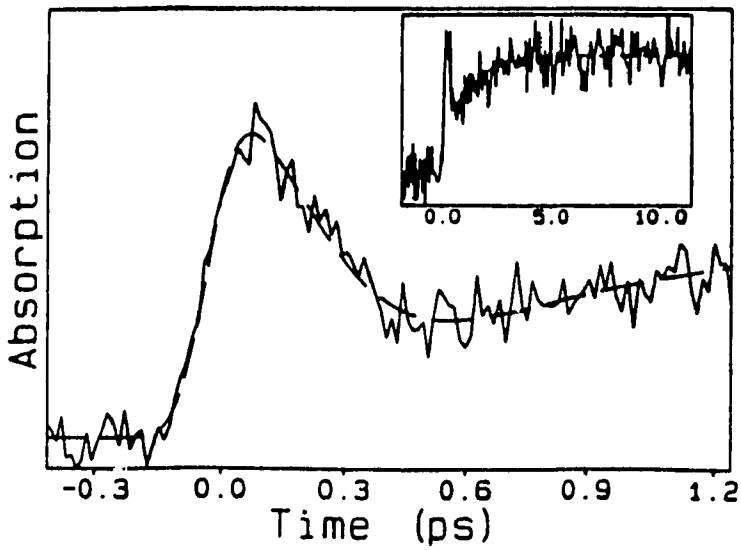

Figure 1.1. Transient absorption spectrum of $Cr(CO)_6$ in MeOH using a 308 nm pump pulse and a 480 nm probe pulse. The inset shows the spectral behaviour over 10 ps. This spectrum was taken from Reference 6a.

similar carbonyl systems revealed that $M(CO)_5S$ (M = Cr, Mo, W; S = a solvent molecule) are initially formed "hot" and have vibrational relaxation times $\geq$ 15-20 ps on the ground state potential surface[4-8]. In all probability, these reactions involve initial excitation of specific vibrational degrees of freedom of the molecule. This is not limited to dissociative reactions. Other examples include the femtosecond stilbene isomerization recently described by Hochstrasser[1].

Excitation of *trans*-stilbene at 312 nm induces an isomerization reaction. In order for the *trans* --> *cis* isomerization to take place, the system must cross over a barrier thus making the process relatively slow (60-200 ps, depending on the solvent). Consequently, the reaction products (*cis*-stilbene) are thermally equilibrated by the time they are observed. Conversely, excitation of the *cis* isomer at 312 nm leads to an excited

state with a rise time of less than 100 fs. The isomerization to the *trans* isomer is complete in about 1 ps, depending on the solvent. This indicates only a small barrier to reaction. Furthermore, the product (*trans*-stilbene) is formed "hot" and cools down by energy transfer to the surrounding solvent molecules. The difference in the behaviour of *cis* and *trans* stilbene at early times after the 312 nm excitation shows that different vibrational regions of the potential surface are involved in the isomerization process. Another example of such behaviour is the initial step in the isomerization of rhodopsin[7]. In this case, observation of products at 50 fs reveal breakdown of the Born-Oppenheimer approximation.

Previous work by Langford *et al*[9] has shown that wavelength dependence of quantum yields over narrow spectral regions can be used as a diagnostic of chemical processes (e.g. ligand substitution, isomerization) which compete with vibrational relaxation. For example, the photoracemization of (+)-[Cr(1,10-phenanthroline)$_3$]$^{3+}$ yields a rather interesting wavelength dependence[9b] which is attributed to an effective competition between photoisomerization and vibrational deactivation. In this case, there are two excited states involved: the ^{2}E state which is "quenchable" and a residual non-quenchable component which was assigned the initially excited ^{4}T state. At high quencher concentrations (i.e. where only reaction from the ^{4}T state is important), the quantum yield increased with increasing initial vibronic excitation across the low energy side of the first quartet band. Similar results were observed in the absence of quencher thus indicating that the quantum yield reflects the efficiency of intersystem crossing and that the photoisomerization competes effectively with vibrational deactivation. The

aquation[9c] of $[Co(NH_3)_5Cl]^{2+}$ with loss of either NH_3 or Cl^- follows a monotonic decline of quantum yield with decreasing excitation energy. The quantum yield decreased across the envelope of the first spin-allowed LF band (the singlet manifold), although the yield for Cl^- loss was greater than that for loss of NH_3 in the low energy region of the singlet manifold. Direct irradiation into the triplet region (647 nm) produced even smaller quantum yields. In order to account for the wavelength dependence, the substitution of NH_3 was explained a direct reaction from the singlet state which precedes intersystem crossing. Cl^- loss was assigned to the triplet state which is populated via intersystem crossing from the singlet. This intersystem crossing competes with vibrational relaxation in the singlet (if it were simply crossing to the triplet, the quantum yield upon excitation directly into the triplet region should be higher than that observed in the singlet manifold). More recently it was found[5a] that the quantum yield of substitution of the unique ligand, L, in $W(CO)_5L$ (L = Piperidine, Pyridine) varied in a complex fashion with decreasing excitation energy. The quantum yields increased with decreasing excitation energy upon irradiation into the singlet region (313-436 nm), whereas the quantum yields decreased with decreasing excitation energy upon irradiation into the triplet region (457.5 - 488.0 nm), thus bearing a remarkable similarity to the previous example. This was also interpreted as a reaction which occurs promptly from a minimum of two excited states and is competitive with vibrational relaxation.

This thesis examines in detail the mechanistic aspects of the photochemistry and/or photophysics of selected transition metal complexes: $[M(S_2C_2(CN)_2)_2]^{2-}$ (M = Ni, Pt), $W(CO)_5$(4-X-Pyridine) (X = CN, Formyl), $W(CO)_4$(phen) (phen = 1,10-

phenanthroline), and L_nM-$Re(CO)_3(bpy')$ (L_nM = $(CO)_5Re$-, $(Ph)_3Sn$-; bpy' = 4,4'-2,2'-dimethylbipyridine) in search of more information on non Born-Oppenheimer processes. Contrary to the systems previously investigated, all molecules studied in this thesis possess excited states with charge transfer character. The research described below was, in a large part, motivated by the intriguing question of how will charge transfer excitation and the resulting short-lived spatial charge separation be reflected in the primary photoprocesses and photoreactivity. As we see below, solvent dependence is the natural complement to wavelength dependence in diagnosis of a reaction mechanism. Solvent variation will therefore be an important theme of the thesis.

1.2. Objectives of the Research

This research project was divided into four related areas. The first area involved a detailed examination of the wavelength dependent behaviour of the photooxidation of $[M(mnt)_2]^{2-}$ (M = Ni, Pt; mnt = $S_2C_2(CN)_2$) in $CHCl_3$ upon near UV excitation. Using the same wavelengths of excitation, this was extended into an analysis of the dependence of the quantum yields of photooxidation on solvent composition which also corresponds to the study of the dependence on electron acceptor concentration. The complexes and reaction were chosen since the charge redistribution in the process makes it a candidate system in which solvent polarity and dipolar relaxation times might be important. This expectation was not realized.

The second area involved the reactivity of metal-to-ligand-charge-transfer, MLCT, and LF excited states in CO substitution reactions and was examined as a function of

wavelength, solvent, and substituting ligand in $W(CO)_4$(phen). Earlier studies have revealed that in this complex, ligand substitution processes occur from both an MLCT excited state and a LF excited state via an associative and a dissociative pathway, respectively[10,11]. Another interesting feature of $W(CO)_4(\alpha,\alpha'$- diimine) complexes, including $W(CO)_4$(phen) derivatives, is the observation of multiple luminescence[12], suggesting rather unusual photophysics in this family. We will see evidence for the role of differential rates of vibrational relaxation.

The early stages of the photoreaction of $W(CO)_5$(4-X-Pyridine); X = CN, Formyl were also examined. Unlike $W(CO)_4$(phen), substitution of the pyridine ligand occurs via a dissociative pathway upon LF *and* MLCT excitations as suggested by common pressure dependence[13]. Pressure dependence normally involves the calculation of the volume of activation associated with a chemical reaction. Volumes of activation are concepts in transition state theory. Because of the fundamental assumption in transition state theory that a quasiequilibrium of all degrees of freedom is maintained except on the reaction coordinate, volumes of activation cannot be directly applied to pressure dependence of ultrafast photoreactions where this condition is not fulfilled. Nevertheless pressure dependence indicates that the overall photobehaviour of pentacarbonyl complexes is different from that of analogous tetracarbonyl-diimine complexes of group 6 metals[14-18]. Furthermore, these earlier investigations have shown that the MLCT state is of crucial importance for photosubstitutional reactivity of $W(CO)_5$(4-X-Py) (X = CN, Formyl) under visible excitation and the processes following the population of the MLCT state are well understood. However, nothing is known about the early excited state

dynamics of these complexes (i.e. about the non Born-Oppenheimer processes that populate the MLCT states and that are thus responsible for selection of the photoreactive pathway). To this goal, we have investigated the picosecond time-resolved absorption spectra of $W(CO)_5$(4-NC-Pyridine) and $W(CO)_5$(4-Formyl-Pyridine) following excitations into their LF and MLCT absorption bands.

The fourth area involved the investigation of the complexes $(CO)_5Re$-$Re(CO)_3$(bpy') and $(Ph)_3Sn$-$Re(CO)_3$(bpy'). These compounds, which possess both a direct metal-metal bond and a π-accepting diimine ligand, can give rise to excited states resulting from excitation of the electrons involved in the metal-metal bond and/or the MLCT transitions. Low lying electronic excited states of metal-metal bonded complexes, unlike the mononuclear analogues, often involve significant changes in the electron density associated with the metal-metal bond, compared to the ground electronic state thus creating the potential for some very interesting homolytic photochemistry which cannot occur in other complexes. What is intriguing about these complexes is their remarkably high photosensitivity, in contrast to what is commonly observed upon MLCT excitation[15,18-21]. Luminescence studies by Larson *et al*[22] have revealed that $(CO)_5Re$-$Re(CO)_3$(bpy') exhibits multiple emission (both fluorescence and phosphorescence were observed) from an MLCT excited state thereby indicating unique photophysics in this complex. In the past, research conducted by Stufkens and co-workers of the University of Amsterdam has revealed only a small amount of mechanistic information on this type of organometallic compound. Thus, in order to gain further insight into the mechanism of reaction, the primary photoprocesses of $(CO)_5Re$-$Re(CO)_3$(bpy') and $(Ph)_3Sn$-

$Re(CO)_3(bpy')$ upon MLCT excitation have been investigated using a combination of wavelength dependence of the quantum yield of homolytic bond cleavage (induced by MLCT excitation) and picosecond laser flash photolysis.

These complexes were chosen because they all exhibit unique photochemistry and are therefore good candidates to probe early time behaviour in detail. The combination of steady-state photochemistry and transient absorption spectroscopy is used to gain new insight into early excited state dynamics. Having introduced the families of compounds used and the reasons they were expected to exhibit novel and interesting fast photoprocesses, this chapter will next provide the necessary introduction to their chemistry and photochemistry and introduce some of the theoretical considerations which figure in the analysis of mechanisms in the short time domain.

1.3. Review of Metal Carbonyls

1.3.1. History[23]

The first interaction between a transition metal and carbon monoxide (CO) was discovered accidentally by L. Mond in 1890[24] when he noticed that the reaction vessels containing valves made of nickel used for the production of sodium bicarbonate corroded severely during the reaction. This observation motivated him to conduct a detailed study. His investigation revealed that Ni reacted slowly with CO at about 100°C to form a mixture of gases which included nickel tetracarbonyl, $Ni(CO)_4$, in yields above 30%. Attempts to prepare similar compounds with cobalt, iron, copper and platinum failed. Despite the lack of success in these early experiments, research continued and in 1891,

iron pentacarbonyl, $Fe(CO)_5$, was synthesized simultaneously by L. Mond and F. Quincke in England[25] and M. Berthelot in France[26]. The first photochemical reaction of a metal carbonyl was observed in 1903: diiron nonacarbonyl, $Fe_2(CO)_9$, was formed by exposing $Fe(CO)_5$ to sunlight[27]. These results inspired much research into the synthesis of other compounds with the preparation of the carbonyl complexes of chromium, molybdenum, tungsten, cobalt, ruthenium, and iridium between 1910 and 1940. Preparation of these complexes with the general formula $M_x(CO)_y$ was generally straightforward. The major criteria were: i) high pressures of CO, ii) reaction temperatures in excess of 100°C and iii) the presence of a reducing agent. The latter was essential because most syntheses began with the metal in a high oxidation state and the stable metal carbonyls required a metal with an oxidation state of 0 or ± 1. The inherent stability of these metal carbonyls is associated with an inert-gas configuration around the central metal atom. In these, and most other organometallic compounds, the 18 electron rule is obeyed and the complexes form so as to produce this configuration.

1.3.2. Geometric Structure

Metal carbonyl complexes of the Cr, Mo, W triad exist as stable six-coordinate molecules. Four metal carbonyl complexes will be examined in this thesis, all of which exhibit very fast photochemistry. The simplest of these complexes are $W(CO)_5$(4-X-Py); X = CN, Formyl (Figure 1.2). This molecule possesses C_{4v} symmetry. The electronic configuration of the free W atom is $5d^46s^2$ and the valence orbitals available for bonding are the 5d, 6s, and 6p orbitals. The substituted pyridine ligand is bonded to the W metal

(a)

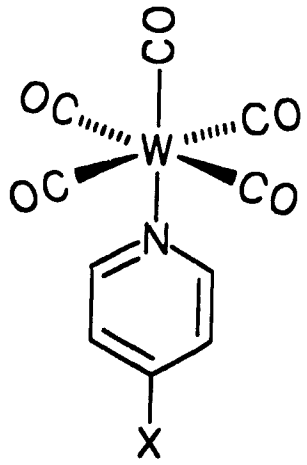

(b)

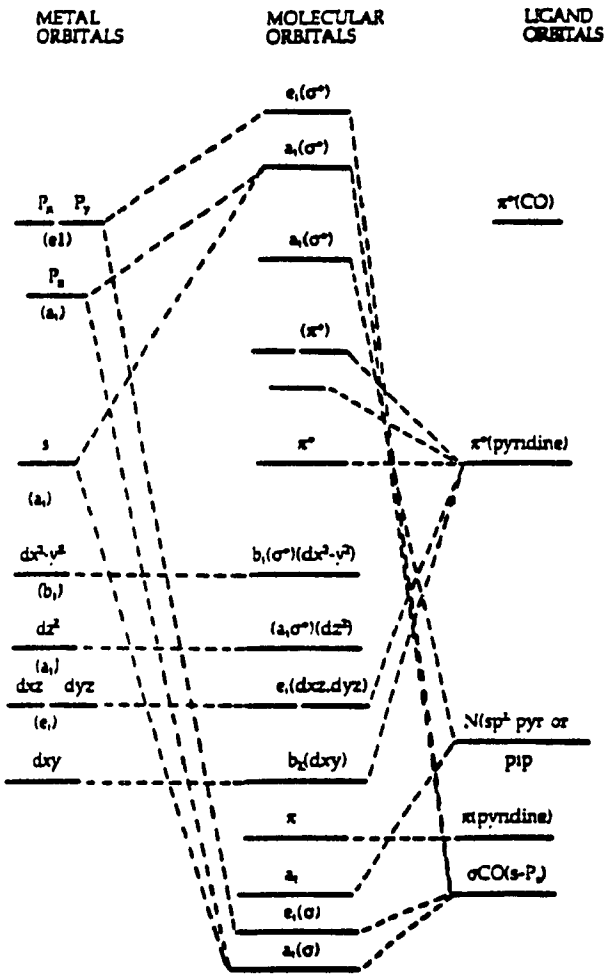

Figure 1.2. Geometric structure (a) and the simplified molecular orbital diagram (b) for $W(CO)_5$(4-X-Py); X = CN, Formyl. The molecular orbital diagram was obtained from Reference 5c.

through the lone pair of electrons on the nitrogen atom and possesses low-lying π-orbitals which can accept electron density.

The bonding between carbon and oxygen in carbon monoxide consists of a filled σ orbital and two filled π orbitals which are localized between the carbon and the oxygen. There is one lone electron pair localized on each of the carbon and oxygen atoms which are directed away from the molecule and two empty π^* orbitals which are directed away from the carbon-oxygen internuclear region. When CO acts as a ligand, the σ orbital serves as a weak donor to the metal atom and forms a σ bond with it (Figure 1.3).

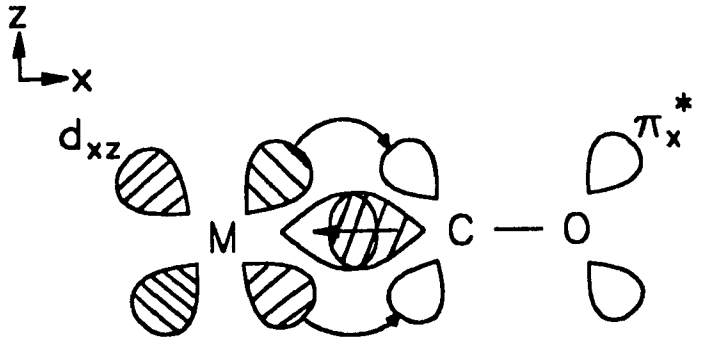

Figure 1.3. Schematic diagram of bonding between a metal atom and CO.

The two π^* orbitals of CO are crucial in the bonding process since they can overlap metal orbitals possessing π symmetry with respect to the M-C bond (refer to Figure 1.3). The π interaction leads to the delocalization of electron density from the filled d-orbitals on to the CO ligands, resulting in the stabilization of the complex with the metal in a low

oxidation state. A molecular orbital diagram of this complex is shown in Figure 1.2b.

$W(CO)_4$(phen) is structurally similar to $W(CO)_5$(4-X-Py) (X = CN, Formyl). The only difference between these two molecules is that in the former complex, a bidentate ligand (phenanthroline) replaces a monodentate ligand (4-X-Py) and one CO ligand. This results in the reduction of the molecular symmetry from C_{4v} to C_{2v}.

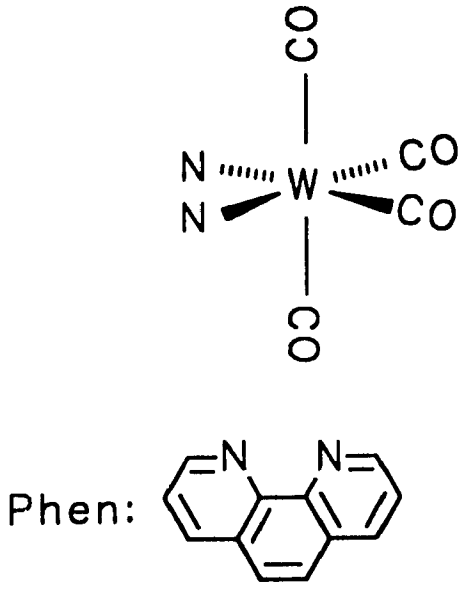

Figure 1.4. Geometric structure of $W(CO)_4$(phen).

The phenanthroline ligand is bonded to the W atom via the lone electron pair on each nitrogen atom. As in the complex discussed above, there are empty low-lying π^* orbitals on the phenanthroline ligand which can accept electron density. Bonding between the metal and the CO ligands is the same as described for $W(CO)_5$(4-X-Py) (X = CN, Formyl). The structure of this complex is shown in Figure 1.4.

The two other carbonyl complexes examined in this thesis are more complicated in that they possess a direct metal-metal bond in addition to M-CO bonds, as described

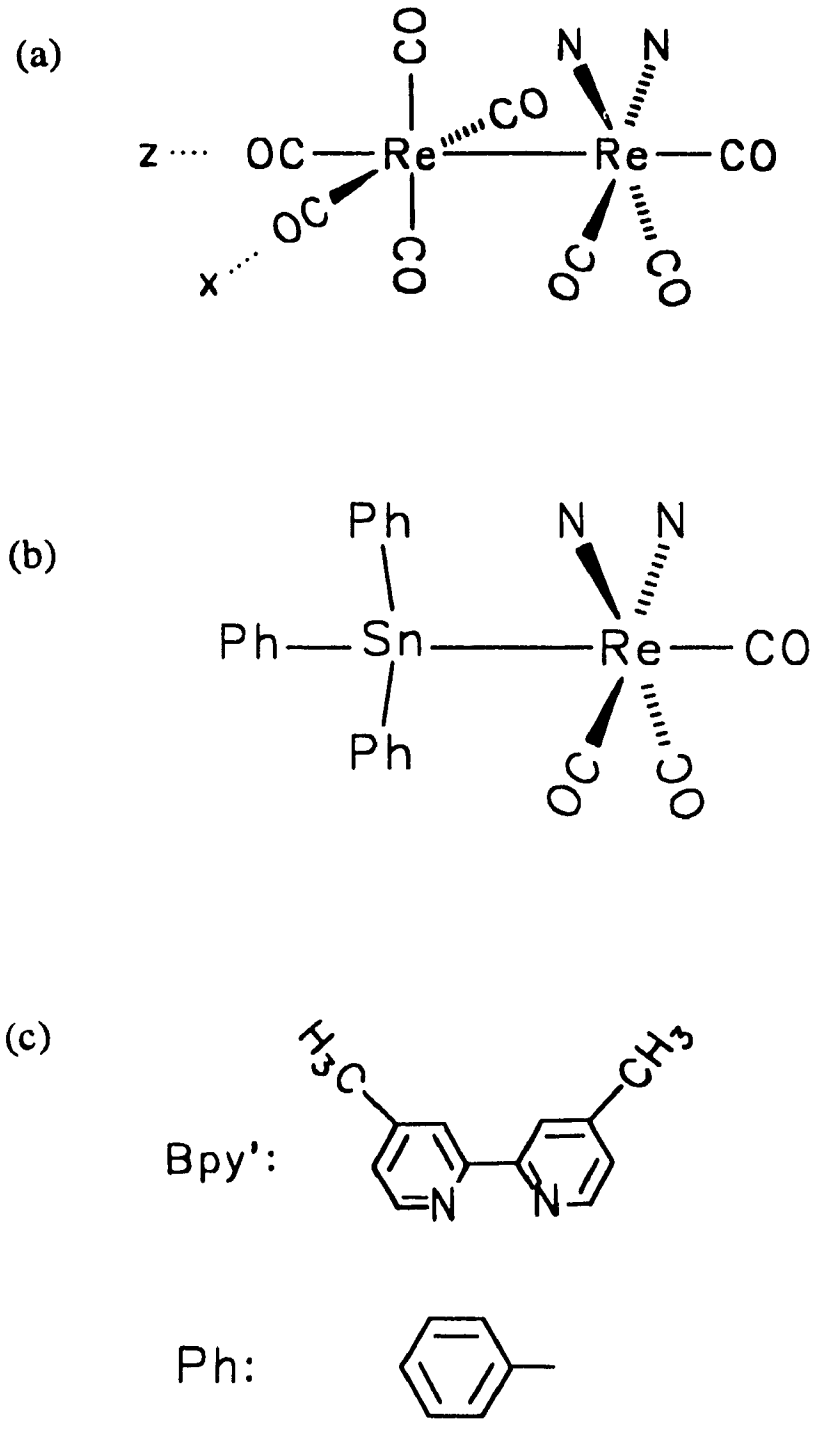

Figure 1.5. Geometric structure of $(CO)_5Re\text{-}Re(CO)_3(diim)$ (a) and $(Ph)_3Sn\text{-}Re(CO)_3(diim)$ (b), and the diimine (bpy') ligand (c).

above. These complexes are of the general form L_nM-$Re(CO)_3(bpy')$ (M = Re, Sn; L = CO, C_6H_5-) and possess the structure shown in Figure 1.5.

1.4. Review of Metal Maleonitriledithiolate Complexes

1.4.1. History[28]

1,2-dithiols were first studied in the mid and late 1930's when R.E.D. Clarke and co-workers investigated the reactions of toluene-3,4-dithiol and 1-chlorobenzene-3,4-dithiol with metal halides, including those of zinc, cadmium, mercury and tin[29]. They discovered that these dithiols readily formed complexes with metals, and with tin, species of the type [Sn(dithiol)$_2$] were isolated. Work on the analytical aspects of toluene-3,4-dithiol was carried out in the 1940's and 1950's[30]. However, there was no serious work to characterize the metal complexes of unsaturated 1,2-dithiols until 1957 when Bahr and Schleitzer in Munich noted that a ligand which they prepared, $Na_2S_2C_2(CN)_2$, readily formed complexes with palladium[31]. These complexes were formulated as $Pd(NH_3)_2S_2C_2(CN)_2$ and $Na_2[Pd(S_2C_2(CN)_2)_2]$. They further observed that the latter was oxidized by iodine, although they could not identify the reaction product. In 1962, G.N. Schrauzer and V.P. Mayweg prepared[32] an unusual Ni complex, $NiS_4C_4Ph_4$. It was formed by the reaction of $Ni(CO)_4$, sulfur and diphenylacetylene. This complex was unlike any Ni complex known at that time; it was intensely coloured (green), diamagnetic and volatile. In pyridine or piperidine solution, the green colour was replaced by a red-brown colour and the final solution was paramagnetic. Also in 1962, H.B. Gray and his co-workers prepared complexes of the type $[MS_4C_4(CN)_4]^{2-}$ where M = Cu, Ni, Pd and

Co[33]. In 1963, Davison *et al* discovered that the only difference[34] between the neutral complex of Schrauzer, $NiS_4C_4Ph_4$, and the dianionic complex of Gray, $[MS_4C_4(CN)_4]^{2-}$ (M = Cu, Ni, Pd, Co) was in the number of electrons (the latter complex contains 2 more electrons on the ligand). Thus, they reasoned that it should be possible to effect an oxidation of the dianion to the neutral species or a reduction of the neutral species to the dianionic complex via an intermediate monoanionic complex. They discovered that this indeed was possible and isolated several different paramagnetic monoanions.

1.4.2. Geometric Structure

The electronic configuration of the Ni^{2+} ion is $3d^8$ and the valence orbitals available for bonding are the 3d, 4s, and 4p orbitals. X-ray crystallography[35a] was used to show that the nickel maleonitrilelitholate anion, $[Ni(mnt)_2]^{2-}$ (mnt^{2-} = $(NC)_2C_2S_2]^{2-}$), is a four-coordinate complex with square planar geometry (Figure 1.6a). This molecule possesses D_{2h} symmetry. The mnt ligand consists of two sp^2-hybridized carbon atoms, each of which is bound covalently to a CN group (by a σ bond to the sp-hybridized carbon of the CN group) and the sulfur of the thiolate group, $-S^-$ (also by a σ bond).

The mnt ligand is bonded to the metal via the sulfur atom. The four-coordinate geometry is stabilized by the involvement of metal d(xz), d(yz), and p(z) valence orbitals in an extensive π orbital network spanning the entire complex in order to delocalize as much of the charge as possible. Interatomic distances for $[Ni(mnt)_2]^{2-}$ are summarized in Table 1.1. Manoharan *et al* has performed a detailed analysis[35b] of the electronic spectrum of $[Ni(mnt)_2]^{2+}$. The resulting energy level diagram is shown in Figure 1.6b.

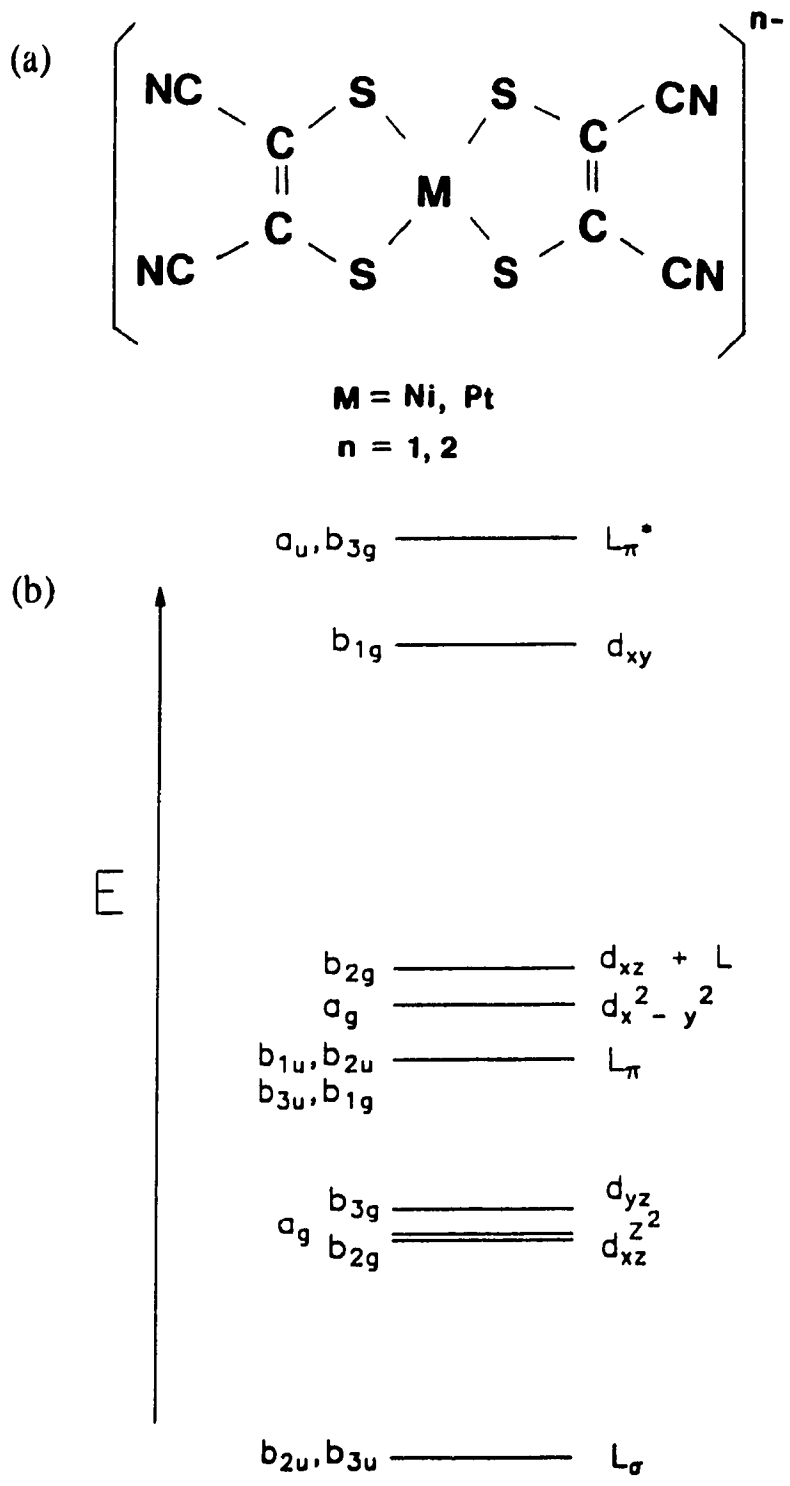

Figure 1.6. Geometrical structure of $[M(mnt)_2]^{2-}$ (M = Ni, Pt) (a) and the energy level diagram (b). The energy level diagram was obtained from Reference 35b.

Note that the structure of the Pt analogue is identical[35a] to that determined for $[Ni(mnt)_2]^{2-}$ and the bands can be assigned using data for the Ni complex as a guide.

Table 1.1. Bond lengths[21] in $[(C_2H_5)_4N][NiS_4C_4(CN)_4]$.

Bond	Length (Å)
Ni-S	2.16
S-C	1.75
C=C	1.30
C-C	1.44
C-N	1.13

1.5. Hollebone's Octupole Rule

We turn now to some theoretical considerations we will need to interpret fast events. Identifiable factors we must now consider include the nature of the electronic (vibronic) transitions, rates of vibrational relaxation, and rates of solvent reorientation. We take up electronic factors first. Two approaches are discussed in the literature, the Heller-Zink approach based on the Fourier transform of absorption and emission spectra[36a] and the Hollebone octupole rule[37]. As work on $W(CO)_5$(Pyridine) by Zink and Tutt[36b] illustrates, it remains difficult to exploit the Heller-Zink approach in the picosecond/sub-picosecond domain. However, we will see below some opportunities for accessible insights using the octupole rule developed by Hollebone.

In order to interpret what is occurring on very fast time scales, it is necessary to adopt an approach which is somewhat different from the "conventional" Born-

Oppenheimer approximation. One approach which may help to identify the specifically excited vibrational modes was introduced in the early 1980's by Hollebone *et al*[37]. This method offers an approach in the spirit of Woodward - Hoffman or Longuet-Higgins - Abrahamson rules. The Hollebone model consists of symmetry selection rules for prompt relaxation which indicate the preferred nuclear coordinate connecting two electronic states if overall angular momentum is to be conserved in the vibronic transition process. It is used to identify the vibrational mode coupling the excited state to the ground state. Similarly, it may provide rules for connecting two excited states. The theory is based on subduction from spherical symmetry to a lower symmetry (e.g. octahedral, O_h). It allows definition of angular momentum quantum numbers for vibration analogues to those for electronic orbital and spin angular momentum. This is accomplished by considering the modes of vibration of a sphere of uniform mass density. The mathematics is well known from the "liquid drop" model of the nucleus.

During the photochemically productive absorption, the translational and rotational momentum of the photochemically active photon is converted into internal motions of the molecule - but not into its net translation or rotation. For this to be possible, the centre of gravity and the axes of symmetry must remain unchanged, a condition realized only if all electronuclear accelerations from the photon event are compensated by opposing accelerations in the molecule. This requires that the molecule invoke all internal degrees of freedom in 3D space, requiring a complete description to have 2^3 distinct components. This leads to Hollebone's octupole selection rule[37]: $\Delta T = 3$. It can be factored into the following components:

$$\Delta J + \Delta V = \Delta L + \Delta S + \Delta V = \Delta T = 3 \qquad (1.1)$$

where ΔT is the total change in momenta for the transition, ΔV is the change of a vibrational angular momentum quantum number, ΔJ is the change in electronic angular momentum, ΔS is the change in spin momenta, and ΔL is the change in orbital momenta.

If the octupole rule is applied to a d^6 complex (such as $W(CO)_4(phen)$) approximated as an O_h system, the LF transitions can be described as follows:

Transition	ΔL	ΔS	ΔV	O_h vibration
$^1T_1(I) <-- {}^1A_1(I)$	0	0	3	t_{1u} buckle
$^3T_1(P) <-- {}^1A_1(I)$	1	1	1	t_{1u} stretch

The letters in parenthesis refers to the system in its "free ion state" - that is the case where the system is not perturbed by the octahedral field. Here, all orbitals are degenerate. Under the influence of an octahedral field, the degeneracy is removed and the states are split. The new states are described using labels which arise from group theory. They are related to the symmetry of the particular state. Note that these transitions can be predicted from the Tanabe-Sugano diagram (the Tanabe-Sugano diagram correlates the free ion states with the states in the octahedral ligand field) for a d^6 system in an octahedral field (Figure 1.7). The number in the superscript to the left of the term describing the state is related to the number of unpaired electrons in the system. The individual spin quantum numbers are +1/2 or -1/2. These numbers are additive. In the case of two electrons, there are thus two possibilities. If the spins are opposed, the resultant spin is 0; whereas if the electrons have the same spin, quantum number, the resultant spin is 1. In general, the multiplicity is related to the resultant spin

by:

$$\textit{Multiplicity} = (2S + 1) \tag{1.2}$$

So, when S = 0, the multiplicity is 1 and when S = 1, the multiplicity is 3. These are referred to as singlet and triplet, respectively.

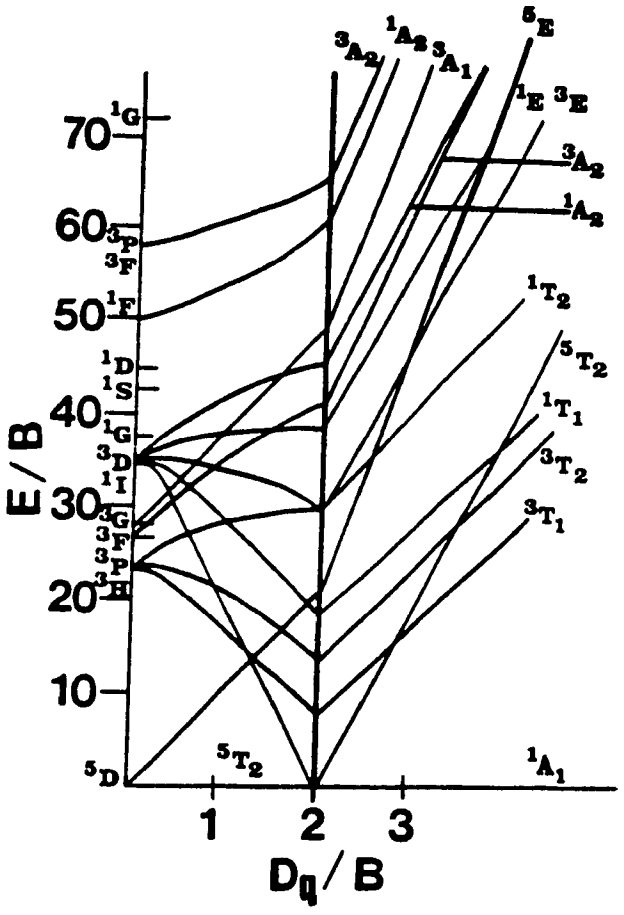

Figure 1.7. Tanabe-Sugano Diagram for a d^6 system in an octahedral field.

Transitions into the LF bands (or transitions from the LF bands to the ground state) have $\Delta V = 1$ or $\Delta V = 3$, and can show prompt dissociation because the response

is an asymmetric bond stretch which can readily lead to rapid dissociation of one ligand. In octahedral symmetry, the requirements of the point group imply coupling of LF (d-d, gerade transitions) with two types of t_{1u} vibrations. The vibration associated with the triplet excited state and corresponding to $\Delta V = 1$ is the asymmetric stretch shown in Figure 1.8a. In this mode, there is substantial extension along one axis, hence the ligand on that axis should be susceptible to substitution via a square pyramid intermediate. The singlet excited state ($\Delta V = 3$) is associated with a buckling mode of vibration as shown in Figure 1.8b. This mode, which is also responsible according to the Hollebone model for the efficient fast photosubstitution from Cr(III) d^3 species[38], is expected to be very reactive toward substitution via a stereochemically non-selective path because the metal is highly exposed to solvating molecules on four octahedral faces above the x,y plane. Hence, loss of CO is expected upon excitation into the singlet LF state. This idea has recently been successfully employed[5a] to explain excitation wavelength dependent photosubstitution of the C_{4v} complex $W(CO)_5L$ (L = Pyridine, Piperidine). This is accomplished by consideration of the coupling of vibration and electronic quantum numbers in C_{4v}. Octahedral ^1T correlates with ^1E and ^1A in C_{4v} symmetry where ^1E is the lower of the two electronic states. Because vibronic coupling is a vector product that must conserve overall degeneracy[39], the splitting of the octahedral t_{1u} vibration into e_u and a_u components requires the combination of the E electronic state with the a_u vibration (the vibration weakening the bond to L) and the A electronic state with the e_u vibration. Thus, excitation of the lower electronic state (^1E) leads to selection of a relaxation pathway buckling to release L. On the other hand, excitation into the higher energy ^1A

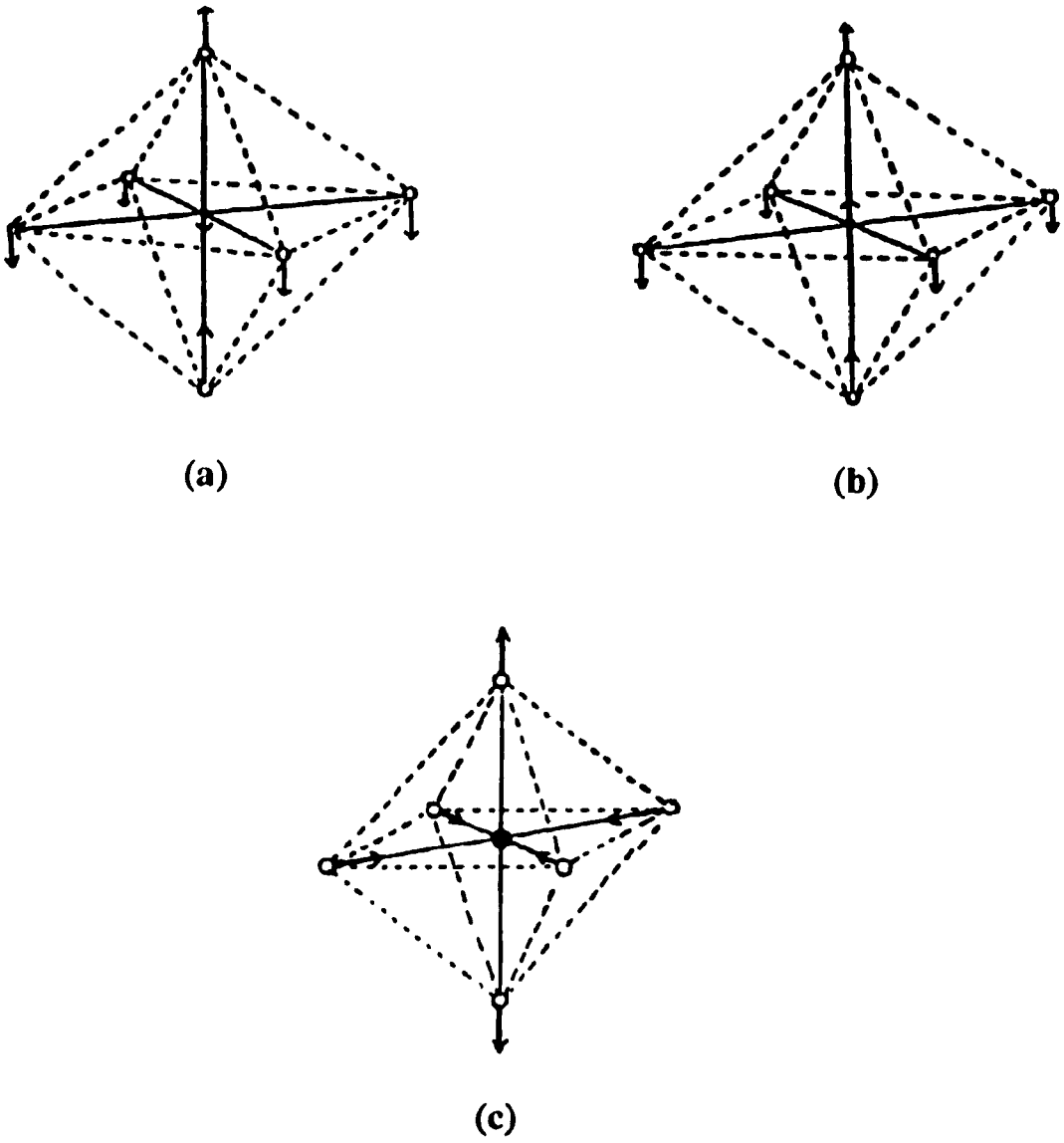

Figure 1.8. Simplified diagrams representing (a) the asymmetric stretch mode of a t_{1u} vibration, (b) the buckle mode of a t_{1u} vibration and (c) the υ_2 mode of vibration in O_h.

electronic state leads to selection of a relaxation pathway where the more exposed ligand is an unreactive CO. This is why the quantum yields are higher upon excitation at lower energy across the singlet LF manifold.

It is interesting to see whether the Hollebone octupole selection rule can also provide an explanation for an associative reaction from a MLCT state. According to the Hollebone selection rules, spin allowed ($\Delta S = 0$) CT bands with electric dipole character must have $\Delta L + \Delta S = 1$ (therefore, $\Delta V = 2$; Figure 1.8c)[37]. Thus, quadrupolar vibrations maintaining gerade structure (often detectable by Raman spectroscopy) will accompany allowed MLCT excitation. However, there is a low probability of driving a prompt dissociative response like those possible for LF excitation of $M(CO)_4(phen)$ (M = Cr, Mo, W) because at least 2 atoms are put into motion to maintain gerade structure. Thus, Hollebone's selection rule can account for the common low reactivity toward substitution of MLCT states. It can also explain reactivity on the basis of conformational change which may favour associative processes.

1.6. Effect of the Solvent

The study of the behaviour of a molecular system in the condensed phase presents a challenge resulting from the intimate contact between the molecule of interest with the surrounding solvent molecules. On the other hand, solvent variation provides an additional diagnostic parameter. Consequently, in order to understand the behaviour of the solute, a clear understanding of solvent-solute interactions is required.

A large fraction of our experiments are concerned with the influence of the solvent on relaxation pathways. One interest is the role of the solvent in electron transfer reactions involving maleonitriledithiolate complexes of Ni and Pt. An acetonitrile-chloroform mixed solvent system was selected for these experiments so that polarity of

the system could be readily changed while the concentration of the electron acceptor is varied in a simple way. These solvents also vary significantly in the role they play as acceptors of energy during vibrational relaxation. In addition, we used solvents of varying polarities to change the position of the electronic absorption bands in $W(CO)_4(phen)$ in order to probe in detail the quantum yields across the MLCT band envelope (the specific solvents used and reasons for using them will be discussed in detail in Chapter 4). This allows use of a fixed set of laser wavelengths to make a more comprehensive survey using "solvent tuning" rather than tuning the laser. Results from continuous photolysis experiments and picosecond spectroscopy in various solvents are combined in an effort to elucidate the photophysics and photochemistry of these complexes. In order to interpret the results of these studies, it is necessary to review the different solvent parameters which may be important in these reactions.

There are three important determinants of processes which occur on timescales faster than or competitive with vibrational relaxation. Each factor is directly proportional to a particular physical property of the solvent which is readily attainable and is thus diagnostic. These are summarized in Table 1.2 and will be considered separately in the following sections.

Table 1.2. Factors affecting the relaxation process

Solvent Parameter	Physical Parameter
cage effect	viscosity
thermal cage effect	thermal conductivity
solvent reorientation	longitudinal dielectric relaxation time

1.6.1. The Cage Effect[40]

One of the earliest recognized interactions between solvent and solute molecules is the so called "cage effect"[41]. In general, when in solution, the number of solvent molecules is greater than the number of solute molecules so that the solute is always completely surrounded by solvent. Constant motions between the solvent and solute molecules allows for the movement of solute through the solvent at a finite rate. Upon absorption of a photon of light, the solute molecule is promoted to some excited state in which the atoms of the molecule vibrate at an increased amplitude. If sufficient kinetic energy is available, the molecule may dissociate and the dissociated fragment will move a given distance away from the remaining fragment and retain a given amount of kinetic energy. The immediate products generated by this dissociation (i.e. a pair of radicals or molecular fragments) are termed *geminate* or *primary* species and are at most separated by only a few molecular diameters. The solvent functions to keep these fragments together as they rebound from collision with the solvent (i.e. the solvent deflects them back toward each other). During these collisions, any excess kinetic energy is lost. If a solvent molecule does not get between the geminate species, recombination becomes probable. This is termed *primary or geminate recombination*, a process which competes with diffusion out of the cage. Products failing to undergo primary recombination will diffuse into the bulk solution and either undergo diffusion-controlled secondary recombination or enter into chemical reactions. Thus, the probability that the fragmented species will recombine is limited by the rate of diffusion

of the molecules through the solvent. The rate of diffusion is inversely proportional to the rate of diffusional separation which is proportional to the bulk viscosity of the solvent[42]. Generally, elementary diffusion steps in common solvents at room temperature occur on the nanosecond timescale, thus, sub-nanosecond processes are not controlled by diffusional events except for the case of competition between escape from the cage and recombination with a partner product of prompt dissociation. This competition may depend on the initial kinetic energy of the dissociating fragment. The probability of geminate recombination is dependent upon both the viscosity of the solvent and the wavelength of excitation and is inversely proportional to the distance between the primary products. Classically, recombination was assumed to be less likely at higher excitation energy since the possibility of increased excess momentum of the molecular fragments allows them to penetrate the solvent cage and enter into the bulk solution more readily.

The cage effect has been studied extensively by several groups[43-54]. In particular, the solvent dependence of the dissociative reaction of I_2 was studied. Noyes and co-workers investigated the geminate recombination yield as a function of both excitation wavelength and solvent viscosity[43,44,53-55]. They found that the quantum yield decreased with increasing wavelength and viscosity. Despite all of these efforts, a complete characterization of geminate atom recombination did not emerge until the advent of short time laser techniques in the mid 1970's when Chuang *et al*[45] used picosecond laser flash photolysis to further probe the reaction dynamics of the I_2 molecule. These experiments revealed that the time for decrease of the signal due to I atoms was approximately 100 ps, much to the dismay of the theoreticians. This was interpreted as the characteristic

timescale for primary recombination. However, subsequent molecular dynamic simulations by Bunker and Jacobson showed that recombination occurs in 1-2 ps[46]. In fact, recent picosecond experiments on the recombination dynamics of I_2 in inert solvents supported the molecular dynamics simulations[52]. The 100 ps decay time was attributed to vibrational relaxation of the recombined I_2 molecules[48-50] which was a surprising result at that time. Once geminate recombination has occurred, vibrational and electronic energy relaxation occurs surprisingly slowly.

Solvent dependence studies revealed important information regarding the importance of energy transfer from the vibrationally excited I_2 molecule to either solvent translational (V-T) or vibrational (V-V) degrees of freedom. In inert solvents (e.g. Xe), only V-T energy transfer is possible. In this case, vibrational relaxation occurs in about 1 ns. A combination of V-V and V-T energy transfer to a CCl_4 vibrational mode accounted for faster (150 ps) relaxation time[56] in CCl_4. It has been speculated that the relaxation of I_2 in CCl_4 is due to pure V-T transfer in the first 50 ps and that after this time, V-V transfer becomes more important, although this is yet to be experimentally proven. This shows that the "timescale" for vibrational relaxation is dependent upon the solvent.

As will be seen with the example discussed in chapter three, there may be little evidence of control by a geminate pair primary product which can undergo recombination or separation. Other factors must be considered. Three important determinants of processes which occur on time scales competitive with vibrational relaxation can be identified and will be discussed subsequently.

1.6.2. Excited State Vibrational Relaxation (The Thermal Cage Effect)[57]

Vibrational relaxation and related energy redistribution play an important role in many photoinduced processes. Of particular interest are reactions in the condensed phase where collision-induced relaxation can occur. The process of collision-induced relaxation occurs on a very rapid timescale - between several tens of femtoseconds and 100 picoseconds[58]. Time resolved spectroscopy has been recently employed to elucidate the dynamics and physical mechanisms of intra- and inter-molecular energy redistribution[59,60] - processes which up until now have eluded adequate explanation.

In large organic molecules such as naphthalene (18 atoms) or coumarin 6 (43 atoms), there are a large number of vibrational states per energy level giving rise to many possible pathways for vibrational relaxation. Pump-probe experiments with picosecond time resolution were used by Gottfried and co-workers[61,62] to show the intramolecular equilibration of vibrational energy in ground state naphthalene and anthracene occurs within 5 ps following infrared excitation (i.e. within 5 ps, the vibrational levels attain a quasiequilibrium).

Vibrational relaxation processes in anthracene and selected organic dye molecules were investigated in the electronic ground state and, to a lesser extent, in the first excited state using time resolved laser techniques[63-66]. The solute molecules were vibrationally excited by a picosecond infrared pulse or, indirectly, by internal conversion from a higher-lying electronic state. Results showed that the transient signal consists of two components: an initial fast component (2 ps) followed by a slower kinetics with a decay time $>$ 10 ps. The 2 ps time is attributed to intramolecular redistribution creating a

quasiequilibrium population of vibrational levels. The redistribution of the excess energy supplied by the pump pulse creates a hot vibrational system with a distribution function characterized by an elevated vibrational temperature (the energy transfer was monitored via the thermal broadening of the absorption band[62,65,67] or the corresponding emission spectrum[68-70]. The hot molecules cool by collisional interaction with the solvent on a timescale of 7-50 ps, depending on the solvent.

Femtosecond pulses (70 fs pump and probe) were used by Kaiser and co-workers in order to further probe relaxation of the vibronic levels of the excited state in several organic dye molecules. They found that the bleaching kinetics was ultrafast (one kinetic component occurred in the tens of femtoseconds, the other in the hundred femtosecond domain). This was attributed to the depopulation of the vibronic S_1 states. Thus, strong coupling of vibronic levels leads to ultrafast intramolecular relaxation[70]. Relaxation dynamics of the higher lying states in dye molecules also occurs promptly (fs timescale). In this case, two types of relaxation processes are observed: (1) the fast intramolecular S_n --> S_1 redistribution (due to strong coupling within the S_n manifold) and (2) the cooling of vibrationally hot molecules via collisional interaction with neighbouring solvent molecules, a process which occurs in the picosecond time domain. Because of the high density of the liquid (with respect to gas phase), the hot solute interacts with the essentially fixed local arrangement of surrounding solvent molecules of the solvent cage which are heated by the energy received from the solute. The resulting temperature gradient between the inner shell and the bulk (cold) solvent leads to heat conduction which continues until an equilibrium temperature is reached for the entire solution.

Thus, as the solvent cage molecules become hot, energy transfer from the excited state is slowed (because once all the energy has been transferred from the excited molecule to the immediate surroundings, the energy must then be transferred to the bulk solvent before the excited solute molecule can transfer any more energy to the molecules in the first solvation sphere). That is, there is a ***thermal*** cage effect. For heat conduction, the diffusivity K (which is proportional to thermal conductivity λ) represents the most important physical parameter. Thus, the retention of heat at the excited centre as its solvent neighbours become "hot" and a poorer heat sink is closely related to the bulk solvent thermal conductivity and correlation of behaviour to that parameter is diagnostic.

1.6.3. Solvent Reorientation

It is well established that the surrounding solvent medium plays an important role in solution reactions involving ionic molecules or molecules that possess dipoles. The first type of solvent effect involves the solvation of reactants, products and transition states due to strong electrostatic interactions[71] - a static effect. This is most clearly illustrated by the large difference between gas and solution phase rates for associative substitution reactions[72].

The second type of solvent effect is dynamic in nature and is much less understood. In fact, probing the influence of the solvent at early times has only recently become possible upon the advent of picosecond and sub-picosecond pulsed laser techniques. When charge becomes displaced either in a chemical reaction or by electronic excitation, the surrounding solvent dipoles will respond to this motion in a time

dependent fashion. If the reaction is fast, the charges may move so rapidly that the solvent dipoles are essentially "frozen". On the other hand, if the charge moves sufficiently slowly, the solvent dipoles will have time to rearrange thereby clothing the charge with an equilibrium solvation at each stage of the reaction. It is the latter case where details of the structure and motion of the surrounding solvent become important factors which can control fast chemical reactions and excited state relaxations.

In non-equilibrium phenomena, the solvent is treated as a dielectric continuum where the solvent is modeled as a structureless fluid with a frequency-dependent constant (i.e. the system is of constant charge and both the molecular structure of the solvent and of the first solvation shell is disregarded). This is expressed as

$$\epsilon(\omega) = \epsilon_o + \frac{\epsilon_o - \epsilon_\infty}{1 + i\omega\tau_D} \qquad (1.3)$$

where ε_o and ε_∞ are the zero- and high-frequency dielectric constants, respectively, and τ_D is the Debye relaxation time constants (which is a measure of the solvent dipole reorientation). This relaxation time represents the "traditional" view of solvent relaxation. It is based on a constant field approach which states that a charge will tend to move towards an oppositely charged electrode upon application of an electric potential. With it, it will bring an entourage of oppositely charged ions. Thus, the "ionic atmosphere" around the ion is not symmetrical resulting in retarding the motion of the ion. However, the longitudinal solvent relaxation time[74], τ_L, is the term usually invoked to gauge dynamic solvent effects. For example, if the solvent induces changes in the potential energy and free energy barrier to reaction[73], solvent reorientation about a

redistributed charge distribution can control the relaxation pathways. The timescale of this process will be determined by τ_L. It depends slightly on the nature of the perturbation and the dielectric constant[75,76]. This term is used because it accounts for the polarity of the solvent by considering the system as a constant charge (rather than a constant field). τ_L is related to the Debye relaxation time as follows:

$$\tau_L = (\frac{\varepsilon_\infty}{\varepsilon_o})\tau_D \qquad (1.4)$$

In polar solvents, $\varepsilon_o >> \varepsilon_\infty$ and $\tau_L << \tau_D$. Since τ_D is commonly in the range between 10^{-10} and 10^{-11} s, and for polar liquids, $\varepsilon_\infty/\varepsilon_o$ is between 10 and 50, τ typically can vary from 3 to 300 ps for common solvents[76a,77]. The importance of τ_L in solvent dynamics has been discussed by Kosower *et al*[74] who established the intramolecular charge-transfer rates of several organic molecules (e.g. 4-N,N-dimethylaminobenzonitrile) in alcohols are well correlated with τ_L indicating intimate connection between solvent reorientation rates and the rates of intramolecular electron transfer. Thus, solvent motion limits the rate of intramolecular charge transfer reactions.

1.7. References

1. a) Repinec, S.T.; Sension, R.J.; Szarka, A.P.; Hochstrasser, R. M. *J. Phys. Chem.* **1991**, *95*, 10380.

   b) Sension, R.J.; Repinec, S.T.; Hochstrasser, R.M. *J. Chem. Phys.* **1990**, *93*, 9185.

   c) Abrash, S.; Repinec, S.T.; Hochstrasser, R.M. *J. Chem. Phys.* **1990**, *93*, 1041.

   d) Doany, F.E.; Hochstrasser, R.M.; Greene, B.I.; Millard, R.R. *Chem .Phys. Lett.* **1985**, *118*, 1.

2. a) Schoenlein, R. W.; Peteanu, L. A.; Mathies, R. A.; Shank, C. V. *Science* **1991**, *254*, 412.

   b) Tallent, J.R.; Hyde, E.W.; Findsen, L.A.; Fox, G.C.; Birge, R.R. *J. Am. Chem. Soc.* **1992**, *114*, 1581.

3. Langford, C.H.; Moralejo, C.; Sharma, D.K. *Inorg. Chim. Acta.* **1987**, *126*, L11.

4. Lee, M.; Harris, C.B. *J. Am. Chem. Soc.* **1989**, *111*, 8963.

5. a) Moralejo, C.; Langford, C.H.; Sharma, D.K. *Inorg. Chem.* **1989**, *28*, 2205.

   b) Langford, C.H.; Moralejo, C.; Lindsay, E.; Sharma, D.K. *Coordination Chemistry Reviews* **1991**, *111*, 337.

   c) Moralejo, C. Ph.D. Thesis, Concordia University, 1989.

6. a) Joly, A.G.; Nelson, K.A. *Chemical Physics* **1991**, *152*, 69.

   b) Joly, A.G.; Nelson, K.A. *J. Phys. Chem.* **1989**, *93*, 2876.

   c) Simon, J.D.; Xie, X. *J. Phys. Chem.* **1986**, *90*, 6751.

7. Moralejo, C.; Langford, C.H.; Sharma, D.K. *Inorganic Chemistry* **1989**, *28*, 2205.

8. Yu, S.; Xu, X.; Lingle, R.; Hopkins, J.B. *J. Am. Chem. Soc.* **1990**, *112*, 3668.

9. a) Langford, C.H. *Acc. Chem. Res.* **1984**, *17*, 96.

b) Sasseville, R.; Langford, C.H. *J. Am. Chem. Soc.* **1979**, *101*, 5834.

c) Langford, C.H.; Malkashian, A.Y.S. *J. Chem. Soc., Chem. Commun.* **1982**, 1210.

10. Weiland, S.; Reddy, K.B.; van Eldik, R. *Organometallics* **1990**, *9*, 1802-1806.

11. van Dijk, H.K.; Servaas, P.C.; Stufkens, D.J.; Oskam, A. *Inorg. Chim. Acta* **1985**, *104*, 179.

12. Rawlins, K.A.; Lees, A.J. *Inorg. Chem.* **1989**, *28*, 2154-2160.

13. Wieland, S.; van Eldik, R.; Crane, D.R.; Ford, P.C. *Inorg. Chem.* **1989**, *28*, 3663.

14. Víchová, J.; Hartl, F.; Vlček, A., Jr. *J. Am. Chem. Soc.* **1992**, *114*, 10903.

15. Balk, R.W.; Snoeck, T.; Stufkens, D.J.; Oskam, A. *Inorg. Chem.* **1980**, *19*, 3015.

16. Manuta, D.M.; Lees, A. *Inorg. Chem.* **1986**, *25*, 1354.

17. Wieland, S.; Reddy, K.B.; van Eldik, R. *Organometallics* **1990**, *9*, 1802.

18. Lindsay, E.; Vlcek, A., Jr.; Langford, C.H. *Inorg. Chem.*, in press.

19. Van Dijk, H.K.; Stufkens, D.J.; Oskam, A. *J. Am. Chem. Soc.* **1989**, *111*, 541.

20. Meyer, T.J. *Pure and Appl. Chem.* **1986**, *58*, 1193.

21. Ford, P.C.; Wink, D.; DiBenedetto, J. *Prog. Inorg. Chem.* **1983**, *30*, 213.

22. Larson, L.J.; Oskam, A.; Zink, J.I. *Inorg, Chem.* **1991**, *30*, 42.

23. Thayer, J.S. *Adv. Organomet. Chem.* (**1974**), *13*, 1.

24. Mond, L.; Langer, C.; Quincke, F. *J. Chem. Soc.* (**1890**), *57*, 749.

25. Mond, L.; Quincke, F. *J. Chem. Soc.* (**1891**), *59*, 604.

26. Berthelot, M. *Acad. Soc.* (**1891**), *112*, 1343.

27. Dewar, J.; Jones, H.O. *Proc. Roy. Soc. (London) A* **(1905)**, *76*, 558.

28. Cotton, F.A. *Prog. Inorg. Chem.* **1968**, *10*, 49.

29. a) Mills, W.H.; Clark, R.E.D. *J. Chem. Soc.* **1936**, 175.

    b) Clark, R.E.D. *Analyst* **1936**, *60*, 242.

    c) Clark, R.E.D. *Analyst* **1937**, *62*, 661.

30. a) Hamence, J. *Analyst* **1940**, *65*, 152.

    b) Miller, C.C.; Lowe, A.J. *J. Chem.Soc.* **1940**, 1258.

    c) Short, H.G. *Analyst* **1951**, *76*, 710.

31. Bahr, G.; Schleitzer, H. *Chem. Ber.* **1957**, *90*, 438.

32. Schrauzer, G.N.; Mayweg, V.P. *J. Am. Chem. Soc.* **1962**, *84*, 3221.

33. Gray, H.B.; Williams, R.; Bernal, I.; Billig, E. *J. Am. Chem. Soc.* **1962**, *84*, 3596.

34. Davison, A.; Edelstein, N.; Holm, R.H.; Maki, A.H. *J. Am. Chem. Soc.* **1963**, *85*, 2029.

35. a) Eisenberg, R.; Ibers, J.A.; Clark, R.J.H.; Gray, H.B. *J. Am. Chem. Soc.* **1964**, *86*, 113.

    b) Chandramouli, G.V.R.; Manoharan, P.T. *Inorg. Chem.* **1986**, *25*, 4680.

36. a) Heller E.J.; *Acc. Chem. Res.* **1981**, *14*, 368.

    b) Tutt, L.; Zink, J.I.; *J. Am. Chem. Soc.* **1986**, *108*, 5830.

37. Hollebone, B.R.; Langford, C.H.; Serpone, N. *Coord. Chem. Rev.* **1981**, *39*, 181.

38. Hollebone, B.R. *Theor. Chim. Acta* **1980**, *56*, 45.

39. Hollebone, B.R.; Stillman, M.J. *J. Chem. Soc. Faraday Trans. 2* **1978**, 2107.

40. Harris, A.L.; Brown, J.K.; Harris, C.B. *Ann Rev. Phys. Chem.* **1988**, *39*, 341.

41. Franck, J.; Rabinowitch, E. *Trans. Farad. Soc.* **1934**, *30*, 120.

42. Debye, P. *Trans. Electrochem. Soc.* **1977**, *81*, 265.

43. Zimmerman, R.M.; Noyes, J. *J. Chem. Phys.* **1950**, *18*, 658.

44. Lampe, F.W.; Noyes, J. *J. Am. Chem. Soc.* **1954**, *76*, 2140.

45. Chuang, T.J.; Hoffman, G.W.; Eisenthal, L.B. *Chem. Phys. Lett.* **1974**, *25*, 21.

46. Bunker, D.L.; Jacobson, B.S. *J. Am. Chem. Soc.* **1972**, *94*, 1843.

47. Murrell, J.N.; Stace, A.J.; Dammel, R. *J. Chem. Soc. Farad. Trans.* **1978**, *274*, 1532.

48. Nesbitt, D.J.; Hynes, J.T. *J. Chem. Phys.* **1982**, *77*, 2130.

49. Bado, P.; Berens, P.H.; Wilson, K.R. *Proc. Soc. Photo-optic Instrum. Eng.* **1982**, *322*, 230.

50. Bado, P.; Berens, P.H.; Bergsma, J.P.; Coladonato, M.H.; Edelsten, C.G.; Kahn, P.M.; Wilson, J.D.; Wilson, R.K. in Photochemistry and Photobiology, Ed. A. Zewail, 1983, 1, 615.

51. Harris, A.L.; Berg, M.; Harris, C.B. *J.Chem. Phys.* **1988**, *84*, 788.

52. Brown, J.K.; Harris, C.B.; Tully, J.C. *J. Chem. Phys.* **1988**, *89*, 6687.

53. Marshall, R.; Davidson, N. *J. Chem. Phys.* **1953**, *21*, 2086.

54. Booth, D.; Noyes, R.M. *J. Am. Chem. Soc.* **1960**, *82*, 1868.

55. Meadows, L.F.; Noyes, R.M. *J. Am. Chem. Soc.* **1960**, *82*, 1872.

56. Nesbitt, D.J.; Hynes, J.T. *J. Chem. Phys.* **1982**, *77*, 6002.

57. Elsaesser, T.; Kaiser, W. *Ann. Rev. Phys. Chem.* **1991**, *42*, 83.

58. Hinze, J. Ed. Energy Storage and Redistribution in Molecules Plenum, New York, 1983.

59. Kaiser, W. Ed. Ultrafast Laser Pulses and Applications Springer, Berlin, 1988.

60. Harris, C.B.; Ippen, E.P.; Mourou, E.P; Zewail, A. Eds. Ultrafast Phenomena VII Springer, Berlin, 1990.

61. Gottfried, N.H.; Kaiser, W. *Chem. Phys. Lett.* **1983**, *101*, 331.

62. Gottfried, N.H.; Seilmeier, A. Kaiser, W. *Chem. Phys. Lett.* **1984**, *111*, 326.

63. Scherer, P.O.J.; Seilmeier, A. Kaiser, W. *J. Chem. Phys.* **1985**, *83*, 3948.

64. Seilmeier, A; Scherer, P.O.J.; Kaiser, W. *Chem. Phys. Lett.* **1984**, *105*, 140.

65. Wondrazek, F.; Seilmeier, A. Kaiser, W. *Chem. Phys. Lett.* **1984**, *111*, 316.

66. Kaiser, W.; Bauerle, R.J.; Elsaesser, T.; Hubner, H.J.; Seilmeier, A. in Ultrafast Phenomena VI, Eds. T. Yajima, K. Yoshihara, C.B. Harris, S. Shinoya, Springer, Berlin, p. 453.

67. Wild, W.; Seilmeier, A.; Gottfried, N.H.; Kaiser, W. *Chem. Phys. Lett.* **1985**, *119*, 159.

68. Mokhtari, A.; Chesnoy, J.; Laubereau, A. *Chem. Phys. Lett.* **1989**, *155*, 593.

69. Laermer, F.; Elsaesser, T.; Kaiser, W. *Chem. Phys. Lett.* **1989**, *156*, 381.

70. Laermer, F.; Israel, W; Elsaesser, T. *J. Opt. Soc. Am.* **1990**, *B7*, 1604.

71. a) Abraham, M.H. *Progress in Physical Organic Chemistry*, Vol. 11, Ed. A. Streitwieser, Jr. and R.W. Taft, Wiley and Sons, New York, 1974.

    b) Parker, A.J. *Chem Rev.*, **1969**, *69*, 1.

72. a) Tanaka, K.; Mackay, G.I.; Payzant J.D.; Bohme, D.K. *Can. J. Chem.*, **1976**, *54*, 1643.

    b) Olmstead, W.N.; Brauman, J.I. *J.Am. Chem. Soc.* **1977**, *99*, 4219.

    c) Bohme, D.K.; Mackay, G.I. *J.Am. Chem. Soc.* **1981**, *103*, 978.

73. Hynes, J.T. *Ann. Rev. Phys. Chem.* **1985**, *36*, 573.

74. Kosower, E.M.; Huppert, D. *Ann. Rev. Phys. Chem.* **1986**, *37*, 127.

75. Sumi, H.; Marcus, R.A. *J. Chem. Phys.* **1986**, *84*, 4272.

76. a) Frolich, H. *Theory of Dielectrics* Oxford University Press, London, 1949.

    b) Hubbard, J.B. *J. Chem. Phys.* **1978**, *68*, 1649.

77. Hill, N.E.; Vaughn, W.E.; Price, A.H.; Davies, M. *Dielectric Properties and Molecular Behavior*, Van Nostrand, Princeton, 1969, chs. 1,4,5.

2. Experimental

2.1. Materials

Commercially available materials were used in all synthetic procedures and in all photochemical experiments with further purification only as specified below. A list of the reagents used, their grade and supplier is given in Tables 2.1 and 2.2.

Table 2.1. List of reagents used in the preparation of the Re carbonyl complexes.

Compound	Grade	Supplier
Acetonitrile	Reagent	Janssen Chimica
Bromine	Reagent	Merck
Carbon tetrachloride	Reagent	Merck
Dichloromethane	Reagent	Janssen Chimica
4,4'-Dimethyl-2,2'-dipyridyl	Reagent	Fluka
Hexanes	Reagent	Janssen Chimica
Petroleum ether	Reagent	Janssen Chimica
1,10-Phenanthroline	Reagent	Fluka
Dirhenium decacarbonyl	Reagent	Fluka
Silicagel-60	Reagent	Merck
Tetrahydrofuran	Reagent	Janssen Chimica
Triphenyl tin chloride	Reagent	Fluka

The tetrahydrofuran was purified by the ketyl method[1] and the hexane was dried over sodium metal and distilled under nitrogen prior to use. All other reagents were used as received.

Table 2.2. List of reagents used in picosecond flash photolysis measurements, steady state photolysis and in the synthesis of $W(CO)_4$(phen), $W(CO)_5$(4-Formyl-Pyridine) and $[(n\text{-}C_2H_5)_4N]_2[Ni(mnt)_2]$.

Compound	Grade	Supplier
Aberchrome 540	-	Aberchromics Ltd.
Aberchrome 999P	-	Aberchromics Ltd.
Acetone	Reagent	ACP
Acetonitrile	HPLC	Aldrich
Benzene	Reagent; HPLC	Caledon; Aldrich
Carbon disulfide	Reagent	Baker
Chloroform	HPLC	Aldrich
Dichloromethane	Reagent; Spectrophotometric	Aldrich
Dimethylformamide	Reagent	Aldrich
Ethanol	Reagent	ACP
Hexanes	Reagent; HPLC	Aldrich; Baxter
Iodine	Reagent	Shawinigan
Iron chloride hexahydrate	Reagent	Fisher
Isobutanol	Reagent	Fisher
Methanol	Reagent	ACP
Nickel(II) chloride	Reagent	Fisher
n-Pentane	Spectrophotometric	Anachemia
1,10-Phenanthroline	99+%	Aldrich
Potassium oxalate	Reagent	Shawinigan
Pyridine	HPLC	Aldrich
4-Formyl-Pyridine	98%	Aldrich
Silicagel-60	Reagent	Merck, Baker
Tetraethylammonium bromide	98%	Anachemia
Tetrahydrofuran	Reagent	BDH
Toluene	Spectrophotometric	Aldrich
n-tributyl phosphine	99%	Aldrich
Trimethylamine N-oxide-dihydrate	98%	Aldrich
$W(CO)_6$	99%	Aldrich

Carbon disulfide and isobutanol were distilled and tetrahydrofuran was purified by the ketyl method[1] prior to use. All other reagents were used without further purification unless otherwise noted.

2.2. Preparation of the Complexes.

2.2.1. Sodium *cis*-1,2-dicyanato-1,2- ethylenedithiolate, $Na_2(S_2C_2(CN)_2)$.

$$NaCN + CS_2 + 3HCON(CH_3)_2 \text{ --> } NCCS_2Na \cdot 3HCON(CH_3)_2 \qquad (2.1)$$

$$2NCCS_2Na \cdot 3HCON(CH_3)_2 \text{ --> } Na_2S_2C_2(CN)_2 + 6HCON(CH_3)_2 + 2S \qquad (2.2)$$

A modification of the method described by Bahr and Schleitzer[2a,b] was used. 10 g (0.61 mol) of finely crushed NaCN was added to 120 mL of DMF in a 3-neck, standard-taper round-bottomed flask equipped with a dropping funnel and a stirring bar and stirred for 3 days. 30.2 g (24 mL; 0.4 mol) of CS_2 was then added dropwise with vigorous stirring over a period of 20 minutes. A yellow-green colour developed initially and rapidly darkened to the characteristic red-brown colour of sodium dithiocyanate. When the addition was complete, the mixture was stirred for 4 hours. The solution was then stored at -10°C for 24 hours. During this time, sodium dithiocyanate precipitated out of solution along with any excess NaCN. The solid was collected by suction filtration and air dried. A super-saturated solution of the solid in a 1:1 mixture of hot isobutanol/isopropanol was made in order to remove excess NaCN (sodium dithiocyanate is soluble in alcohols, whereas NaCN is not). The hot solution was filtered under vacuum. The filtrate was then transferred into a 500 mL Erlenmeyer flask, sealed tightly, and stored at -10°C for 24 hours. The cold solution was filtered under vacuum

and air dried thus affording pale brown crystals (sodium dithiocyanate). The yield was 18.6 g.

The following steps of the synthesis were carried out in the dark in a glove bag filled with pre-purified nitrogen. About 250 mL of deaerated $CHCl_3$ was added to a 500 mL Erlenmeyer flask containing approximately 18.6 grams of sodium dithiocyanate. The mixture was thoroughly stirred, then sealed tightly (the rubber stopper was wrapped with aluminum foil to prevent any possible reaction between the $CHCl_3$ vapours and the rubber) and left to stand in the inert atmosphere. Spontaneous dimerization of sodium dithiocyanate occurred thus affording a yellow precipitate of Na_2mnt (the ligand $S_2C_2(CN)_2$ will be subsequently abbreviated as mnt) and sulfur. After a period of 1 week, the flask was removed from the glove bag and the precipitate was filtered by suction and air dried (exposure to air should be minimized and exposure to light avoided during the filtration and drying). The precipitate was then dissolved in a minimum amount of a 1:1 methanol/ethanol mixture. The resulting solution was filtered under vacuum to remove insoluble sulfur. This filtrate was concentrated to 25 mL. A copious amount of $CHCl_3$ was added, with stirring, to the filtrate and Na_2mnt immediately precipitated. The solution was cooled on ice to ensure complete precipitation. The product was collected by vacuum filtration, washed with 5 mL of cold $CHCl_3$ and air-dried. The purity was checked by thin layer chromatography using a 50% acetone-ethanol mixture as the mobile phase. The yield was 19 g (52% based on NaCN). Na_2mnt is a highly electrostatic yellow powder and was stored in the dark in a calcium chloride desiccator under nitrogen.

2.2.2. Tetra-*n*-ethylammonium bis(*cis*-1,2-dicyano-1,2-ethylenedithiolato)-nickelate(2-), $[(C_2H_5)_3N]_2[Ni(mnt)_2]$

$$Ni^{2+} + 2S_2C_2(CN)_2^{2-} + 2(n\text{-}C_2H_5)_4N^+ \text{---> } [(n\text{-}C_2H_5)_4N]_2[NiS_4C_4(CN)_4] \qquad (2.3)$$

The preparation developed by Billig *et al* was used[3a,b]. A solution of 2.05 g (0.0011 mol) of Na_2mnt (Section 2.2.1) in 30 mL of a 1:1 (v/v) mixture of ethanol-water was prepared. To this, a solution of 1.19 g (0.005 mol) of nickel chloride hexahydrate dissolved in 7.5 mL of water was slowly added, with stirring. The dark red solution was filtered by suction. A solution of 2.42 g (0.0115 mol) of tetra *n*-ethylammonium bromide in 12.5 mL of ethanol was slowly added to the filtrate with stirring. Small orange-red crystals of crude $[(n\text{-}C_2H_5)_4N]_2[Ni(mnt)_2]$ separated immediately and were collected by suction filtration, washed with 10 mL of water, followed by 10 mL of ethanol-water (1:1 (v/v)) and sucked dry. $[(n\text{-}C_2H_5)_4N]_2[Ni(mnt)_2]$ was purified by recrystallization using an acetone-isobutyl alcohol solvent mixture.

The crude product was dissolved in 40 mL of hot acetone and filtered while still hot. The filtrate was heated to boiling and 17.5 mL of isobutyl alcohol was added slowly, with stirring. Most of the acetone was then evaporated by heating on a steam bath. When the volume was approximately 20 mL, the solution was set aside. Large, well formed deep red crystals separated upon cooling. These were collected by suction filtration and washed with 12.5 mL of isobutyl alcohol followed by three 25 mL portions of *n*-pentane. The yield was 86%. The product was characterized by UV-visible spectroscopy. The spectrum was identical to those which were previously reported[4a,b]. The extinction coefficient is 3800 $M^{-1}cm^{-1}$ for the MLCT band (476 nm) in acetonitrile. $[(n\text{-}C_2H_5)_4N]_2[Ni(mnt)_2]$ can be stored safely under nitrogen in the dark.

2.2.3. Tetra-*n*-ethylammonium bis(*cis*-1,2-dicyano-1,2-ethylenedithiolato)-nickelate(1-), $[(n\text{-}C_2H_5)_3N][Ni(mnt)_2]$

$$[(n\text{-}C_2H_5)_4N]_2[NiS_4C_4(CN)_4] + 1/2I_2 \text{ -----> } [(n\text{-}C_2H_5)_3N]I + [(n\text{-}C_2H_5)_4N][NiS_4C_4(CN)_4] \quad (2.4)$$

This compound was prepared[5a,b] by the iodine oxidation of $Ni(mnt)_2^{2-}$ (Section 2.2.2). 4.0 g (0.016 mol) of iodine was dissolved in 8 mL of dimethyl sulfoxide. This solution was added in one portion to a solution of $[(n\text{-}C_2H_5)_4N]_2[Ni(mnt)_2]$ in 60 mL of dimethyl sulfoxide and stirred for one minute. The mixture was poured, with stirring, into 210 mL of 95% ethanol, then allowed to sit for 20 minutes. During this time, the product precipitated out of solution as tiny black crystals. The crystals were collected by suction filtration and washed repeatedly with 10 mL portions of ethanol (150 mL). The black crystals were then washed with three 25 mL portions of anhydrous ether followed by three 25 mL portions of *n*-pentane and air dried. The yield was 77%. The product was characterized by UV-visible spectroscopy. The spectrum agreed well with that which was previously reported[4a,b]. The extinction coefficient of the LMCT band (477 nm) is 2500 $M^{-1}cm^{-1}$. $[(n\text{-}C_2H_5)_4N][Ni(mnt)_2]$ can be stored in the dark for long periods of time.

2.2.4. $W(CO)_4$(phen); phen = 1,10-phenanthroline

$$W(CO)_6 + \text{phen} + (CH_3)_3NO \cdot 2H_2O \text{ ---> } W(CO)_4(\text{phen}) + 2CO \quad (2.5)$$

Preparation of this complex was based the method developed by Bock and tom Dieck[6]. All procedures were carried out in the dark. 1 g (3.4 mmol) of $W(CO)_6$, 0.56 g (2.8 mmol) of phen and 0.9 g (8.0 mmol) of trimethylamine N-oxide dihydrate were

refluxed in 50 mL of acetonitrile at 50°C for 1.5 hours. Evaporation of the acetonitrile solution yielded crude $W(CO)_4$(phen). The product was purified using column chromatography.

A column of silicagel-60 was prepared using hexane as the solvent. A 1:1 (v/v) mixture of hexane and dichloromethane followed by neat dichloromethane were used to elute the product. The dichloromethane solution was then evaporated to dryness, affording pure $W(CO)_4$(phen). The yield was 34%. The compound was characterized using UV-visible and infrared (IR) spectroscopies. The spectra agreed well with those previously reported[7]. The extinction coefficients are 6040 $M^{-1}cm^{-1}$ and 3040 $M^{-1}cm^{-1}$ for the MLCT band (486 nm) and the LF band (394 nm), respectively, in THF. $W(CO)_4$(phen) can safely be stored for long periods of time in the dark.

2.2.5. $W(CO)_5$(4-X-Pyridine); X = CN, Formyl

$$W(CO)_6 \xrightarrow[THF]{h\nu} W(CO)_5THF + CO\uparrow \qquad (2.6)$$

$$W(CO)_5(THF) \xrightarrow[X]{\Delta} W(CO)_5(4\text{-X-Pyridine}) + THF \qquad (2.7)$$

The preparation of $W(CO)_5$(4-X-Pyridine) was carried out via the corresponding tetrahydrofuran (THF) complex, $W(CO)_5$(THF), as described by Strohmeier[8]. 1.3 g (3.7 mmol) of $W(CO)_6$ was dissolved in 60 mL of dry, deaerated THF and then irradiated with 350 nm light using a Rayonet photochemical reactor. The solution was continually purged with nitrogen throughout the irradiation to avoid oxidation effects and to remove

the CO produced. After 1.5 hours, the solution became deep yellow-green, characteristic of $W(CO)_5(THF)$. A stoichiometric amount of X (either 4-Formyl Pyridine or 4-CN-Pyridine) was then added to the solution containing $W(CO)_5(THF)$. The mixture became yellow-orange in colour indicating substitution of THF by X. The THF was then removed by rotary evaporation thus affording crude $W(CO)_5(4\text{-}X\text{-}Py)$. The product was purified under atmospheric conditions using column chromatography.

A column of silicagel-60 was prepared using hexane as the solvent. The crude product was dissolved in benzene and brought onto the column. Unreacted hexacarbonyl was removed from the column by successive hexane washings; these were monitored by UV-visible spectroscopy. $W(CO)_5(4\text{-}X\text{-}Pyridine)$ was then eluted with benzene. The benzene solution was evaporated to dryness affording $W(CO)_5(4\text{-}X\text{-}Pyridine)$. This procedure was repeated to ensure complete removal of $W(CO)_6$. The product was further purified by recrystallization from benzene/hexane (1:1) solution. The yield of $W(CO)_5(4\text{-}Formyl\text{-}Pyridine)$ was 35%. The compound was characterized using UV-visible and IR spectroscopies. The spectra agreed well with those previously reported[9]. $W(CO)_5(4\text{-}Formyl\text{-}Pyridine)$ can safely be stored for long periods of time under nitrogen in the dark. $W(CO)_5(4\text{-}NC\text{-}Pyridine)$ was generously donated by Prof. A.J. Lees.

2.2.6. $Re(CO)_5Br$

$$Re_2(CO)_{10} + Br_2 \text{ ---> } 2Re(CO)_5Br \qquad (2.8)$$

$Re(CO)_5Br$ was prepared according to the procedure described in reference 10. 3.25 g (4.98 mmol) of $Re_2(CO)_{10}$ was dissolved in 75 mL of CCl_4 and cooled to 0°C.

A solution of 6.8 mmol (0.35 mL) Br_2 in 10 mL CCl_4 was then added very slowly to the cold $Re_2(CO)_{10}$ solution. The resulting mixture was stirred at room temperature for two hours. During this time, a white precipitate ($Re(CO)_5Br$) formed. The precipitate was collected by suction filtration and washed twice with 30 mL of CCl_4 followed by 30 mL of hexane. Further purification was unnecessary. The yield was 84%. The product was characterized by IR spectroscopy. The spectrum agreed with that previously reported[10].

2.2.7. $Re(CO)_3(CH_3CN)_2Br$

$$Re(CO)_5Br + 2CH_3CN \xrightarrow{\Delta} Re(CO)_3(CH_3CN)_2Br + 2CO \qquad (2.9)$$

The method developed by Wehman[11] was used for the preparation of $Re(CO)_3(CH_3CN)_2Br$. 1.5 g (3.7 mmol) of $Re(CO)_5Br$ (Section 2.2.6) was dissolved in a minimum amount of CH_3CN and refluxed under nitrogen for 24 hours. The acetonitrile was removed under vacuum thus affording crude $Re(CO)_3(CH_3CN)_2Br$ (a pale brown powder). The product was recrystallized from a dichloromethane/petroleum ether mixture under atmospheric conditions. Infrared spectroscopy was used to characterize the compound; the spectrum agreed with that which was previously reported[11]. The yield was 88%.

2.2.8. $Re(CO)_3(bpy')Br$; bpy' = 4,4'-dimethyl-2,2'-bipyridyl

$$Re(CO)_3(CH_3CN)_2Br + bpy' \longrightarrow Re(CO)_3(bpy')Br \qquad (2.10)$$

$Re(CO)_3(bpy')Br$ was prepared by a modification of the method developed by Staal *et al*[12]. All procedures were carried out in an inert environment using standard

Schlenk techniques. 0.5 g (1.1 mmol) of $Re(CO)_3(CH_3CN)_2Br$ (Section 2.2.7) and 1.3 mmol of 4,4'-dimethyl-2,2'-bipyridyl were dissolved in a minimum amount of dry, deaerated THF and stirred at room temperature for two hours. The solution was filtered by suction to remove insoluble impurities. The yellow product was then precipitated out of solution by the slow addition of petroleum ether to the filtrate and was collected using suction filtration. The yield was 80%. The product was characterized by its IR spectrum (Figure 2.1) which was similar to that previously reported for the analogous 1,4-diazobutadiene complex[12]. $Re(CO)_3(bpy')Br$ can be safely stored in the dark.

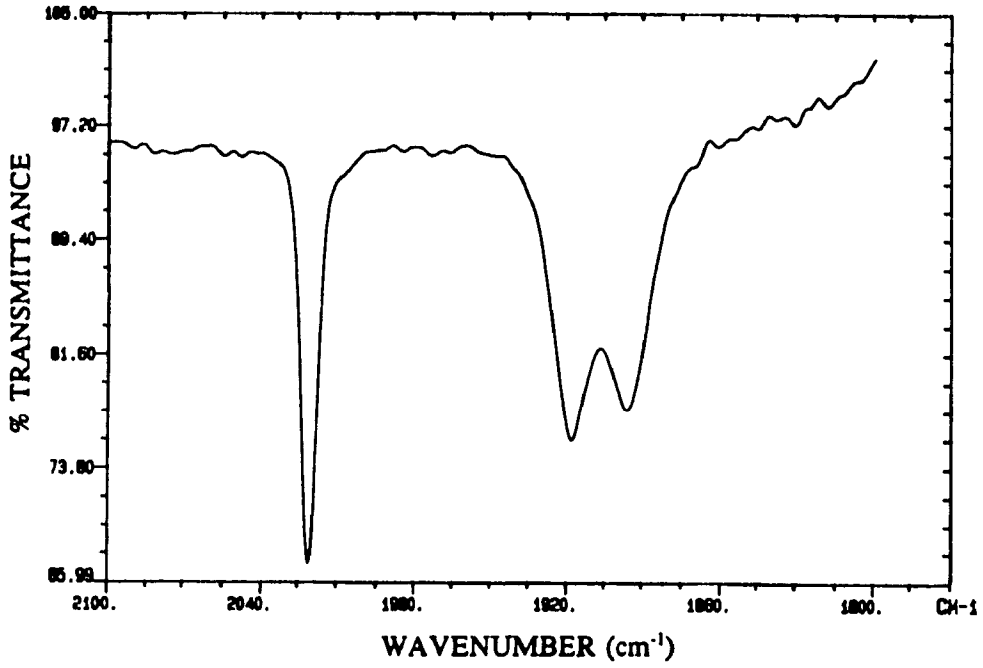

Figure 2.1. Infrared spectrum (CO stretching region) of $Re(CO)_3(bpy')Br$ in CH_2Cl_2.

2.2.9. $(CO)_5Re\text{-}Re(CO)_3(bpy')$; bpy' = 4,4'-dimethyl-2,2'-bipyridyl

$$Re_2(CO)_{10} \xrightarrow[NaK_{2.8}]{THF} Na^+Re(CO)_5^- \qquad (2.11)$$

$$Na^+Re(CO)_5^- + Re(CO)_3(bpy')Br \text{ -----} > (CO)_5Re\text{-}Re(CO)_3(bpy') + NaBr \qquad (2.12)$$

A modification of the method described in reference 13 was used to prepare this compound. All procedures were carried out in the dark and in an inert atmosphere using standard Schlenk techniques. 1.3 g (2 mmol) of $Re_2(CO)_{10}$ was dissolved in dry, freshly distilled THF. Approximately 0.5 mL of $NaK_{2.8}$ (this material was prepared by Ms. Brenda Rossenaar at the University of Amsterdam based on the method developed by Ellis and Flom[14]) was added to this solution and the resulting mixture was stirred vigorously for 24 hours. The mixture was then filtered (under nitrogen) to remove any excess $NaK_{2.8}$.

0.19 g (0.35 mmol) of $Re(CO)_3(bpy')Br$ (Section 2.2.8) was dissolved in 50 mL of dry, freshly distilled THF. The solution of $Re(CO)_3(bpy')Br$ was then added to the $Re(CO)_5^-$ solution and stirred for 24 hours. The solvent was removed under vacuum thus affording crude $(CO)_5Re\text{-}Re(CO)_3(bpy')$, a red powder. The red compound was purified using column chromatography.

The manipulations described for the purification of $(CO)_5Re\text{-}Re(CO)_3(bpy')$ were also performed under nitrogen and in the dark. All solvents were freshly distilled and dried prior to use. A column of silicagel-60 was prepared using hexane as the solvent. The $(CO)_5Re\text{-}Re(CO)_3(bpy')$ was dissolved in 3 mL of THF and brought on to the

column with a syringe. A 10% (v/v) solution of THF in hexane was used to elute the product. The solvent was then removed under vacuum, thus affording pure $(CO)_5Re$-$Re(CO)_3(bpy')$. The compound was characterized using UV-visible and IR spectroscopies. The spectrum was similar to that which has been previously reported for the analogous phen compound[13b] as shown in Figure 2.2. $(CO)_5Re$-$Re(CO)_3(bpy')$ can be stored in the dark, under nitrogen.

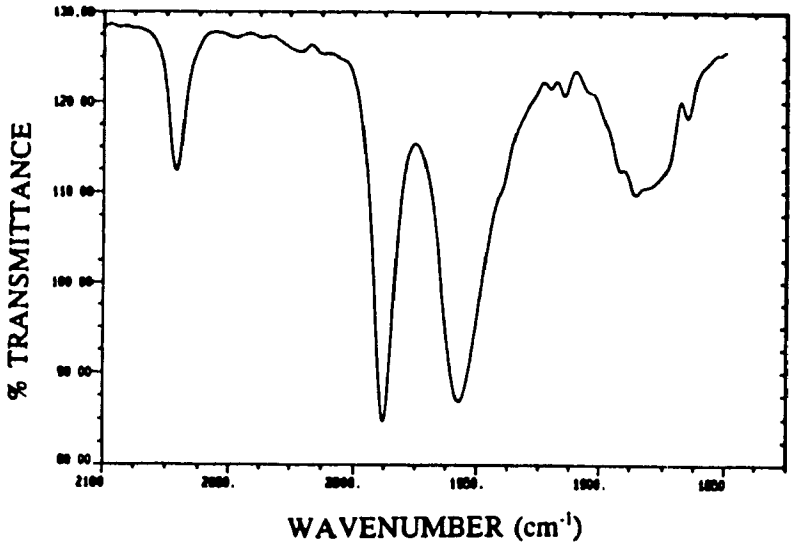

Figure 2.2. Infrared spectrum (CO stretching region) of $(CO)_5Re$-$Re(CO)_3(bpy')$ in CH_2Cl_2.

2.2.10. $(CO)_3(bpy')Re$-$Sn(C_6H_5)_3$; bpy' = 4,4'-dimethyl-2,2'-bipyridyl

$$Re(CO)_3(bpy')Br \xrightarrow[NaK_{2.8}]{THF} Re(CO)_3(bpy')^- + Br^- \qquad (2.13)$$

$$Re(CO)_3(bpy')^- + Sn(C_6H_5)_3Cl \longrightarrow (C_6H_5)_3Sn\text{-}Re(CO)_3(bpy') + Cl^- \qquad (2.14)$$

This compound was prepared according to the procedure developed by Luong *et al*[15]. All manipulations were carried out in the dark and in an inert environment using

standard Schlenk techniques. 0.5 g (1 mmol) of $Re(CO)_3(bpy')Br$ (Section 2.2.8) was dissolved in dry, distilled THF. Approximately 0.3 mL of $NaK_{2.8}$ was added to this solution and the resulting dark blue mixture was stirred for two hours. The mixture was then filtered (under nitrogen) to remove any excess $NaK_{2.8}$. A solution of 0.39 g (1 mmol) of $Sn(C_6H_5)_3Cl$ in 20 mL THF was then added dropwise, with stirring, to the filtrate. The resulting mixture was stirred for two hours. The solvent was removed under vacuum, thus affording crude $(C_6H_5)_3Sn\text{-}Re(CO)_3(bpy')$, an orange powder. The product was purified using column chromatography.

Manipulations described for the purification of $(C_6H_5)_3Sn\text{-}Re(CO)_3(bpy')$ were also performed in the dark and under nitrogen. All solvents were freshly distilled and dried prior to use. A column of silicagel-60 was prepared using hexane as the solvent. The $(C_6H_5)_3Sn\text{-}Re(CO)_3(bpy')$ was dissolved in 3 mL of THF and brought on to the column with a syringe. A 5% (v/v) solution of THF in hexane was used to elute the product. The solvent was then removed under vacuum, thus affording pure $(C_6H_5)_3Sn\text{-}Re(CO)_3(bpy')$. The orange compound was characterized by its IR spectrum which was similar to that which has been previously reported for the analogous phen compound[15] as shown in Figure 2.3. $(C_6H_5)_3Sn\text{-}Re(CO)_3(bpy')$ can be stored in the dark, under nitrogen.

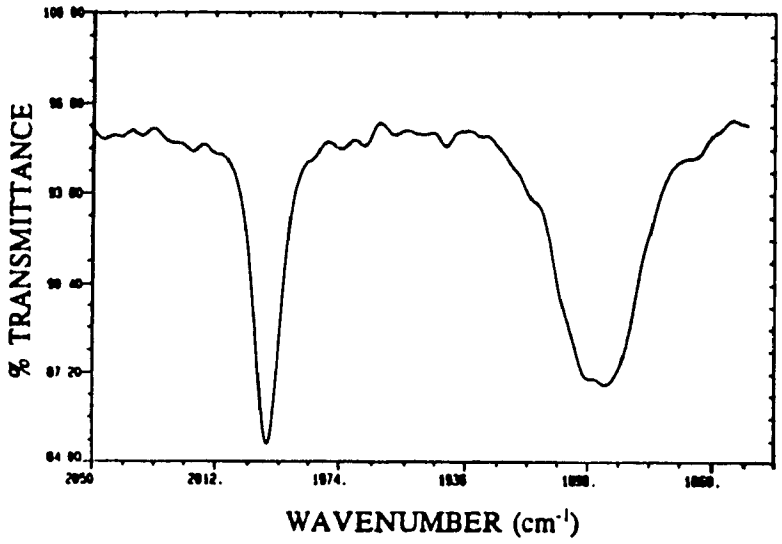

Figure 2.3. Infrared spectrum (CO stretching region) of $(C_6H_5)_3Sn\text{-}Re(CO)_3(bpy')$ in CH_2Cl_2.

2.2.11. Potassium Ferrioxalate, $K_3Fe(C_2O_4)_3 \cdot 3H_2O$

$$3K_2(C_2O_4) + FeCl_3 \text{ ---> } K_3Fe(C_2O_4)_3 + 3KCl \qquad (2.15)$$

Potassium ferrioxalate was prepared according to the procedure described by Calvert and Pitts[16]. All manipulations were carried out in the dark. 3 volumes of 1.5 M potassium oxalate solution was mixed with 1 volume of a 1.5 M ferric chloride solution. The green crystals of $K_3Fe(C_2O_4)_3 \cdot 3H_2O$ were allowed to precipitate out overnight. They were recrystallized 3 times from warm water and dried in an oven at 40°C oven. The yield was 89%.

2.3. Steady-State Photochemistry

2.3.1. Sample Preparation

Solutions of $[(n\text{-}C_2H_5)_4N]_2[Ni(mnt)_2]$ in acetonitrile-chloroform mixtures were prepared under atmospheric conditions and then transferred to a quartz cuvette (Hellma, 1 cm path length, volume = 3.0 mL) for photolysis. Solution concentrations ranged from 10^{-3} M to 10^{-4} M.

Solutions of $W(CO)_4(phen)$ in carefully deaerated solvents (pyridine, toluene, dichloromethane, tetrachloroethylene) were prepared under an atmosphere of pre-purified nitrogen using standard Schlenk techniques. When a non-coordinating solvent (toluene, dichloromethane or tetrachloroethylene) was used, the ligand *n*-tributylphosphine (also carefully degassed) was added to the reaction mixture to produce concentrations of either 0.015, 0.33 or 0.36 M. A 3.0 mL aliquot of the $W(CO)_4(phen)$ solution was then transferred (under nitrogen) to a Schlenk tube with an attached quartz cuvette (Hellma, 1 cm path length, volume = 3 mL) for photolysis. Solution concentrations ranged from $9x10^{-4}$ to $1.5x10^{-3}$ M.

Solutions of $(CO)_5Re\text{-}Re(CO)_3(bpy')$ were prepared in carefully deaerated dichloromethane under an atmosphere of pre-purified nitrogen using standard Schlenk techniques. A 3.0 mL aliquot of the $(CO)_5Re\text{-}Re(CO)_3(bpy')$ solution was then transferred (under nitrogen) to a Schlenk tube with an attached quartz cuvette (Hellma, 1 cm path length, volume = 3 mL) for photolysis. Solution concentrations were $9.9x10^{-4}$ M.

2.3.2. Instrumentation

The IR spectra used to characterize the carbonyl complexes were recorded on a Nicolet 7199B FTIR spectrometer using a liquid nitrogen cooled MCT detector (resolution 1.0 cm^{-1}).

A PRA Model No. ALH215 xenon medium pressure arc lamp (150 W) coupled with an interference filter (Oriel; bandwidth $\pm$ 12 nm) was used for photolysis at 313 nm and 365 nm. A block diagram of the optical train is given in Figure 2.4. An argon ion laser (Coherent Innova 70, 4 W (all line)) was used for photolysis at 488.0 nm, 496.0 nm, and 514.5 nm. For irradiation at 610.9 nm, a dye laser (Coherent CR-590) using Rh-6G was employed. The beam was expanded to the diameter of the photolysis cell by passing it through a convex lens. A block diagram of the optical trains is given in Figure 2.5.

All steady-state photolyses were monitored by UV-visible absorption spectroscopy using a Hewlett-Packard Model No. 8452A diode array spectrophotometer interfaced with an IBM PC. Each sample was irradiated for successive time intervals, and a full spectrum taken after each interval. All solutions were stirred continuously during irradiation. All compounds were thermally stable on the time scale of the photochemical experiments. Photolysis and spectroscopic analysis were carried out using the same cell.

2.4. Measurement of Light Intensity

The amount of light absorbed by the reactants (i.e. $[(C_2H_5)_3N]_2[Ni(mnt)_2]$, $(CO)_5Re\text{-}Re(CO)_3(bpy')$, and $W(CO)_4(phen)$) in all steady-state photolyses was

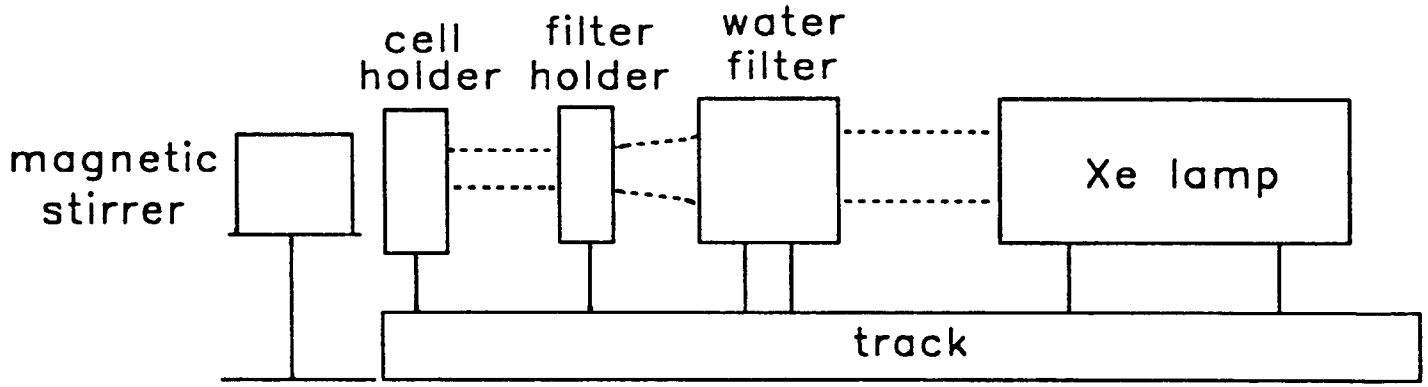

Figure 2.4. Optical train for 313 nm and 365 nm irradiation.

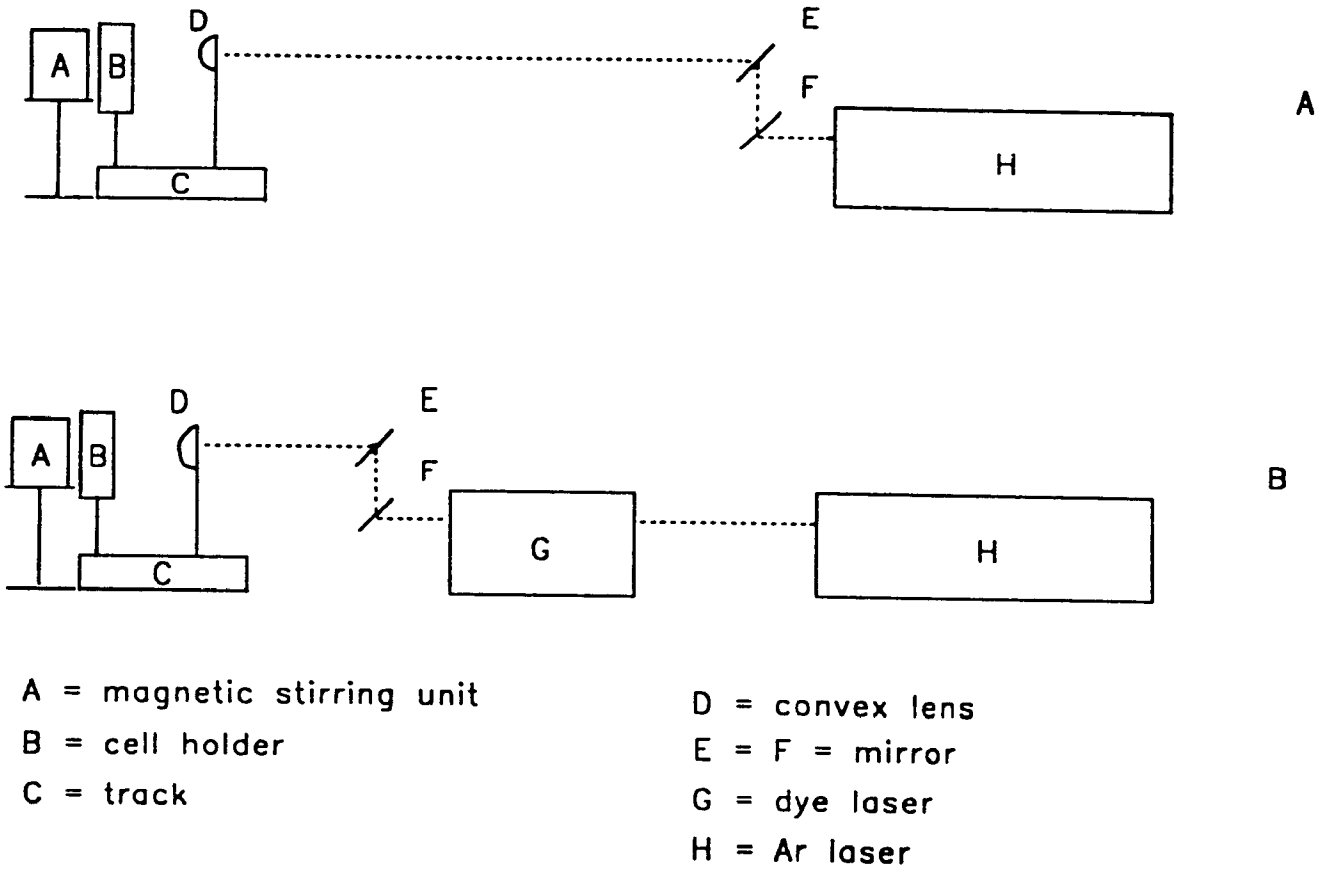

Figure 2.5. Optical trains for (A) 488.0 and 514.5 nm irradiation and (B) 610.9 nm irradiation.

determined using chemical actinometry. Chemical actinometry has the advantage that the actinometer can be irradiated under conditions similar to those of the photoreactions being studied. Two compounds were used for actinometry during the course of this work: (1) potassium ferrioxalate[17], the "traditional" chemical actinometer developed by Hatchard and Parker in the late 1950's and (2) photochromic fulgides[18] which were developed by Heller and Langan in the early 1980's.

2.4.1. Ferrioxalate Actinometry

Exposure of tris(oxalato)ferrate(III) to light between 254 and 514 nm reduces the Fe^{3+} to Fe^{2+} according to the following reaction:

$$[Fe^{III}(C_2O_4)_3]^{3-} \xrightarrow{h\upsilon} [Fe^{II}(C_2O_4)_2]^{2-} + 2CO_2 \qquad (2.16)$$

Quantum yields for the reduction are wavelength-dependent and have been well established[17]. For irradiations at 313 and 365 nm, the fraction of the light absorbed by the actinometer for concentrations of $\geq$ 0.06 M was > 99%. Solutions of $[(C_2H_5)_3N]_2[Ni(mnt)_2]$ were made sufficiently concentrated so that the total light absorbed by the sample was > 99% for these two wavelengths. The number of photons/second entering the photolysis cell was easily determined using the equations described in Section 2.5.2.

2.4.2. Fulgide Actinometry

Fulgide actinometry is able to determine the light intensity entering the cell window under either ultraviolet or visible irradiation. Irradiation at 313 or 365 nm

promotes a conrotatory ring closure of aberchrome 540 (X = O; R = CH_3; Equation 2.17) to yield the deep red aberchrome 540P.

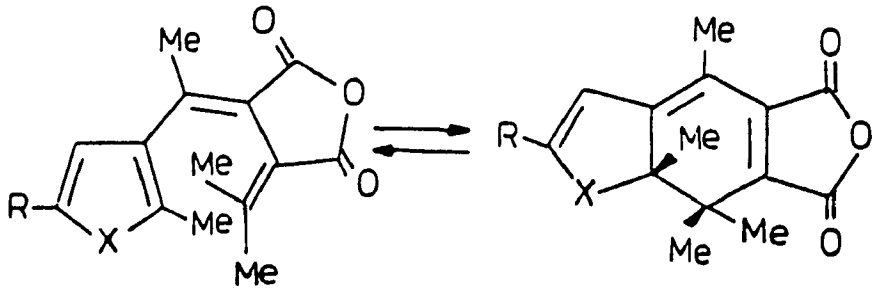

(2.17)

540 540P

The quantum yield for this reaction has been well established as 0.20[18b] when toluene is the solvent and is independent of both temperature and irradiating wavelength. For irradiations at 313 and 365 nm, the light absorbed by the actinometer was > 99%. The number of photons per second entering the photolysis cell was easily determined using the equations in Section 2.5.3. Solutions of $W(CO)_4$(phen) were made sufficiently concentrated such that the light absorbed by the sample was > 99% for these two wavelengths.

The ring opening reaction (ie: the reverse of reaction 2.17) was followed when the irradiation was 488.0 or 514.5 nm, although, a more dilute solution (absorbance < 1) was employed than when irradiating in the ultraviolet region. Unlike the forward reaction, the ring opening reaction is dependent on both the wavelength of excitation and on the temperature. When the exciting wavelength was 610.9 nm, aberchrome 999P (X = S; R = C_6H_5- in Equation 2.17.) was the actinometer used since it absorbs light

in this spectral region. It reacts similarly to aberchrome 540P. As with irradiations at 488.0 and 514.5 the absorbance by the actinometer for excitation at 610.9 nm was less than 1. These effects (temperature, wavelength and absorptivity) were taken into account in the calculations (Section 2.5.4).

In all cases, several actinometer readings were obtained during the course of each experiment and averaged. The standard deviation was less than 5%. As in the photolysis experiments, the actinometer solution was stirred constantly during the irradiation using a magnetic stirring bar. The average number of photons/second entering the cell through the 313 and 365 nm filters was 6.0×10^{14} and 1.5×10^{15} ($\pm$ 5%), respectively. The average power emitted by the laser at both 488.0 and 514.0 nm was 100 mW/cm^2. However, the laser power was limited to 10 mW/cm^2 for the photolysis of $(CO)_5Re\text{-}Re(CO)_3(bpy')$ (488.0, 496.0, 514.5 nm irradiation) because of its extreme sensitivity to light. At 610.9 nm, the average power emitted by the laser was 60 mW/cm^2.

2.5. Analysis of the Steady-State Photolysis Data

2.5.1. Photolysis of $[(C_2H_5)_3N]_2Ni(mnt)_2$

The increase of the absorbance of the photoproduct, $[(C_2H_5)_3N]Ni(mnt)_2$, was monitored as a function of time of irradiation for solutions of $[(C_2H_5)_3N]_2Ni(mnt)_2$ in various chloroform-acetonitrile mixtures. The wavelength of analysis was chosen to be 818 nm because the photoproduct is the only species which absorbs light in this region. There was no loss of isosbestic point during the course of the measurements. The molar

extinction coefficient of the photoproduct was determined using a Beer-Lambert plot of $[(C_2H_5)_3N][Ni(mnt)_2]$ in chloroform-acetonitrile mixtures of the same composition that was used for the photolyses. For 313 and 365 nm, data used for calculation of product formation was limited to 10% conversion. There was no evidence for a competing thermal process during the irradiation period, as shown by a dark control experiment. The amount of photoproduct formed was calculated based on the absorbance change at 818 nm. The calculations used to determine the number of moles of product formed in a given amount of time are given below.

$$n_p(at\ time\ t) = \frac{A_p \cdot V}{\epsilon_p \cdot t \cdot l} \qquad (2.18)$$

where n_p = number of moles of $[(C_2H_5)_3N]Ni(mnt)_2$

A_p = absorbance of $[(C_2H_5)_3N]Ni(mnt)_2$ at 818 nm

V = volume of reactant (3.0 mL)

ϵ_p = molar extinction coefficient of $[(C_2H_5)_3N]Ni(mnt)_2$ at 818 nm

l = pathlength of the photolysis cell (1.0 cm)

t = time of irradiation in seconds

2.5.2. Analysis of Fe^{2+} Produced Upon Irradiation of $K_3Fe(ox)_3$.

The amount of Fe^{II} produced during the photolysis of potassium ferrioxalate (Section 2.4.1) was determined as follows: an aliquot of the actinometer (2.8 mL) was irradiated for a given amount of time. 2.5 mL of the irradiated volume was transferred into a 25 mL volumetric flask containing 5 mL of developing solution (0.05% 1,10-

phenanthroline/0.75 M sodium acetate/0.1N H_2SO_4)[19] and then diluted to the mark with deionized water. The absorbance of the red solution was recorded at 510 nm after allowing the solution to stand for 30 minutes. The entire procedure was carried out in the presence of red safety lights. The amount of Fe^{2+} produced was calculated as follows:

$$\frac{\Delta n}{\Delta t} = \frac{(A_{510} \cdot V_1 \cdot V_2)}{(V_3 \cdot \epsilon \cdot t \cdot l)} \tag{2.19}$$

where $\Delta n/\Delta t$ = number of moles of Fe^{2+} formed per unit time of irradiation

A_{510} = absorbance of the Fe^{2+}-phenanthroline solution at 510 nm

V_1 = volume of the aliquot irradiated (2.8 mL)

V_2 = total volume (25.0 mL)

V_3 = volume of the aliquot complexed (2.5 mL)

ϵ = molar extinction coefficient of Fe^{2+}-phenanthroline at 510 nm (1.11 x 10^4 $M^{-1} \cdot cm^{-1}$)

t = time of irradiation in seconds

l = pathlength of the photolysis cell (1.0 cm)

The number of einsteins per second entering the photolysis cell through the 313 and 365 nm filters is given by:

$$I_a = \frac{n(Fe^{2+})}{[\Phi(Fe^{2+}) \cdot I_f \cdot t](6.023 \times 10^{23})} \tag{2.20}$$

where I_a = light intensity expressed in einsteins/second

$\Phi_{Fe(2+)}$ = quantum yield of formation of Fe^{2+} (1.24 at 313 nm; 1.21 at 365 nm)[16]

I_f = fraction of light absorbed at 313 and 365 nm (1.00)

t = time of irradiation in seconds

The overall quantum yield is defined as the ratio of the total amount of product to the total amount of light absorbed[20]. The determination of quantum yield for the photooxidation of $[(C_2H_5)_3N]_2[Ni(mnt)_2]$ can therefore be readily determined by combining equations 2.19 and 2.20:

$$\Phi_p = \frac{\Delta n_p}{I_a} \qquad (2.21)$$

where Φ_p = quantum yield of product formation

Δn_p = number of molecules of product formed in time t

I_a = number of photons/second entering the photolysis cell

2.5.3. Fulgide Actinometry; Ultraviolet Irradiation

The ring closing reaction of aberchrome 540 was monitored as follows: a volume of the actinometer (4.6 mL) was irradiated for a given amount of time. The reaction was followed spectrophotometrically at 494 nm (the band maximum of the photoproduced aberchrome 540P); the amount of aberchrome 540P increased with increasing irradiation time. The entire procedure was carried out in the presence of red safety lights. The measured absorbancies of aberchrome 540P produced was related to the incident light

intensity as follows:

$$I=\frac{A\cdot V}{\Phi\cdot\epsilon\cdot t\cdot l} \qquad (2.22)$$

where I = light intensity (einsteins • s-1)

A = absorbance at 494 nm

V = volume irradiated (4.6 mL)

Φ = 0.20 (for 300 nm < λ_{ex} < 380 nm)[18b]

ϵ = 8200 $M^{-1}\cdot cm^{-1}$ at 494 nm

t = time of irradiation in seconds

l = pathlength of photolysis cell (1.0 cm)

2.5.4. Fulgide Actinometry; Visible Irradiation

The quantum yield of bleaching (ie: colour loss) is evaluated for a toluene solution of aberchrome 540P at 21°C[18b] using the empirical equation:

$$\Phi_b=0.178-(2.4\ x\ 10^{-4}\cdot\lambda_{ex}) \qquad (2.23)$$

where Φ_b = quantum yield of bleaching

λ_{ex} = wavelength of excitation (in nm)

The light intensity entering the photolysis cell can then be calculated according to equation 2.24.

$$I = -\frac{V}{\Phi\cdot\epsilon\cdot t\cdot l}\left[\log\frac{T^o}{(1-T^o)} - \log\frac{T^t}{(1-T^t)}\right] \qquad (2.24)$$

where I = light intensity at the cell window (einsteins $\cdot s^{-1}$)

T^t = transmittance at time t at λ_{ex}

T^o = transmittance at time 0 at λ_{ex}

V = volume irradiated (4.5 mL)

Φ_b = quantum yield of bleaching.

ϵ = 8030.8 $M^{-1}cm^{-1}$ and 7447 $M^{-1}cm^{-1}$ at 488 nm and 514.5 nm, respectively.

t = time of irradiation in seconds.

l = pathlength of photolysis cell (1.0 cm)

The light intensity entering the cell when using the actinometer 999P is calculated as in equation 2.24, except the Φ_b is evaluated as follows:[18c,21]

$$\Phi_b = 0.0737 - [\lambda_{ex} - (2.31 \times \theta)] \times 10^{-4} \qquad (2.25)$$

where θ = temperature in degrees Celcius.

λ_{ex} = wavelength of excitation (in nm)

Φ_b = quantum yield of bleaching

2.5.5. Photolysis of $W(CO)_4$(phen) and $(CO)_5Re\text{-}Re(CO)_3$(bpy')

2.5.5.1. UV Excitation of $W(CO)_4$(phen)

For irradiation at 313 and 365 nm, the increase of the absorbance of the photoproduct, $W(CO)_3$(phen)L (L = *n*-Bu_3P or pyridine), was monitored as a function of time of irradiation for solutions of $W(CO)_4$(phen) in neat pyridine and solutions of

n-Bu_3P in dichloromethane. The wavelength of analysis was chosen to be 720 nm because the absorbance difference between the reactant and the photoproduct was large at this wavelength. The molar extinction coefficient of the band maximum of the photoproduct at 720 nm was determined by converting the reactant to 100% photoproduct using visible irradiation. The molar extinction coefficient of the reactant in all solvents was determined at zero irradiation time using the Beer-Lambert relationship. In all solvents, irradiation of $W(CO)_4$(phen) at 313 nm and 365 nm produced no loss of isosbestic points in the absorption spectrum during the course of the experiment.

2.5.5.2. Visible Excitation of $W(CO)_4$(phen) and $(CO)_5Re\text{-}Re(CO)_3$(bpy')

The absorbance change at the wavelength of excitation was used to monitor the photolysis of $(CO)_5Re\text{-}Re(CO)_3$(bpy') in CH_2Cl_2 and solutions of $W(CO)_4$(phen) in neat pyridine and solutions of *n*-Bu_3P in dichloromethane, toluene, and tetrachloroethylene as a function of time for irradiations at 488.0, 496.0, 514.5 nm, and 610.9 nm. The wavelength of analysis was chosen to be the wavelength of excitation in order to account for the partial absorbance of the reactant in this region. In all solvents, irradiation of $W(CO)_4$(phen) at wavelengths $\leq$ 610.9 nm produced no loss of isosbestic points in the absorption spectrum throughout the reaction period indicating that complications resulting from side reactions do not occur up to the levels of conversion used in the experiment (generally 15%). An isosbestic point was not observed in the spectra for the photolysis of $(CO)_5Re\text{-}Re(CO)_3$(bpy') at wavelengths $\leq$ 514.5 nm. This is because the product spectrum contains only one absorption band which is much less intense than any of the

absorption bands in the spectrum of $(CO)_5Re\text{-}Re(CO)_3(bpy')$.

There was no evidence for a competing thermal process for either complex during the irradiation time, as shown by dark control experiments. The entire procedure was carried out in the presence of red safety lights. For 313, 365, 488.0, 496.0, 514.5, and 610.9 nm irradiation, data corresponding to less than 15% conversion were used for calculation of photoproduct quantum yield of formation except in the case of $(CO)_5Re\text{-}Re(CO)_3(bpy')$ where the conversion was limited to 10%. This was done in order to ensure that side reactions were avoided during the course of the experiments. The calculations used to determine the quantum yields are given in Section 2.5.7.

2.5.6. Quantum Yield Determination for 313 and 365 nm Irradiation

The calculation of the quantum yield for the photosubstitution of $W(CO)_4(phen)$ upon ultraviolet excitation was carried as follows. Because the amount of light absorbed by both the reactant and the actinometer was > 99%, the following equation was used to calculate the quantum yield.

$$\Phi = \frac{A \cdot V}{I \cdot \epsilon \cdot t \cdot l} \qquad (2.26)$$

where A = absorbance of the photoproduct

V = volume irradiated (L)

I = Intensity (einsteins $\cdot s^{-1}$)

ϵ = molar extinction coefficient of the photoproduct ($M^{-1} \cdot cm^{-1}$) at 720 nm

t = time of irradiation in seconds

l = pathlength of photolysis cell (cm)

2.5.7. Quantum Yield Determination for 488.0, 496.0, 514.5, and 610.9 nm Irradiation

2.5.7.1. Integration Method

Since the fraction of light absorbed by both the reactant and actinometer was ≤ 100%, the integration method[6] was employed to determine the quantum yields for the photosubstitution of $W(CO)_4(phen)$ under visible excitation. This method requires the area under the curve of the decay of the reactant absorbance with time be evaluated.

$$\ln\left(\frac{A_t - A_\infty}{A_o - A_\infty}\right) = \frac{-\Phi \cdot I \cdot \epsilon_\lambda \cdot l}{V} \int_{t_0}^{t_1} \frac{(1-10^{(-A_t)})}{A_t}\, dt \qquad (2.27)$$

where A_t = absorbance at the wavelength of excitation at time $t = t_1/2$

A_∞ = absorbance of the photoproduct at the wavelength of excitation at 100% conversion

A_o = absorbance at the wavelength of excitation at zero time

Φ = quantum yield

I = light intensity entering the photolysis cell measured in einsteins $\cdot s^{-1}$.

ϵ_λ = molar extinction coefficient of the reactant at the excitation wavelength

l = pathlength of the photolysis cell (1.0 cm)

t_1 = time of irradiation (s)

The quantum yield is determined as the slope of the plot of $\ln[(A_o - A_\infty)/(A_o - A_\infty)]$ vs

$$(I \cdot \epsilon_\lambda \cdot l)/V \int_{t_0}^{t_1} (1-10^{(-A_t)})/A_t \, dt.$$

2.5.7.2. Isosbestic Method

When the irradiation wavelength coincided with an isosbestic point, the "isosbestic method" was used to determine the quantum yield[22].

$$\ln(C_t/C_o) = \frac{-(\Phi \cdot I)}{(C_o \cdot V)} (1-10^{-A_o})\Delta t \qquad (2.28)$$

where C_t and C_o = concentration of the reactant at time t and zero time, respectively

Φ = quantum yield

I = intensity of the light absorbed by the sample

V = volume irradiated (3.0 mL)

Δt = time of irradiation in seconds

The quantum yield is determined as the slope of the plot of $\ln(C_t/C_o)$ vs $(I/C_o \cdot V)(1-10^{(-A_o)})\Delta t$.

2.6. Nanosecond Flash Photolysis

Nanosecond spectroscopy was carried out under the auspices of Dr. D.J. Stufkens at the University of Amsterdam. The system has been previously described[23]. Nanosecond spectra were recorded using second harmonic Nd/YAG excitation (532 nm) with pulse energies of either 20 mJ or 40 mJ and a pulse width of approximately 10 ns and monitored with a 400-800 nm probe pulse. An OMA was used for data collection.

2.7. Picosecond Laser Flash Photolysis

Picosecond time resolved spectroscopy was carried out at the Canadian Centre for Picosecond Laser Flash Photolysis at Concordia University using a mode-locked Nd/YAG laser (Quantel YG 402G) for excitation and a 425-675 nm probe pulse for detection. An OMA was used for data collection. The diameter of the laser beam at the sample is 1.5 mm. A block diagram of the system is given in Figure 2.6[24]. Details regarding the operation of the system is described in Reference 24.

Picosecond spectra were recorded using either second or third harmonic Nd/YAG excitation (532 nm or 355 nm excitation, respectively) with a pulse energy of either 2.5 mJ or 1.2 mJ and a pulse width of approximately 30 ps (1 ps = 10^{12} s). The probe pulse was generated by focusing a fraction of the fundamental pulse (1064 nm) into a solution of D_3PO_4. The probe continuum was then split into a reading pulse (I) which enters the sample cell and a reference pulse (I_o) which passed beside the cell. A background spectrum was taken before each set of four excited state absorptions by blocking the pump beam. The I_o and I values detected therefore correspond to the ground state absorption. When the pump beam entered the sample cell, the detection of the absorption of the sample corresponds to the excited state absorption. The spectra reported are the average of six to nine recordings and two to three blanks for each time delay (a delay line enabled the spectra to be recorded at delays from 0 ps to 10 ns after the exciting pulse).

A sample shot may be rejected during the experimental stage or later during the calculation stage. During the experimental stage, a shot may be rejected for the

Figure 2.6. Schematic representation of the picosecond flash photolysis laser system.

1. Laser: a)head (contains laser material and light source)
   b) mode-locking cell (contains mirror and dye)
   c) partial mirror
2. Beam Expander
3. Glan-air Polarizers
4. Pulse Selector
5. Amplifier
6. Second Harmonic Crystal
7. Third Harmonic Crystal
8. Delay Ramp
9. Continuum Cell
10. Energy Detector
11. Energy Meter
12. Sample Cell
13. Double Monochromator
14. Photodiode Array Detector
15. Multichannel Analyzer
16. Computer

DM. Dichroic Mirror

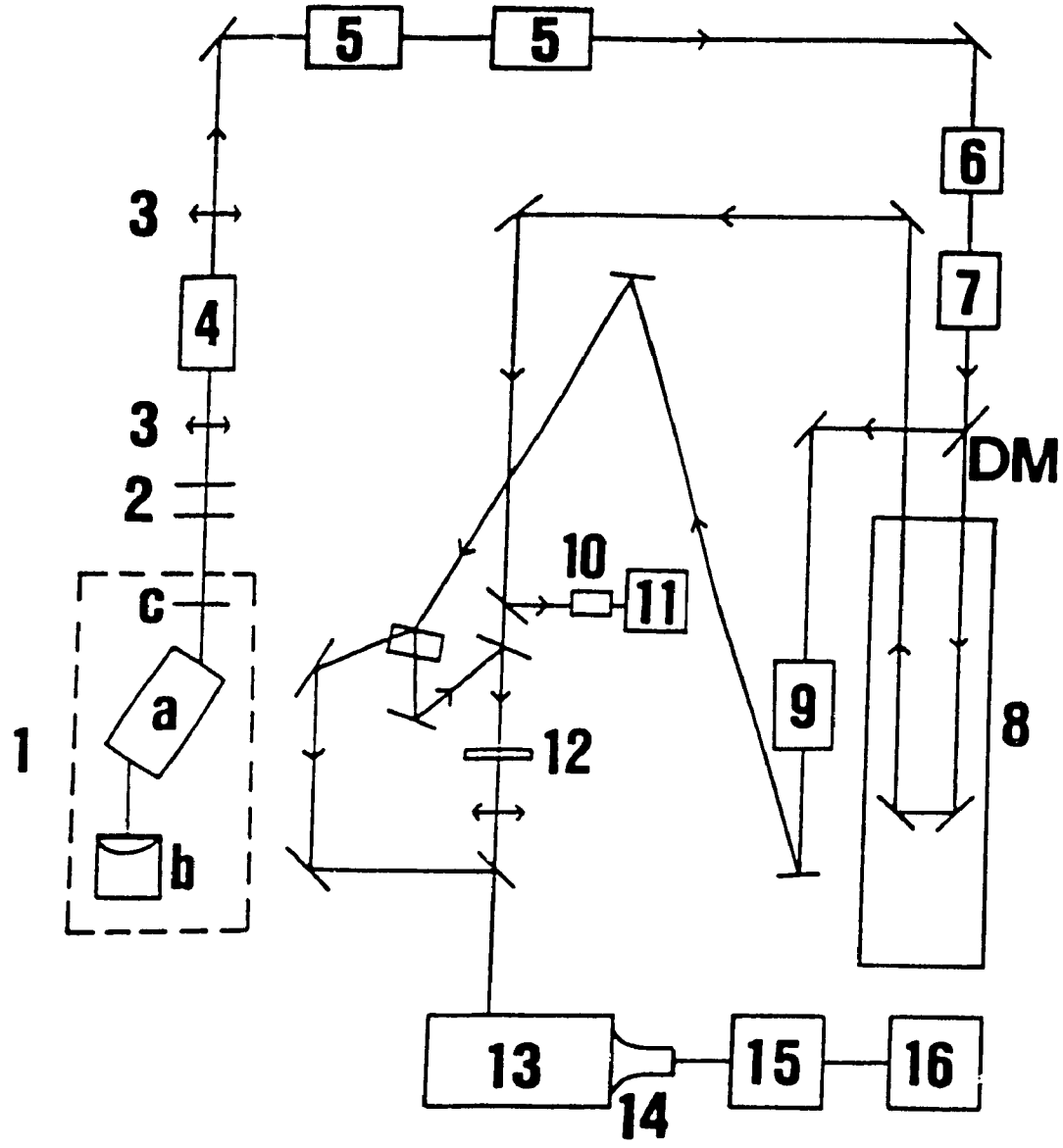
5
5
6
3
7
4
3
DM
2
10
11
c
a
1
9
8
12
b
13
15
16
14

following reasons: (1) there is a double train of pulses created in the oscillator; (2) the pulse energy of the pump beam may be too high or too low; (3) an unsatisfactory continuum pulse may be generated; or (4) saturation of one of the photodiodes by one of the probe beams may occur. During the calculation stage, a shot may be rejected because of an unacceptable noise level. Any shot whose noise value was higher than 10 was rejected. The absorbance of each shot at each wavelength is calculated by a minicomputer (PDP-11) using the formula a = log (I_o/I). The noise is calculated by:

$$N_i=\frac{\Sigma_k(a_{ik}-a_k)^2}{a_k} \qquad (2.29)$$

where N_i = noise for the curve

a_{ik} = absorbance of the shot at wavelength k

a_k = average absorbance value at the same wavelength for all the shots on a specific state

An average value for the excited state and the ground state is also calculated by the computer. The absorbance change for every wavelength is calculated by the computer by subtracting the ground state absorbance from the excited state absorbance. The absorbance change (ΔA) vs wavelength (425-675 nm) is reported.

Sources of error must be taken into account when interpreting the spectra. High noise levels can be a major source of error in the 425-440 nm and 635-675 nm spectral regions. This problem arises because the number of counts in these regions are low due to the bell shape of the continuum curve. In our experiments, there was excited state absorption, ESA, within the 425-440 nm region and between 550 and 650 nm. However,

because the ESA of interest to most of our experiments fell in the 550-650 nm, no additional precautions were made when interpreting the majority of the spectra. The second source of error involves the appearance of a "DC shift" in the ESA spectra of $W(CO)_4$(phen) at time delays of 10 ns and $W(CO)_5$(4-X-Py); X = CN, Formyl at time delays of > 500 ps upon 355 nm excitation. This "DC shift" appears at a significant absorbance (approximately 0.1 absorbance unit) at all wavelengths. This shift is believed to result from the scattering of the probe beam as the beam passes through the cell. For example, scattering may be caused by the formation of bubbles in the reaction cell as the result of CO loss. This effect was reduced by running the picosecond experiments using a "low energy" excitation pulse. The energy was therefore intentionally limited to 1.2 mJ for the $W(CO)_4$(phen) and $W(CO)_5$(4-X-Py) (X = CN, Formyl) experiments using 355 nm excitation. Such shifts were not observed in the ESA spectra of $M(mnt)^{2-}$ (M = Ni, Pt) and L_nM-$Re(CO)_3$(bpy') (L_nM = $(C_6H_5)_3Sn$-, $(CO)_5Re$-).

2.8. Spectroelectrochemistry

The spectroelectrochemical measurements were carried out by Dr. F. Hartl of the J. Heyrovský Institute of Physical Chemistry and Electrochemistry, Prague, Czech Republic. $W(CO)_4$(phen) was electrochemically reduced by one electron[25] to its corresponding anion $W(CO)_4(phen)^{\cdot-}$. Absorption spectra were obtained spectroelectrochemically by a reduction of their THF solutions containing 0.1M (n-$Bu)_4NPF_6$ on a Pt minigrind electrode in an Optically Transparent Thin Layer (OTTLE) cell[26].

2.9. References

1. Herzog, S.; Dehnert, J. *Z. Chem.*, **1964**, *4*, 1.

2. (a) Bahr, G.; Schleitzer, G. *Chem. Ber.* **1957**, *90*, 438.

   (b) *Inorganic Synthesis* Vol.X, ed. E.L. Muetterties, McGraw-Hill: U.S.A., 1967, pp. 10-13.

3. (a) Billig, E.; Williams, R.; Bernal, I.; Waters, J.H.; Gray, H.B. *Inorg. Chem.* **1964**, *3*, 663.

   (b) *Inorganic Synthesis* Vol.X, ed. E.L. Muetterties, McGraw-Hill: U.S.A., 1967, pp. 13-15.

4. (a) Shupack, S.I.; Billig, E.; Clark, R.J. H.; Williams, R.; Gray, H.B. *J. Am. Chem. Soc.* **1964**, *86*, 4594.

   (b) Biro, D. *Ph.D. thesis* Concordia University, 1989.

5. (a) *Inorganic Synthesis* Vol.X, ed. E.L. Muetterties, McGraw-Hill: U.S.A., 1967, pp. 15,16.

   (b) Davison, A.; Edelstein, N.; Holm, R.H.; Maki, A.H. *Inorg. Chem.* **1963**, *2*, 1227.

6. Bock, H.; tom Dieck, H. *Chem. Ber.* **1967**, *100*, 228.

7. Manuta, D.M.; Lees, A.J. *Inorg. Chem.* **1986**, *25*, 1354.

8. Strohmeier, W. *Angew. Chem. Internal. Edit.* **1964**, *3*, 730.

9. Wrighton, M.S.; Abrahamson, H.B.; Morse, D.L. *J. Am. Chem. Soc.* **1976**, *98*, 4105.

10. Brauer, G. *Handbuch der Praparatiuen Anorganischen Chemie* 1981, p. 1950.

11. Wehman, P. University of Amsterdam, Unpublished results, 1990.

12. Staal. L.H.; Oskam, A.; Vrieze, K. *J. Organomet. Chem.* **1979**, *170*, 235.

13. (a) Ellis, .E.; Flom, E.A. *J. Organomet. Chem.* **1977**, *125*, 71.

   (b) Morse, D.L.; Wrighton, M.S. *J. Am. Chem. Soc.*, **1976**, *98*, 3931.

14. Ellis, J.E.; Flom, E.A. *J. Organomet. Chem.* **1975**, **99**, 263.

15. Luong, J.C.; Faltynek, R.A.; Wrighton, M.S. *J. Am. Chem. Soc.* **1980**, *102*, 7892.

16. Pitts, J.N.; Calvert, J.G. *Photochemistry* John Wiley and Sons, Ltd. New York, 1966, pp. 783-785.

17. Hatchard, C.G.; Parker, C.A. *Proc. R. Soc. London, Ser. A*, **1956**, *235*, 518.

18. (a) Heller, H.G. in *ELECTRONIC MATERIALS from Silicon to Organics* ed. L.S. Miller, J.B. Mullin, Planum Publishing Corporation, 1991, pp. 471-483.

    (b) Heller, H.G.; Langan, J.R. *J. Chem. Soc., Perkin Trans. I*, **1981**, 341.

    (c) Kuhn, H.J.; Braslavsky, S.E.; Schmidt, R. *Pure Appl. Chem.* **1989**, *61*, 187.

19. Kirk, A.D.; Namasivayam, C. *Anal. Chem.*, **1983**, *55*, 2429.

20. Ferraudi, G.J. *Elements of Inorganic Photochemistry* John Wiley and Sons, Inc. U.S.A., 1988, pp. 13-14.

21. Heller, H.G.; Glaze, A.P.; Morgan, C.J.; Oliver, S.N.; Whittal, J.; Rubin, M. Unpublished results

22. Bunce N.J. *J. Photochem.* **1987**, *38*, 99.

23. Martens, F.M.; Verhoeven, J.W.; Varma, C.A.G.O.; Bergwerf, P. *J. Photochem.*, **1983**, *22*, 99.

24. Moralejo, C. Ph.D thesis, Concordia University, 1989.

25. Miholová, D.; Gaš, B.; Záliš, S.; Klíma, J.; Vlček, A.A. *Journal of Organometallic Chemistry* **1987**, *330*, 75.

26. Krejčík, M.; Daněk, M.; Hartl, F. *J. Electroanal. Chem.*, **1991**, *317*, 179.

3. Solvent Dependence of the Fast Photooxidation of $[M((S_2C_2(CN)_2))_2)]^{2-}$ (M = Ni,Pt) in Acetonitrile-Chloroform Mixtures

3.1. Background

Femtosecond time resolution spectroscopy appears to be an ideal technique to directly investigate chemical reactions in which the product is determined by events which occur on the timescale of vibrational relaxation or less[1,2]. The major indirect experimental probe is the observation of wavelength dependence across a single electronic band[3]. As mentioned in Section 1.1, one common form of such wavelength dependence is a systematic monotonic increase of quantum yield as excitation energy increases with no discontinuities where absorption band boundaries arise.

Three different types of photoreactivity have been reported for $[M(mnt)_2]^{2-}$ (M = Ni, Pd, Pt; $S_2C_2(CN)_2))_2$ = mnt): (1) deep UV excitation leads to the initiation of hydrogen evolution from solvents, probably by charge transfer to solvent (CTTS) excitation[4]; (2) a photocurrent is observed upon irradiation into the visible region[5]; and (3) near UV excitation promotes a photooxidation reaction in the presence of an electron acceptor[6]. In a preliminary investigation[6a], Vogler and Kunkely observed a particularly interesting feature in the latter case: irradiation in the presence of chlorocarbon solvents leads to wavelength dependent one-electron photooxidation of $[M(mnt)_2]^{2-}$ (M = Ni, Pd, Pt)[6] and reduction of the halocarbon. The reaction also exhibits the characteristic monotonic increase of quantum yield with excitation energy across absorption bands of different character[6].

The classical account of such a phenomenon concerns the competition between geminate recombination and cage escape (Section 1.6.1), but picosecond studies of I_2 dissociation[7] showed some years ago that this view was oversimplified. As will be seen from the example discussed in this chapter, there may be little evidence of the formation of a "geminate pair" primary product which can undergo recombination or separation. An alternative explanation must therefore be considered. There are three important determinants of processes which occur on time scales faster or are comparable with vibrational relaxation which can be identified. These are: (1) electronic factors, which may be approached using the Hollebone selection rules (Section 1.5); (2) vibrational relaxation controlled predominantly by the thermal cage effect (Section 1.6.2). Note that this process is probably more complicated in that it also involves intramolecular factors and vibronic coupling between the excited molecule and the solvent; and (3) solvent reorientation about a new charge distribution (Section 1.6.3). It is therefore apparent that the solvent can play a very important role in elucidating events in prompt chemical reactions[8-10] thus indicating that solvent dependence will be a crucial tool for identification of these controlling factors.

In order to distinguish which factor(s) regulates the reaction, the wavelength dependence and solvent dependence of the quantum yields of photooxidation of $[M(mnt)_2]^{2-}$ (M = Ni, Pt) in mixtures of acetonitrile (CH_3CN) and chloroform ($CHCl_3$) will be compared. These results will then be combined with absorption spectra acquired in the picosecond time domain after electronic excitation of both complexes in the presence and in the absence of $CHCl_3$ in order compare initial "in cage" quantum yields

to those obtained under continuous photolysis. The combination of these results will provide new insight into the early stages of these prompt photochemical processes.

3.2. Quantum Yield Measurements

Irradiation of $[M(mnt)_2]^{2-}$ (M = Ni, Pt) in the presence of an electron acceptor using either 313 nm or 365 nm light causes photooxidation of the reactant and concomitant reduction of the solvent yielding the spectroscopically distinct species $[M(mnt)_2]^-$ (M = Ni, Pt) according to the following equation.

$$[M(mnt)_2]^{2-} \xrightarrow[CHCl_3]{h\upsilon} [M(mnt)_2]^- + \underset{\text{photoproducts}}{CHCl_2^\bullet} + Cl^- \qquad (3.1)$$

During the photooxidation, the spectra show a clean progression towards the spectral features of $[M(mnt)_2]^-$ (M = Ni, Pt) as evidenced by the grow-in of a band in the 800 nm region (Figures 3.1 and 3.2). The reaction was limited to 10% conversion in order to avoid any complications due to side or subsequent reactions and to minimize inner filter effects ($[Ni(mnt)_2]^-$ and $[Pt(mnt)_2]^-$ absorb in the same region as the reactant).

In order to learn the way in which the excitation wavelength and the solvent affect the reaction, the quantum yield for photooxidation of $[M(mnt)_2]^{2-}$ (M = Ni, Pt) using both 313 nm and 365 nm excitation was examined as a function of mole fraction (χ) of $CHCl_3$ for each irradiation wavelength. The results for $[Ni(mnt)_2]^{2-}$ are summarized in Tables 3.1 and 3.2 and shown graphically in Figures 3.3 and 3.4. Similar results for the analogous Pt complex were obtained by Dr. A.Y.S. Malkhasian[11] and are summarized

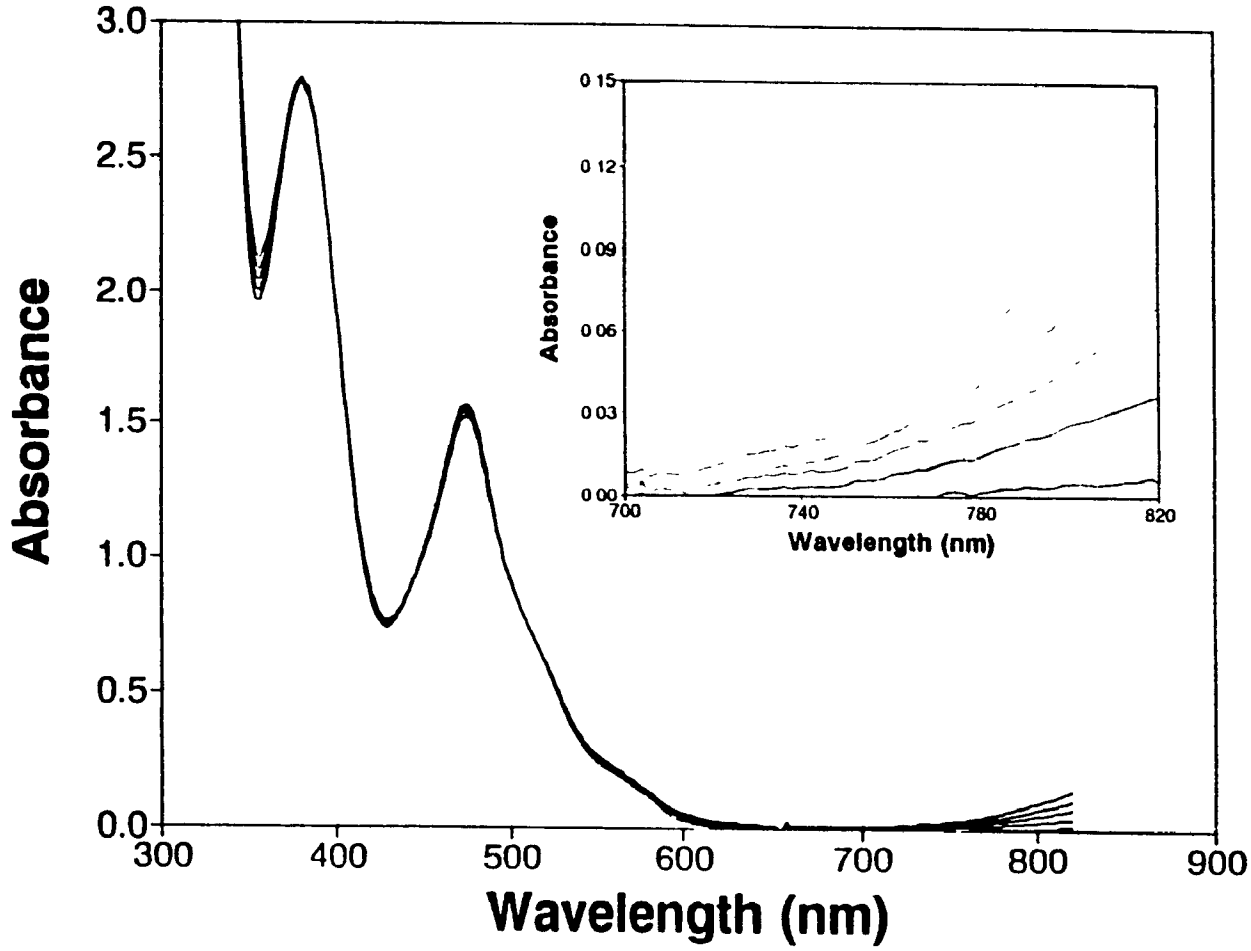

Figure 3.1. Electronic spectral changes observed upon 313 nm photolysis of $[Ni(mnt)_2]^{2-}$ in a $CHCl_3$-CH_3CN mixture ($\chi(CHCl_3) = 0.4947$). The times of irradiation from reactant A to product B are: 0, 60, 120, 180, and 240 minutes. The inset shows the grow-in of the band due to the photoproduct.

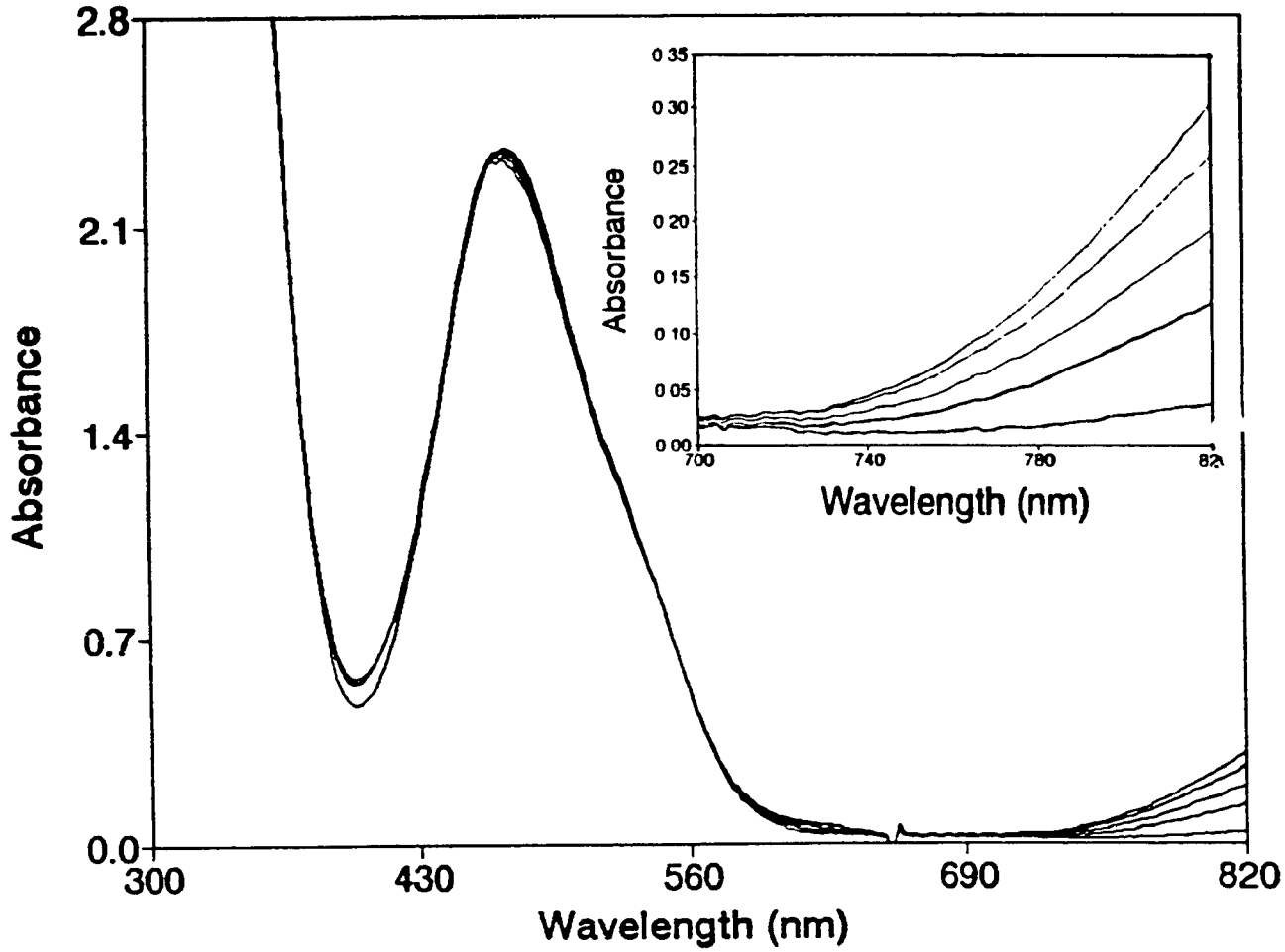

Figure 3.2. Electronic spectral changes observed upon 365 nm photolysis of $[Pt(mnt)_2]^{2-}$ in a 3:2 mixture of $CHCl_3$ and CH_3CN. The times of irradiation from reactant A to product B are 0, 5, 8, 11, and 13 minutes in order of increasing absorbance. The inset shows the grow-in of the photoproduct.

in Tables 3.3 and 3.4 and shown graphically in Figures 3.5 and 3.6.

Table 3.1. Solvent dependence of the quantum yield of photooxidation of $[Ni(mnt)_2]^{2-}$ upon 313 nm excitation.

$\chi(CHCl_3)$	Φ ($[Ni(mnt)_2]^-$)[a]
0.000	0.00
0.0676	0.07
0.1403	0.14
0.2186	0.21
0.3032	0.22
0.3949	0.25
0.4947	0.23
0.7230	0.26
0.8545	0.23

a) The error in quantum yields is $\pm$ 10% except where $\chi(CHCl_3) = 0.0676$. In this case, the error is $>$ 10% due to difficulty in measuring a minimal absorbance change near the end limit of the detector.

Table 3.2. Solvent dependence of the quantum yield of photooxidation of $[Ni(mnt)_2]^{2-}$ upon 365 nm excitation.

$\chi(CHCl_3)$	Φ ($[Ni(mnt)_2]^-$)[a]
0.0000	0.0001
0.0676	0.0036
0.1402	0.0058
0.3000	0.010
0.4000	0.012
0.5000	0.013
0.9400	0.013

a) The error in quantum yields is $\pm$ 10% except where $\chi(CHCl_3) = 0.0676$. In this case, the error is $>$ 10% due to difficulty in measuring a minimal absorbance change.

Table 3.3. Solvent dependence of the quantum yield of photooxidation of $[Pt(mnt)_2]^{2-}$ upon 313 nm excitation.

$\chi(CHCl_3)$	Φ ($[Pt(mnt)_2]^{2-}$)[a]
0.0000	0.000_0
0.0300	0.020_0
0.1000	0.047_0
0.2000	0.071_4
0.3000	0.089_9
0.4000	0.10_9
0.5000	0.11_1
0.6000	0.12_0
0.7000	0.12_3
0.8500	0.12_5

a) The error in quantum yields is ± 10%.

Table 3.4. Solvent dependence of the quantum yield of photooxidation of $[Pt(mnt)_2]^{2-}$ upon 365 nm excitation.

$\chi(CHCl_3)$	Φ ($[Ni(mnt)_2]^{2-}$)[a]
0.0000	0.000_0
0.0310	0.0003_8
0.1000	0.007_8
0.2000	0.011_2
0.3000	0.015_5
0.4000	0.018_3
0.5000	0.019_8
0.6000	0.022_8
0.7000	0.022_7
0.8500	0.022_0

a) The error in quantum yields is ± 10%.

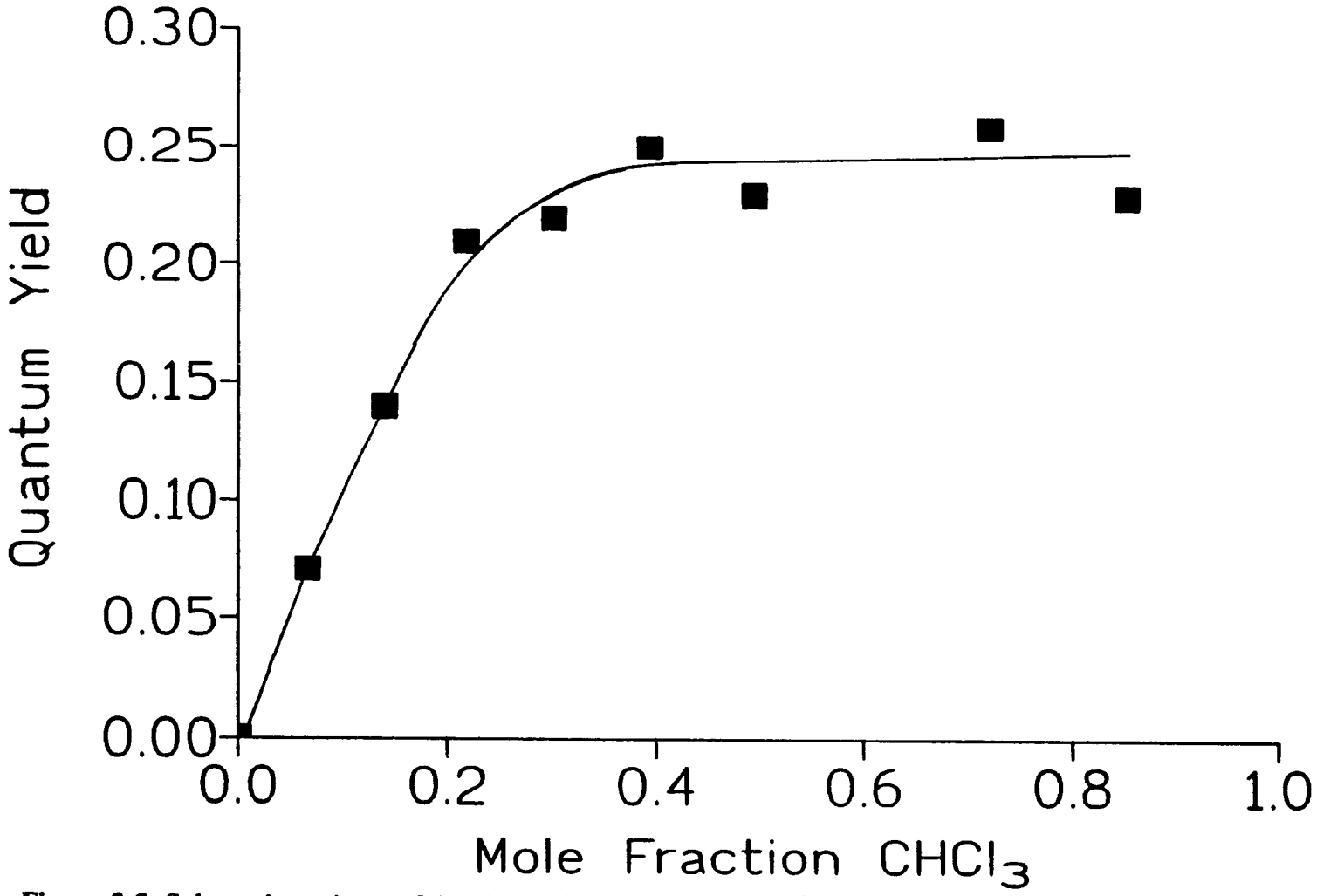

Figure 3.3. Solvent dependence of the photooxidation of $[Ni(mnt)_2]^{2-}$ using 313 nm excitation in $CHCl_3$-CH_3CN mixtures.

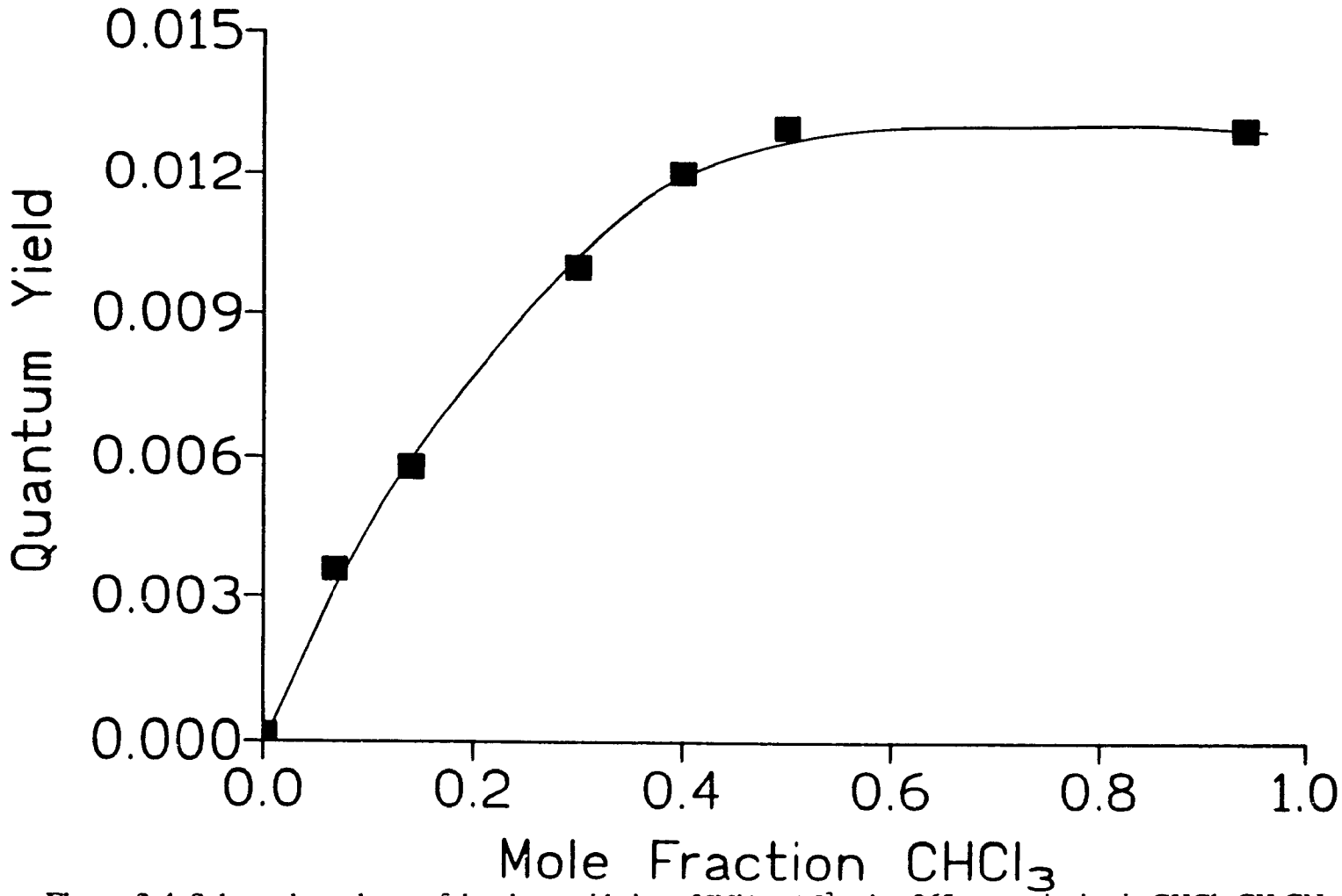

Figure 3.4. Solvent dependence of the photooxidation of $[Ni(mnt)_2]^{2-}$ using 365 nm excitation in $CHCl_3$-CH_3CN mixtures.

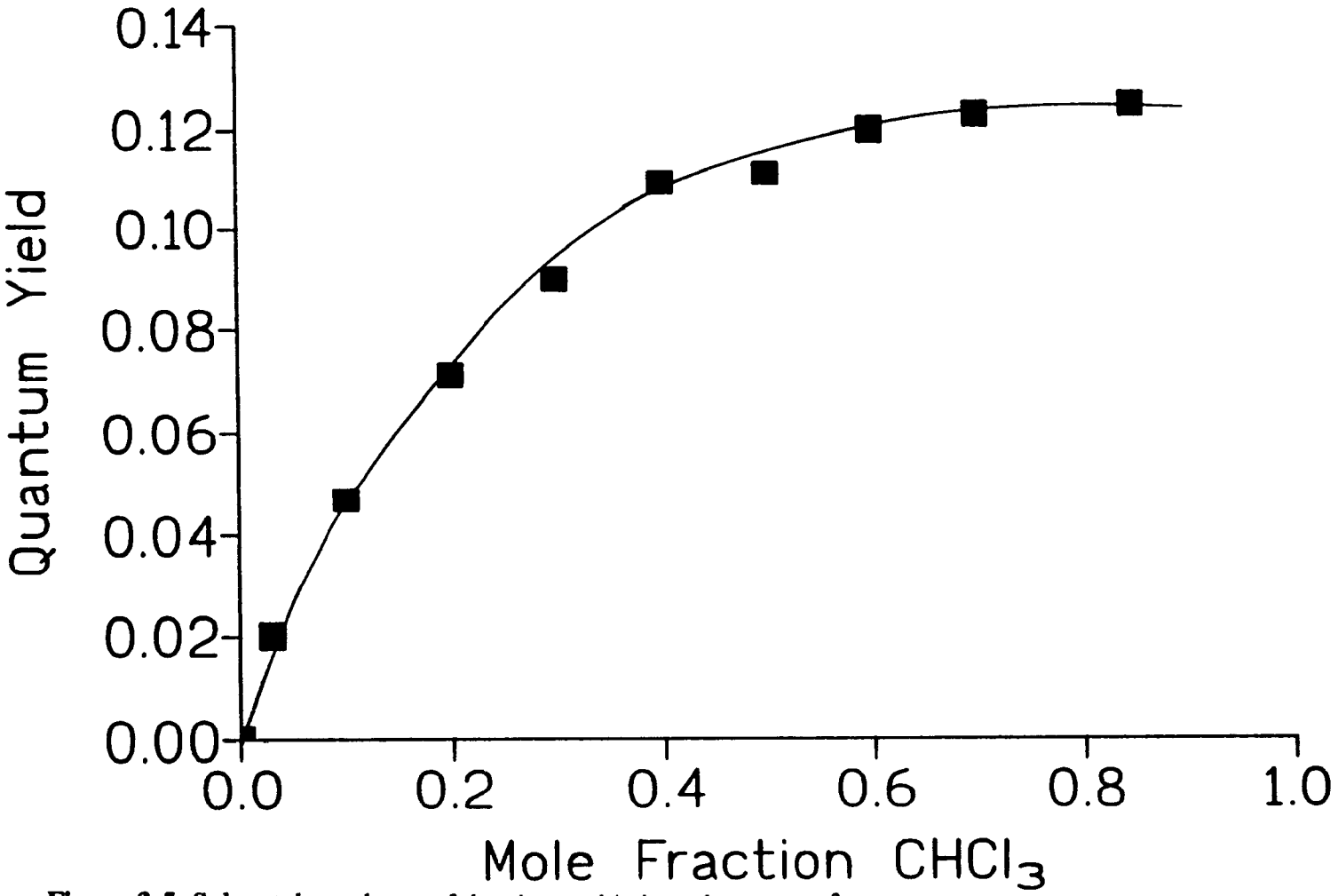

Figure 3.5. Solvent dependence of the photooxidation of $[Pt(mnt)_2]^{2-}$ using 313 nm excitation in $CHCl_3$-CH_3CN mixtures.

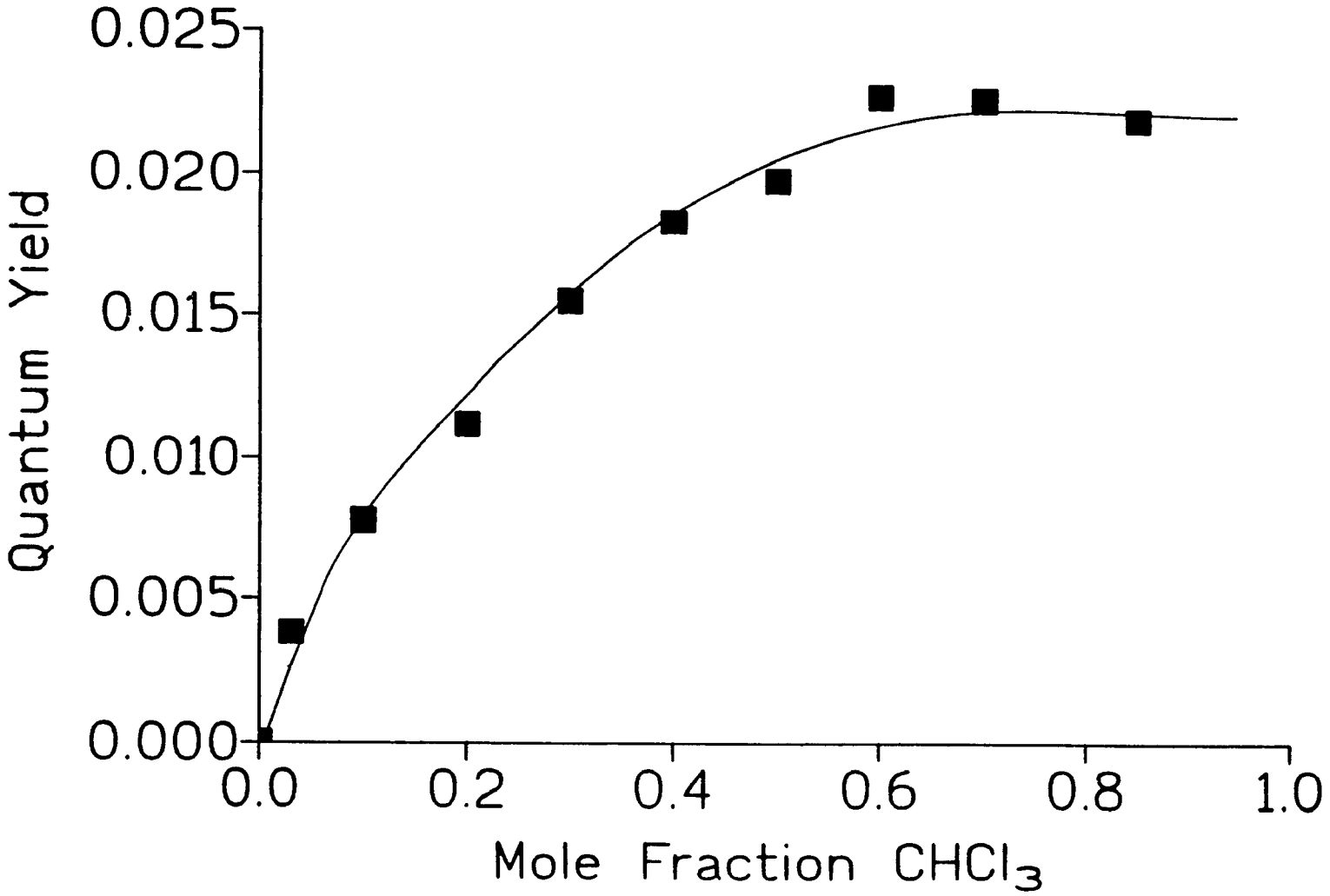

Figure 3.6. Solvent dependence of the photooxidation of $[Pt(mnt)_2]^{2-}$ using 365 nm excitation in $CHCl_3$-CH_3CN mixtures.

It is evident that the photooxidation of $[M(mnt)_2]^{2-}$ (M = Ni, Pt) is dependent upon the solvent and the wavelength of excitation. The quantum yield for the photooxidation at either wavelength is essentially zero in CH_3CN and increases with increasing $CHCl_3$ concentration. A limiting quantum yield is approached at high $CHCl_3$ concentration. This value can be estimated by plotting the data in a double reciprocal form ($1/\Phi$ *vs* $1/\chi$); this aids accurate extrapolation to find the high $CHCl_3$ limit (the complexes are not soluble in neat $CHCl_3$ thereby preventing experimental measurements at $\chi(CHCl_3) > 0.94$). The equations that describe the system mathematically and justify this plot are given on Page 91 as Equations 3.4 and 3.5. The reasons for selecting this equation will subsequently be discussed in detail. Note that the double reciprocal curve was extrapolated to the reciprocal quantum yield value corresponding to $1/\chi(CHCl_3) = 1$ since this is the maximum possible value for mole fraction. In all cases, except the 313 nm photolysis of $[Ni(mnt)_2]^{2-}$, this procedure gave a good linear correlation (Figures 3.7 to 3.9). The plot parameters are summarized in Table 3.5.

Table 3.5. Plot parameters for the double reciprocal plots for $[M(mnt)_2]^{2-}$ (M = Ni, Pt).

Wavelength (nm)	$[Ni(mnt)_2]^{2-}$			$[Pt(mnt)_2]^{2-}$		
	R^2	1/slope[a]	Φ_{lim}	R^2	1/slope[a]	Φ_{lim}
313	0.956	1.3	0.25[b]	0.999	0.77	0.14
365	0.991	0.064	0.014	0.988	0.14	0.024

a) This value equals the initial slope of the solvation curve at low mole fractions of $CHCl_3$ (see Equations 3.4 and 3.5).
b) Because the double reciprocal treatment does not produce a good correlation for the case of 313 nm photolysis of $[Ni(mnt)_2]^{2-}$, the limiting quantum yield was estimated as 0.25 directly from the solvation curve.

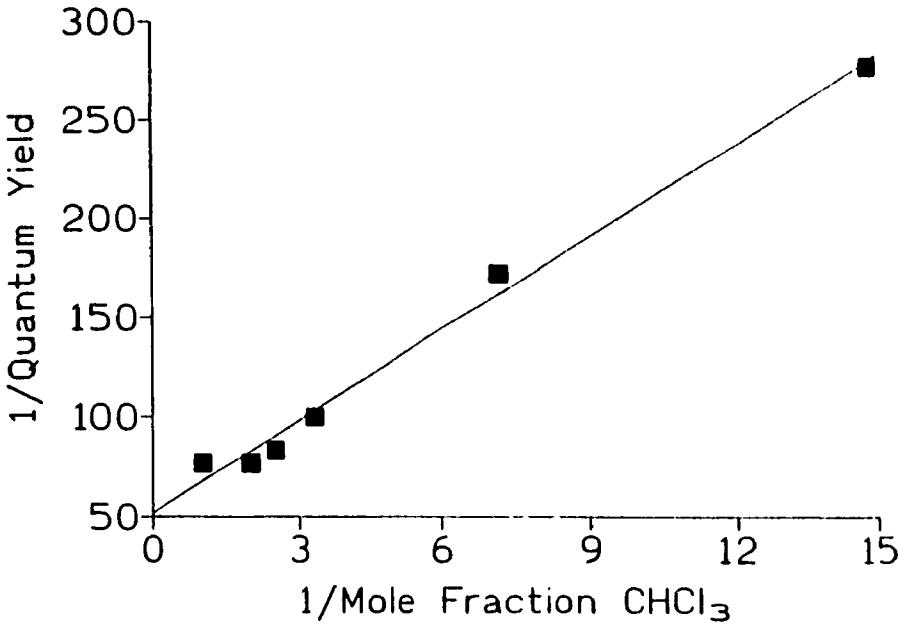

Figure 3.7. Double reciprocal plot for the solvent dependence of the photolysis of $[Ni(mnt)_2]^{2-}$ in CH_3CN-$CHCl_3$ mixtures using 365 nm excitation.

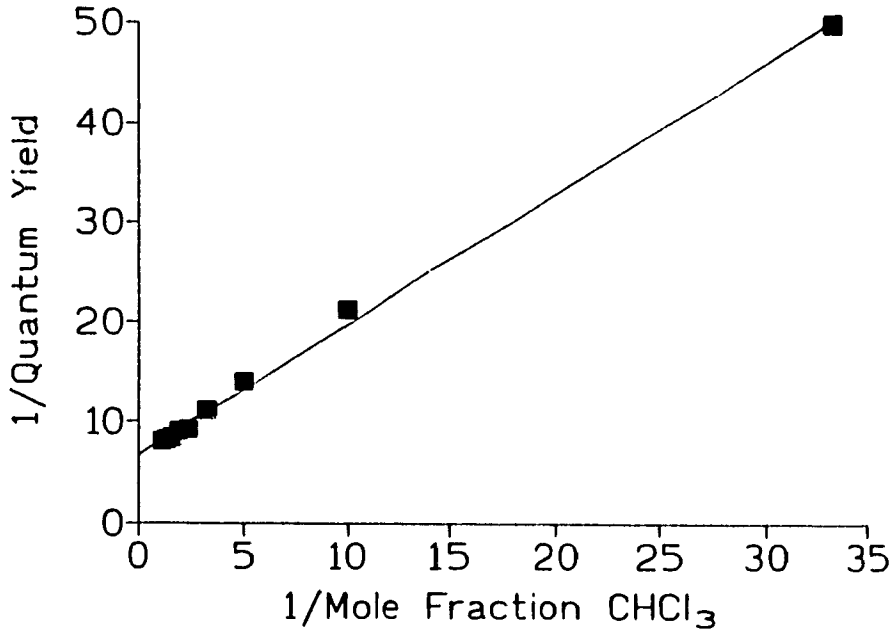

Figure 3.8. Double reciprocal plot for the solvent dependence of the photolysis of $[Pt(mnt)_2]^{2-}$ in CH_3CN-$CHCl_3$ mixtures using 313 nm excitation.

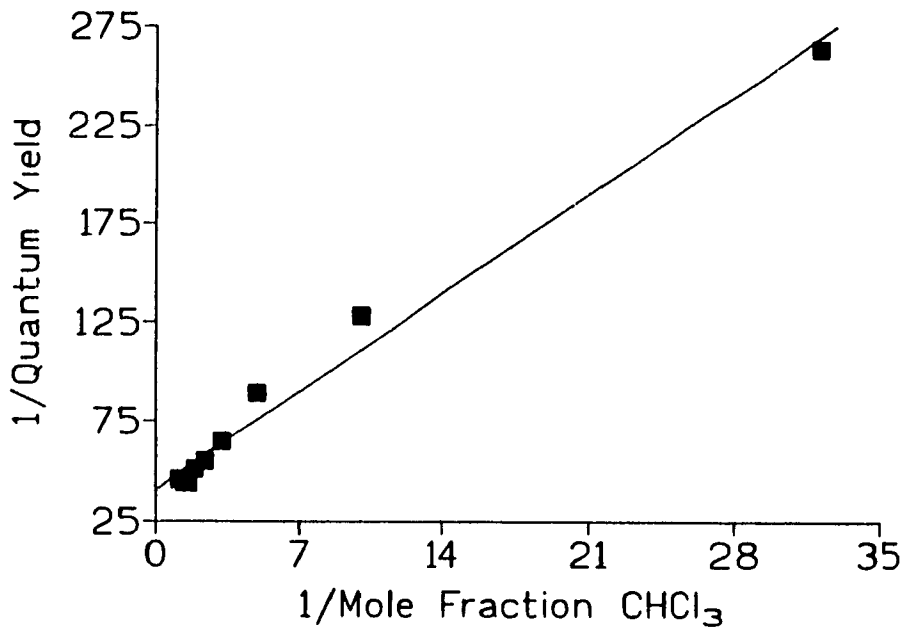

Figure 3.9. Double reciprocal plot for the solvent dependence of the photolysis of $[Pt(mnt)_2]^{2-}$ in CH_3CN-$CHCl_3$ mixtures using 365 nm excitation.

The double reciprocal treatment can be justified upon consideration of the algebraic expression that describes the chemistry of the system if $CHCl_3$ is acting simply as a reactant and bulk solvent effects are small. Since this reaction involves the transfer of an electron from the metal to $CHCl_3$, an encounter complex must form prior to the event of electron transfer. Thus, the chemistry must proceed according to the following equation where K_E is the equilibrium constant for the formation of the encounter complex.

$$[M(mnt)_2]^{2-} \underset{CHCl_3}{\overset{K_E}{\rightleftharpoons}} [M(mnt)_2]^{2-}\cdots CHCl_3] \xrightarrow{h\upsilon} [M(mnt)_2]^{2-}\cdots CHCl_3]^{*} \quad \text{(encounter complex)} \qquad (3.3)$$

$$\xrightarrow{\Phi_{lim}} [M(mnt)_2]^{-}\cdots CHCl_2^{\bullet}\cdots Cl^{-}] \longrightarrow [M(mnt)_2]^{-} + CHCl_2^{\bullet} + Cl^{-}$$

(primary products; photoproducts)

The following equation can be used to express the chemistry of the preequilibrium situation.

$$\phi = \frac{K_E \cdot \phi_{lim} \cdot \chi}{1 + K_E \cdot \chi} \qquad (3.4)$$

where Φ and Φ_{lim} are the quantum yield and limiting quantum yield, respectively, and χ is the mole fraction of $CHCl_3$. The reciprocal can thus be expressed as:

$$\frac{1}{\phi} = \frac{1 + K_E \cdot \chi}{K_E \cdot \phi_{lim} \cdot \chi} = \frac{1}{K_E \cdot \phi_{lim}} \cdot \left(\frac{1}{\chi}\right) + \frac{1}{\phi_{lim}} \qquad (3.5)$$

From the above two equations, it is obvious that the reciprocal of the initial slope of the solvation curve is directly related to the slopes obtained in the reciprocal plots.

Evidence for the lack of bulk solvent effects and the separation of solvent dependence from wavelength dependence is obtained by using the yield for the high $CHCl_3$ limit (Table 3.5), to normalize the quantum yields as a fraction of the limiting value (Φ/Φ_{lim}). This allows direct comparison of the solvent dependence at different wavelengths. Examination of Figures 3.10 and 3.11 points to identical solvent behaviour under both 313 nm and 365 nm excitation for $[M(mnt)_2]^{2-}$ (M = Ni, Pt).

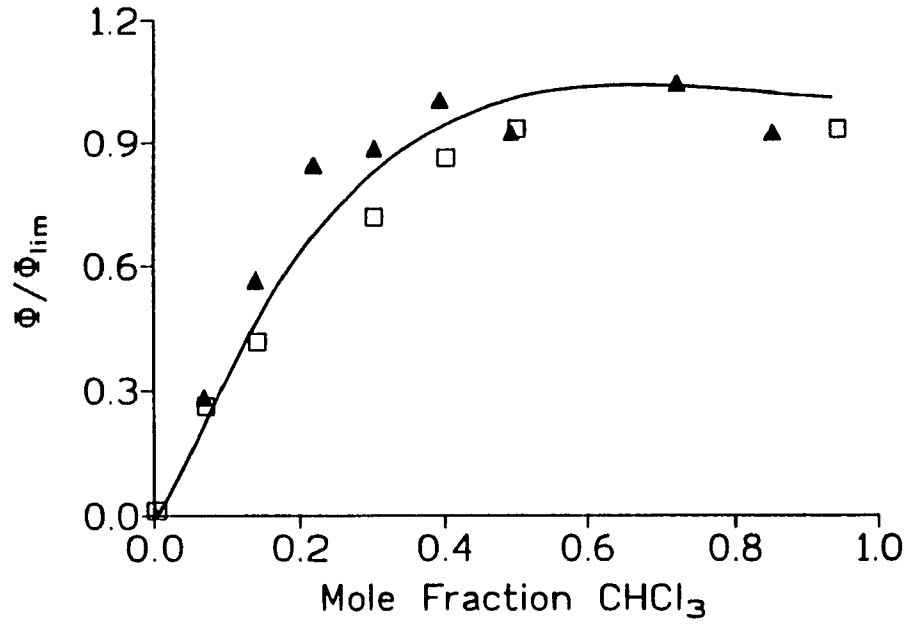

Figure 3.10. Comparison of the observed solvent dependence for the photooxidation of $[Ni(mnt)_2]^{2-}$ using 313 nm (▲) and 365 nm (□) excitation.

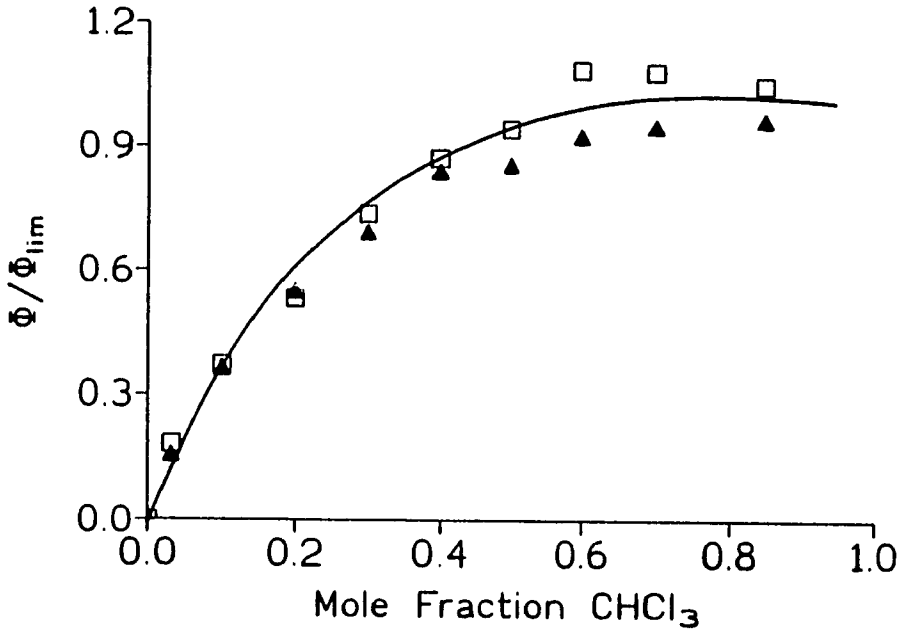

Figure 3.11. Comparison of the observed solvent dependence for the photooxidation of $[Pt(mnt)_2]^{2-}$ using 313 nm (▲) and 365 nm (□) excitation.

This behaviour can be verified by considering the implications of normalizing Equation 3.4:

$$\frac{\phi}{\phi_{lim}} = \frac{K_E \cdot \chi}{1 + K_E \cdot \chi} \tag{3.6}$$

It thus follows that the reciprocal of the normalized curve is:

$$\frac{\phi_{lim}}{\phi} = \frac{1 + K_E \cdot X}{K_E \cdot \chi} = 1 + \frac{1}{K_E} \cdot \frac{1}{\chi} \tag{3.7}$$

From this, it is obvious that the slope of the normalized double reciprocal plot is equivalent to the reciprocal of the equilibrium constant for encounter complex formation, K_E. The normalized double reciprocal plots for $[Pt(mnt)_2]^{2-}$ are shown in Figures 3.12 and 3.13. Both give good linear correlations (R^2 for 313 nm data and 365 nm data is 0.997 and 0.984, respectively). The slopes are 0.171 and 0.149 for the 313 nm and 365 nm data, respectively. Fisher's Z transformation[12] was used to establish that the slopes of these curves (and thus K_E) are statistically indistinguishable (refer to Appendix A for the calculation). The slope of the normalized double reciprocal plot (Figure 3.14) of the 365 nm photolysis data of $[Ni(mnt)_2]^{2-}$ is 0.217 (R^2 = 0.991). However, as mentioned earlier, the 313 nm photolysis data does not yield a good correlation (R^2 = 0.956). Thus, the plot parameters cannot be directly evaluated as was done in the Pt case. Assuming the Ni system behaves similarly to the Pt case (i.e. identical K_E's for 313 nm

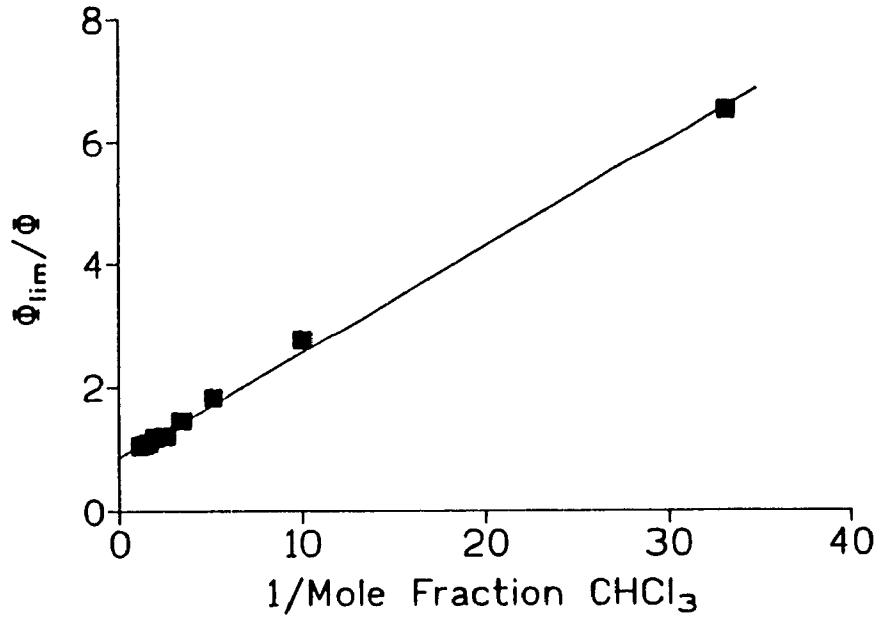

Figure 3.12. Normalized double reciprocal plot for the 313 nm photolysis of $[Pt(mnt)_2]^{2-}$.

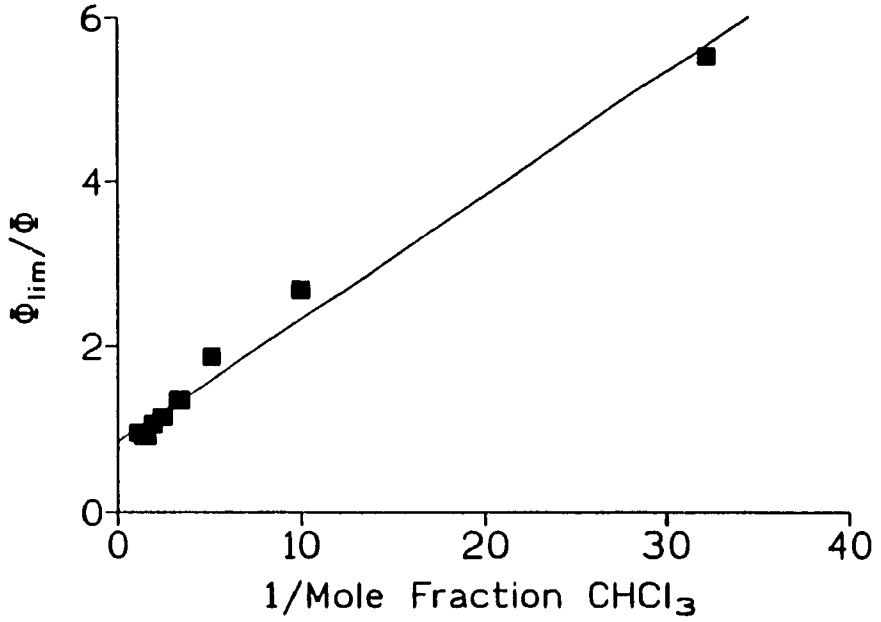

Figure 3.13. Normalized double reciprocal plot for the 365 nm photolysis of $[Pt(mnt)_2]^{2-}$.

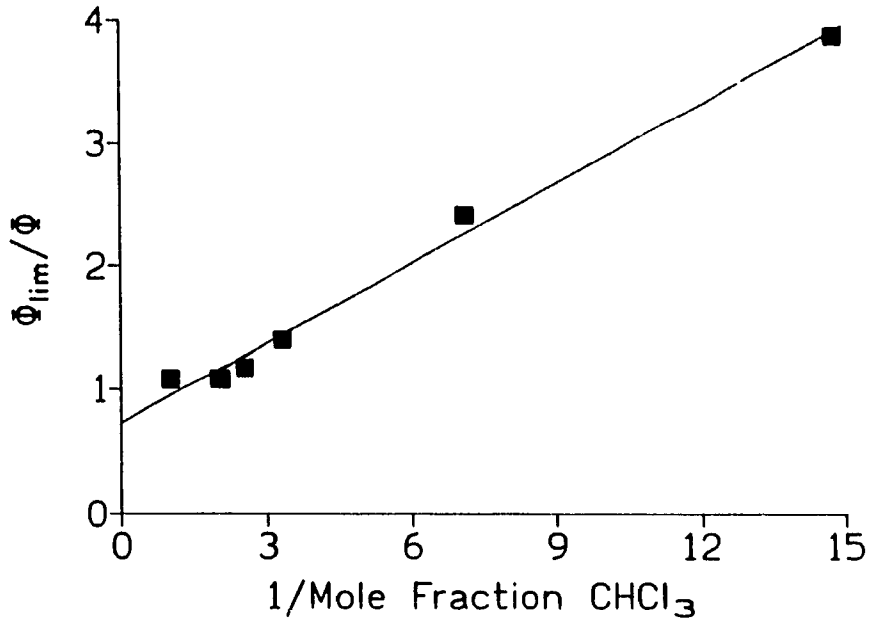

Figure 3.14. Normalized double reciprocal plot for the 365 nm photolysis of $[Ni(mnt)_2]^{2-}$.

and 365 nm excitation), the ratio of the slopes of the two Pt curves should equal that of the two Ni curves. Hence, the slope of the Ni curve using 313 nm excitation can be calculated (it is 0.249). A t-test[13] shows that this calculated slope is statistically equivalent to that obtained from the 365 nm data (the calculation is included in Appendix A). Thus, it is reasonable to suggest that the Ni system is behaving similarly to the Pt system and that K_E is again independent of the excitation wavelength. This demonstrates that *the solvent dependence is independent of the excitation wavelength.* That is, there are two separable phenomena. This suggests that the wavelength dependence must be controlled by the degree of coupling between the non-reactive and the reactive excited states.

3.3. Picosecond Spectroscopy

In order to further investigate the role of $CHCl_3$ as a reactant, the spectral behaviour at short times was explored using time-resolved picosecond laser spectroscopy. In particular, it is important to know whether the steady state oxidation yield is substantially lower than the primary yields as a result of recombination. This information is essential to the interpretation of the wavelength dependence. Unfortunately, the probe pulse and detector do not permit search for the oxidized product at 800 nm. However, bleaching of the band of the starting complex can be examined. Spectra of both the Ni and Pt complexes in $CHCl_3$-CH_3CN ($\chi(CHCl_3)$ = 0.7231) mixtures and neat CH_3CN were recorded under identical conditions at various time delays following excitation by a 355 nm, 30 ps pulse. Spectra of the Ni system in a $CHCl_3$-CH_3CN mixture and in neat CH_3CN are shown for delay times up to 100 ps in Figures 3.15 and 3.16, respectively. In both cases, bleaching of the initial ground state band is seen at 475 nm. This corresponds to the depletion of the ground state absorption upon excitation. A broad excited state absorption, ESA, band is seen between 525 nm and 625 nm. This decays within 100 ps to leave a residual transient whose intensity remains constant until 5 ns (in a separate experiment, nanosecond spectroscopy in a $CHCl_3$-CH_3CN mixture where $\chi(CHCl_3)$ = 0.7231 revealed that there is no observable transient (even within the 10 ns pulse), thereby indicating that all the important excited state processes occur in the picosecond time domain). However, a small amount of bleaching persists at longer times (i.e. 5 ns) indicating the presence of some excited states or products which do not fully return to the initial ground state complex until nearly 10 ns.

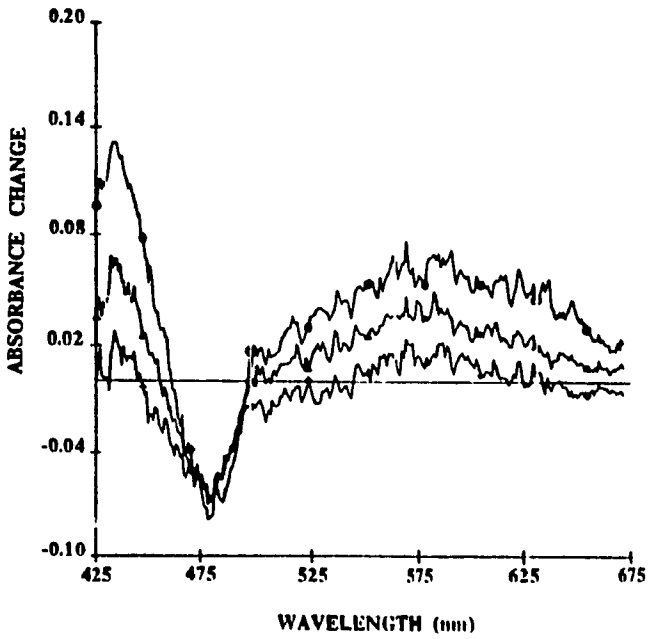

Figure 3.15. Transient absorption spectra of $[Ni(mnt)_2]^{2-}$ in a $CHCl_3$-CH_3CN mixture ($\chi(CHCl_3) = 0.7231$) using 355 nm excitation recorded at probe delays of 20, 50 and 100 ps in order of decreasing absorbance change.

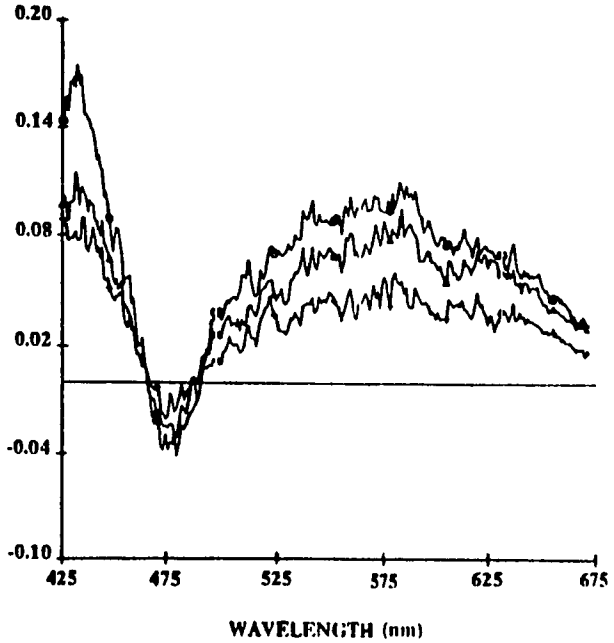

Figure 3.16. Transient absorption spectra of $[Ni(mnt)_2]^{2-}$ in neat CH_3CN using 355 nm excitation recorded at probe delays of 20, 50 and 100 ps in order of decreasing absorbance change.

Analogous changes were reported in a preliminary study[14] of $[M(mnt)_2]^{2-}$ (M = Ni, Pd, Pt) in the unreactive solvent CH_3CN. These small changes were explained in terms of excited state processes. Importantly, the picosecond spectra are identical in both halogenated and non-halogenated solvents (Figures 3.15 and 3.16). If the primary quantum yield is significantly greater than the observed steady state yield of 0.014 ($[Ni(mnt)_2]^{2-}$; 365 nm excitation), some evidence of the oxidized product should be present in the time-resolved spectrum. Also, if there is a significant formation of radicals which subsequently recombine, it would be expected that the magnitude of the bleached absorption in the picosecond spectra would decrease with increasing time delays indicating return of the system to the initial state. Thus, it can be concluded that the initial electron transfer quantum yield must be as low as the final quantum yield rendering the small amount of photoproduct undetectable above the noise level of the transient spectra. The fact that the picosecond spectra are identical in both halogenated and non-halogenated solvents also suggests that solvent effects such as vibrational relaxation may occur on a still shorter timescale (i.e. femtosecond) and are already completed within the excitation pulse (possibly, changes are obscured by the broad ESA).

Very similar spectra were obtained for the analogous Pt complex in both a $CHCl_3$-CH_3CN mixture and in neat CH_3CN (Figures 3.17 and 3.18, respectively) with a broader bleaching feature caused by the breadth of the main visible band of the starting Pt complex. Again, the spectra are very similar to those obtained[14] in the unreactive solvent CH_3CN which also were explained in terms of excited state processes. As in the case of the Ni complex, no evidence for the net oxidation of the complex is found and it can

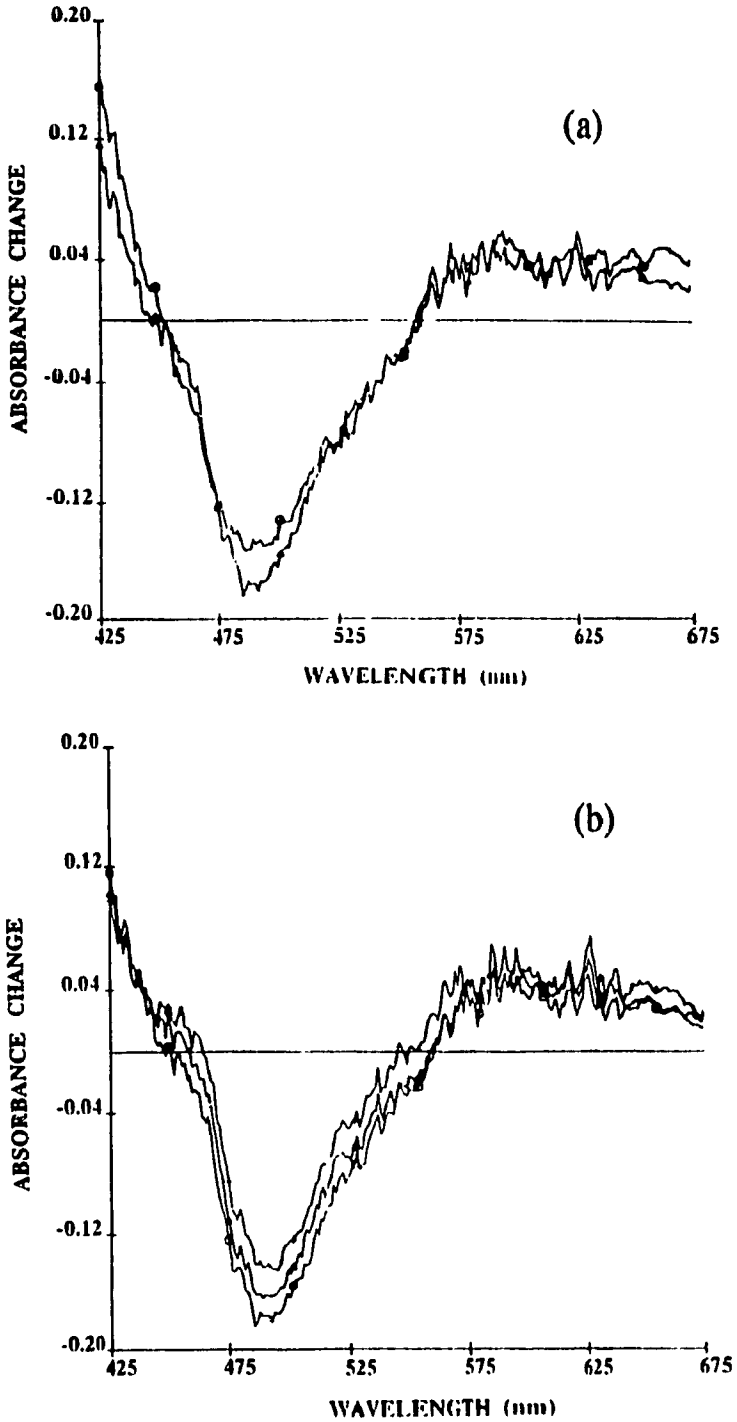

Figure 3.17. Transient absorption spectra of $[Pt(mnt)_2]^{2-}$ in a $CHCl_3$-CH_3CN mixture ($\chi(CHCl_3) = 0.7231$) using 355 nm excitation recorded at probe delays of (a) 50 and 500 ps and (b) 500 ps and 2 and 5 ns in order of increasing absorbance change of the bleach.

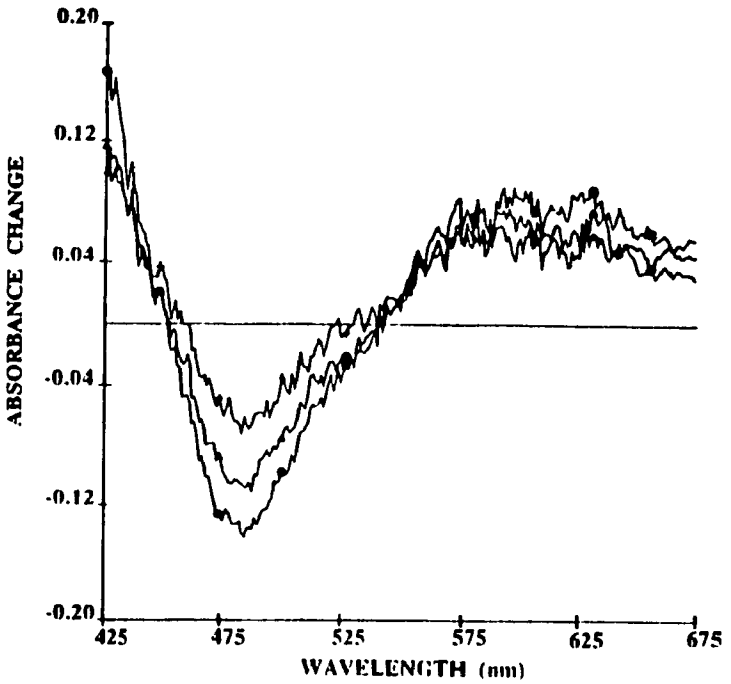

Figure 3.18. Transient absorption spectra of $[Pt(mnt)_2]^{2-}$ in neat CH_3CN using 355 nm excitation recorded at probe delays of 500 ps and 2 and 5 ns in order of increasing absorbance change of the bleach.

be again concluded that the primary yield cannot significantly exceed the overall steady state yield (0.024; 365 nm excitation). One interesting point regarding the spectra of the Pt complex in $CHCl_3$ is that some recovery of the transient bleach is observed. Furthermore, the transient absorption (between 550 nm and 650 nm) forms within the pulse (30 ps) and does not decay, even at times as long as 5 ns. This indicates that there is clearly something different occurring in the Pt complex[14]. This concept will be explored further in Section 3.5.

3.4. Effect of Chloroform Concentration on the Photooxidation

Evidence obtained from transient spectroscopy suggests that the overall steady state quantum yields are at most little different from primary radical yields. The

explanation of the wavelength dependence on the basis of the classical competition between radical geminate recombination versus escape from the solvent cage is thus excluded. Moreover, in such a situation, the yield is expected to be reduced by increasing viscosity[15] which means that $CHCl_3$ with a viscosity 1.6 times[16] that of CH_3CN should retard the reaction. This could lead to a yield downturn rather than levelling at high $CHCl_3$ concentrations or, at least, a more complex mole fraction dependence than the simple linear reciprocal plot.

There are two critical processes in which the solvent is involved that deserve consideration. In the first, the primary product, which is a pair of monoanions (Equation 3.3), can be stabilized by solvent reorganization from the solvation shell of the dianionic starting material. A solvent with shorter longitudinal dielectric relaxation time might provide a greater opportunity for this to occur during relaxation of the excited state and thus allow higher yields as a consequence of greater initial excitation. The dielectric relaxation times of CH_3CN and $CHCl_3$ are both relatively short[17] (0.19 ps and 6.4 ps, respectively). The relaxation times move in the wrong direction (as does the solvent viscosity) to be considered important to the changing yields.

The second process in which the solvent plays a major part is dissipation of the excitation energy via vibrational relaxation. In ordinary fluids at room temperature, this is a 10 to 100 ps process[7]. The major determinant in the outcome of the reaction is the "thermal cage" effect (Section 1.6.2). A solvent molecule receiving energy from a "hot" centre (i.e. $[M(mnt)_2]^{2-}$ (M = Ni, Pt)) becomes excited and can back transfer energy in competition with dissipation to the thermal bath. The rate of dissipation will be closely

linked to the bulk thermal conductivity.

The thermal conductivity for pure liquids can be readily approximated using Equation 3.8 which was developed by Sato and Riedel[18] (the physical parameters used in the approximation can be found in Reference 16).

$$\lambda_L = \frac{2.64x10^{-3}}{M^{1/2}} \cdot \frac{3 + 20(1-T_r)^{(2/3)}}{3 + 20(1-T_{rb})^{(2/3)}} \qquad (3.8)$$

where λ_L is the liquid thermal conductivity of the solvent, M the molecular mass, T_r the reduced temperature (i.e. T/T_c; T_c = critical temperature), and T_{rb} is the reduced temperature at the normal boiling point (i.e. T_b/T_c; T_b = boiling point of the solvent). The values are 5.1 x 10^{-4} cal cm^{-1} s^{-1} K^{-1} and 2.6 x 10^{-4} cal cm^{-1} s^{-1} K^{-1} for CH_3CN and $CHCl_3$, respectively.

Vibrational cooling times for dyes have been measured[8] in $CHCl_3$ and CH_3OH (which probably models CH_3CN adequately) as 35 $\pm$ 10 ps and 13 $\pm$ 5 ps, respectively. The implication is that $CHCl_3$ is approximately two times *less* efficient at dissipating excess energy than CH_3CN and the difference between CH_3CN and $CHCl_3$ is in the right direction for explanation of the increasing yields. At high initial excitation energy, the reduced rate of loss of excitation in $CHCl_3$ may allow increased probability of crossing to a primary product surface in competition with relaxation to the ground state which explains the higher yield under 313 nm excitation. This carries the interesting implication that the timescale of the reaction is that of vibrational cooling - the ten ps domain (or even shorter). However, this should also lead to the breakdown of the simple

model leading to the double reciprocal plots. The linearity of these plots argues against a major role for this factor.

3.5. Mechanism of Reaction

Studies on the photochemistry of iron dithiocarbamato complexes and the carbonyl(η^5-cyclopentadienyl)iron(I)tetramer[19a,b] revealed that near UV excitation induced an electron transfer reaction in the presence of a halogenated species. In these studies, it was noticed that the near UV region of the electronic spectrum was slightly perturbed in the presence of halocarbons (the band intensity increased in the presence of halogenated solvent). Careful inspection of the spectra of these iron complexes in both halogenated and non-halogenated solvents revealed that this increased absorptivity is due to the presence of an additional transition, probably charge-transfer-to-solvent (CTTS) in nature. The existence of a CTTS state was verified by an observed dependence of the quantum yield of photoreaction on the wavelength of excitation and the fact that the CTTS maximum correlated with the ease of reduction of the halocarbon. Furthermore, numerous reports[6a,19a,20] (including that of Vogler and Kunkely) have implicated such states in photoreactions of other complexes in chlorinated solvents. Vogler and Kunkely postulated that the photooxidation of $[M(mnt)_2]^{2-}$ (M = Ni, Pt) in $CHCl_3$ depends upon crossing into a CTTS state, but were unable to prove this. Their study focused only on the wavelength dependence of the steady state quantum yield.

CTTS states usually appear between 250 and 350 nm in the electronic spectrum[19]. Vogler and co-workers searched for the presence of such transitions in the $[M(mnt)_2]^{2-}$

(M = Ni, Pt) complexes. Careful examination revealed two "new" maxima (possibly due to a CTTS transition) at 318 nm and 363 nm for the Pt complex[6a]. For the Ni analogue, there was a less pronounced band at 335 nm[6a]. However, due to the small extinction coefficients, these bands are not reliably identifiable because they are obscured by intraligand and charge-transfer (CT) bands which have very large extinction coefficients[21] (although it is important to realize that even though the CTTS transition cannot directly be observed in the UV-visible spectrum, it does not necessarily mean that it is not present).

In order to gain further insight into the nature of the reactive excited state, the minimum energy required to go from ground state reactants to ground state products was estimated from the $E_{1/2}$ values of the solvent and the complex using a hypothetical electrochemical cell (it is important to realize that the one electron oxidation of $[M(mnt)_2]^{2-}$ (M = Ni, Pt) is a reversible process[6a], whereas the reduction of $CHCl_3$ is an irreversible process[22]). Also, an $E_{1/2}$ value rather than an E° is used to describe the reduction of $CHCl_3$ since it is the most appropriate potential to use. This is because it describes the energy required to reach the unstable primary products, $CHCl_2^\bullet$ and Cl^-, (i.e. it is parallel to our reaction). Since the oxidation of the complex ($E_{1/2}$(Ni) = 0.23 V)[6a] occurs at the anode and the reduction of the solvent ($E_{1/2}$ = -1.67 V)[23] at the cathode, the "cell potential" can be calculated as:

$$E_{cell} = E_{cathode} - E_{anode} \qquad (3.6)$$

$$= -1.67 - 0.23$$

$$= -1.90 \text{ V}$$

The familiar relationship between free energy and cell potential can be used to show that -1.90 V corresponds to -184 $kJ \cdot mol^{-1}$. The absolute value of this energy represents the absolute cutoff wavelength of excitation required to cause a reaction (i.e. $\lambda_{cutoff} > \Delta G_{thermodynamic}$). Vogler and Kunkely showed[6a] that this reaction is not limited to just near UV excitation. Irradiation of $[Ni(mnt)_2]^{2-}$ and $[Pt(mnt)_2]^{2-}$ with 405 nm light promotes a reaction with a quantum yield of 0.001 and 0.009, respectively[6a]. Therefore, comparison of the "cell potential" to the energies of a 313 nm (382 $kJ \cdot mol^{-1}$), a 365 nm (328 $kJ \cdot mol^{-1}$), and a 405 nm (295 $kJ \cdot mol^{-1}$) photon shows that this reaction is thermodynamically permitted from UV through to visible excitation. The low value of E_{cell} suggests that the reactive excited state is relatively low in energy and can readily be populated, even with a 405 nm photon.

Excitation in the near UV, as mentioned above, causes an electron transfer such that $[M(mnt)_2]^{2-}$ (M = Ni, Pd, Pt) is oxidized and $CHCl_3$ is reduced. The products of this reaction are $[M(mnt)_2]^{-}$ (M = Ni, Pt), Cl^- and $CHCl_2^{\bullet}$. Furthermore, the reaction is probably best represented by a "dissociative" potential energy surface because of the irreversibility of the reduction of $CHCl_3$. This explains why this reaction cannot be interpreted in terms of the classical competition between geminate radical recombination versus escape from the solvent cage. Once the electron has been transferred, the system dissociates and there is no opportunity for recombination. These considerations suggest the dominant coordinate of the reactive surface. Following electron transfer, a covalent two electron bond (C-Cl) is converted into a carbon based radical and a Cl^- ion. This involves mainly the lengthening of the C-Cl bond and solvent reorganization. Thus,

there is much structural change in $CHCl_3$. It has been shown using X-Ray crystallography[24] that there is little structural change between $[M(mnt)_2]^{2-}$ and $[M(mnt)_2]^{-}$ (M = Ni, Pd, Pt). Consequently, the dominant coordinate on the potential energy surface must be the C-Cl bond length which is known to be dissociative in the $CHCl_3$ reduction[22]. The CTTS state therefore must be identical to the product potential energy surface which must also be dissociative in nature. A diagram describing the states involved in the photooxidation is shown in Figure 3.19. This representation can provide the basis for an account of both the observed wavelength and solvent dependencies.

A vertical (Franck-Condon) transition from the ground state terminates in a high vibrational state where the vibrational levels are very dense (the CTTS would appear as a weak, broad band in the electronic spectrum, and hence would be masked by other intense transitions (such as intraligand and LMCT) occurring in the same region). Thus, the more likely explanation is that the absorbed photon will directly populate one of the more intense electronic transitions. The CTTS state is then populated from the optically excited state at or near the Franck-Condon configuration (the efficiency of this conversion of course depends on the excitation wavelength since CTTS population occurs from different vibronic levels of the initially excited state and (perhaps) also because of the population of a different electronic excited state at 313 and 365 nm (i.e. LMCT *vs* MLCT).

From the lack of bleach recovery in the transient absorption spectra of $[Ni(mnt)_2]^{2-}$ in the halogenated system (Figure 3.15), there is no evidence for back-reaction in this time domain, hence it is concluded that this is not an important factor in the reaction.

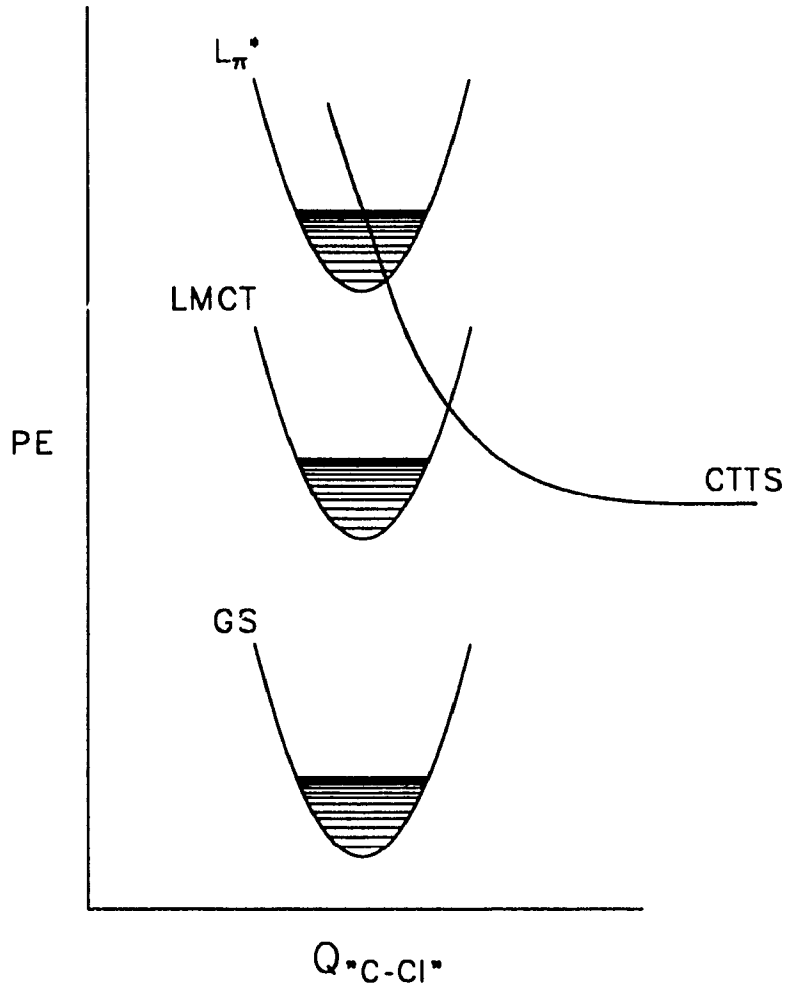

Figure 3.19. Potential energy diagram for $[M(mnt)_2]^{2-}$; M = Ni, Pt. The dominant coordinate, $Q_{"C-Cl"}$, is assumed to be the C-Cl bond length.

Low quantum yields for photooxidation indicate that there are radiationless pathways which successfully compete with the chemical reaction (i.e. the possibility of relaxation to other excited states, as observed in CH_3CN, cannot be excluded). The overall quantum yield must therefore reflect either the degree of mixing between the two states or the efficiency of crossing from the initially excited state to the CTTS state. Based on the lack of solvent dependence and the relationship between thermal conductivity and

vibrational cooling times (discussed in Section 3.4), the main factor controlling the reaction is probably the degree of mixing of the CTTS state with a non-reactive excited state in the transition.

3.6. Conclusions

The photooxidation of $[M(mnt)_2]^{2-}$ (M = Ni, Pt) is a sub-picosecond process which is governed by both solvent and excitation wavelength. The quantum yield of photooxidation of $[Ni(mnt)_2]^{2-}$ increases with increasing $CHCl_3$ concentration up to a limiting value of 0.014 and 0.25 for 365 nm and 313 nm excitation, respectively. $[Pt(mnt)_2]^{2-}$ exhibits similar behaviour; the limiting values of the quantum yield are 0.021 and 0.13 for 365 nm and 313 nm excitation, respectively. The solvation data were found to fit to the mathematical expression used to describe kinetics involving preequilibria thus indicating that no important solvent effects exist beyond the role of $CHCl_3$ as a reactant. The interesting point regarding the quantum yield is that after normalization with respect to the limiting yield, the normalized solvation profiles have identical initial slopes for different excitation wavelengths while the solvent dependence is retained. Thus, the wavelength dependence is independent of the solvent dependence. This points to an electronic effect which controls the reaction. This is accomplished via mixing of a non-reactive excited state with one of CTTS character. It is this process that controls the quantum yield.

Picosecond spectra reveal no solvent dependence in the early excited state dynamics for both $[Ni(mnt)_2]^{2-}$ and $[Pt(mnt)_2]^{2-}$. Importantly, there is no evidence for an

efficient primary formation of the oxidized products, even in 80% (v/v) $CHCl_3$ demonstrating the overall steady state quantum yields are the same as the primary yields. The observed steady-state quantum yield must therefore be related to the electronic factors governing the mixing of a non-reactive excited state with the CTTS state. Thus, the dominant factor determining the fast photooxidation of $[M(mnt)_2]^{2-}$ (M = Ni, Pt) is the mixing of the higher energy non-reactive CT excited state with the reactive CTTS state. That is, "electronic factors" appear to control the process.

3.7. References

1. a) Repinec, S. T.; Sension, R. J.; Szarka, A. P.; Hochstrasser, R. M. *J. Phys. Chem.* **1991**, *95*, 10380.

   b) Sension, R. J.; Repinec, S. T.; Hochstrasser, R. M. *J. Chem. Phys.* **1990**, *93*, 9185.

2. a) Schoenlein, R. W.; Peteanu, L. A.; Mathies, R. A.; Shank, C. V. *Science* **1991**, *254*, 412.

   b) Tallent, J.R.; Hyde, E.W.; Findsen, L.A.; Fox, G.C.; Birge, R.R. *J. Am. Chem. Soc.* **1992**, *114*, 1581.

3. Langford, C.H. *Acc. Chem. Res.* **1984**, *17*, 96.

4. Rainer, H.; Schlumann, W.; Kisch, H. *Angew. Chem.* **1980**, *19*, 645.

5. Persaud, L.; Langford, C. H. *Inorganic Chemistry* **1985**, *24*, 3562.

6. a) Vogler, A.; Kunkely, H. *Inorganic Chemistry* **1982**, *21*, 1172.

   b) Dooley, D.M.; Patterson, B.M. *Inorganic Chemistry* **1982**, *21*, 1172.

7. a) Hynes, J. T. *Ann. Rev. Phys. Chem.* **1986**, *35*, 573.

   b) Harris, A. L.; Brown, J. K.; Harris, C. B. *Ann. Rev. Phys. Chem.* **1988**, *39*, 341.

8. Elsaesser, T.; Kaiser, W. *Ann. Rev. Phys. Chem.* **1991**, *42*, 83.

9. a) Abraham, M.H. *Progress in Physical Organic Chemistry*, Vol. 11, Ed. A. Streitwieser, Jr. and R.W. Taft, Wiley and Sons, New York, 1974.

   b) Parker, A.J. *Chem. Rev.* **1969**, *69*, 1.

10. Kosower E.M.; Huppert, D. *Ann. Rev. Phys. Chem.* **1986**, *37*, 127.

11. Malkhasian, A.Y.S. *Personal Communication*, **1993**.

12. Kleinbaum, D.G.; Kupper, L.L.; Muller, K.E. *Applied Regression Analysis and Other Multivariable Methods* 2nd ed., PWS-Kent Publishing Co., Boston, **1988**, pp. 91-92.

13. Christian, G.D. *Analytical Chemistry* 3rd ed., John Wiley and Sons, New York, **1980**, p. 74.

14. Persaud, L.; Sharma, D. K.; Langford, C. H. *Inorg. Chim. Acta* **1986**, *114*, L5-L6.

15. Adamson, A.; Fleischauer Concepts of Inorganic Photochemistry John Wiley and Sons, USA, 1975.

16. Riddick, J. A.; Bunger, W. B.; Sakano, T. K. in *Techniques of Chemistry, Vol. II, Organic Solvents Physical Properties and Methods of Purification*, 4th edition; John Wiley and Sons, Inc.: U.S.A., 1986, pp.492, 582.

17. a) Rips, I.; Klafter, J.; Jortner, J. in Photochemical Energy Conversion, Ed. J.R. Norris, D. Meisel, Elsevier, New York, 1989.

    b) Potapov, A.A. *Russian J. Phys. Chem.* **1992**, *66*, 708.

18. Reid, R. C.; Prausnitz, J. M.; Sherwood, T. K. in *The Properties of Gases and Liquids*, 3rd edition; McGraw-Hill Book Company: U.S.A., 1958, pp. 204-210, 518-520.

19. a) Bock, C.R.; Wrighton, M.S. *Inorg. Chem.* **1977**, *16*, 1309.

    b) Miessler, G.L.; Zoebisch, E.; Pignolet, L.H. *Inorg. Chem.* **1978**, *17*, 3636.

20. Traverso, O.; Scandola, F. *Inorg. Chim. Acta.* **1970**, *4*, 493.

21. Schupack, S.I.; Billig, E.; Clark, R.J.H.; Williams, R.; Gray, H.B. *J. Am. Chem. Soc.* **1964**, *86*, 4594.

22. a) Bertran, J.; Gallardo, I.; Moreno, M.; Savéant, J. *J. Am. Chem. Soc.* **1992**, *114*, 9576.

    b) Savéant, J. *J. Am. Chem. Soc.* **1987**, *109*, 6788.

23. Mann, C.K.; Barnes, K.K. *Electrochemical Reactions in Nonaqueous Systems*, Ed. Marcel Dekker, New York, **1970**.

24. Eisenberg,R.; Ibers, J.A.; Clark, R.J.H.; Gray, H.B. *J. Am. Chem. Soc.* **1964**, *86*, 113.

4. Mechanistic Aspects of the Photosubstitution of CO in $W(CO)_4$(phen)

4.1. Background

It is known that ligand field, LF, excitation promotes rapid loss of CO via a dissociative pathway in $M(CO)_6$ (M = Cr, W) complexes[1-3] (Section 1.1). Replacement of two CO ligands by the π accepting diimine ligand 1,10-phenanthroline (phen) yields the complex $W(CO)_4$(phen) which possesses metal-to-ligand charge transfer, MLCT, states in addition to LF states, the former states being lower in energy. $W(CO)_4$(phen) can undergo substitution of the CO ligand, as can the hexacarbonyl analogues. It is here where the similarity between the hexacarbonyl and the tetracarbonyl complexes appears to end. This is because CO loss in $W(CO)_4$(phen) occurs from both MLCT and LF excited states. What makes this reaction particularly intriguing is the fact that not only does the substitution occur from both states, but it proceeds via different pathways. Stufkens and co-workers found that CO substitution was dependent on the concentration of the entering ligand upon MLCT excitation[4], thus suggesting that this is an associative process upon MLCT excitation. Pressure dependence studies carried out by van Eldik *et al*[5] have shown a negative volume of activation upon MLCT excitation indicating an associative pathway thus corroborating the evidence from the earlier concentration dependence study (i.e. ligand substitution follows an associative mechanism upon MLCT excitation). However, the volume of activation was positive upon irradiation into the LF band[5] indicating a dissociative pathway. Furthermore, multiple luminescence has been observed for many $W(CO)_4(\alpha,\alpha'$- diimine) complexes, including $W(CO)_4$(phen)

derivatives[6], suggesting rather unusual photophysics in this family.

It is thus clear that MLCT states effect rather interesting behaviour with regards to photochemical ligand substitutions which is not seen in complexes possessing only LF states. In order to probe the nature of the reactive states (both LF and MLCT) in organometallics and their reactivity towards photosubstitution, the primary processes of $W(CO)_4$(phen) upon irradiation into the MLCT and the LF bands have been explored via (1) the concentration dependence of the quantum yield under LF excitation, (2) the wavelength and solvent dependence of the quantum yield upon excitation into the MLCT band, and (3) sub-nanosecond spectroscopy.

4.2. Electronic Spectroscopy

4.2.1. Solvatochromism

Solvent effects on the absorption spectra of organometallic complexes have been recognized for a number of systems. These effects are usually the result of a shift in energy of transitions which are predominantly CT in character. There is minimal effect on the energy of LF transitions. In fact, the variation in the energy of the MLCT state for $W(CO)_4(\alpha,\alpha'$-diimine) (M = Cr, Mo, W) complexes is one of the largest known among both inorganic and organometallic species[7]. An earlier study has shown[8] that $W(CO)_4$(bpy) exhibits *negative solvatochromism*. That is, the MLCT absorbtion band undergoes a hypsochromic shift as the medium becomes increasingly polar. Negative solvatochromism has been interpreted in terms of a reduced excited state electric dipole[9,10]. This is a consequence of the Franck-Condon principle and implies that there

is a substantial electric dipole moment associated with the ground state solute molecule which is reduced, reversed, or realigned with the MLCT transition. Thus, a polar medium can be considered to stabilize the ground state to a greater extent than the excited state species (since during the transition, there is not sufficient time for the solvent molecules to re-orient with respect to the new charge distribution). From the electronic spectra shown in Figure 4.1, it is evident that $W(CO)_4(phen)$, the complex of interest in this chapter (its geometrical structure is given in Figure 1.4), exhibits behaviour similar to that observed for the analogous bpy complex.

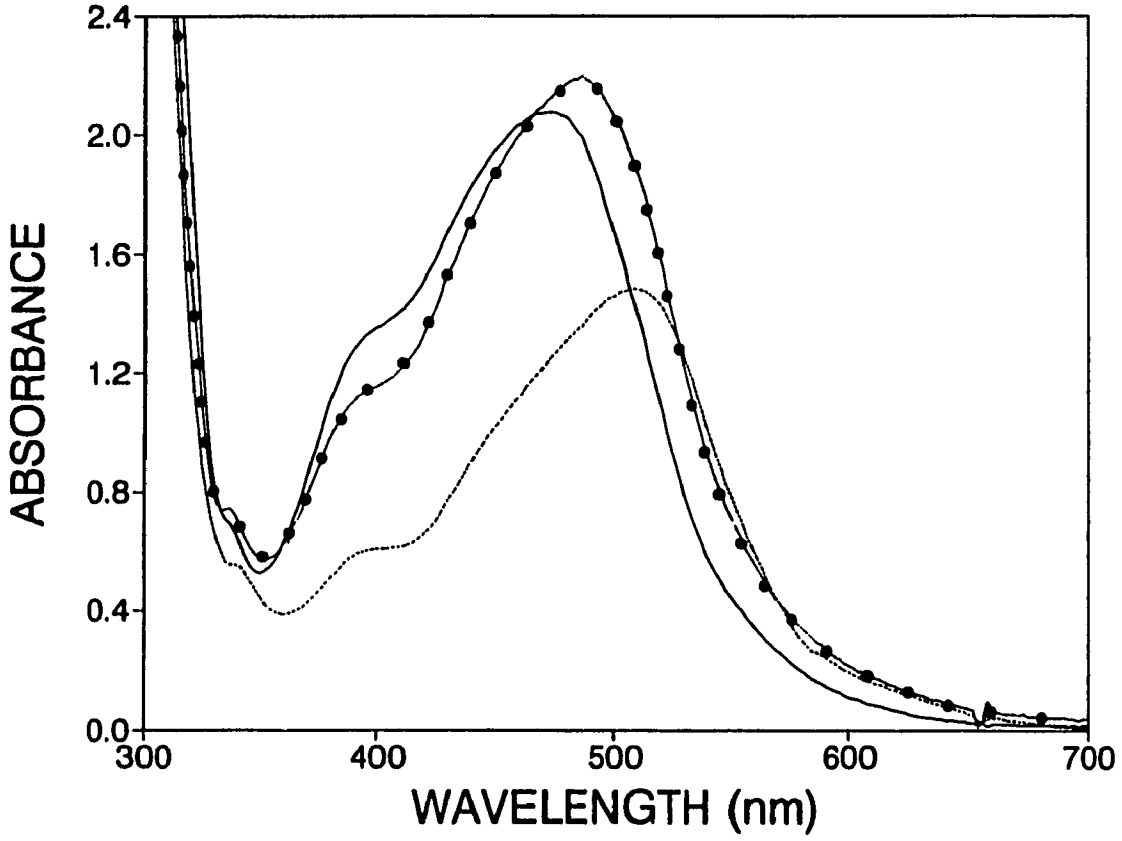

Figure 4.1. Electronic absorption spectra of $W(CO)_4(phen)$ at 293 K in pyridine (—), dichloromethane (-•-•-) and toluene (---).

Thus, solvatochromism is important in that it (1) provides a relatively simple means to assign transitions (i.e. LF *vs* CT) and (2) affords the opportunity to easily probe different regions of the MLCT envelope without varying the wavelength of the excitation source (i.e. we tune the complex, rather than the laser!). This is desirable since it provides a straightforward means of examining the quantum yields of reaction while populating different regions of the MLCT band envelope. As mentioned in Section 1.1, wavelength dependence of the quantum yield across narrow spectral regions is indicative of processes which compete with vibrational relaxation.

4.2.2. Band Assignments

The electronic spectra of $W(CO)_4$(phen) in pyridine, dichloromethane and toluene at 25°C are shown in Figure 4.1. Negative solvatochromism of the low-lying band is observed, indicating CT character. This band has been assigned as a W ---> phen π^* CT transition in closely analogous $W(CO)_4(\alpha,\alpha'$ diimine) complexes[11,12]. Servaas *et al* have analyzed such MLCT band envelopes and assigned three MLCT transitions. The most intense transition is a z-polarized $(d_{yz})b_2$ ---> $b_2(\pi^*)$ transition[11]. This intense low energy system will be referred to as MLCT<1>. The higher energy absorption at around 400 nm does not exhibit solvatochromism. It has been assigned as predominantly LF with a contribution from a higher energy a_2 ---> $a_2(\pi^*)$ MLCT transition[6,12] which will be referred to as MLCT<2>. The band in the 300-350 nm region is also not solvatochromic, indicating LF character. These absorptions have been assigned to transitions to the two higher energy d_σ orbitals[12].

4.3. Concentration Dependent Behaviour

The quantum yield of photochemical reactions whose mechanisms are uncomplicated by subsequent thermal processes is directly related to the quantum yields of the primary photochemical steps involved. Dependencies of quantum yields on reaction conditions (excitation wavelength, temperature, ligand concentration...) thus reveal detailed information on primary photochemical dynamics. Quantum yields of dissociative photosubstitution reactions are independent of the concentration of the substituting ligand[5]. On the other hand, extended concentration dependence of the quantum yield is a good diagnostic for an associative mechanism[4]. As mentioned in Section 4.1, quantum yields of CO photosubstitution in $W(CO)_4(\alpha,\alpha'$-diimine) complexes are concentration dependent upon MLCT excitation in the visible region of the spectrum[4] such that the quantum yield of the reaction increases with increasing concentration of the substituting ligand. Consequently, the photosubstitution follows a two-term rate law:

$$\phi_{obs} = \phi_{dis} + \phi_{ass}[(n\text{-}Bu)_3P] \qquad (4.1)$$

Thus, at low phosphine concentrations, the associative term is too small to be outside the experimental error and cannot be observed (i.e. the only instance where it may be possible to see this term is at high phosphine concentrations). In order to examine whether there is a contribution from the associative pathway even under LF excitation, dependence of the photosubstitution quantum yields of $W(CO)_4$(phen) were measured as a function of the $(n\text{-Bu})_3P$ concentration in CH_2Cl_2 at 365 nm (As may be seen in Figure 4.1, this excitation wavelength falls into the high energy onset of the LF absorption band. The possibility of simultaneous excitation of both MLCT and LF transitions thus can

clearly be neglected).

Irradiation of $W(CO)_4(phen)$ in either a coordinating solvent (neat pyridine) or in the presence of an excess of tri-*n*-butyl phosphine (*n*-Bu_3P), a potential ligand, in dichloromethane leads to the substitution of one CO ligand to form $W(CO)_3(L)(phen)$ which has a unique electronic spectrum (Figures 4.2 and 4.3) thus can be readily differentiated from the reactant (although the electronic spectrum of the photoproduct $W(CO)_3(L)(phen)$ has not been characterized in the literature, it is similar to that observed[13] for $Mo(CO)_3(L)(phen)$). The electronic spectrum of the photoproduct possesses a band in the red region of the spectrum which is not present in the electronic spectrum of $W(CO)_4(phen)$. The red shift of the band is expected upon substitution of a strong field ligand by a weaker field ligand. Throughout the photolysis, the spectra show a clean progression to the spectral features of $W(CO)_3(L)(phen)$ as indicated by the retention of isosbestic points at 392 nm and 514 nm and 372 nm and 514 nm in neat pyridine and solutions of (*n*-$Bu)_3P$ in dichloromethane, respectively, throughout the reaction (Figures 4.2 and 4.3; refer to Appendix B for spectral changes observed in other solvents). This indicates that there are no complications arising from side or subsequent reactions for the duration of the reaction. Hence, it is concluded that $W(CO)_3(L)(phen)$ is the sole product of the photolysis of $W(CO)_4(phen)$. The results are summarized in Table 4.1. Notice that the quantum yields are virtually identical in neat pyridine and in solutions of 0.36 M (*n*-$Bu)_3P$ in dichloromethane. This suggests we are approaching the upper limit of the quantum yield at this concentration of (*n*-$Bu)_3P$. This can be explained upon consideration of the amounts of incoming ligand present in solution. In neat

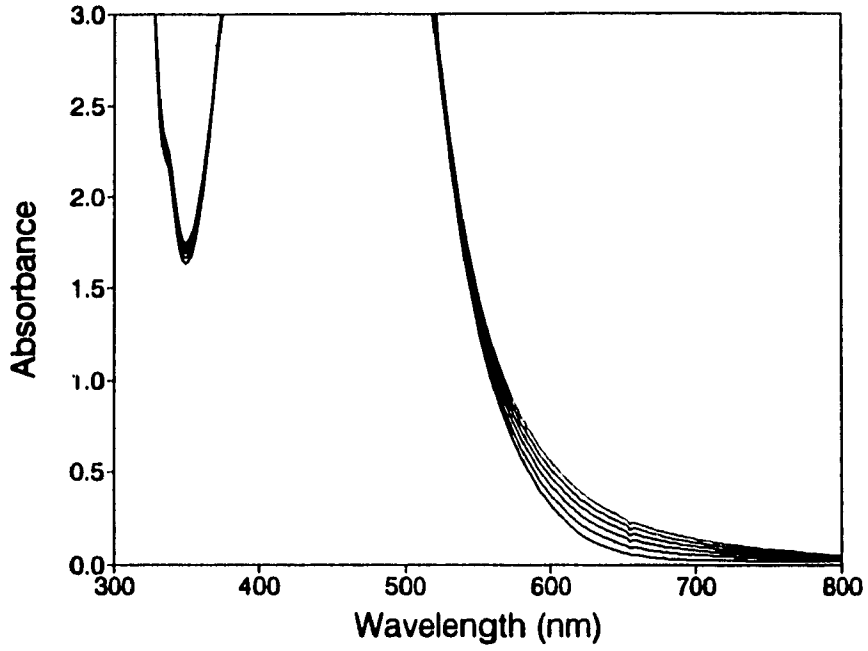

Figure 4.2. Electronic spectral changes observed upon photolysis of $W(CO)_4$(phen) in neat pyridine at 365 nm. The times of irradiation from reactant A to product B are: 0, 607, 1832, 2432, 3032, and 3632 s in order of increasing absorbance.

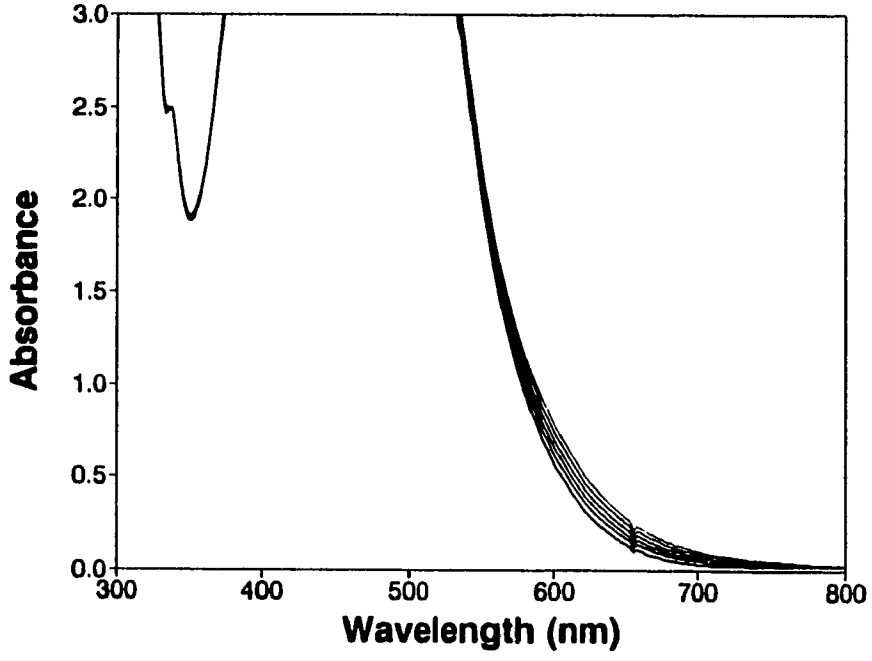

Figure 4.3. Electronic spectral changes observed upon photolysis of $W(CO)_4$(phen) in a 0.015 M solution of $(n\text{-Bu})_3P$ in CH_2Cl_2 at 365 nm. The times of irradiation from reactant A to product B are: 0, 600, 1200, 1800, 2400, and 3000 s in order of increasing absorbance.

pyridine, the complex is always in encounter with a potential ligand and as a result, the quantum yield will be at its maximum at this wavelength. On the other hand, in (n-Bu)$_3$P, there are fewer substituting ligands in encounter with the W complex, hence the quantum yield is expected to be lower in this situation. However, at this concentration of (n-Bu)$_3$P, the quantum yield is approximately the same as that in neat pyridine, suggesting that nearly 100% of the W complexes may be in encounter with (n-Bu)$_3$P. This concept will subsequently be examined in more detail.

Table 4.1. Quantum yields[a] for the 365 nm photolysis of W(CO)$_4$(phen) in neat pyridine and in CH_2Cl_2 containing (n-Bu)$_3$P.

SOLVENT	QUANTUM YIELD[b]
neat pyridine	0.016(6.8)
0.015 M (n-Bu)$_3$P in CH_2Cl_2	0.011(7.8)
0.36 M (n-Bu)$_3$P in CH_2Cl_2	0.017(3.0)

a) All quantum yields were obtained at room temperature.
b) The standard deviation (percent) is in parenthesis.

The results in Table 4.1 indicate a dependence of the quantum yield upon the concentration of the substituting ligand ((n-Bu)$_3$P) under LF excitation in CH_2Cl_2. The quantum yield increases from 0.011 to 0.017 upon increasing the concentration of (n-Bu)$_3$P in the reaction mixture from 0.015 M to 0.36 M. This unambiguously supports the presence of an associative term upon LF excitation. The associative contribution at a (n-Bu)$_3$P concentration of 0.36 M, can be estimated simply by subtracting the quantum yield obtained in the low [(n-Bu)$_3$P] limit from that obtained in the upper [(n-Bu)$_3$P] limit to give a value of 0.006. This increase is comparable to that observed upon excitation

into the MLCT band in the same solvent/ligand system (Table 4.2). This suggests that photosubstitution following LF excitation occurs by two pathways: a major dissociative pathway ($\Phi \cong 0.01$) accompanied by a smaller contribution from an associative pathway.

4.4. Wavelength Dependent Behaviour

Dependence of the quantum yields on the excitation wavelength within the MLCT absorption band envelope was investigated in order to obtain more detailed information regarding the reactivity of the MLCT states. As described above, irradiation of $W(CO)_4$(phen) in either a coordinating solvent (neat pyridine) or in the presence of an excess of the potential ligand (n-Bu)$_3$P in dichloromethane leads to the substitution of one CO ligand. No secondary photolysis was observed during the irradiation at wavelengths $\geq$ 488.0 nm. Clean isosbestic points persist in all solvents (Figures 4.4 and 4.5 and Appendix B) until the reaction has gone nearly to completion. Towards 100% conversion, the photolysis of the product becomes significant (but at a lesser rate than that of the reactant). However, irradiation times were limited such that during the course of the reaction $W(CO)_3$(L)(phen) is the sole product. Representative spectra are shown in Figures 4.4 and 4.5. The results for visible excitation of $W(CO)_4$(phen) are shown in Table 4.2.

Although the quantum yield observed upon MLCT excitation in neat pyridine remains unchanged (approximately 0.0028) when irradiating at 488.0 nm and 514.5 nm, the quantum yield increases slightly from 0.0070 (488.0 nm excitation) to 0.0079 (514.5 nm excitation) in a solution of 0.3 M (n-Bu)$_3$P in toluene. However, the quantum yield

Table 4.2. Wavelength dependence of the quantum yield[a] for the photochemical reaction of $W(CO)_4$(phen) in various solvents[b].

WAVELENGTH (nm)	SOLVENT	QUANTUM YIELD[c]
488.0	neat pyridine	0.0028(4.1)
	0.3 M (n-Bu)$_3$P in toluene	0.0070(3.6)
	0.33 M (n-Bu)$_3$P in CH_2Cl_2	0.0024(2.9)
	0.3 M (n-Bu)$_3$P in C_2Cl_4	0.0079(2.1)
514.5	neat pyridine	0.0027(3.0)
	0.3 M (n-Bu)$_3$P in toluene	0.0079(5.8)
	0.36 M (n-Bu)$_3$P in CH_2Cl_2	0.0061(0.6)
	0.3 M (n-Bu)$_3$P in C_2Cl_4	0.010(4.4)
610.9	0.3 M (n-Bu)$_3$P in C_2Cl_4	0.028(4.0)

a) All quantum yields were obtained at room temperature.
b) When C_2Cl_4 was the solvent, 8% (v/v) CH_2Cl_2 was added to the solution to enhance the solubility of $W(CO)_4$(phen).
c) The standard deviation (percent) is in parenthesis.

is found to increase from 0.0024 (488.0 nm excitation) to 0.0061 (514.5 nm excitation) in solutions of (n-Bu)$_3$P in dichloromethane. Likewise, the quantum yield is found to increase from 0.0079 (488.0 nm excitation) to 0.010 (514.5 nm excitation) to 0.028 (610.9 nm excitation) in solutions of (n-Bu)$_3$P in tetrachloroethylene. These results show that a substantial increase in the quantum yield values with increasing excitation wavelength (i.e. decreasing excitation energy) is typical for chlorinated solvents. The wavelength dependence thus points to higher reactivity upon excitation into the low-energy part of the MLCT band. It is interesting to note that this is in the opposite direction to the "conventional" wavelength dependence[14] (as addressed in Section 1.1).

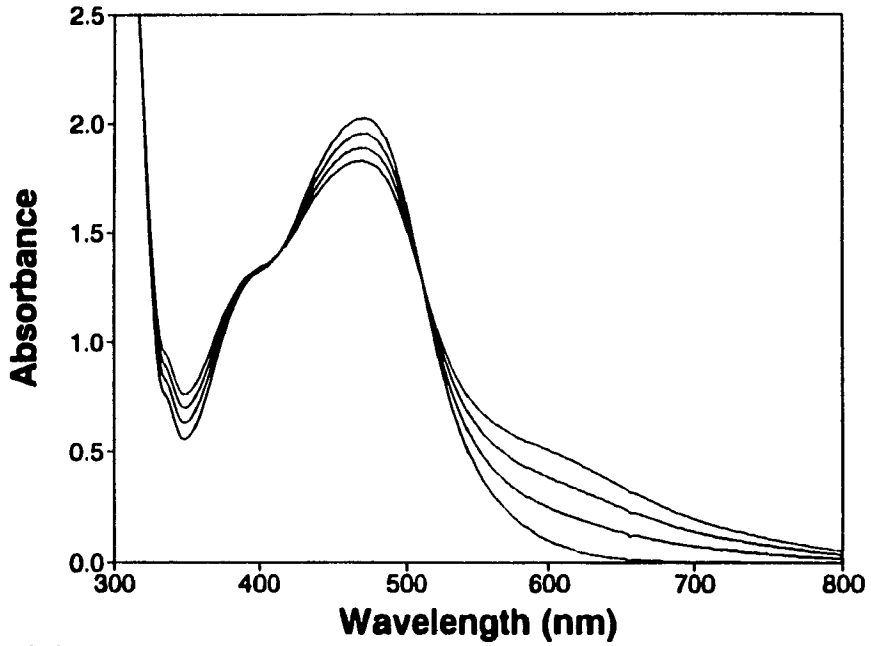

Figure 4.4. Electronic spectral changes observed upon 514.5 nm photolysis of $W(CO)_4$(phen) in neat pyridine. The times of irradiation from reactant A to product B are: 0, 180, 360, and 540 s in order of increasing absorbance.

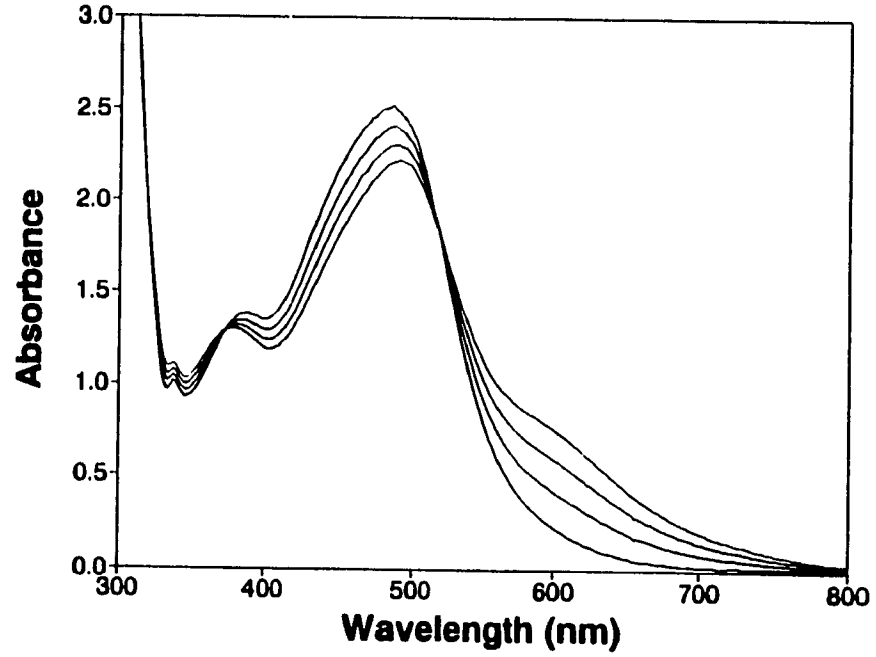

Figure 4.5. Electronic spectral changes observed upon 514.5 nm photolysis of $W(CO)_4$(phen) in 0.33 M (n-Bu)$_3$P in CH_2Cl_2. The times of irradiation from reactant A to product B are: 0, 61, 120, and 180 s in order of increasing absorbance.

This will subsequently be discussed in more detail.

Due to the solvatochromism, the 488.0 nm and the 514.5 nm excitation wavelength falls into the low-energy side of the band in CH_2Cl_2, close to the band-maximum in toluene, and to the high-energy side of the band in C_2Cl_4 (c.f. from Section 4.2.1, we are "tuning" the complex rather than the laser so as to obtain more detailed information regarding the different regions of the MLCT band envelope). The quantum yields increase with increasing wavelength of the MLCT band maximum in the solvent series CH_2Cl_2 (λ_{max} = 486 nm), toluene (λ_{max} = 510 nm), and C_2Cl_4 (λ_{max} = 534 nm), if the nucleophile, (*n*-Bu)$_3$P, and its concentration is kept constant. What is important to notice is that there are coupled wavelength and solvent dependencies upon excitation into various regions of the MLCT band envelope which do not correlate with the solvatochromism and are thus not attributable to changes in initial distribution of Franck-Condon excited state population. This establishes the importance of events at very early times after excitation. Furthermore, the magnitude of the quantum yield upon MLCT excitation (10^{-3}) is the same as that estimated for the MLCT contribution under LF excitation (0.006). This indicates that LF ---> MLCT conversion must be an ultrafast process, kinetically competitive with both CO dissociation from the excited LF state(s) and with their relaxation to the ground state. This observation clearly points to a population of reactive MLCT state(s), which are known to react associatively[1,2], even from LF state(s).

It is known that the rates of vibrational relaxation are dependent on thermal conductivity of the solvent medium[15]. As discussed in Section 3.4, halogenated

hydrocarbons have a lower thermal conductivity than the non-halogenated hydrocarbons, slowing the dissipation of excess vibrational energy and hence, the relaxation into the reactive excited state. The thermal conductivities of the solvents used in this study were estimated using the equation developed by Sato and Riedel (Section 3.4) and are summarized in Table 4.3.

Table 4.3. Thermal conductivity[a] of various solvents as estimated using the Sato-Riedel equation.

Solvent	Thermal Conductivity ($cal \cdot cm^{-1} \cdot s^{-1} \cdot K^{-1}$)
Pyridine	3.55×10^{-4}
Toluene	3.31×10^{-4}
Dichloromethane	2.98×10^{-4}
Tetrachloroethylene	2.48×10^{-4}

a) The data used in the estimation of thermal conductivity of each solvent was obtained from Reference 16.

Upon excitation, the "hot" solute can transfer excess vibrational energy to the surrounding solvent molecules. Because the non-halogenated solvents dissipate the surplus heat more efficiently, it is expected that the solute should remain in an excited state for only a very short time thus reducing the possibility of relaxation to the reactive MLCT state, thus the quantum yields are expected to be low in non-halogenated systems. Conversely, the reduced loss of the excess energy generated upon excitation in chlorinated solvents suggests that the solute should remain excited for a longer period of time, hence the probability of relaxation into the reactive excited state increases. Therefore, the quantum yields are expected to be larger in this case. However, examination of the data in Table 4.2 clearly shows that the quantum yields decrease in

the order C_2Cl_4 > toluene > pyridine > CH_2Cl_2. From this, and the fact that the values of thermal conductivity of these solvents cover a very small range, it can be concluded that the thermal conductivity of the solvent is not an important factor in this reaction. However, both solvent and wavelength dependence clearly show that the partition between various relaxation channels, one of them being the reactive one, must be decisively influenced by events occurring in competition with vibrational relaxation. That is, the molecule must "decide" which pathway it will follow within the few picosecond time domain of vibrational relaxation[14] following the initial MLCT excitation.

4.5. Transient Absorption Spectroscopy

Transient absorption spectra of $W(CO)_4$(phen) were recorded using LF (355 nm) and MLCT (532 nm) excitation in both polar and non-polar solvents, and using both nanosecond and picosecond pulses. The nanosecond spectra obtained between 400 and 800 nm with 532 nm excitation (Figures 4.6 and 4.7) indicate the presence of a transient (band maximum at approximately 580 nm and 592 nm in acetonitrile and toluene, respectively) that is formed within the pulse and decays completely in about 8 ns. This work makes clear that no excited state absorption (ESA) of lifetime longer than 8 ns is important in the primary processes of $W(CO)_4$(phen) and that the bands observed between 425-650 nm are the only significant ESA bands. Consequently, only the picosecond spectra are presented in detail.

Representative ESA spectra of $W(CO)_4$(phen) in pyridine and dichloromethane recorded using 30 ps excitation pulses with both 355 nm and 532 nm excitation are

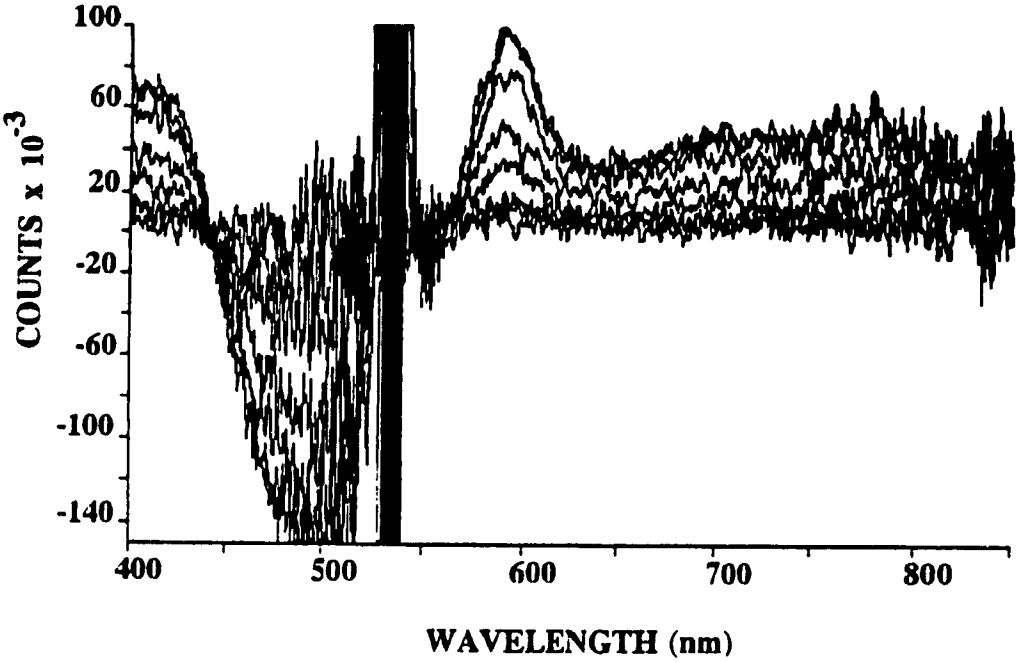

Figure 4.6. Nanosecond absorption spectra of $W(CO)_4(phen)$ in acetonitrile using 532 nm excitation recorded at probe delays of 0, 2, 4, 6, and 8 ns in order of decreasing counts. The pulse energy is 40 mJ.

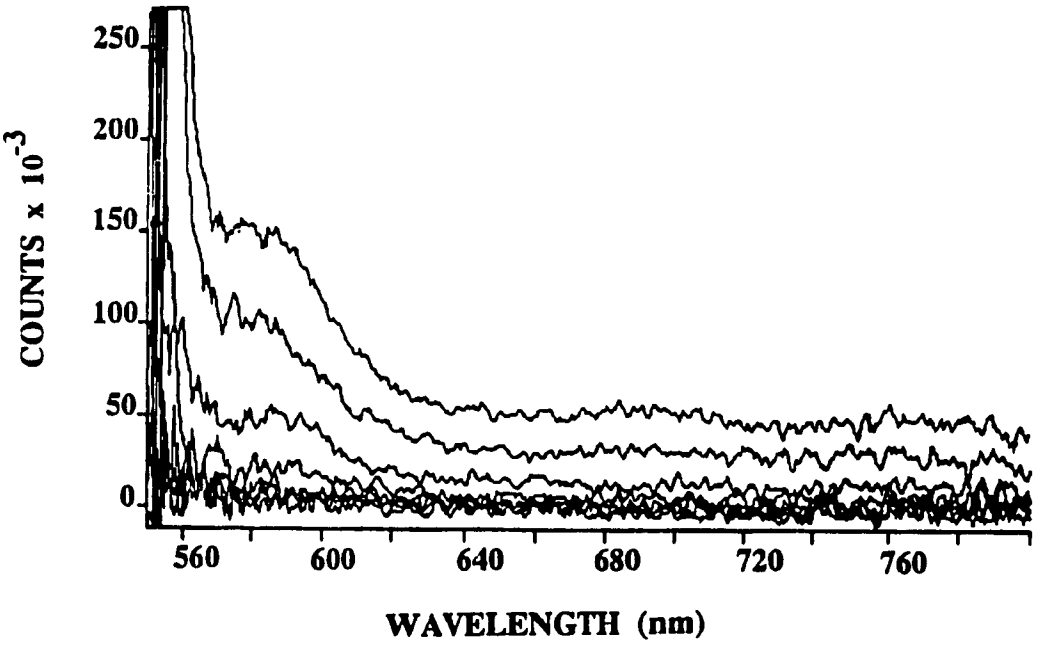

Figure 4.7. Nanosecond absorption spectra of $W(CO)_4(phen)$ in toluene using 532 nm excitation recorded at probe delays of 0, 2, 4, 6, 8 and 10 ns in order of decreasing counts. The pulse energy is 20 mJ.

shown in Figures 4.8 to 4.12. For clarity, all other picosecond spectra are presented in Appendix C. Inspection of the transient absorption spectra show that the transients are fully developed in less than 20 ps under both 355 nm and 532 nm excitation. They decay subsequently. Spectra obtained in other solvents showed similar behaviour. Numerical results are summarized in Tables 4.4 and 4.5.

Table 4.4. Data for picosecond flash photolysis of $W(CO)_4(phen)^a$ in various solvents. λ_{pump} = 355 nm.

Solvent	Acetonitrile[b]	Pyridine	Benzene[c]
Tau (ns) (HE[d] ESA)	1.1 ± 0.1	1.0 ± 0.1	e)
Tau (ns) (LE[d] ESA)	0.7 ± 0.1	2.0 ± 0.1	1.6 ± 0.2
Tau (ns) (bleach)	3.6 ± 0.8	1.8 ± 0.1	0.9 ± 0.1
Ground State Band Maxima (nm)	452 ± 2 390(sh) ± 2	472 ± 2 390(sh) ± 2	508 ± 2 390(sh) ± 2
Bleach Minimum (nm)	452 ± 10	480 ± 10	495 ± 10
HE ESA (nm)	538 ± 10	550 ± 10	e)
LE ESA (nm)	582 ± 10	590 ± 10	584 ± 10
Dielectric Constant[f]	35.95	12.01	2.28

a) All transient absorption spectra were obtained at room temperature (22^{0}C).
b) To enhance the solubility of $W(CO)_4(phen)$ in acetonitrile, 0.02 M H_2O was added to the reaction mixture.
c) To enhance the solubility of $W(CO)_4(phen)$ in benzene, 0.05 M pyridine was added to the reaction mixture.
d) HE and LE refer to the high energy and the low energy components of the ESA, respectively.
e) The ESA blue shifted (with respect to what was observed in the other solvents) and no HE component was resolved when benzene was the solvent.
f) Data was obtained from Reference 17.

Table 4.5. Data for picosecond flash photolysis on $W(CO)_4(phen)^a$ in various solvents. λ_{pump} = 532 nm.

Solvent	Acetonitrile	Pyridine	Benzene	C_2Cl_4
Tau (ns) (HE^b ESA)	0.4 ± 0.1	1.1 ± 0.1	c)	e)
Tau (ns) (LE^b ESA)	1.0 ± 0.2	1.2 ± 0.2	1.2 ± 0.2	e)
Tau (ns) (bleach)	1.8 ± 0.2	1.3 ± 0.1	1.3 ± 0.2	e)
Ground State Band Maxima (nm)	452 ± 2 390(sh) ± 2	472 ± 2 390(sh) ± 2	508 ± 2 390(sh) ± 2	538 ± 2
Bleach Minimum (nm)	460 ± 10	479 ± 10	495 ± 10	500 ± 10[f]
HE ESA (nm)	560 ± 10	560 ± 10	c)	580 ± 10
LE ESA (nm)	587 ± 10	596 ± 10	597 ± 10	630 ± 10
Dielectric Constant[d]	35.95	12.01	2.28	2.30

a) All transient absorption spectra were obtained at room temperature (22°C).
b) HE and LE refer to high energy and low energy components of the ESA, respectively.
c) The ESA blue shifted (with respect to what was observed in the other two solvents) and no high energy ESA was resolved when benzene was the solvent.
d) Data was obtained from Reference 17.
e) The rate constant was not obtained since the transient absorbance did not change sufficiently during the time of observation.
f) The spike at 532 nm due to the green laser pulse makes the bleach maximum difficult to see.

There are three characteristic features which can be found in each spectrum. In all, the ground state band is bleached within 20 ps and recovers subsequently. Two initial ESA maxima are identified by a "higher" energy and "lower" energy band maximum wavelength. The decay yields, within approximately 1 ns (Table 4.4), a longer lived residual absorption with a single band still seen at 5 ns but, as seen in the nanosecond spectra, decays completely shortly after 8 ns.

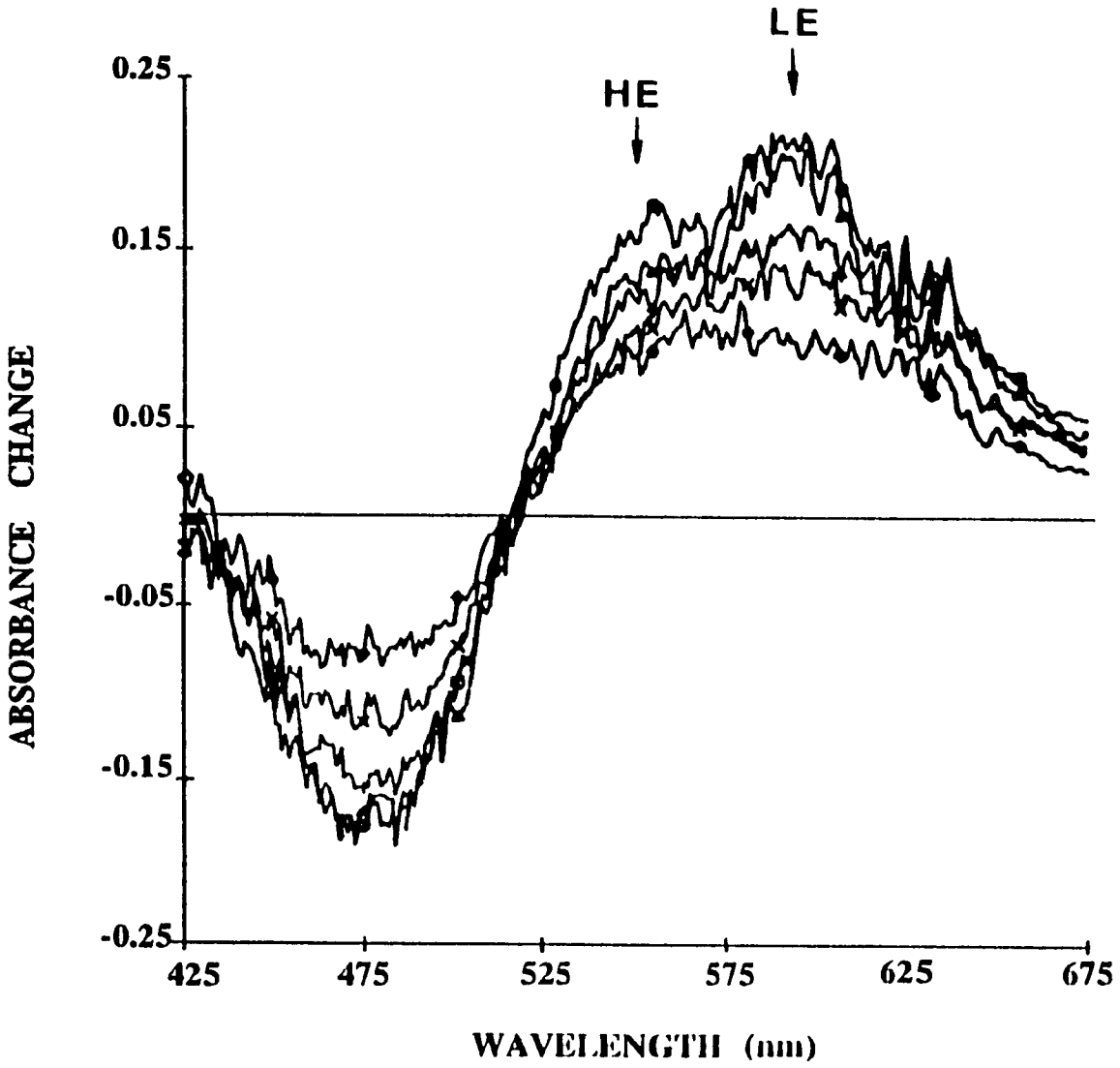

Figure 4.8. Picosecond absorption spectra of $W(CO)_4(phen)$ in neat pyridine using 355 nm excitation recorded at probe delays of 50 and 500 ps and at 1, 2 and 5 ns in order of decreasing absorbance change. The arrows indicate the "high energy" (HE) and "low energy" (LE) components of the ESA. The pulse energy is 1.2 mJ.

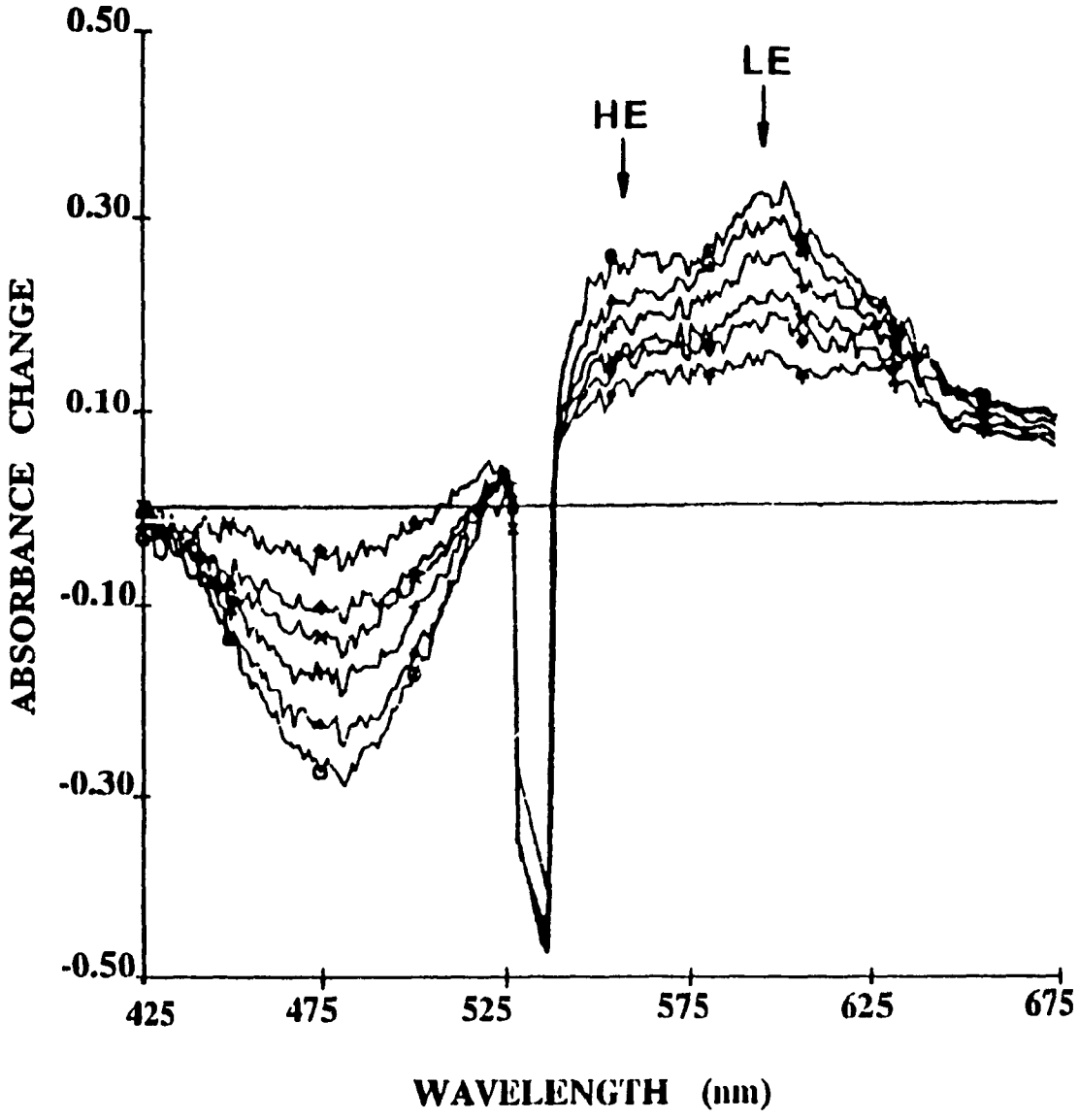

Figure 4.9. Picosecond absorption spectra of $W(CO)_4(phen)$ in neat pyridine using 532 nm excitation recorded at probe delays of 50 and 500 ps and at 1, 1.5, 2 and 5 ns in order of decreasing absorbance change. The arrows indicate the "high energy" (HE) and "low energy" (LE) components of the ESA. The pulse energy is 2.5 mJ.

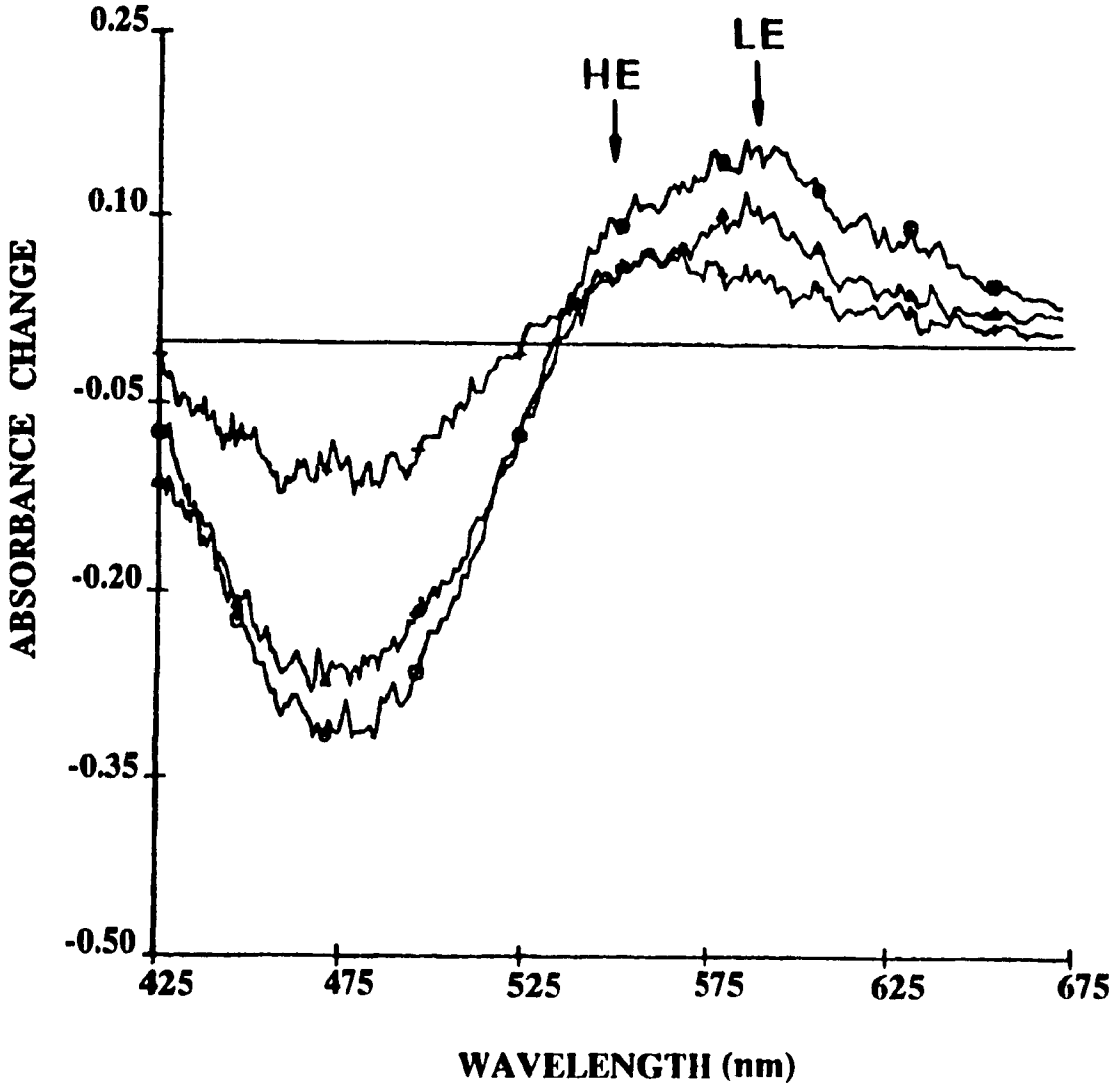

Figure 4.10. Picosecond absorption spectra of $W(CO)_4(phen)$ in dichloromethane using 355 nm excitation recorded at probe delays of 50 and 500 ps and at 5 ns in order of decreasing absorbance change. The arrows indicate the "high energy" (HE) and "low energy" (LE) components of the ESA. The pulse energy is 1.2 mJ.

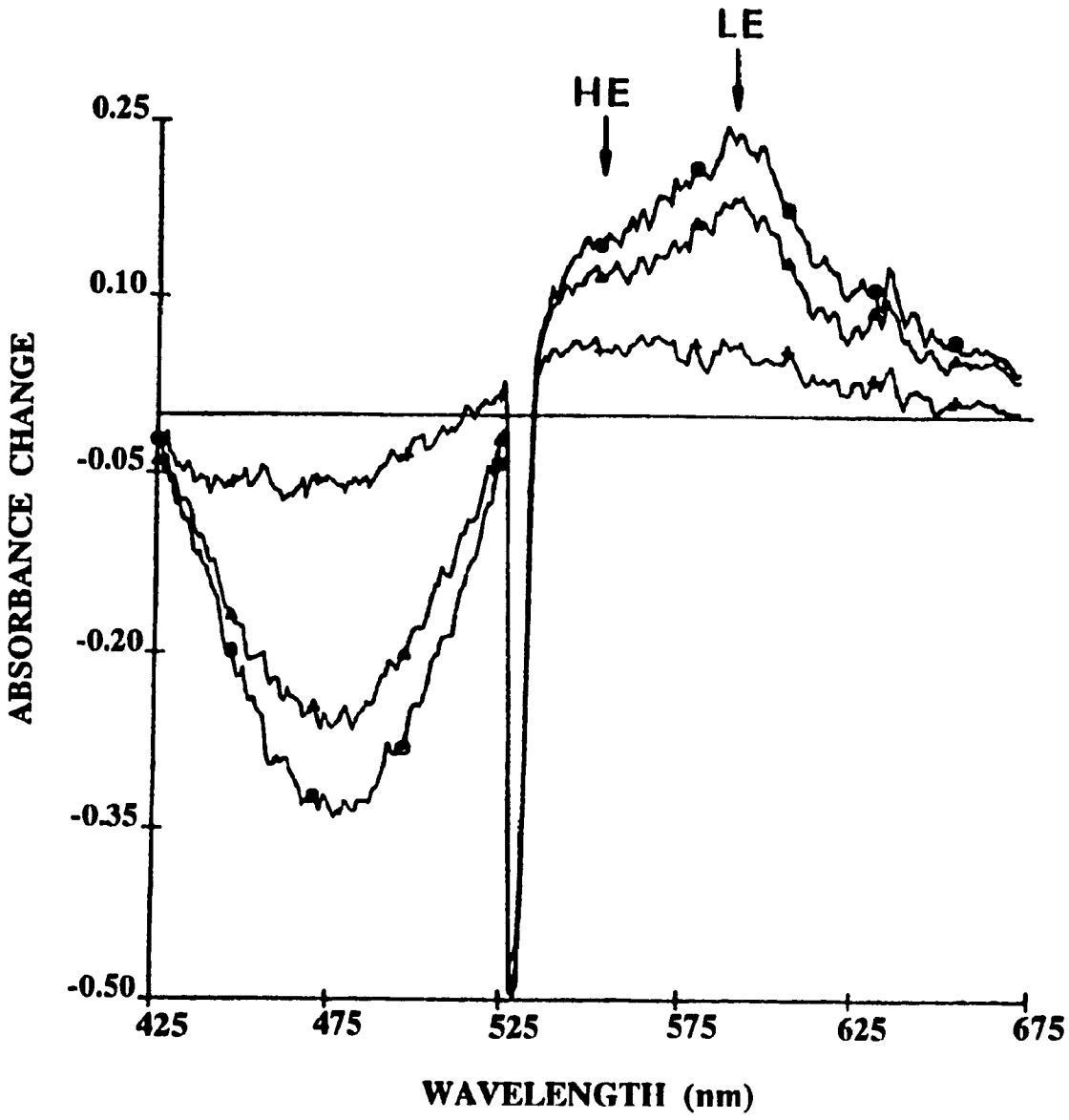

Figure 4.11. Picosecond absorption spectra of $W(CO)_4(phen)$ in neat dichloromethane using 532 nm excitation recorded at probe delays of 50 and 500 ps and at 5 ns in order of decreasing absorbance change. The arrows indicate the "high energy" (HE) and "low energy" (LE) components of the ESA. The pulse energy is 2.5 mJ.

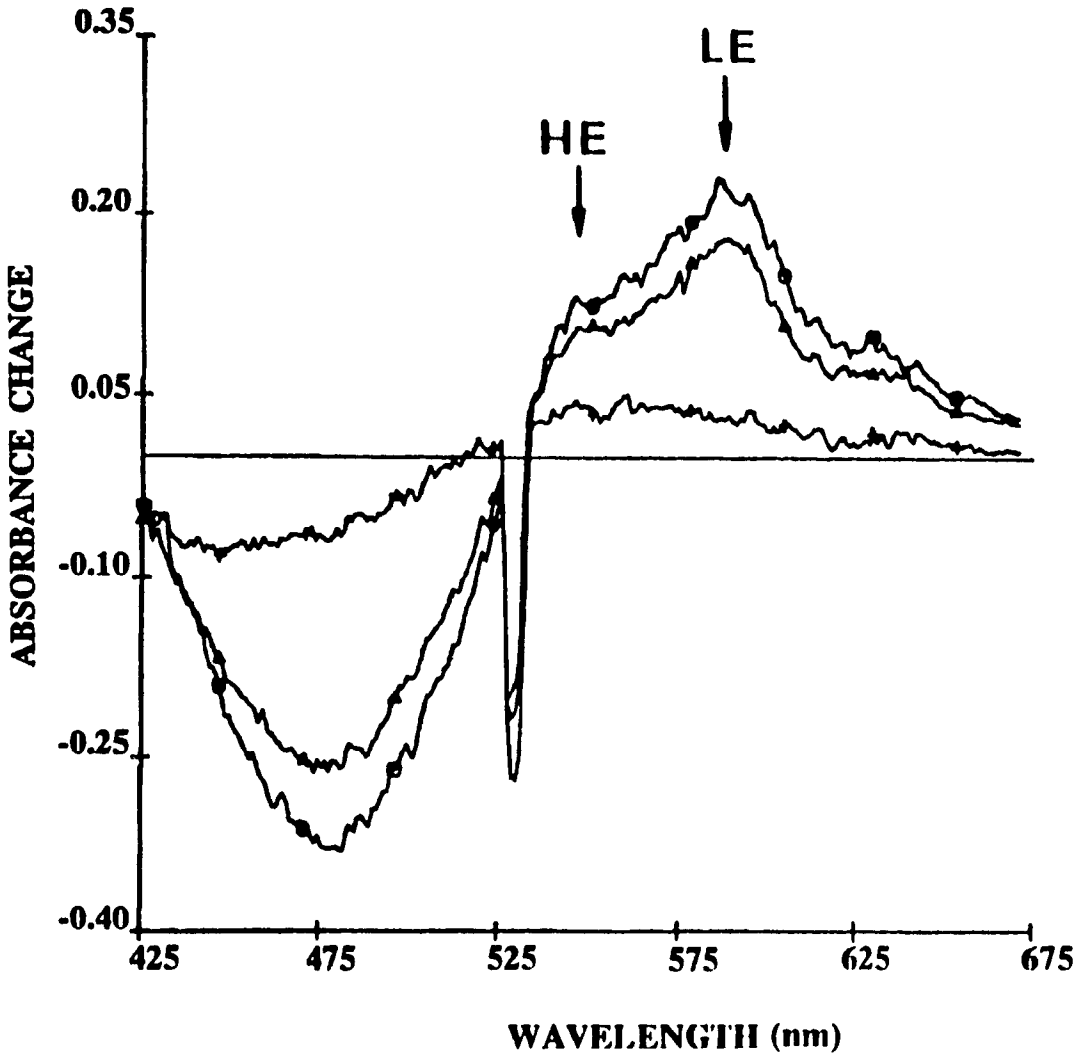

Figure 4.12. Picosecond absorption spectra of $W(CO)_4$(phen) in a solution of 0.3 M $(n\text{-}Bu)_3P$ in CH_2Cl_2 using 532 nm excitation recorded at probe delays of 50 and 500 ps and at 5 ns in order if decreasing absorbance change. The arrows indicate the "high energy" (HE) and "low energy" (LE) components of the ESA. The pulse energy is 2.5 mJ.

The general features of the ESA spectra under both 355 nm and 532 nm excitation are similar. However, quantitative examination reveals unequivocally that the initial (20 ps) contributions of the higher energy and the lower energy band maxima vary with excitation wavelength and solvent. This is most reliably demonstrated by calculation of the ratio of the absorbance change of the ESA band to the depth of the absorbance change minimum where the ground state is bleached. This is done simply by averaging the absorbance change for several wavelengths near the ESA band maximum and dividing by the corresponding average absorbance change near the bleach minimum. By doing this, any effects due to pulse intensity variation are eliminated, thereby rendering the comparison of all ESA spectra reliable and exhibiting the subtle differences between them. The results are summarized in Appendix D. The two components (higher and lower energy) form in different ratios at the two excitation wavelengths and decay with distinguishable solvent dependent rates. Thus it is clear that ESA is observed for two distinct excited states which are both fully formed at 20 ps and which are formed in different ratios under different irradiation wavelengths. Again, evidence is seen for a decisive influence of early events prior to 20 ps.

In all cases, bleach recovery follows biexponential kinetics, the faster component being comparable with the decay rate constant of the faster part of the transient absorption (See Tables 4.2 and 4.3). As in the ESA, the longer-lived component of the bleached ground state absorption is still present at 5 ns. The observed ESA extends into the blue region, over the same area as the bleach (475 nm). This is concluded because the absorbance change for the bleach (475 nm) is approximately -0.3 whereas the ground

state spectrum has an absorbance of 0.9 at 475 nm when pyridine is the solvent. That is, not "enough" bleaching occurs for there to be no ESA at the bleach minimum.

4.6. Assignment of ESA

The low overall quantum yields for substitution allow for the elimination of the possibility that primary photoproducts account for the transients observed at 20 ps. Because the quantum yield is so low under both LF and MLCT excitation, it is not expected that solvato species, a possible precursor to the photoproduct, will give a resolvable transient in comparison to the observed ESA absorbancies. Further evidence that the transient absorption is not due to the solvato species is the observation that very similar transients are formed in both coordinating (THF, CH_3CN, pyridine) and non-coordinating (CH_2Cl_2, benzene) solvents. Only a very small negative solvatochromism is observed in the transient absorption spectra. It is unlikely that a LF excited state would show any noticeable solvatochromism whereas a ligand-localized electron in a MLCT state is likely to interact with the solvent leading to some solvatochromism in its further excitation. Therefore, the transients are assigned to MLCT states. More direct evidence for this assignment is obtained from the results of spectroelectrochemical experiments (Figure 4.13). The spectrum of the reduced $[W(CO)_4(phen)]^-$ complex is very similar to the spectrum of an uncoordinated radical-anion of the ligand ($phen^-$) (Figure 4.13, inset), indicating that the extra electron is ligand-localized in the reduced complexes which thus can be formulated as a $W(CO)_4(phen^-)$ species. These bands are of similar shape and in the same region as the ESA for $W(CO)_4(phen)$ in the same

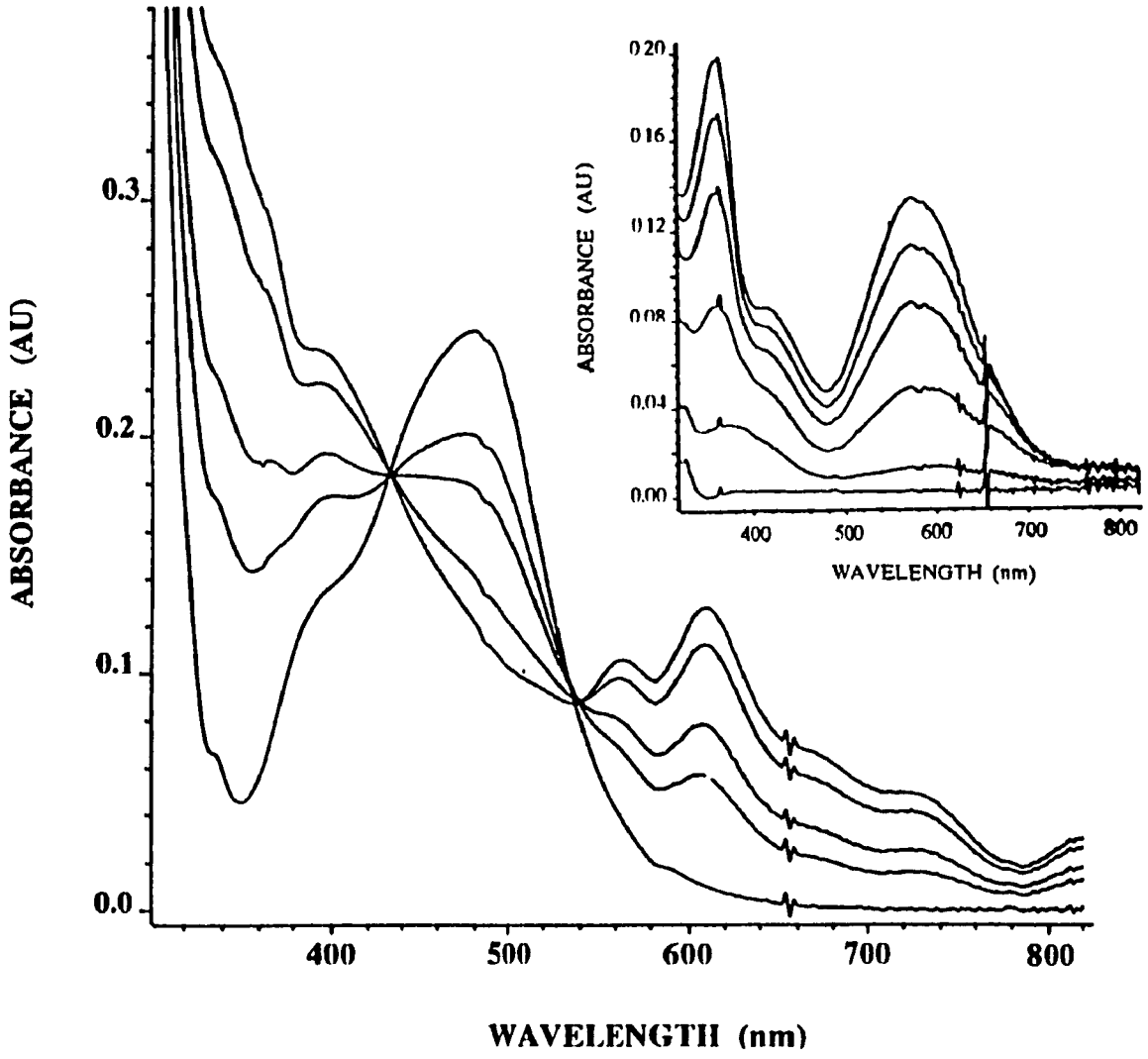

Figure 4.13. Spectroelectrochemical reaction of $W(CO)_4(phen)$ in THF solution containing 0.1 M $(n\text{-}Bu)_4NPF_6$. The spectra displayed in the inset show the reduction of the free phen ligand. Notice the similarity between the band due to the free phen ligand (inset) and the new band growing in at 600 nm. This indicates that upon reduction, the electron is ligand-localized. The reduced complex can be formulated as $[W^I(CO)_4(phen^{\cdot})]$.

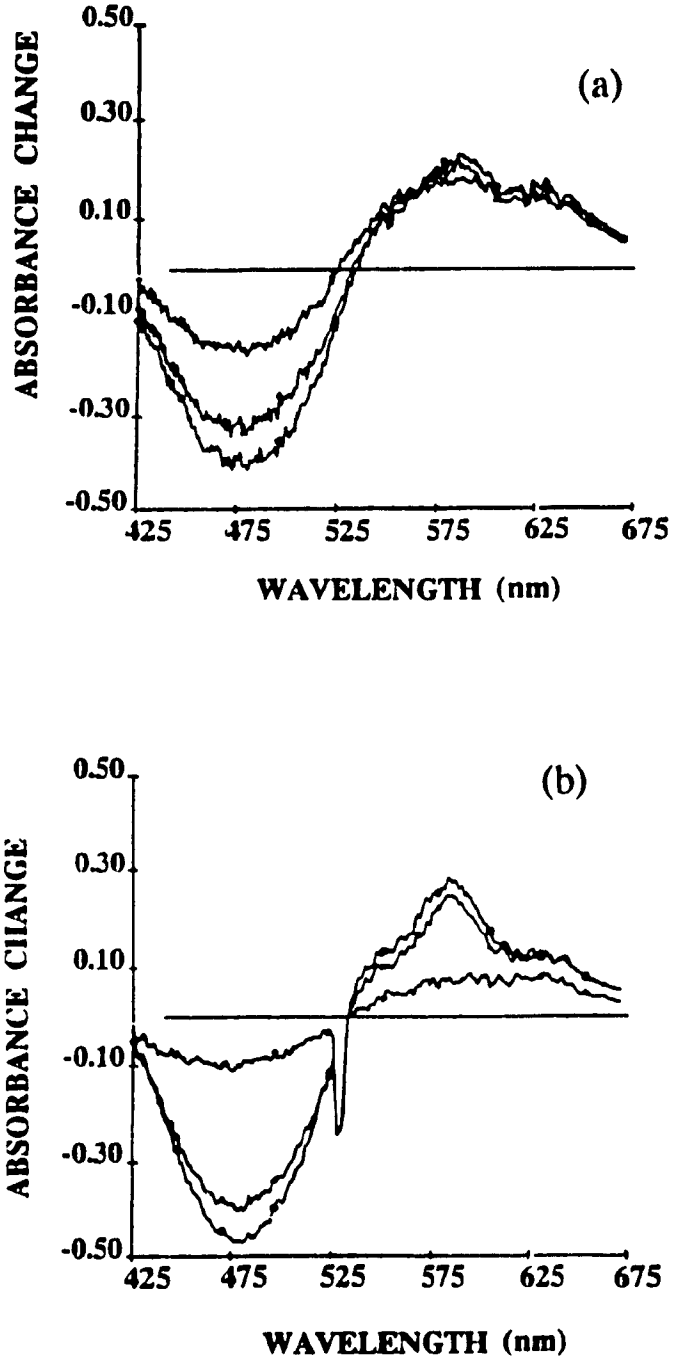

Figure 4.14. Picosecond absorption spectra of $W(CO)_4(phen)$ in neat THF using 355 nm (a) and 532 nm (b) excitation recorded at probe delays of 50 and 500 ps and at 5 ns in order of decreasing absorbance change. The pulse energy is 1.2 and 2.5 mJ for 355 and 532 nm excitation, respectively.

solvent (Figure 4.14). This supports the assignment of the transients as MLCT states which may be viewed as $[W^{I}(CO)_4(phen^{\cdot})]$. Hence, the ESA is assigned as an essentially π ---> π^* transition of the reduced phen$^{\cdot}$ ligand of MLCT excited $W(CO)_4(phen)$. Analogous qualitative correspondence between the ESA spectrum of an MLCT excited state and a spectrum of a one-electron reduced species was observed[18] for $Ru(bipy)_3^{2+}$. In conclusion, the observed transient is most likely a combination of a short lived MLCT excited state (the sharper peak on the low energy side of the transient absorption which rapidly decays; τ = 1.1 ns) and another longer lived MLCT excited state (the broad band which persists at 5 ns). Most probably, these states are members of the MLCT<1> manifold whose presence was inferred[3] from emission spectra of the closely related $W(CO)_4$(4-Me-phen) complex. According to this emission study[3], these individual ^{3}MLCT states are less than 1000cm^{-1} apart. This energy difference is comparable with that between the short-lived (~ 1 ns) and long-lived (~ 5 ns) ESA transients. The observed excited state dynamics occurring between 20 ps and 5 ns may then be viewed as an equilibration[3] of the MLCT<1> excited state manifold.

Observation of ESA due to MLCT states even after excitation at 355 nm indicates that those LF excited states which do not undergo CO dissociation (fraction > 0.98) can relax to an MLCT state(s). This LF ---> MLCT conversion efficiently competes with the CO dissociation from the LF states, limiting the quantum yield observed at 355 nm to about 0.02. Note that the states reached promptly, i.e. in competition with the sub-picosecond CO dissociation from the LF state, are similar to those generated by 532 nm MLCT excitation. This interpretation of the transient absorption spectra fully agrees with

the presence of a minor associative photochemical pathway in addition to the dissociative pathway which operates on LF excitation as was established by the quantum yield measurements. If CO dissociation is a sub-picosecond process[19], it would seem that LF --> MLCT conversion is similarly rapid.

4.7. A Model for the Associative Photochemistry

The prompt appearance of the ESA (< 20 ps) and the similarity in coordinating and non-coordinating solvents suggest that the events initiating the associative pathway (i.e. formation of the *reactive* MLCT state) occur on the same short time scale as those controlling CO dissociation from the LF state. This idea is reinforced by the observed wavelength dependence. In this context, the response of the steady state yield to changes of nucleophile does not suggest prompt formation of a 7-coordinate species incorporating the entering ligand.

In order for the ligand substitution to occur, the incoming ligand must be in encounter with $W(CO)_4$(phen) for a reaction to occur. The first step of the process therefore must be the formation of an encounter complex:

$$A + B \overset{K_E}{\rightleftharpoons} \{E\} \qquad (4.3)$$

where A and B are $W(CO)_4$(phen) and (n-Bu)$_3$P or pyridine, respectively, E the encounter complex, and K_E the equilibrium constant (M^{-1}) for the encounter complex. By definition,

$$K_E = \frac{\{E\}}{[A][B]} \tag{4.4}$$

The Fuoss-Eigen[20] equation (4.5) can be used to estimate the equilibrium constant for the formation of the encounter complex.

$$K_E = \frac{4\pi}{3} a^3 N_A e^{-\frac{V}{kT}} \tag{4.5}$$

where a is the distance of closest approach (estimated as 5×10^{-9} dm), V the electrostatic potential energy at that distance, N_A Avogadro's number, k the Boltzmann constant, and T the temperature. Consequently, for neutral species such as $W(CO)_4$(phen), pyridine, and (n-Bu)$_3$P, V = 0 and the equation reduces to:

$$K_E = \frac{4\pi}{3} a^3 N_A \tag{4.6}$$

From this is evident that the equilibrium constant for encounter complex formation is 0.32 M^{-1}. Since the concentration of (n-Bu)$_3$P is known (0.36 M), Equation (4.4) can be used to estimate that 12% of the $W(CO)_4$(phen) molecules are in encounter with a phosphine molecule at the time of excitation (and in the first nanosecond after). In neat pyridine, where all complexes excited are in encounter with a potential ligand, the observed yield is smaller than that for 0.36 M (n-Bu)$_3$P. At this concentration of (n-Bu)$_3$P, we are therefore *not* near the limit as was postulated above in Section 4.3 and

another explanation must be provided. This explanation lies in the interpretation of the events which occur along the associative pathway. That is, this pathway must involve *bimolecular attack by a nucleophile on a suitable vibrationally excited state.* Alternatively, a relaxed intermediate could be involved.

In pyridine, where all excited states are in encounter with the nucleophile, the kinetics of attack reduce to first order. This is because in pyridine, the solvent is itself a reactant, and all of the $W(CO)_4$(phen) is "associated" (in encounter) at the instant of excitation. Therefore no corrections for the preequilibrium are necessary. If it is assumed that nucleophilic attack and relaxation to the ground state are competing paths of the excited state, the quantum yield of ~ 0.003, if the reaction is with an excited state which decays at about 1×10^9 s^{-1} (i.e. $\tau = 1 \times 10^{-9}$ s), implies an attack rate constant of about 3×10^6 s^{-1}. It thus follows that if the longer lived state is assumed to be reactive, the rate constant would be one order of magnitude smaller. However, a preequilibrium must be considered in the presence of $(n\text{-Bu})_3P$. Since the fraction of $W(CO)_4$(phen) bound in the encounter complex is 0.12, the corresponding phosphine rate constant is about 2×10^7 s^{-1} (i.e. 3×10^6 $s^{-1}/0.12$). Thus, the associative pathway appears to arise in two stages. First, an excited state (or primary intermediate) which is susceptible to facile nucleophilic attack is formed rapidly (< 20 ps). After this step, the species relaxes and reacts with nucleophiles in competition with its nanosecond relaxation back to the ground state. Beyond this statement lies only speculation but some of the speculation is useful in illustrating clearly how the system acquires its sensitivity to nucleophilic attack which is at least ten orders of magnitude greater than the susceptibility of the ground state.

After all, the remarkable accelerations which some pathways experience in excited states has not often been given concrete explanation and even first steps in this direction may fruitfully suggest new experimentation.

Staal *et al* have shown, using resonance Raman (rR) spectroscopy[21], that the $Mo(CO)_4$ moiety in $Mo(CO)_4$(*i*-Pr DAB) (*i*-Pr DAB = $C_{10}H_{16}N_2$) changes from C_{2v} microsymmetry to C_{4v} microsymmetry upon cooling. Clearly such a distortion is not blocked by a high barrier. If it is true that an excited $W(CO)_4$(phen) can also undergo a distortion, this excited state can become more favourable for attack by a nucleophile on the W atom leading to a capped octahedron, a 7-coordinate species. A plausible diagram describing this distortion is shown in Figure 4.15.

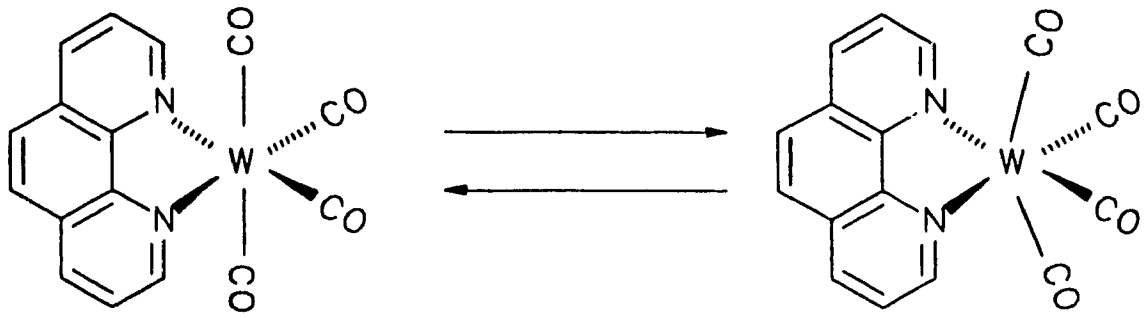

Figure 4.15. Pictorial diagram illustrating the possible conformational change of the $W(CO)_4$(phen) molecule following excitation.

The rate constants calculated above require a specific MLCT species lacking a high barrier to nucleophilic attack. Two other important factors contribute to the reduction

of the barrier for all of the MLCT states. First, the MLCT state has W in the 1+ formal oxidation state[22]. Furthermore, Stufkens *et al* believe that an unrelaxed MLCT is more "+1" than a relaxed MLCT state[23]. As well, the configuration at the metal is d^5 not d^6. Both factors should considerably facilitate nucleophilic attack. These are general factors and the conformational effect or some similar mechanism must select the particular state responsible for reaction.

4.8. Associative vs Dissociative Pathway

The presence of two different photosubstitution pathways emphasizes the important question of why differences between the photochemistry of the LF and MLCT states should arise in these prompt processes. Since it is argued that key events determining the relative efficiency of the partition between the associative, dissociative, and non-reactive relaxation pathways are very fast steps in the domain of breakdown of the Born-Oppenheimer approximation[24,25], it is interesting to see whether the Hollebone octupole selection rule[26] ($\Delta J + \Delta V = \Delta L + \Delta S + \Delta V = 3$; Section 1.5; Page 17) can provide an explanation for the dissociative reaction from a LF state and associative reaction from an MLCT state.

According to the Tanabe-Sugano diagram for d^6 systems (Figure 1.7), the two possible LF transitions for $W(CO)_4(phen)$, if approximated as an octahedral system, are: $^1T_1(I) \leftarrow {}^1A_1(I)$ and $^3T_1(P) \leftarrow {}^1A_1(I)$. These correspond to a ΔV of 3 and 1, respectively. The vibration of the octahedron associated with the triplet excited state and corresponding to $\Delta V = 1$ is the asymmetric stretch (Figure 1.8a; Page 21). In this

mode, there is substantial extension along one axis, hence the ligand on that axis should be susceptible to substitution via a square pyramid intermediate. The singlet excited state ($\Delta V = 3$) is associated with a buckling mode of vibration as shown in Figure 1.8b (Page 21). This mode is expected to be very reactive toward substitution via a non-selective path because the metal is highly exposed to solvating molecules on four octahedral faces above the x,y plane. Hence, loss of CO is expected upon excitation into the singlet LF state. Such variation in selectivity has been observed in $W(CO)_5L$ (L = pyridine, piperidine)[27,28]. If the time scale of the dissociation is fast, as in the case of $W(CO)_6$, dissociation of a CO molecule is the most likely consequence of 355 nm irradiation.

Spin allowed CT bands with electric dipole character[6] have $\Delta V = 2$ (Section 1.5). The vibration associated with a $\Delta V = 2$ is the υ_2 mode in octahedral geometry (Figure 1.8c; Page 21). This υ_2 mode reflects the requirement to put at least two atoms into motion to maintain gerade structure, thus there is low probability of prompt dissociative response. A schematic representation of the consequence of a $\Delta V = 2$ vibration is given in Figure 4.15. From this, it can be seen that the main result of such a vibration is an opening of the faces of the octahedron, a prerequisite for the formation of a 7-coordinated associative intermediate.

This analysis suggests the presence of two distinct reaction pathways for the reaction of $W(CO)_4$(phen). The observation of a dissociative pathway upon excitation into the LF singlet is predicted by the excitation of either $\Delta V = 1$ or 3 t_{1u} vibrations. An associative pathway upon MLCT irradiation is consistent with the prediction of excitation of a $\Delta V = 2$ vibration, leading to a *conformational rearrangement* which

makes the molecule more susceptible to nucleophilic attack.

4.9. Conclusions

The photosubstitution of CO in $W(CO)_4$(phen) is a complex process dependent on both the nature of the solvent and on the wavelength of irradiation. Excitation into the LF bands leads to the substitution of a CO molecule via two pathways: a dissociative pathway which is accompanied by a smaller contribution from an associative pathway.

Excitation into the MLCT bands induces CO substitution via an associative pathway. The quantum yield *increases* with decreasing excitation energy across the MLCT band envelope in halogenated solvents, but varies marginally in toluene and pyridine thus indicating that the wavelength and solvent dependencies are coupled. Therefore, the partition between the various relaxation channels must be decisively influenced by events occurring in competition with vibrational relaxation.

Picosecond spectroscopy reveals that identical excited states (MLCT) are produced under LF and MLCT excitation. In both cases, the ESA has two distinct components which undergo rapid equilibration ($\tau \sim 1$ ns): a short lived MLCT state and another MLCT excited state that is longer lived. It can thus be concluded that MLCT states play an important role in the substitutional reactivity of $W(CO)_4$(phen). The population of the reactive MLCT states from LF states must be competitive with the sub-picosecond CO dissociation from the LF state and with relaxation to the ground state.

Furthermore, it has been shown that the reactivity of this complex can be predicted using the Hollebone rules. Upon LF excitation, this complex undergoes a

distortion of one of the W-CO bonds which leads to CO loss via a dissociative pathway. MLCT excitation, on the other hand, excites a different vibration which leads to the opening of one of the faces on the octahedron, a prerequisite for the formation of a 7-coordinated associative intermediate. The two geometries of the excited state (i.e. distorted and non-distorted octahedron) correspond to the ESA seen in the picosecond spectra. These rules have now given fruitful insight into the reactivity of $W(CO)_4$(phen) in addition to two other d^6 systems ($W(CO)_5L$; L = piperidine, pyridine[3,27,28] and the complex[29] $[Co(NH_3)_5X]^{2+}$; X = halogen). Thus, the combination of experimental evidence acquired using picosecond laser flash photolysis in conjunction with both solvent and wavelength dependence of the quantum yields and predictions made by Hollebone theory provide a powerful means by which to address complex mechanistic questions. It remains a matter of considerable interest to see how widespread are the predictive successes in elucidating short time behaviour of more complex systems.

4.10. References

1. Langford, C.H.; Moralejo, C.; Sharma, D.K. *Inorg. Chim. Acta.* **1987**, *126*, L11.

2. Lee, M.; Harris, C.B. *J. Am. Chem. Soc.* **1989**, *111*, 8963.

3. a) Moralejo, C.; Langford, C.H.; Sharma, D.K. *Inorg. Chem.*, **1989**, *28*, 2205.

   b) Langford, C.H.; Moralejo, C.; Lindsay, E.; Sharma, D.K. *Coordination Chemistry Reviews* **1991**, *111*, 337.

4. Van Dijk, H.K. Servaas, P.C.; Stufkens, D.J.; Oskam, A.; *Inorg. Chim. Acta* **1985**, *104*, 179.

5. Weiland, S.; Reddy, K.B.; van Eldik, R. *Organometallics* **1990**, *9*, 1802-1806.

6. Rawlins, K.A.; Lees, A.J. *Inorg. Chem.* **1989**, *28*, 2154-2160.

7. Manuta, D.M.; Lees, A.J. *Inorg. Chem.* **1983**, *22*, 3825.

8. Manuta, D.M.; Lees, A.J. *Inorg. Chem.* **1986**, *25*, 3212.

9. a) Dance, I.G.; Miller, T.R. *J. Chem. Soc., Chem. Commun.*, **1973**, 433.

   b) Miller, T.R.; Dance, I.G. *J. Am. Chem. Soc.* **1973**, *95*, 96.

10. Renk, I.W.; tom Dieck, H. *Chem. Ber.* **1972**, *105*, 1403.

11. Servaas, P.C.; van Dijk, H.K.; Snoeck, T.L.; Stufkens, D.J.; Oskam, A. *Inorg. Chem.* **1985**, *24*, 4494.

12. Manuta, D.M.; Lees, A.J. *Inorg. Chem.* **1986**, *25*, 1354.

13. Balk, R.W.; Stufkens, D.J.; Oskam, A. *Inorg. Chim. Acta*, **1978**, *28*, 133.

14. Langford, C.H. *Acc. Chem. Res.* **1984**, *17*, 96.

15. Elsaesser, T.; Kaiser, W. *Ann. Rev. Phys. Chem.* **1991**, *42*, 83.

16. Riddick, J. A.; Bunger, W. B.; Sakano, T. K. in *Techniques of Chemistry, Vol. II, Organic Solvents Physical Properties and Methods of Purification*, 4th edition; John Wiley and Sons, Inc.: U.S.A., 1986, pp.372,373.

17. Nonaqueous Electrolyte Handbook, Vol.1, Janz, Tomkins, Academic Press, Inc., 1972, N.Y.

18. Braterman, P.S.; Harriman, A.; Heath, G.A.; Yellowlees, L.J. *J.C.S. Dalton Trans.* **1983**, 1801.

19. a) Joly, A.G.; Nelson, K.A. *Chemical Physics* **1991**, *152*, 69.

    b) Joly, A.G.; Nelson, K.A. *J. Phys. Chem.* **1989**, *93*, 2876.

20. Shriver, D.F.; Atkins, P.W..; Langford, C.H. in *Inorganic Chemistry*, Oxford University Press, Great Britain, 1990, p. 479.

21. Staal, L.H.; Terpstra, A.; Stufkens, D.J. *Inorg. Chim. Acta.* **1974**, *34*, 97.

22. Perng, J.H.; Zink, J. *Inorg. Chem.*, **1990**, *29*, 1158.

23. Stufkens, D.J. *Private communication.*

24. a) Repinec, S.T.; Sension, R.J.; Szarka, A.Z.; Hochstrasser, R.M.; *J. Phys. Chem.* **1991**, *95*, 10380.

    b) Sension, R.J.; Repinec, S.T.; Hochstrasser, R.M.; *J. Chem. Phys.* **1990**, *93*, 9185.

25. a) Schoenlein, R.W.; Peteanu, L.A.; Mathies, R.A.; Shank, C.V.; *Science* **1991**, *254*, 412.

    b) Tallent, J.R.; Hyde, E.W.; Findsen, L.A.; Fox, G.C.; Birge, R.R.; *J. Am. Chem. Soc.* **1992**, *114*, 1581.

26. Hollebone, B.R.; Langford, C.H.; Serpone, N. *Coord. Chem. Rev.* **1981**, *39*, 181.

27. a) Moralejo, C.; Langford, C.H. *Journal of Photochemistry and Photobiology A: Chemistry* **1991**, *59*, 285.

    b) Moralejo, C.; Langford, C.H.; Sharma, D.K.; *Inorganic Chemistry* **1989**, *28*, 2205.

28. Moralejo, C. Ph.D Thesis, Concordia University, 1989.

29. Malkhasian, A.Y.S.; Langford, C.H. *J. Am. Chem. Soc.* **1987**, *109*, 2682.

5. Early Excited State Dynamics of $W(CO)_5$(4-NC-Pyridine) and $W(CO)_5$(4-Formyl-Pyridine)

5.1. Background

Metal-to-ligand charge transfer, MLCT, excited states are best known for electron-transfer reactivity. However, they have also been implicated in other chemical processes which involve bond activation. For example, a CO ligand was found[1] to dissociate promptly from the spin-singlet MLCT state of $Cr(CO)_4$(bpy) leading to CO-substitution[2-4] via a dissociative pathway. The analogous tungsten complex, $W(CO)_4$(phen), undergoes associative substitution of the CO[4,5] ligand from its MLCT states which are apparently populated on a sub-picosecond timescale (Chapter 4 and Reference 6).

As in these tetracarbonyls, MLCT states are the lowest lying excited states in $W(CO)_5$(4-X-Pyridine) complexes where X is an electron withdrawing substituent (e.g. a cyano, formyl, benzoyl, or acetyl group)[7]. Recent research[7-13] on these compounds has focused on the mechanism of reaction and the nature of the excited states involved. Pressure dependence studies[11] have suggested that substitution of the pyridine ligand follows a dissociative mechanism upon both ligand field, LF, and MLCT excitations thus suggesting a different type of reactivity than what was observed in $W(CO)_4$(phen). However, a similarity to the tetracarbonyl complex lies in the observation of multiple luminescence[8] for $W(CO)_5$(4-NC-Pyridine), a phenomenon which implies rather unusual photophysics. Thus, there is a remarkable resemblance to what is observed for the excited states in the tetracarbonyl analogues. However, despite all of this work, little is known about the processes that populate the reactive states and that are thus responsible

for selection of the photoreactive pathway. In order to learn more about the behaviour of MLCT states in the early stages of reaction, we have investigated the picosecond time resolved absorption spectra of $W(CO)_5$(4-NC-Pyridine) and $W(CO)_5$(4-Formyl-Pyridine) following excitations into their LF and MLCT absorption bands. In order to interpret the time resolved spectra, it is advantageous to first have a clear understanding of the steady state photochemistry of these complexes. This will be presented in Section 5.2.

5.2. Review of the Photochemistry of $W(CO)_5$(4-X-Pyridine); X = CN, Formyl

As mentioned above, MLCT states are the lowest lying excited states in these $W(CO)_5$(4-X-Pyridine) complexes[7]. In a temperature dependence study of the luminescent properties of $W(CO)_5$(4-NC-Py), Lees *et al* showed that this complex possesses two MLCT states[8]. These states correspond to long-lived (292 ns at room temperature) emissive ^{3}MLCT states and are separated by 990 cm^{-1}. They are in thermal equilibrium in fluid solution. Other $W(CO)_5$(4-X-Pyridine) complexes exhibit qualitatively similar behaviour[7,9]. Nanosecond time-resolved spectra reported previously[9,10] show that the lower ^{3}MLCT state is populated within 10 ns following the laser excitation (355 or 510nm) for all of the investigated $W(CO)_5$(4-X-Pyridine) complexes.

$W(CO)_5$(4-X-Pyridine) complexes undergo photosubstitution[7] of the pyridine ligand according to Equation 5.1.

$$W(CO)_5(\text{4-X-Pyridine}) + S \xrightarrow{h\nu} W(CO)_5S + \text{4-X-Pyridine} \qquad (5.1)$$

The quantum yield of this reaction is approximately 0.1 when the complexes are irradiated into the higher energy ligand-field, LF, absorption band[11] and drops to about 0.02 when the irradiation is into the MLCT absorption band[7,9,11,12] in the visible. The low lying MLCT states are clearly involved in the photosubstitution reaction (Equation 5.1) under direct MLCT excitation as both the phosphorescence and the reaction quantum yield are quenched by anthracene with identical quenching constants[9,14]. Moreover, the absorption spectrum of $W(CO)_5S$, the reaction product, appears between 150 ns and 5μs after MLCT excitation alongside the decay of the MLCT excited state spectrum[9,10]. The activation energy of this reaction is 2660 cm^{-1} for $W(CO)_5$(4-NC-Py) under MLCT excitation[9,12], is rather high for a direct substitution from the ^{3}MLCT state. It was thus suggested that a highly reactive, presumably ^{3}LF, state is thermally populated from the long-lived ^{3}MLCT states. Pressure dependence of the photochemical quantum yields strongly supports this mechanism[11]. Positive volumes of activation suggest a dissociative mechanism for both LF and MLCT excitations. Furthermore, apparent volumes of activation found for the substitution under MLCT excitation are larger than those measured for direct photosubstitution from LF states. Observed differences (4.3 and 1.8 cm^3mol^{-1} for 4-Acetyl-Pyridine and 4-NC-Pyridine, respectively)[11] correspond to the usual expansion of the molecule when going from the MLCT to the LF state[14].

It is thus obvious that the MLCT excited states in $W(CO)_5$(4-X-Pyridine) complexes do not possess a chemical reactivity of their own. In this way, the photobehavior of pentacarbonyl complexes strongly contrasts that of analogous tetracarbonyl-diimine complexes of group 6 metals[1-6]. However, the ^{3}MLCT state(s) are

of crucial importance for the photosubstitutional reactivity of $W(CO)_5$(4-X-Pyridine) complexes under visible irradiation. They act as a long-lived "excitation energy sink" from which another reactive excited state can be subsequently populated.

5.3. Band Assignments in the Electronic Spectra of $W(CO)_5$(4-X-Py); X = CN, Formyl

$W(CO)_5$(4-NC-Pyridine) and $W(CO)_5$(4-Formyl-Pyridine), hereafter abbreviated as $W(CO)_5$(4-NC-Py) and $W(CO)_5$(4-FM-Py), respectively, exhibit similar features in their electronic absorption spectra. The absorption spectra shown in Figure 5.1 reveal two distinct absorption maxima for each of the complexes in methylcyclohexane.

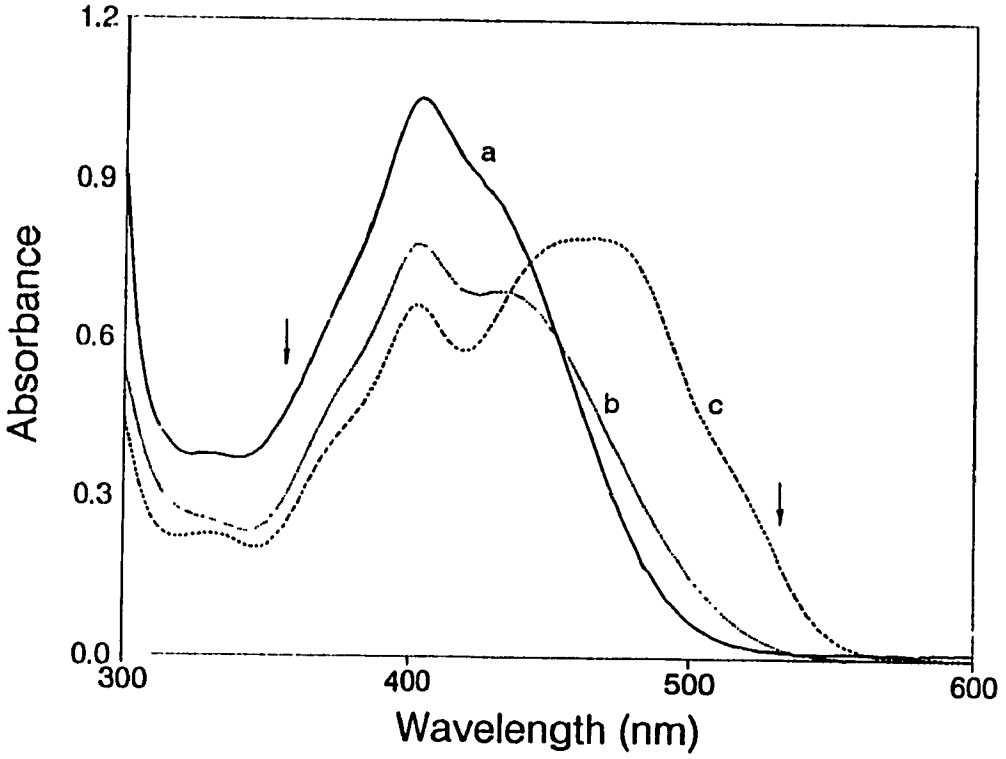

Figure 5.1. Electronic absorption spectra at 293 K of (a) $W(CO)_5$(4-NC-Py) (—) and (b) $W(CO)_5$(4-FM-Py) (---) in toluene, and (c) $W(CO)_5$(4-FM-Py) in methylcyclohexane (• • •). Fig. 5.1. The arrows indicate the area of the band irradiated during the picosecond flash photolysis measurements.

$W(CO)_5$(4-NC-Py) exhibits absorptions at 404 nm (ϵ = 7280 $M^{-1}cm^{-1}$) and 454 nm (ϵ = 8680 $M^{-1}cm^{-1}$), respectively[9]. In $W(CO)_5$(4-FM-Py), the bands occur at 402 nm (ϵ = 5990 $M^{-1}cm^{-1}$) and 470 nm (ϵ = 7640 $M^{-1}cm^{-1}$), respectively[9].

The two bands overlap in the spectra of toluene solutions of both complexes (Figure 5.1). $W(CO)_5$(4-NC-Py) shows a band with a maximum at 404 nm and a shoulder at 432 nm. For $W(CO)_5$(4-FM-Py), an almost identical spectrum (402 nm, 430 nm, sh) was observed. Comparison of these spectra to those recorded in methylcyclohexane (Figure 5.1) reveals that the low lying band exhibits negative solvatochromism (Section 4.2.1). Furthermore, this band undergoes a red shift as the substituent on the pyridine ligand becomes more electron withdrawing (i.e. as one moves from L = 4-NC-Py to L = 4-FM-Py). This indicates that this band possesses CT character. Lees and co-workers have shown that this band is composed of two MLCT states derived from $d_\pi(e)$ ---> π^*(Py) and $d_\pi(b_2)$ ---> π^*(Py) excitations[8] (the notations "e" and "b_2" refer to the symmetry of the d orbitals involved in the transition). The band at higher energy is essentially unshifted by variations in the solvent medium and hence must be LF in character. Wrighton *et al* have assigned this band to a LF $^1A_1(e^4b_2^2)$ ---> $^1E(e^3b_2^2a_1^1)$ transition[7].

5.4. Picosecond Absorption Spectroscopy

Transient absorption spectra of $W(CO)_5$(4-NC-Py) and $W(CO)_5$(4-FM-Py) were recorded between 0 ps (coincident with the excitation pulse) and 500 ps (5 ns for $W(CO)_5$(4-FM-Py) when toluene was the solvent) after the maximum of the excitation

pulse. Spectra observed following LF (355nm) and MLCT (532nm) excitations of $W(CO)_5$(4-FM-Py) in methylcyclohexane are presented in Figures 5.2 and 5.3, respectively.

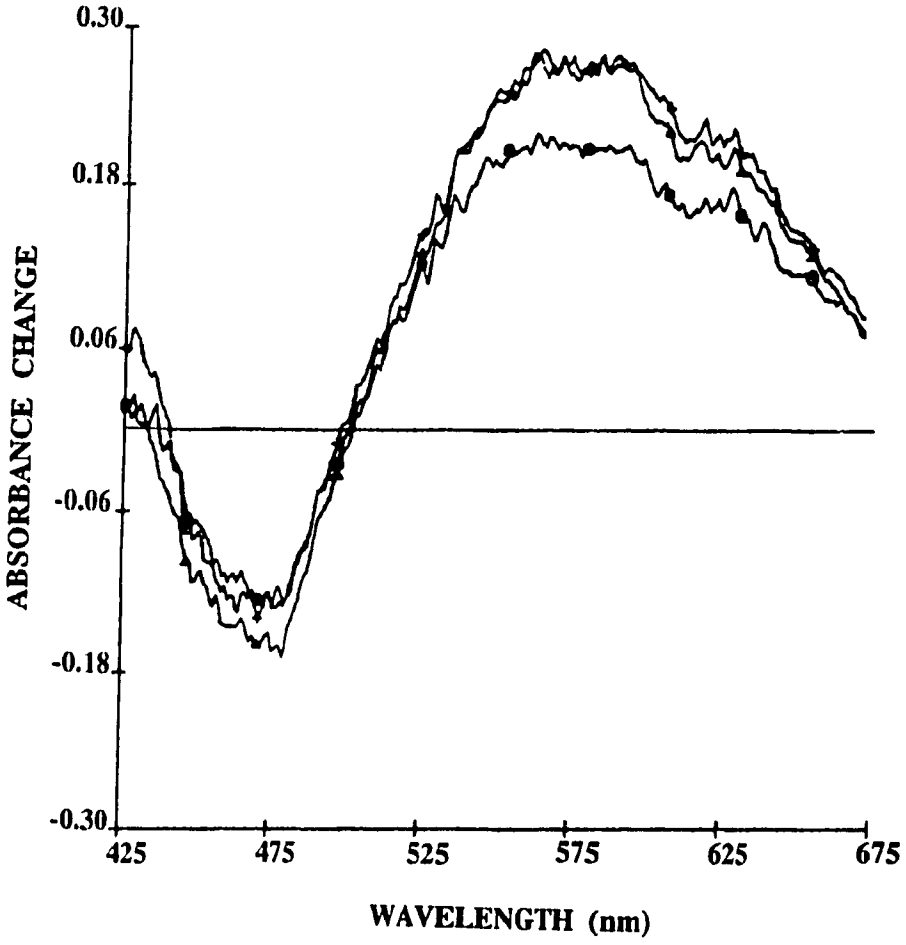

Figure 5.2. Transient absorption spectra of $W(CO)_5$(4-FM-Py) in neat methylcyclohexane using 355 nm excitation recorded at probe delays of 0, 40, and 500 ps in order of increasing absorbance change. The pulse energy was 1.2 mJ.

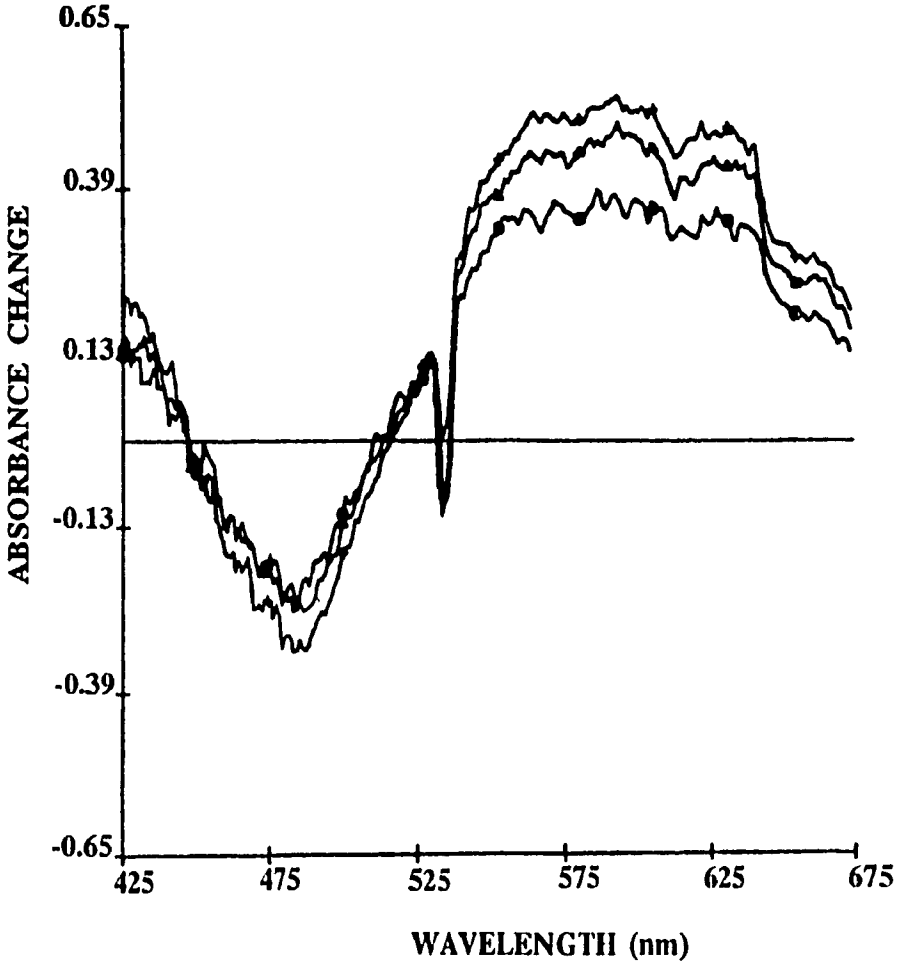

Figure 5.3. Transient absorption spectra of $W(CO)_5$(4-FM-Py) in neat methylcyclohexane using 532 nm excitation recorded at probe delays of 0, 40, and 80 ps in order of increasing absorbance change. The pulse energy was 2.5 mJ.

In both cases, the ground state absorption is bleached and strong excited state absorption in the visible spectral region is formed very rapidly, within the 30 ps width of the excitation pulse. The growth of absorption between 0 and 20 ps is expected for the formation of a long-lived transient as the sample is still being excited in this time

interval[15]. More importantly, a further small growth in absorbance was observed between 20 and 80 ps after the MLCT excitation at 532 nm. After 80 ps, the absorbance was constant. The spectrum obtained with LF (355nm) excitation revealed that the transient forms within the laser pulse as observed at time delays 0 and 20 ps. After 20 ps, the spectrum does not change.

Transient spectra of $W(CO)_5$(4-FM-Py) obtained in a toluene solution (Figure 5.4a) show that approximately 70% of the transient is formed within the excitation pulse. This was determined simply by taking the ratio of the delta absorbance values at t = 20 ps and t = 100 ps. However, a significant growth in intensity was observed between 20 and 100 ps with an apparent 36 ps lifetime followed by a small gradual decrease in absorbance (by about 22%) between 100 ps and 5 ns (Figure 5.4b).

Because of limited solubility and negligible absorbance at 532 nm, the transient spectra of $W(CO)_5$(4-NC-Py) were measured only in toluene solution using 355 nm excitation (i.e. into the LF absorption band). The spectra are shown in Figure 5.5. The formation of an intense broad transient absorption with a maximum at approximately 575 nm is 75% complete within the excitation pulse (this value was obtained in a similar manner as the 4-FM-Py complex as described above). Its formation is then completed between 20 and 100 ps with an apparent rate constant 2.5×10^{10} s^{-1} (i.e. with a 45 ps lifetime).

The intensity loss in the bleached ground state absorption is always much smaller than the initial absorbance before the excitation (1.8 for $W(CO)_5$(4-FM-Py) and 1.1 for $W(CO)_5$(4-NC-Py)) despite the fact that the number of photons in the laser pulse is more

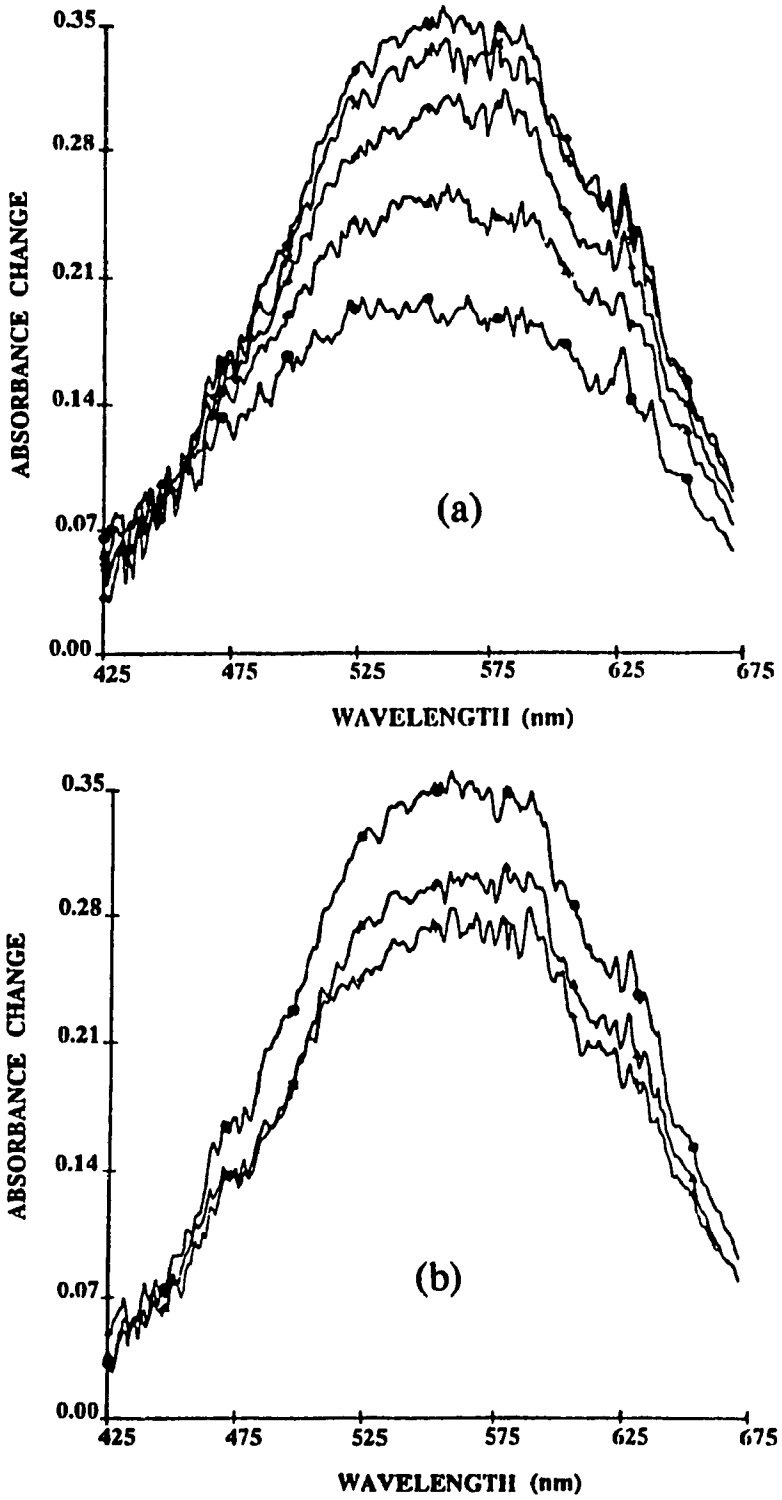

Figure 5.4. Transient absorption spectra of $W(CO)_5$(4-FM-Py) in neat toluene using 355 nm excitation recorded at probe delays of (a) 0, 20, 40, 80, and 100 ps and (b) 5 ns, 500 ps, and 100 ps in order of decreasing absorbance change. The pulse energy was 2.5 mJ.

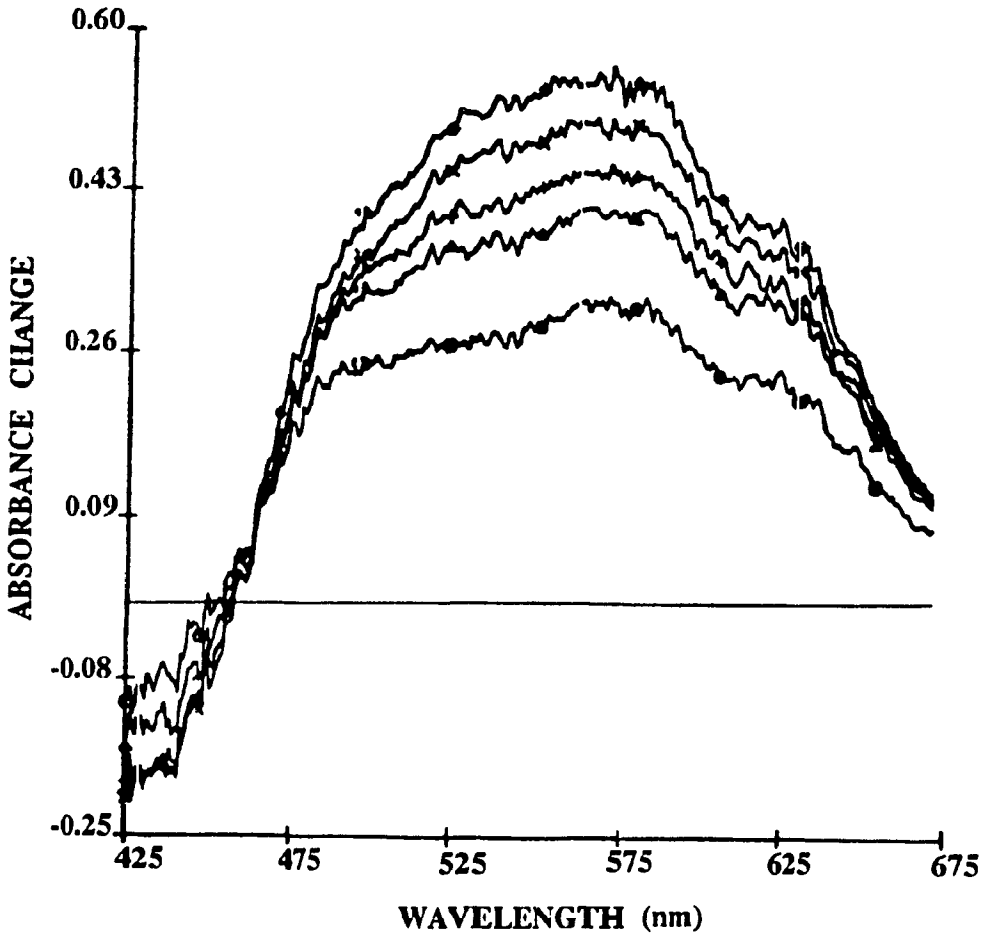

Figure 5.5. Transient absorption spectra of $W(CO)_5$(4-NC-Py) in neat toluene using 355 nm excitation recorded at probe delays of 0, 17, 40, 70 and 100 ps in order of increasing absorbance change. The pulse energy was 2.5 mJ.

than enough to excite all molecules in the irradiated zone of the sample. This observation indicates that the strong transient absorption extends into the blue and near-UV spectral region. Because of large ground state absorption of both samples, the transient spectra are inaccurate in the spectral region of the ground state absorption. No conclusions can thus be drawn from the temporal changes in the bleach region (note that

due to low extinction coefficients at the excitation wavelengths, the measurements could not have been performed in more dilute solutions).

5.5. Assignment of ESA

Picosecond absorption spectra of $W(CO)_5$(4-X-Py); X = CN, Formyl may be assigned to the lowest energy MLCT excited states. Direct evidence for this assignment is provided by the shape of the transient absorption band in that the shape of the absorption band observed for $W(CO)_5$(4-NC-Py) upon picosecond excitation resembles that previously found in the nanosecond transient spectrum[9]. It is not expected that the shape of the band for $W(CO)_5$(4-FM-Py) will differ significantly from that observed for $W(CO)_5$(4-NC-Py) since the ligand functions only to alter the location of the absorption maximum. This band is attributed to the ^{3}MLCT state[16]. Furthermore, its intensity does not decrease with time in accord with known 292 ns lifetime. Alternative assignments of the transient absorption band can easily be excluded. It is too long-lived for either LF or ^{1}MLCT states. The photochemically induced substitution reaction to form $W(CO)_5S$ occurs on a μs timescale[9,10] and the product spectrum[9] is very different from that observed in the picosecond spectra. Note that even though the picosecond spectrum of $W(CO)_5$(4-FM-Py) can also be assigned to the lowest MLCT excited state, the observation that it slowly decays in toluene but not in methylcyclohexane is in accord with the much shorter excited state lifetime previously[9] found in benzene compared with methylcyclohexane. However, our experiment suggests either a faster or a more complicated decay mechanism than that reported earlier[9].

5.6. Mechanism of Photophysical Deactivation

The time-independent shape of the picosecond absorption spectrum observed over the entire time range investigated (starting at 0 ps[15]) does not indicate vibrational relaxation or thermal equilibration of the ^{3}MLCT manifold on this timescale (these processes should be indicated by a blue-shift of the absorption band with increasing delays). However, it cannot be excluded that such subtle changes are obscured by the broadness of the transient absorption and by very strong bleaching of the ground state absorption band. However, the temporal changes observed are most probably due to the kinetics of the formation of a vibrationally cold ^{3}MLCT state by a ^{1}MLCT --> ^{3}MLCT or a ^{1}LF --> ^{3}MLCT intersystem crossing, ISC, under 532 nm or 355 nm excitation, respectively. The spectra show that population of the lowest ^{3}MLCT excited state follows a biphasic kinetics. The dominant component occurs within the excitation pulse whereas the slower minor component has lifetimes of approximately 36 ps and 45 ps for $W(CO)_5$(4-FM-Py) and $W(CO)_5$(4-NC-Py), respectively. The slower component manifests itself by an increase in the transient absorbance at time delays longer than 20 ps[15]. Only the fast component was observed under LF excitation of $W(CO)_5$(4-FM-Py) in methylcyclohexane but the slow component is more prominent in toluene (Figure 5.4). The slow component significantly contributes to the excited state dynamics of $W(CO)_5$(4-NC-Py) in toluene as well (Figure 5.5). It is important to note that the ^{3}MLCT is efficiently formed even under excitation into the LF transition. This observation agrees with earlier measurements[7] of quantum yields of the reaction induced by near UV excitation into the most reactive[17] ^{1}LF state. Their values significantly drop[7]

going from $W(CO)_5$(4-X-Py) complexes with lowest LF excited states to those which possess an MLCT lowest lying excited state where the LF --> MLCT relaxation pathway is available.

Picosecond absorption spectra together with known[7,10,18] quantum yields of the ^{3}MLCT formation allows the upper limit of the rate of the fast kinetic component of the ^{3}MLCT formation to be estimated. The extinction coefficient of the visible absorption band of the ^{3}MLCT excited state of $W(CO)_5$(4-NC-Py) was previously estimated[9] as $2.5x10^3$ $M^{-1}cm^{-1}$. From this value and observed picosecond absorbance values at 17 ps (i.e. within the pulse) and 100 ps (t_∞), the ratio of the concentration of the excited state formed within the pulse to that formed at completion can be estimated using the Beer-Lambert relationship:

$$C_{ex}(t) = \frac{\Delta A(t)}{\epsilon_{ex} \cdot l} \qquad (5.2)$$

where ϵ_{ex} is the extinction coefficient of the ^{3}MLCT excited state (previously estimated as $2.5x10^3$ $M^{-1}cm^{-1}$), l the pathlength (0.2 cm), $\Delta A(t)$ the value of the absorbance change at time t (Taken from Figure 5.5), and $C_{ex}(t)$ the concentration of the ^{3}MLCT state at time t. From this, it can be concluded that the conversion of the ground state $W(CO)_5$(4-NC-Py) complex into its ^{3}MLCT state is at least 70% complete within the 30 ps excitation pulse. Transient nanosecond infrared spectroscopy[10] was used to show that 50% of the ^{3}MLCT excited state relaxes to the ground state while the other 50% of it reacts via the LF state to form the photoproduct. Assuming that this is the only pathway

operating under visible irradiation and knowing that the photosubstitution quantum yield[7] for $W(CO)_5$(4-NC-Py) is 0.02, it is evident that the quantum yield of the ^{3}MLCT formation can be estimated[19] as 0.04. Given this low yield, we conclude that to convert 70% of the molecules present in the irradiated zone to the ^{3}MLCT state requires approximately 18 successive excitations[10] which have to occur within the 30 ps pulse (with a yield of 0.04, 96% of the molecules promptly return to the ground state and can be re-excited within the pulse). That is, it requires only one pulse to promote 4% of the molecules to the ^{3}MLCT state. Therefore, in order to achieve a net 70% population of the ^{3}MLCT state, 18 consecutive pulses (i.e. 70/4) are required. This consideration allows us to estimate the fast component of the time constant for ^{3}MLCT formation. If 18 consecutive excitations occur within the 30 ps pulse, then a single excitation must correspond to 1.7 ps (30 ps/18 excitations). Since this single excitation is all that is required to populate 4% of the ^{3}MLCT state, the fast component can be estimated to form in 1.7 ps. Note that the number of photons absorbed during excitation by the 355 nm and 532 nm pulses of 2.5 mJ energy in the irradiated sample area is sufficient for approximately 26 and 38 excitations, respectively. However, most of the photons are delivered within the short intense central part of the laser pulse. Hence, the actual lifetime for the fast component of the ^{3}MLCT population must be much shorter, on the order of hundreds of femtoseconds. Although no extinction coefficients were reported for the excited state absorption of $W(CO)_5$(4-FM-Py), qualitatively similar behaviour is obvious from Figures 5.2 - 5.4. The fraction of ^{3}MLCT states populated already within the excitation pulse appears to be even larger and, hence, the lifetime of their formation

shorter than that estimated for $W(CO)_5$(4-NC-Py).

One possible interpretation of the biphasic kinetics would be to assign the faster and slower components to ISC from the higher and lower ^{1}MLCT levels, respectively. However, absorption spectra obtained 40 and 80 ps after the 532 nm excitation of $W(CO)_5$(4-FM-Py) shows that the ^{3}MLCT state is populated to about 80% within the excitation pulse (the faster component dominates[20]). Since it is apparent (from Figure 5.1) that 532 nm excitation is directed into the low-energy shoulder of the MLCT band and is energetically insufficient to populate the higher energy ^{1}MLCT level, the faster component cannot be assigned to ISC from this state.

An interpretation of the biphasic kinetics of the formation of the lowest ^{3}MLCT state must take into account the fact that the rate of the faster component of the ISC is comparable to, or even higher than, the rate of vibrational relaxation within an excited state manifold which, in transition metal carbonyls, occurs[21,22] in the femtosecond time domain. Consequently, the dominant sub-picosecond component must involve directly excited Franck-Condon vibronic levels or levels in close energetic proximity. Thus, the fast component is due to the intersystem crossing from the vibrationally unrelaxed Franck-Condon state to the ^{3}MLCT state. The slower, minor, component corresponds to ISC from the vibrationally relaxed ^{1}MLCT state to the ^{3}MLCT state. This interpretation is also corroborated by the observed solvent effect on the rate of the ^{3}MLCT state formation. The slow component (where the ^{1}LF --> ^{1}MLCT ISC terminates in the lower vibrational levels of ^{1}MLCT from which the "slow" ISC occurs) is much more prominent in toluene. In methylcyclohexane, only the ultrafast component

was observed. This corresponds to direct ^{1}LF --> ^{3}MLCT ISC which must be an ultrafast process in order to be competitive with the ultrafast vibrational relaxation of the ^{1}LF level. Alternatively, the relaxing system can go through very high vibrational levels of ^{1}MLCT (resulting from a large degree of separation between the LF and MLCT states; Figure 5.1), from which the faster process must dominate. The only explanation for the fast component which is observed under 532 nm excitation (where ^{3}MLCT is directly populated by the excitation pulse) is vibrational relaxation of the ^{3}MLCT state. Thus, the observed solvent dependence is in accord with the thermal conductivities of toluene and methylcyclohexane (2.7×10^{-4} and 3.2×10^{-4}, respectively; the physical parameters used in the approximation can be found in Reference 23) as estimated using the Sato-Riedel equation (Section 3.4). That is, vibrational relaxation occurs at a slower rate in toluene since this solvent dissipates excess energy less efficiently than methylcyclohexane. The photophysical deactivation pathways are shown schematically in Figure 5.6. Unfortunately, present data do not provide any information on the mechanism of this ISC from optically excited (near) Franck-Condon states. However, this process might be conceptually similar to the ^{1}MLCT ---> ^{5}LF ISC in Fe(II) polypyridyl complexes that was recently found[24,25] to be an ultrafast (< 700 fs) process occurring with no intermediates.

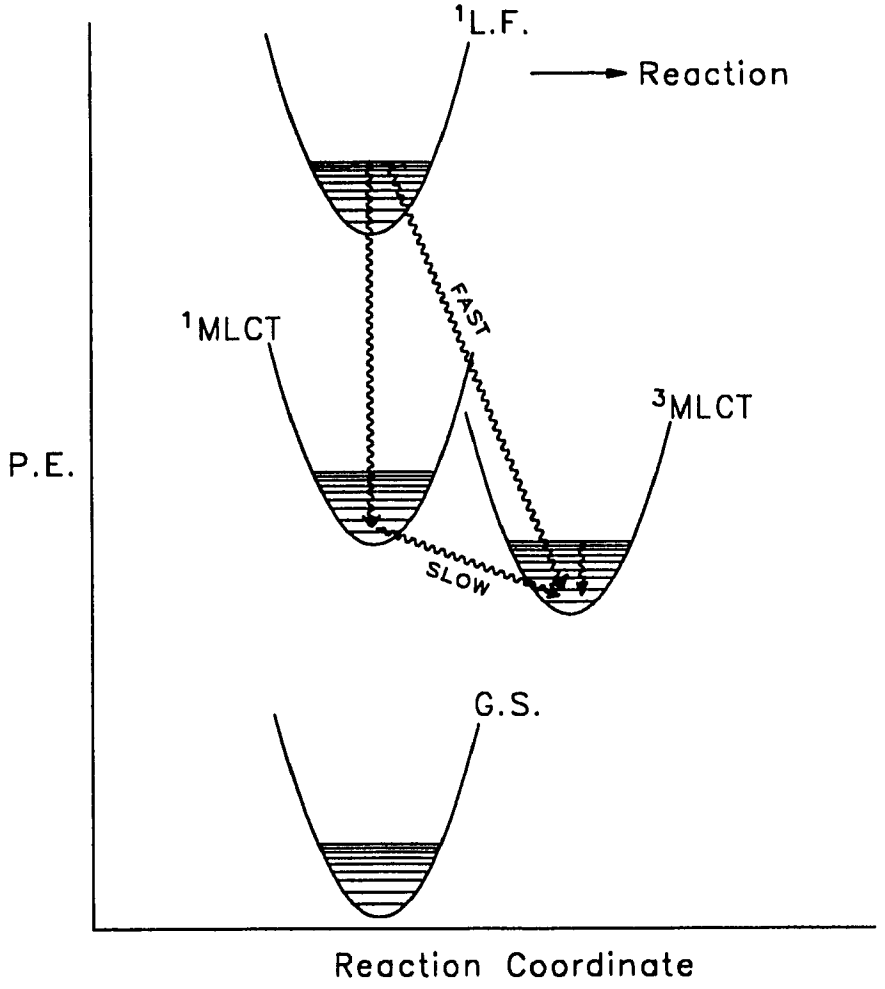

Figure 5.6. Schematic representation of the potential energy surfaces involved in the photophysical deactivation of $W(CO)_5$(4-X-Py); X = CN, Formyl.

5.7. Conclusions

It has been shown for $W(CO)_5$(4-X-Py) complexes that the intersystem crossing, which populates ^{3}MLCT excited state(s) involved in photoreactivity, follows biphasic kinetics. The dominant ultrafast component is assigned to crossing from the vibrationally

unrelaxed ^{1}LF state to the ^{3}MLCT state and occurs at a rate of approximately $6x10^{11}$ s^{-1}. This is seen exclusively when methylcyclohexane is the solvent. The minor component due to ^{1}MLCT --> ^{3}MLCT intersystem crossing occurs at a somewhat slower rate ($2x10^{10}$ and $3x10^{10}$ s^{-1} for $W(CO)_5$(4-NC-Py) and $W(CO)_5$(4-FM-Py) in toluene, respectively). This implies that intersystem crossing occurs on the same timescale as vibrational relaxation (or even faster).

It was also revealed that this intersystem crossing is dependent on the solvent, the slower component being more prominent in toluene than in methylcyclohexane (in the case of population of the LF states of $W(CO)_5$(4-FM-Py) in methylcyclohexane, the slower component is not observed). This solvent dependence is in accord with our ideas regarding the role of the solvent in ultrafast chemical processes presented in Chapter 3. That is, the solvent, through electronic factors, exerts a remarkable control on processes which occur in the sub-picosecond time domain.

The fast photochemistry studied in this and the preceding chapter has revealed that the sub-picosecond population of ^{3}MLCT states is not unique. In fact, these results might bear more general implications for excited state dynamics and photochemistry of organometallic and coordination compounds. In Chapter 4, it was demonstrated that the ^{3}MLCT states of $W(CO)_4$(phen) (which are also implicated in its photoreactivity) are also populated on a sub-picosecond timescale. In this case, complete formation of ^{3}MLCT states was observed to take place within the 30 ps excitation pulse. The only difference between the ^{3}MLCT states in this complex and that studied in this chapter is that the decay of the ^{3}MLCT states in the former complex is quite rapid (approximately 1 ns) as

opposed to the 292 ns lifetime associated with the ^{3}MLCT states of $W(CO)_5$(4-NC-Py). Even in a complex containing a much lighter transition metal, $Cr(CO)_4$(bpy), the ^{3}MLCT states are, in part, produced within the 30 ps excitation pulse, along with a slower, approximately 50 ps, process[1].

It is thus obvious that excited state relaxation pathways are, in these compounds, selected very shortly after the electronic excitation, on timescales where the Born-Oppenheimer approximation is no longer applicable. Involvement of optically excited vibronic levels might provide the specific vibrational coupling needed for activation of particular photophysical (e.g. ISC) as well as prompt photochemical processes. This might be manifested by unusual excitation-wavelength effects[1,6,26] as was observed in the photolysis of $W(CO)_4$(phen) (Chapter 4) and $[M(mnt)_2]^{2-}$ (M = Ni, Pt) (Chapter 3).

It now appears that the usual and convenient interpretation of molecular photochemistry in terms of temporarily well-separated subsequent processes like vibrational relaxation, internal conversion and intersystem crossing, is only of limited use for transition metal compounds such as $W(CO)_4$(phen) and $W(CO)_5$(4-X-Py) (X = CN, Formyl). Our work has shown that in these cases, the photophysical deactivation processes are strongly coupled with each other and not readily separable. This is probably also true for other carbonyl complexes (e.g. $W(CO)_6$) which undergo prompt chemical reaction.

5.8. References

1. Víchová, J.; Hartl, F.; Vlček, A., Jr. *J. Am. Chem. Soc.* **1992**, *114*, 10903.

2. Balk, R.W.; Snoeck, T.; Stufkens, D.J.; Oskam, A. *Inorg. Chem.* **1980**, *19*, 3015.

3. Manuta, D.M.; Lees, A. *Inorg. Chem.* **1986**, *25*, 1354.

4. Wieland, S.; Reddy, K.B.; van Eldik, R. *Organometallics* **1990**, *9*, 1802.

5. van Dijk, H.K.; Servaas, P.C.; Stufkens, D.J.; Oskam, A. *Inorg. Chim. Acta* **1985**, *104*, 179.

6. Lindsay, E.; Vlcek, A., Jr.; Langford, C.H. *Inorg. Chem.*, in press.

7. Wrighton, M.S.; Abrahamson, H.B, Morse, D.L. *J. Am. Chem. Soc.* **1976**, *98*, 4105.

8. Rawlins, K.A.; Lees, A.J.; Adamson, A.W. *Inorg. Chem.* **1990**, *29*, 3866.

9. Lees, A.J.; Adamson, A.W. *J. Am. Chem. Soc.* **1982**, *104*, 3804.

10. Glyn, P.; Johnson, F.P.A.; George, M.W.; Lees, A.J.; Turner, J.J. *Inorg. Chem.* **1991**, *30*, 3543.

11. Wieland, S.; van Eldik, R.; Crane, D.R.; Ford, P.C. *Inorg. Chem.* **1989**, *28*, 3663.

12. Lees, A.J.; Adamson, A.W. *J. Am. Chem. Soc.* **1980**, *102*, 6876.

13. Pyridine ligand photodissociation is much more efficient (0.5 - 0.8) in analogous complexes with lowest excited state of LF character, e.g. $W(CO)_5$(pyridine).

14. van Eldik, R.; Asano, T.; le Noble, W.J. *Chem. Rev.* **1989**, *89*, 549.

15. The effect of the excitation by the "tail" of the laser pulse and/or of the instrument response on the early increase of transient absorption was checked by an independent experiment using $[Ru(bpy)_3]Cl_2$. Its excited state absorption spectrum is known to be formed within a time interval shorter than the time resolution of our instrument (Serpone, N.; Jamieson, M.A. *Coord. Chem. Rev.* **1989**, 93). An aqueous solution containing $[Ru(bpy)_3]^{2+}$ was excited with a 355 nm pulse. Both transient absorbance in the visible as well as the bleached absorbance increased in intensity by less than 4% going from the 20 to 40 ps

time delay after the laser pulse (i.e. the change observed was within the experimental error. It may thus be safely concluded that all changes observed for $W(CO)_5$(4-FM-Py) and $W(CO)_5$(4-NC-Py) at time delays longer than 20 ps are due to the excited state dynamics of the samples investigated. On the other hand, the absorbance changes observed between 0 and 20 ps have no quantitative meaning. However, the comparison of the shape of the transient absorption bands observed at these two time delays is possible, as the band shape is not affected by instrumental factors.

16. Although the use of spin labels for electronic states of heavy-atom organometallic compounds might be disputed,it is an experimental fact that they possess excited states which behave much as spin singlets and triplets of organic compounds and the use of spin labels is thus commonly accepted.

17. Moralejo, C.; Langford, C.H.; Sharma, D.K. *Inorg. Chem.*, **1989**, *28*, 2205.

18. Lees, A.J. *Chem. Rev.* **1987**, *87*, 711.

19. Vlček, A., Jr. *Chemtracts Inorganic* **1991**, *3*, 363-367.

20. It cannot be excluded that a portion of the ^{3}MLCT states are populated by a direct Ground State ---> ^{3}MLCT excitation at 532 nm as the very red shoulder of the absorption band might correspond to this spin-forbidden transition.

21. Joly, A.G.; Nelson, K.A. *Chem. Phys.* **1991**, *152*, 69.

22. Yu, S-C.; Xu, X.; Lingle, R, Jr.; Hopkins, J.B. *J. Am. Chem. Soc.* **1990**, *112*, 3668.

23. Riddick, J. A.; Bunger, W. B.; Sakano, T. K. in *Techniques of Chemistry, Vol. II, Organic Solvents Physical Properties and Methods of Purification*, 4th edition; John Wiley and Sons, Inc.: U.S.A., 1986, pp.85, 107.

24. McCusker, J.K.; Walda, K.N.; Dunn, R.C.; Simon, J.D.; Magde, D.; Hendrickson, D.N. *J. Am. Chem. Soc.* **1992**, *114*, 6919.

25. McCusker, J.K.; Walda, K.N.; Dunn, R.C.; Simon, J.D.; Magde, D.; Hendrickson, D.N. *J. Am. Chem. Soc.* **1993**, *115*, 298.

26. Langford, C.H. *Acc. Chem. Res.* **1984**, *17*, 96.

6. Metal-to-Ligand Charge Transfer Photochemistry of $(CO)_5Re$-$Re(CO)_3(bpy')$ and $(Ph)_3Sn$-$Re(CO)_3(bpy')$

6.1. Background

Transition metal complexes which possess direct metal-metal bonds have been a subject of interest from the point of view of geometric and electronic structure[1-4], synthesis[5], and catalysis[6]. The distribution of electron density in low lying electronic excited states of metal-metal bonded complexes, unlike the mononuclear analogues, is often significantly different compared to the ground electronic state thus creating the potential for some very interesting photochemistry which cannot be observed in other complexes. Earlier mechanistic studies on the photochemistry of metal-metal bonded species have focused on the carbonyl dimers[7-12] $M_2(CO)_{10}$ (M = Mn, Re), $Cp_2Fe_2(CO)_4$, and $Cp_2M_2(CO)_6$ (M = Mo, W). Irradiation of these complexes results in clean, quantum efficient homolysis of the metal-metal bond to yield reactive 17 electron radicals[7,8,11,12] and/or parallel release of CO[8,9].

Substitution of two carbonyl ligands by an α-diimine molecule such as 4,4'-methyl-2,2'-bipyridine (bpy') produces complexes with an absorption band in the visible region, which has all the characteristic features (intensity, solvatochromism, resonance enhancement of the stretching modes of the α-diimine ligand upon MLCT excitation) of a metal-to-ligand charge transfer (MLCT) transition[13,14]. As in $W(CO)_4(phen)$ and $W(CO)_5(4\text{-}X\text{-}Py)$, X = CN, Formyl, (Chapters 4 and 5), the MLCT states are of the lowest energy in $(CO)_5Re$-$Re(CO)_3(bpy')$ and $(Ph)_3Sn$-$Re(CO)_3(bpy')$. What is intriguing about complexes containing both a metal-metal bond and a lowest lying MLCT state is

their remarkably high photosensitivity (the quantum yield observed upon excitation is ~ 0.2[15,16]. This contrasts with the photostability manifested by most other mononuclear α-diimine complexes (e.g. $W(CO)_4$(phen); Chapter 4) having a lowest lying MLCT state (maximum observed quantum yield ≤ 0.03 upon MLCT excitation)[17-21]. The stability of such MLCT states is believed to be caused by the stronger "ionic" interaction between the metal and ligand in the MLCT state which compensates for the weakening of the metal-ligand covalent bond. Emission studies by Larson *et al*[22] have revealed that like $W(CO)_4$(phen) (Chapter 4) and $W(CO)_5$(4-X-Py); X = CN, Formyl (Chapter 5), $(CO)_5Re\text{-}Re(CO)_3$(bpy') exhibits multiple emission (both fluorescence and phosphorescence were observed) from an MLCT excited state thereby indicating unique photophysics in this complex.

In the past, studies of organometallic compounds possessing both a metal-metal bond and lowest lying MLCT state(s) have focused on the investigation of their photochemical reactivities[8,13,23]. Luminescence[22] and resonance Raman spectroscopy[24-26] have also been used to characterize the excited states. Despite this work, much mechanistic information remains to be elucidated for this type of complex. In order to gain further insight into the mechanism of reaction of this class of complexes, the primary photoprocesses of $(CO)_5Re\text{-}Re(CO)_3$(bpy') and $(Ph)_3Sn\ Re(CO)_3$(bpy') upon MLCT excitation have been investigated using a combination of wavelength dependence studies of the quantum yield within the MLCT band envelope and picosecond laser flash photolysis.

6.2. Electronic Spectroscopy

6.2.1. Band assignments in $(CO)_5Re\text{-}Re(CO)_3(bpy')$

The electronic absorption spectrum of $(CO)_5Re\text{-}Re(CO)_3(bpy')$ (the molecular structure of this complex is given in Figure 1.5) in toluene contains an intense low-energy transition (ϵ = 7000 $M^{-1}cm^{-1}$) at 534 nm. This low lying band exhibits negative solvatochromism (Section 4.2.1) as shown in Figure 6.1 thereby indicating CT character. Resonance Raman spectroscopy of an analogous complex differing only in the α-diimine

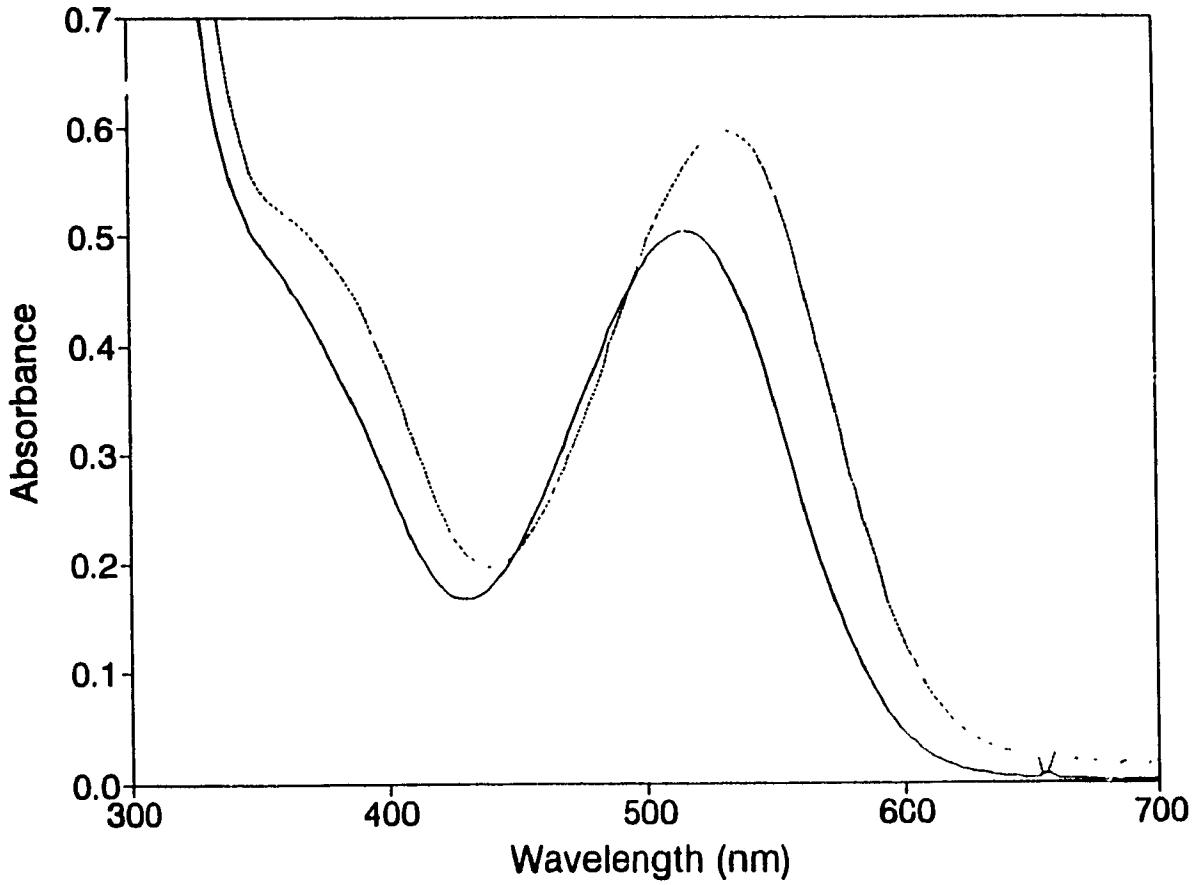

Figure 6.1. Electronic absorption spectra of $(CO)_5Re\text{-}Re(CO)_3(bpy')$ at 293 K in dichloromethane (—) and toluene (• • •).

ligand (i.e. *i*-Pr-DAB (*i*-Pr-N=CH-CH=N-*i*-Pr) was used rather than bpy') has revealed[13,14] a resonance enhancement for several stretching modes of the α-diimine ligand upon excitation into the MLCT band envelope (514.5 nm). Accordingly, this band in $(CO)_5Re\text{-}Re(CO)_3(bpy')$ has been assigned as a Re ---> π^*(bpy') CT transition. Larson *et al* have analyzed the band envelope of the low energy MLCT band and determined that the band consists of a superposition of three transitions: two lowest d_π(Re) ---> π^*(bpy') transitions and the lowest d_δ(Re) ---> π^*(bpy') transition[22]. Note that a σ_b(Re-Re) --> π^*(bpy') transition is also possible. However, resonance Raman experiments done by Kokkes and co-workers[14] showed that it is not a major contributor to the band intensity since only a weak resonance effect for the metal-metal stretching vibration within the lowest energy MLCT band was observed. This intense low energy system will be referred to as $MLCT_2$. Although the higher energy absorption in the 360 nm region has not yet been provided with an unambiguous assignment, it is most likely due to the dipole allowed d_π(Re) --> π^* transition with termination of the transition in a higher level π^* orbital of the diimine[22]. It will be referred to as $MLCT_1$.

6.2.2. Band Assignments in $(Ph)_3Sn\text{-}Re(CO)_3(bpy')$

The electronic absorption spectrum of $(Ph)_3Sn\text{-}Re(CO)_3(bpy')$ (the molecular structure of this complex is given in Figure 1.5) is very similar to that of $(CO)_5Re\text{-}Re(CO)_3(bpy')$. The spectrum consists of an intense low-energy transition (ϵ = 4600 $M^{-1}cm^{-1}$) centred at 465 nm in CH_2Cl_2. Like its Re-Re counterpart, the low lying band exhibits negative solvatochromism (Section 4.2.1) thereby indicating CT character

(Figure 6.2). Resonance Raman spectroscopy on an analogous complex,

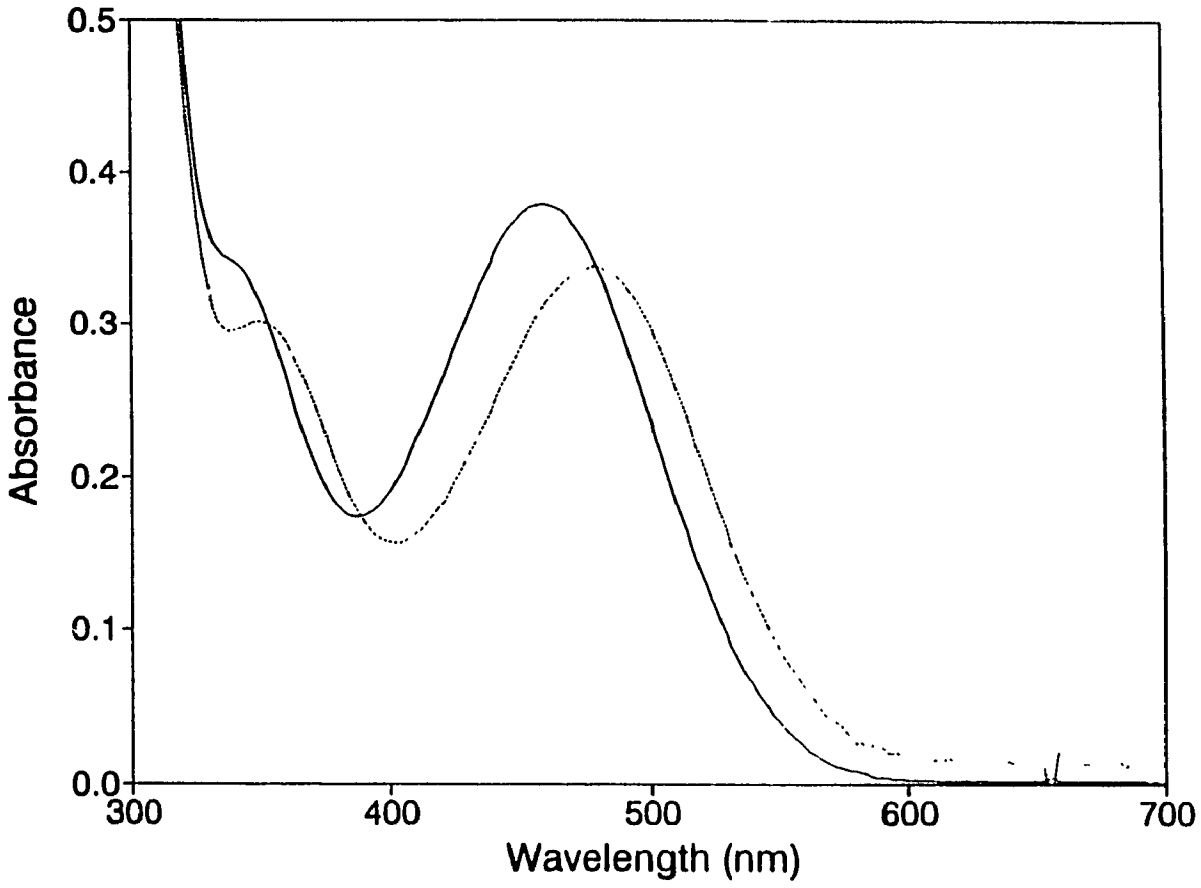

Figure 6.2. Electronic absorption spectra of $(Ph)_3Sn\text{-}Re(CO)_3(bpy')$ at 293 K in THF (—) and toluene (• • •).

$(Ph)_3Sn\text{-}Re(CO)_3$(*t*-Bu-DAB) (*t*-Bu-DAB: *t*-Bu-N=CH-CH=N-*t*-Bu), has revealed strong resonance enhancement for several stretching modes of the α-diimine ligand upon MLCT excitation[24]. Thus, the band has been assigned as a Re ---> π^*(bpy') CT transition.

Unfortunately, there has not yet been a detailed analysis of the band envelope. However, it is expected that the assignments would be very similar to those for the $(CO)_5Re$-$Re(CO)_3(bpy')$ complex (Section 6.2.1) since it contains the identical chromophore, $(bpy')(CO)_3Re$-. The intense low energy system (λ_{max} = 465 nm) will be referred to as $MLCT_2$. The higher energy absorption in the 350 nm region has not yet been assigned. However, as in $(CO)_5Re$-$Re(CO)_3(bpy')$, it is most likely due to a CT transition into a higher level π^* orbital of the diimine[22]. It will be referred to as $MLCT_1$.

6.3. Photoreactivity of $(CO)_5Re$-$Re(CO)_3(bpy')$ Under MLCT Excitation

The photoreactivity of $(CO)_5Re$-$Re(CO)_3(phen)$ upon MLCT excitation in a 0.5 M solution of CCl_4 in CH_2Cl_2 was investigated earlier by Wrighton *et al*[15], although their experiments focused on the photoreactivity across $MLCT_1$ and only a small portion of $MLCT_2$. Their experiments revealed a wavelength independent reaction. In order to prove that this behaviour also applies to the analogous bpy' complex, our experiments probed the reactivity of $(CO)_5Re$-$Re(CO)_3(bpy')$ upon excitation into different regions of the $MLCT_2$ band envelope.

Irradiation into the MLCT band envelope promotes homolysis of the Re-Re bond to yield two 17 electron radicals: $(CO)_5Re^\bullet$ and $(bpy')(CO)_3Re^\bullet$ (Equation 6.1). In the presence of a halogenated solvent (e.g. CH_2Cl_2), which is known to be an efficient radical scavenger, the radicals can abstract a Cl atom to give the final photoproducts $(CO)_5Re$-Cl and $(bpy')(CO)_3Re$-Cl (Equation 6.1).

$$(CO)_5Re\text{-}Re(CO)_3(bpy') \xrightarrow{h\nu} \underbrace{\{(CO)_5Re^{\bullet} + Re(CO)_3(bpy')^{\bullet}\}}_{\text{cage species}} \qquad (6.1)$$

$$\xrightarrow{\qquad} \underbrace{(CO)_5Re^{\bullet} + Re(CO)_3(bpy')^{\bullet}}_{\text{primary radicals}}$$

$$\xrightarrow{CH_2Cl_2} \underbrace{Cl\text{-}Re(CO)_5 + Cl\text{-}Re(CO)_3(bpy')}_{\text{photoproducts}}$$

Representative spectra are shown in Figure 6.3. An isosbestic point was not observed in the spectra for this reaction because the product spectrum contains only one absorption band which is much less intense than the absorption bands in the spectrum of $(CO)_5Re\text{-}Re(CO)_3(bpy')$. However, as a precaution, conversion was limited to approximately 10% in order to eliminate the possibility of interference associated with side reactions due to the reactive radicals generated upon photolysis. The results for visible excitation of $(CO)_5Re\text{-}Re(CO)_3(bpy')$ are presented in Table 6.1.

Table 6.1. Wavelength dependence of the quantum yield[a] for the photoreaction of $(CO)_5Re\text{-}Re(CO)_3(bpy')$ in CH_2Cl_2.

WAVELENGTH (nm)	QUANTUM YIELD[b]
488.0	0.22
496.0	0.23
514.5	0.22

a) All quantum yields were obtained at room temperature.
b) The standard deviation was less than 5%

Unlike the monometallic $W(CO)_4(phen)$ complex discussed in Chapter 4, the quantum yields of reaction upon MLCT excitation of $(CO)_5Re\text{-}Re(CO)_3(bpy')$ are quite large (0.23) and are clearly *independent* of the excitation wavelength (i.e. it does

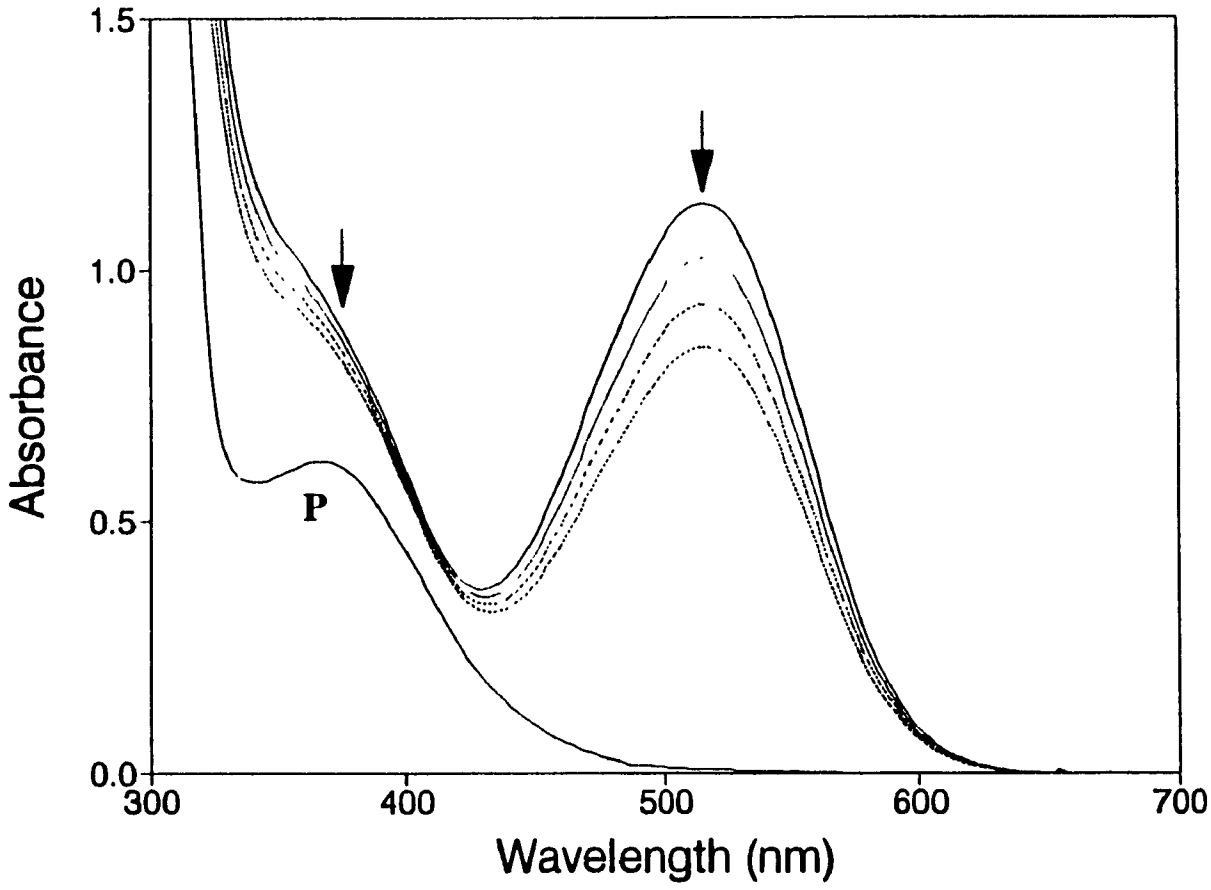

Figure 6.3. Electronic spectral changes observed upon 514.5 nm photolysis of $(CO)_5Re\text{-}Re(CO)_3(bpy')$ in neat CH_2Cl_2. The spectra shown are for 0, 2, 4, and 6 s in order of decreasing absorbance. Also shown is the spectrum of the photoproduct (P).

not matter into which region of the MLCT envelope the excitation occurs). These results are comparable to those published in the preliminary study on the photochemistry of $(CO)_5Re\text{-}Re(CO)_3(phen)$ by Wrighton *et al*[15] indicating that the two complexes react similarly. The combination of our results with those obtained by Wrighton[15], it can be

concluded that the quantum yield is independent of excitation wavelength over the entire MLCT band system.

Wrighton and co-workers also revealed that the photoreaction of $(Ph)_3Sn$-$Re(CO)_3(phen)$ also exhibits a wavelength independent quantum yield upon excitation across $MLCT_1$ and the blue side of the $MLCT_2$ band envelope in halogenated solvents[16]. We did not determine the quantum yield for this complex over the $MLCT_2$ band, however based on the similarity of the yields for the Sn-Re complex and the two Re-Re complexes discussed above and the wavelength independent nature of $(CO)_5Re$-$Re(CO)_3(bpy')$, it can be concluded that Ph_3Sn-$Re(CO)_3(bpy')$ also reacts in a wavelength independent fashion over the entire MLCT band envelope. This contrasts the behaviour of the mononuclear complex $W(CO)_4(phen)$ whose quantum yield is quite low and is both wavelength and solvent dependent under MLCT excitation (Chapter 4). The high quantum yields of this reaction and the observed wavelength independence can be explained in two ways. It could be the result of a fast crossing to some reactive state or, alternatively, a long lived "storage" state (probably ^{3}MLCT) might be involved. In the latter case, the crossing would be slow. This concept will be addressed later.

6.4. Picosecond Absorption Spectroscopy

Unlike what was observed under continuous irradiation, the transient absorption spectra of $(CO)_5Re$-$Re(CO)_3(bpy')$ and $(Ph)_3Sn$-$Re(CO)_3(bpy')$ indicate that these complexes exhibit quite different early time behaviour. Consequently, the transient absorption spectra for each complex will be considered separately.

6.4.1. $(CO)_5Re\text{-}Re(CO)_3(bpy')$

Transient absorption spectra of $(CO)_5Re\text{-}Re(CO)_3(bpy')$ were recorded using 355 nm excitation (i.e. irradiation into $MLCT_1$) and 532 nm excitation (i.e. irradiation into $MLCT_2$) in both toluene and dichloromethane using picosecond laser pulses. The spectra are shown in Figures 6.4 to 6.7. Inspection of the transient absorption spectra recorded in toluene under 355 nm excitation (Figure 6.4) reveal three characteristic features: (1) the bleaching of the ground state band within 20 ps, the bleach minimum being at 550 nm, (2) a broad excited state absorption, ESA, band centred at 625 nm which is fully developed within the laser pulse (30 ps), and (3) a second ESA band overlapping the high energy side of the bleach and extending into the blue region of the spectrum. The presence of this band is inferred from the shift of the bleach minimum with respect to the ground state absorption maximum (532 nm) and the shape of the bleached band at early times.

At delay times of less than 500 ps, the bleach has a "skewed" shape and the bleach minimum is shifted to the red by 16 nm with respect to the maximum absorption of the ground state band (534 nm). This suggests the existence of a second transient extending into the blue region of the visible spectrum (unfortunately, the maximum is not accessible to our detector) which is overlapping it. This transient will be referred to as ESA_1. Furthermore, the absorbance change for the bleach (550 nm) is approximately -0.02 whereas the ground state spectrum has an absorbance of 0.37 at 534 nm when toluene is the solvent. That is, not "enough" bleaching occurs if no ESA is present at the bleach wavelength. Also, as the delay time is increased, the bleach is not recovered

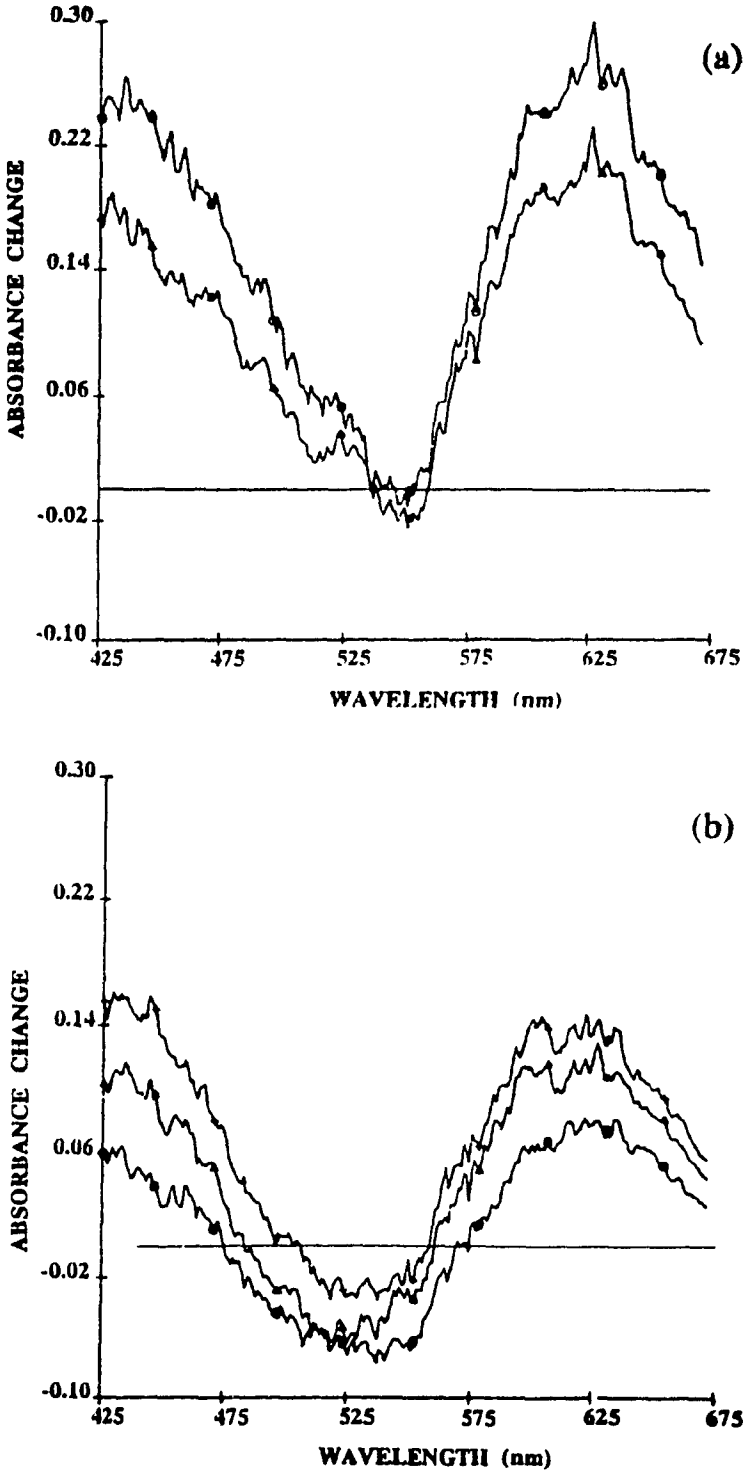

Figure 6.4. Transient absorption spectra of $(CO)_5Re\text{-}Re(CO)_3(bpy')$ in neat toluene using 355 nm excitation recorded at probe delays of (a) 50 and 500 ps and (b) 10, 5, and 2.5 ns in order of decreasing absorbance change.

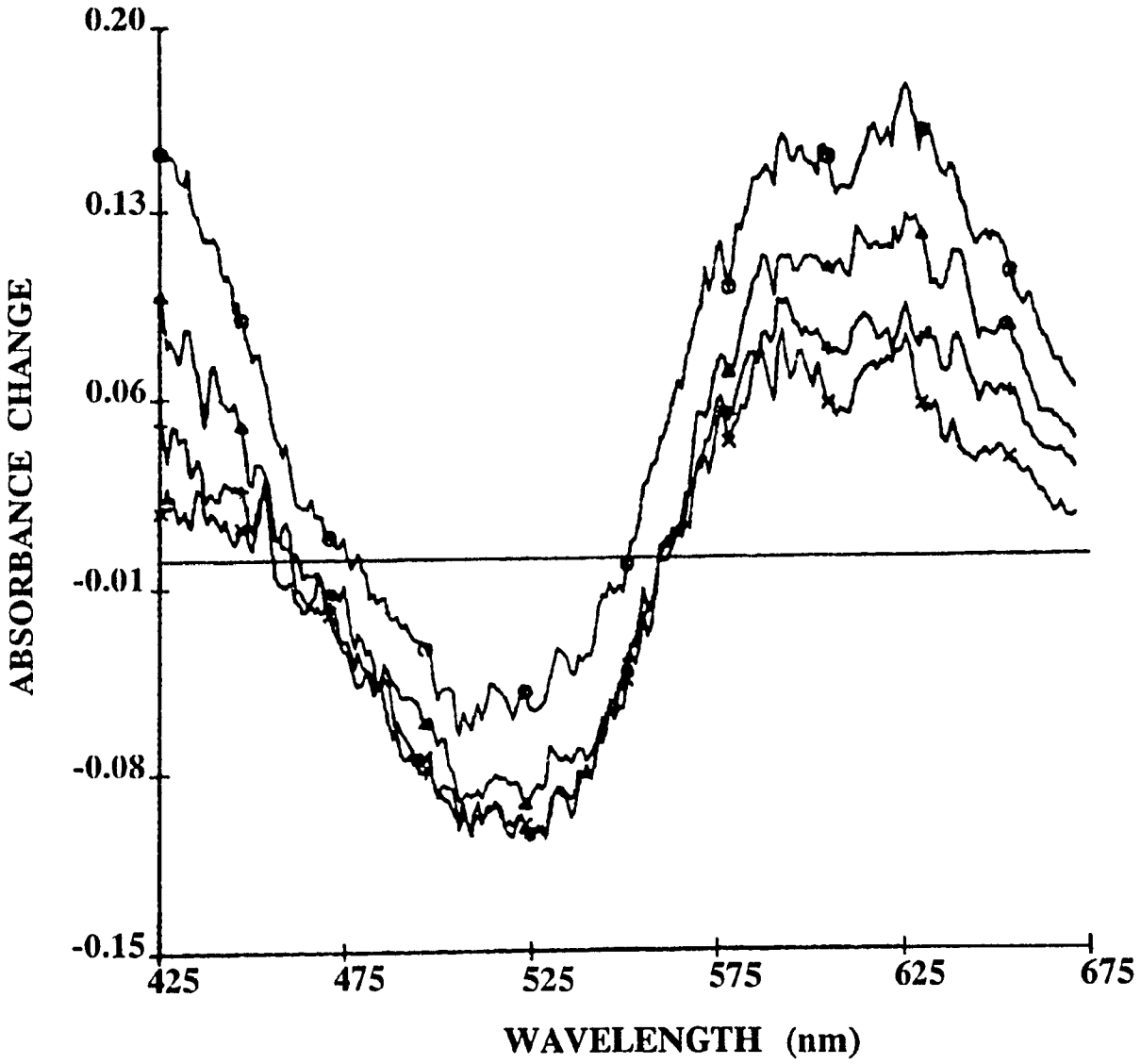

Figure 6.5. Transient absorption spectra of $(CO)_5Re\text{-}Re(CO)_3(bpy')$ in neat dichloromethane using 355 nm excitation recorded at probe delays of 50 and 500 ps and 2.5 ns in order of decreasing absorbance change.

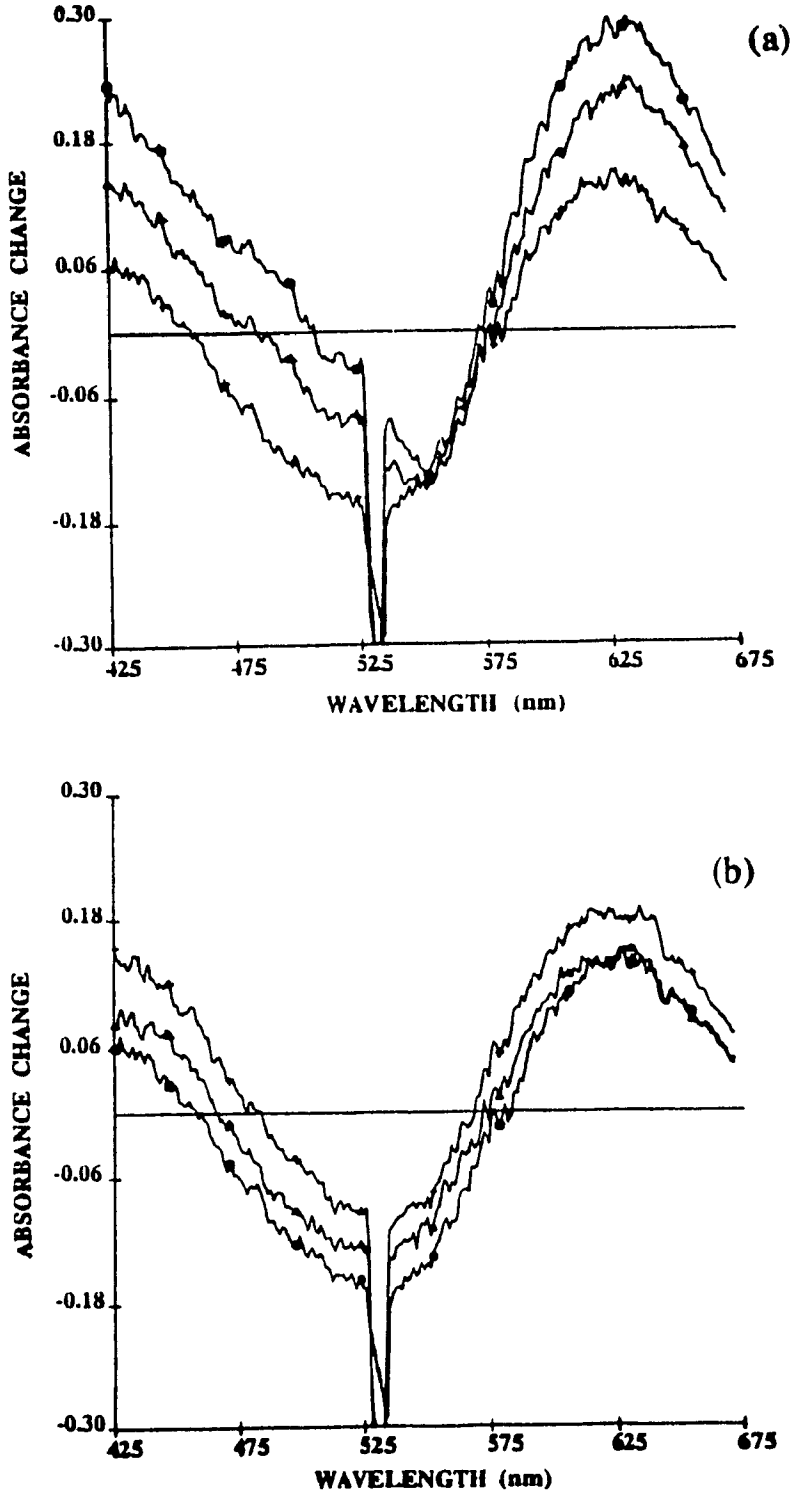

Figure 6.6. Transient absorption spectra of $(CO)_5Re\text{-}Re(CO)_3(bpy')$ in neat toluene using 532 nm excitation recorded at probe delays of (a) 50 and 500 ps, and 2.5 ns and (b) 10, 5, and 2.5 ns in order of decreasing absorbance change.

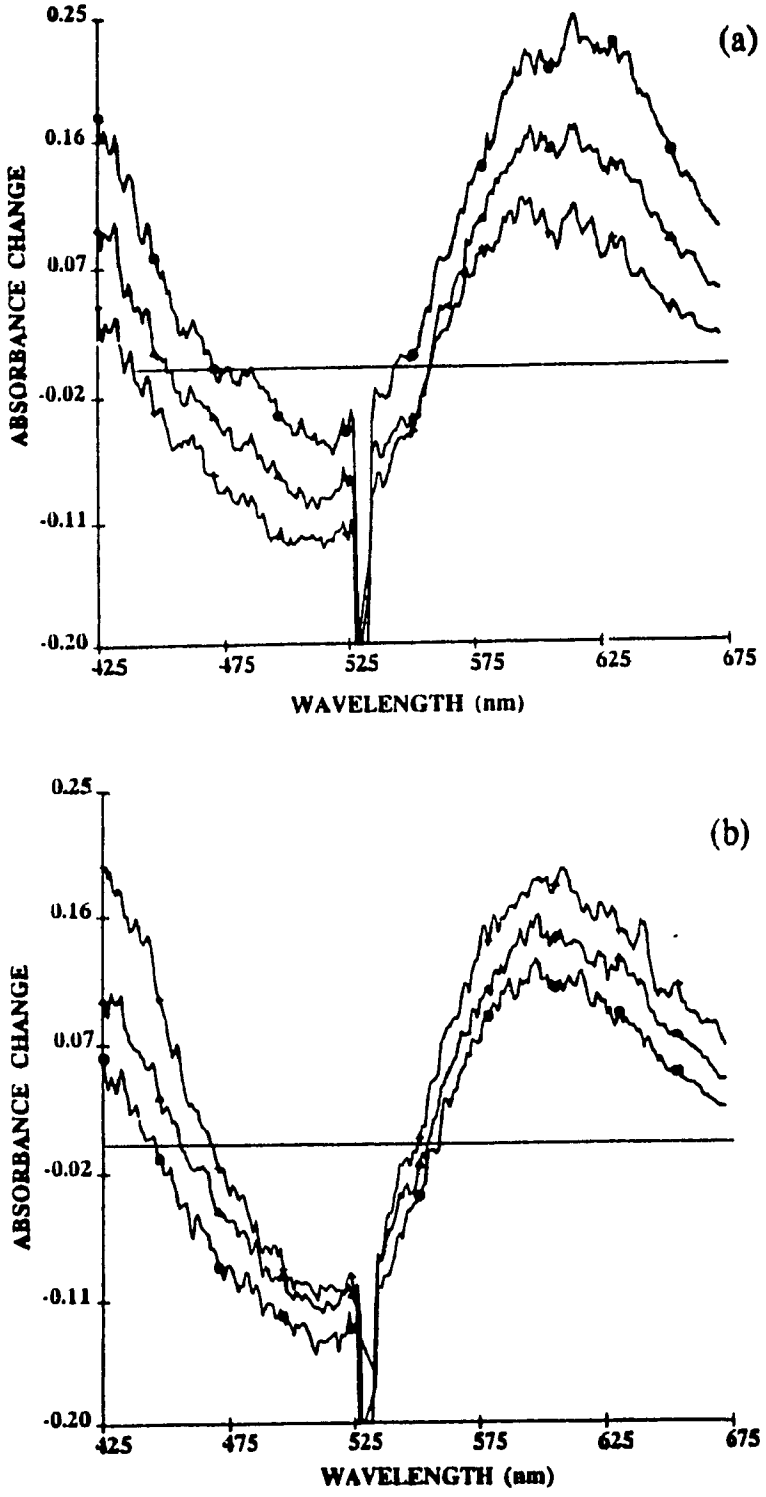

Figure 6.7. Transient absorption spectra of $(CO)_5Re\text{-}Re(CO)_3(bpy')$ in neat dichloromethane using 532 nm excitation recorded at probe delays of (a) 50 and 500 ps and 2.5 ns and (b) 10, 7.5 and 5 ns in order of decreasing absorbance change.

(as was seen in $W(CO)_4(phen)$), nor does it retain its "skewed" shape. Rather, it becomes symmetrical in shape with the bleach minimum shifting to 536 nm, almost exactly the value of wavelength at which the ground state band has maximum absorbance, and more negative. This suggests ESA_1 is relaxing within 1 ns to some other state (not the ground state).

The second feature of the transient absorption spectrum is an ESA band at 625 nm which exhibits rather unusual behaviour. This will be referred to as ESA_2. It decays within 2.5 ns to yield a second band (ESA_3) in the same region which increases in intensity up to 10 ns. Thus, there must be a minimum of three transients, one which relaxes very quickly, but not to the ground state (this is the transient in the blue region), a second one which relaxes at a somewhat slower rate, but not to the ground state (this is the transient which appears in the visible region at early times), and a third which grows in (also in the visible region) at longer times. Note that the band due to ESA_2 is not as broad as that due to ESA_3, thus providing additional evidence for the presence of two separate transients which absorb in the same region.

In CH_2Cl_2, the spectral behaviour upon 355 nm excitation (Figure 6.5) appears at first to be somewhat different than what was observed in toluene. However careful examination of the spectra and consideration of the nature of the solvent reveal that the spectra in both solvents are in fact the same. In CH_2Cl_2 the bleach minimum is symmetrical, even at early times, with a minimum centred at 516 nm (the ground state absorption maximum is at 520 nm). This suggests that ESA_1 is not present in this case. This is not surprising upon consideration of the information presented in the earlier

chapters concerning the rates of relaxation in chlorinated solvents. Examination of the thermal conductivities of chlorinated solvents and how this parameter relates to relaxation processes (Chapter 3) led to the conclusion that a chlorinated solvent will speed up the relaxation process since it tends to dissipate excess energy more rapidly than in a non-halogenated system. From our spectra, it is thus obvious that the relaxation of ESA_1 is dependent upon the solvent in that it appears to be more efficient in CH_2Cl_2 than in toluene. That is, in CH_2Cl_2, the relaxation appears to be so fast that it is not observable in the picosecond time domain. The transient in the 600 nm region is observed to decay leaving a residual ESA at 5 ns which remains constant up to 10 ns when CH_2Cl_2 is the solvent. Therefore, this ESA must correspond to ESA_3, the long lived transient seen to grow in (by 10 ns) when toluene is the solvent. Further evidence linking this transient to ESA_3 is its broadness (the transient due to ESA_3 is also broad in toluene; Figure 6.4b). Thus, the net effect when CH_2Cl_2 is the solvent is an increased rate of relaxation of the excited states such that the only observable state in the picosecond time domain is ESA_3 (i.e. ESA_1 and ESA_2 are not observed). From this, it can be concluded that the solvent induces a change in the rates of interstate transitions. This will subsequently be discussed in detail.

The general features of the ESA spectra under 532 nm excitation are parallel to those observed under 355 nm excitation when toluene is the solvent. That is, there is a "skewed" bleach at short times which becomes symmetrical with increasing time (Figure 6.6a). Also, there is a grow-in of another band at longer times (Figure 6.6b). On the other hand, 532 nm excitation in CH_2Cl_2 yields spectra which are somewhat different

than those obtained using a 355 nm pulse, although the bleach remains symmetrical and coincides with the wavelength of the ground state band maximum of $MLCT_2$ at both short and long times. This indicates that an additional transient extending into the blue region of the visible spectrum is not relaxing in this time domain. Rather than a simple decrease in intensity of the ESA centred at 600 nm, 532 nm excitation leads to an initial decrease in intensity of this band (Figure 6.7a). At longer times, the intensity of this band increases (Figure 6.7b) in much the same way as what is observed when toluene is the solvent. This difference probably arises from different states being populated under 355 nm and 532 nm excitation and/or the effect of the solvent on interstate conversions. This will be subsequently be discussed in detail.

6.4.2. $(Ph)_3Sn\text{-}Re(CO)_3(bpy')$

Transient absorption spectra of $(Ph)_3Sn\text{-}Re(CO)_3(bpy')$ were recorded using 355 nm excitation (i.e. irradiation into $MLCT_1$) and 532 nm excitation (i.e. irradiation into $MLCT_2$) in both a polar (THF) and a non-polar (toluene) solvent using picosecond laser pulses. Spectra are shown in Figures 6.8 and 6.9. Examination of the transient absorption spectra recorded using 355 nm excitation reveals two characteristic features: (1) a broad transient is fully developed within the pulse (30 ps) under both 355 nm and 532 nm excitation and persists for times $>$ 5 ns and (2) a small bleaching of the ground state also occurs within the pulse (30 ps) and persists for long times (i.e $t > 5$ ns). The bleach minimum is at 475 nm as is the band maximum of $MLCT_2$. Unlike what was observed in the $(CO)_5Re\text{-}Re(CO)_3(bpy')$ complex, the bleach is symmetrical at all times,

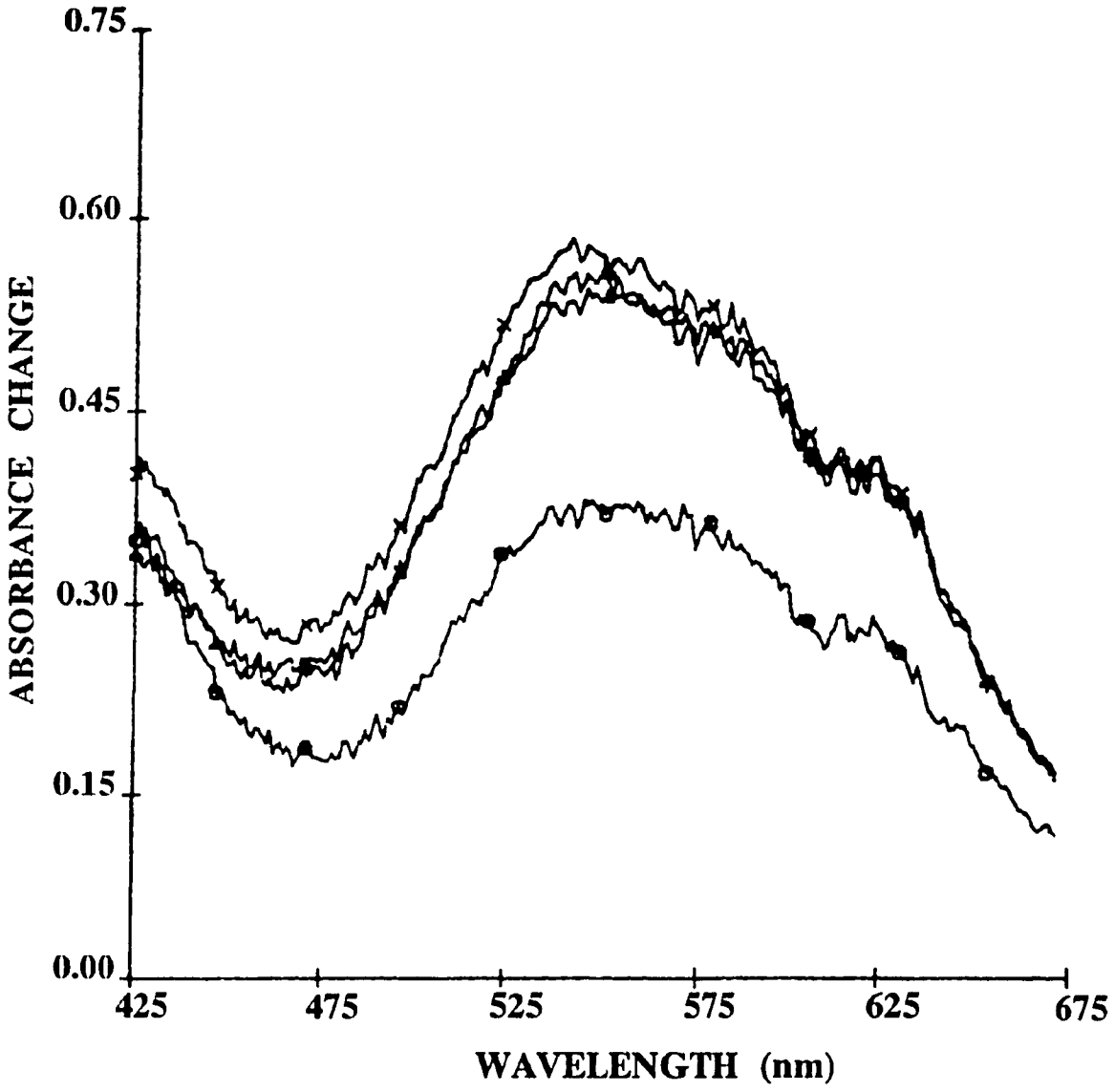

Figure 6.8. Transient absorption spectra of $(Ph)_3Sn$-$Re(CO)_3(bpy')$ recorded in neat toluene using 355 nm excitation recorded at probe delays of 20, 50, and 100 ps and 5 ns.

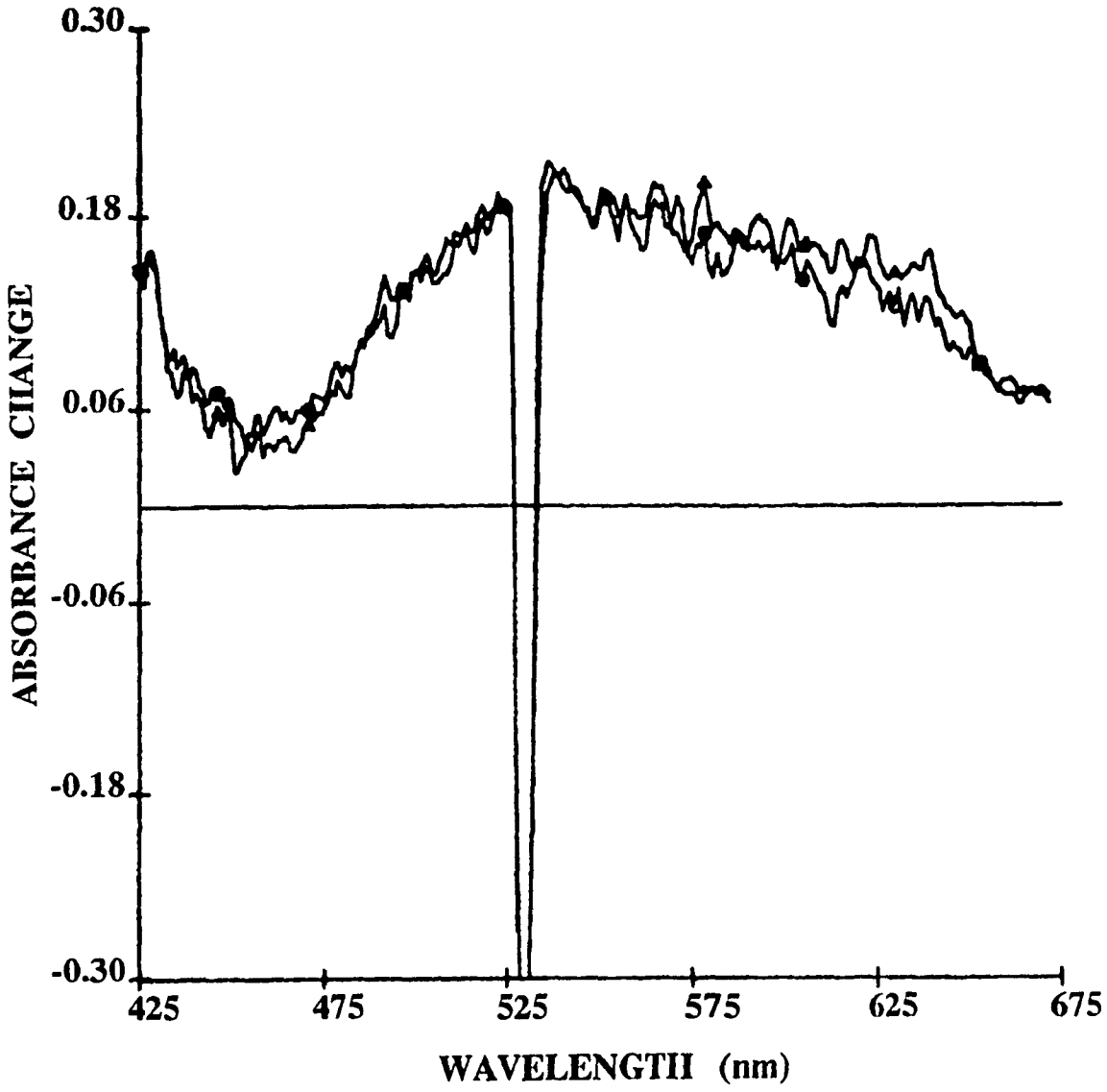

Figure 6.9. Transient absorption spectra of $(Ph)_3Sn$-$Re(CO)_3(bpy')$ in neat THF using 532 nm excitation recorded at probe delays of 50 ps and 5 ns.

and always coincides with the wavelength of the ground state band maximum of $MLCT_2$ thus indicating that an additional transient extending into the blue region of the visible spectrum is not relaxing in this time domain. The second feature of the transient absorption spectrum consists of a single broad ESA band centred at 550 nm which is formed rapidly and does not decay, even at longer times (i.e. 5 ns). In all probability, the ESA spectrum consists of one very intense long lived transient which absorbs over the entire visible spectral region (and thus overlaps the bleach). Evidence supporting this suggestion is gained from the numerical values of the absorbance change of the bleach minimum (475 nm). In the ESA spectra recorded using 355 nm excitation, the bleach minimum has a delta A of approximately 0.18 whereas the ground state spectrum has an absorbance of 0.32 at 475 nm when toluene is the solvent. That is, more bleaching would be expected if there is no ESA at the bleach wavelength. As the delay time is increased, a significant recovery of the bleach is not observed (unlike what was seen in $W(CO)_4(phen)$).

The general features of the ESA spectra under 532 nm excitation (Figure 6.9) are similar to those observed under 355 nm excitation suggesting that the same states are being populated, regardless of the excitation wavelength.

6.5. Assignment of ESA

Although the time dependence of the ESA spectra is somewhat different for $(CO)_5Re\text{-}Re(CO)_3(bpy')$ and $(Ph)_3Sn\text{-}Re(CO)_3(bpy')$, the fact that the temporal behaviour is similar under both excitation wavelengths for each complex suggests that the only

difference between the two compounds is the presence of two additional ESA bands in $(CO)_5Re\text{-}Re(CO)_3(bpy')$. Unequivocal assignment of the transient absorption bands is impossible due to the lack of structural information in the absorption spectra and to their overlap with an intense bleached ground state absorption. As was mentioned above, excitation into the MLCT bands of $(CO)_5Re\text{-}Re(CO)_3(bpy')$ and $(Ph)_3Sn\text{-}Re(CO)_3(bpy')$ yields homolysis of the metal-metal (hereafter abbreviated as M-M) bond to create, in the absence of radical scavenger, the radical fragments $Re(CO)_5^{\bullet}$ (or $Ph_3Sn^{\bullet}$) and $Re(CO)_3(bpy')^{\bullet}$ (Equation 6.1). Initially, these species would be contained in the solvent cage. It is possible for these radicals to recombine prior to escape from the solvent cage thus regenerating the reactant molecules. However, this possibility can be excluded since no recovery of the bleach was observed. Alternatively, the $Re(CO)_3(bpy')^{\bullet}$ and $Ph_3Sn^{\bullet}$ species can dimerize[27] to form $Re_2(CO)_6(bpy')_2$ (which absorbs in the 800 nm region, an area not accessible by our detector) and Sn_2Ph_6 (which absorbs in the UV, so is also not detectable by our system), respectively. However, because the Re dimer was not observed in steady state photolysis experiments (i.e. at long times; Figure 6.1), it is not expected that it will be present in the transient absorption spectra. Furthermore, dimerization is a diffusion limited process (τ = several nanoseconds) limited by the rate at which the radicals can escape the solvent cage, diffuse together and combine. Thus, these species are not expected to be seen on the time scale of our experiments (and even if they are present, their concentrations would be so small that they would not appear above the noise level of the ESA spectra). By inference, it can also be concluded that the Sn dimer (which absorbs in the UV region of the spectrum) is also not present in the

ESA spectra.

Another possibility is that these radicals can coordinate to a solvent molecule thus creating a solvated radical, (S)Re(CO)$_3$(bpy'). As can be seen in Figure 6.10, this species absorbs at around 500 nm. This spectrum was obtained from Reference 28.

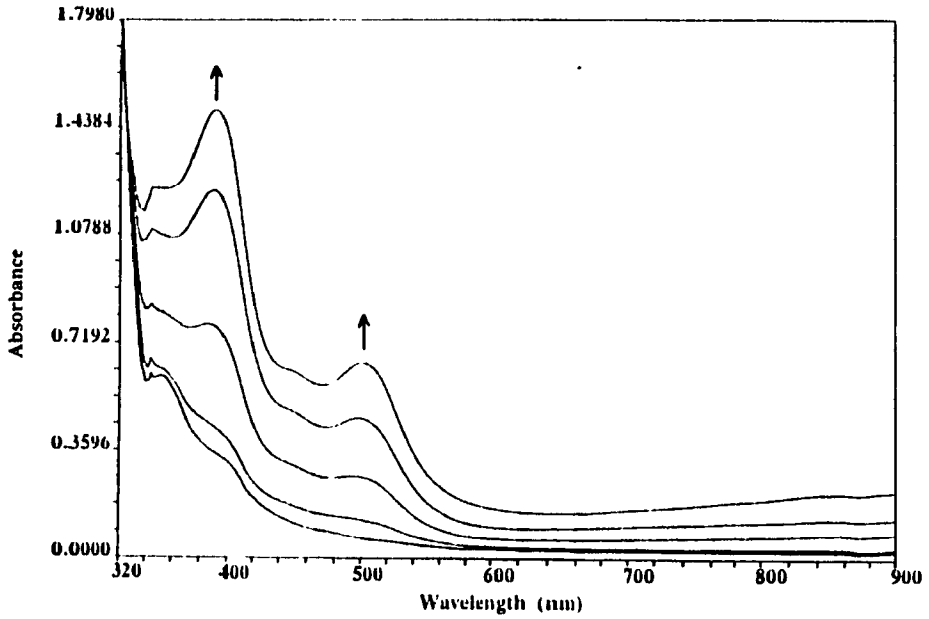

Figure 6.10. Reduction of [Re(CO)$_3$(bpy)]$^+$Otf$^-$ in THF at room temperature in the presence of Ph$_3$P in an OTTLE cell.

The strong bleach of the ground state of (CO)$_5$Re-Re(CO)$_3$(bpy') in this region may make this band difficult to see, hence the presence of this species in the ESA spectrum cannot be ruled out. The possibility of the presence of (S)Re(CO)$_5$ or (S)SnPh$_3$ cannot be eliminated since these species absorb at wavelengths less than 400 nm[29], also a region not accessible to our detector.

The possibility that the transient absorption is due to the molecular fragment

$Re(CO)_5^{\bullet}$ can also be ruled out due to the absence of a distinct absorption peak at 550 nm extending to the red[22] (although the large bleach signal in this region may obscure such a band). Although the quantum yields for homolysis of the Re-Re and the Sn-Re bonds are quite high (with respect to yields observed for $W(CO)_4$(phen); Chapter 4), they are probably not sufficiently high for the radical fragments (solvated, or not) to give a resolvable transient in comparison to the observed ESA absorbancies. Thus, it can be concluded that the observed transients are not due to the radical fragment $Re(CO)_5^{\bullet}$. Furthermore, the lack of bleach recovery in all spectra indicates that all types of recombination (as discussed above) are not important processes on this time scale. It can therefore be safely concluded that the observed transients do not correspond to primary photoproducts of Re-Re or Re-Sn bond homolysis.

Instead, a plausible assignment of the long lived absorption in the ESA observed for $(CO)_5$Re-Re$(CO)_3$(bpy') and $(Ph)_3$Sn-Re$(CO)_3$(bpy') under either 355 nm ($MLCT_1$) or 532 nm ($MLCT_2$) excitation is to the phosphorescent ^{3}MLCT state. This is in accordance with the long emission times found earlier[22]. Direct evidence for this assignment is obtained from the results of picosecond flash photolysis experiments on the non-reactive[29] compound $Re(CO)_3$(bpy')Br in THF. Irradiation into the MLCT band of the non-reactive complex must lead to an MLCT excited state since no other alternatives (other than relaxation to the ground state, a process which is not observed) are possible. The general shape of the ESA spectrum of this complex (Figure 6.11) is very similar in shape and is in the same region as those of the M-M bonded complexes, particularly that of $(Ph)_3$Sn-Re$(CO)_3$(bpy') (Figures 6.8 and 6.9). The high intensity of the ESA observed

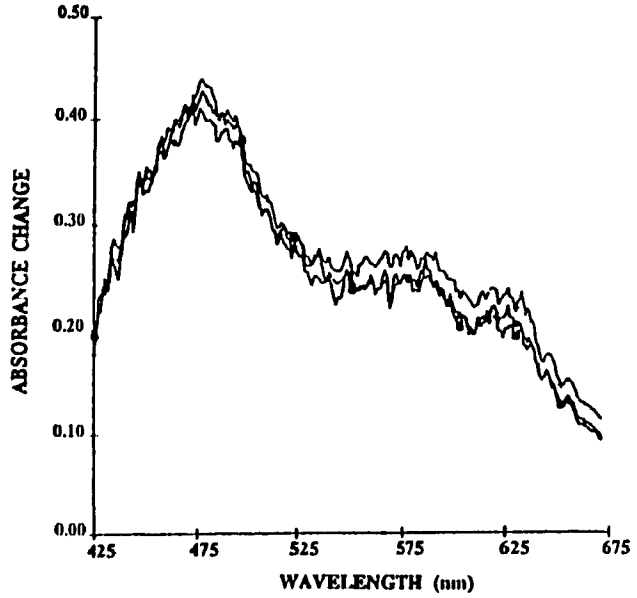

Figure 6.11. Transient absorption spectra of $Re(CO)_3(bpy')Br$ recorded in neat THF using 355 nm excitation recorded at probe delays of 50 and 500 ps and 10 ns.

in $Re(CO)_3(bpy')$ is consistent with the low amount of bleaching observed in the ESA spectra of $(CO)_5Re\text{-}Re(CO)_3(bpy')$ and $(Ph)_3Sn\text{-}Re(CO)_3(bpy')$ thereby confirming the broad transient extending over most of the visible region of the spectrum. Thus, because of the similarity of the ESA upon 355 nm and 532 nm excitation, the long lived transient is assigned to the $^3MLCT_2$ state.

The short lived transient observed only for $(CO)_5Re\text{-}Re(CO)_3(bpy')$ can be identified with the fluorescent ^1MLCT state whose presence was well established by Larson and co-workers[22]. Because (1) the long lived transient in the ESA spectrum is assigned to a $^3MLCT_2$ state and (2) there is an additional short-lived state present in the blue region, this additional state may be due to an efficient conversion from $^1MLCT_2$

---> $^3MLCT_2$ (i.e. $^1MLCT_2$ absorbs in the blue and is rapidly depleted ($t < 500$ ps) thus forming $MLCT_2$ which absorbs over the visible region of the spectrum); alternatively the conversion could be from a higher ^1MLCT state (i.e. $^3MLCT_3$) to $^1MLCT_2$. No short lived emission was observed in $(Ph)_3Sn\text{-}Re(CO)_3(phen)$[15] thus it can be inferred that there should be *no* short lived transient present in the ESA of $(Ph)_3Sn\text{-}Re(CO)_4(bpy')$. This is in accordance with the picosecond flash photolysis data.

6.6. Mechanism of Photophysical Deactivation

From these results, it is evident that we are dealing with the same type of early time behaviour as was observed in $W(CO)_4(phen)$ (Chapter 4): picosecond spectra provide insight into the non-reactive portion of the excited state relaxation whereas evidence on the reactive part must be acquired through quantum yield measurements. Based on the results for the monometallic $W(CO)_4(phen)$ (Chapter 4), MLCT states are not expected to be very reactive and direct population of these states will not give rise to the efficient homolysis reaction observed in these complexes (Section 6.3). Thus, population of the reactive state must be *indirect* in that it must become populated via the MLCT state which is excited directly by the laser (notice that the present data do not allow the specification of the character of the reactive state, although it must either be $\sigma\pi^*$ (where σ represents the σ(M-Re) bonding orbital and π^* the lowest unoccupied orbital of the ligand bpy') in character or the $^3\sigma\sigma^*$ state of the M-Re bond). The high quantum yields and the wavelength and temperature independence (in a separate study, these reactions were shown to be temperature independent[13]) thus can only be explained by a

fast crossing to the reactive state from a higher energy excited state. The slight differences in the ESA spectra might be due to a combination of a variation of the relative position of the potential curves of the MLCT and reactive states for $(CO)_5Re$-$Re(CO)_3(bpy')$ and Ph_3Sn-$Re(CO)_3(bpy')$ and/or the speed at which (a) the system relaxes in the upper excited levels and (b) the subsequent crossing to the reactive state occurs. Note that this must dismiss our earlier notion (Section 6.3) that the reaction might involve a long lived "storage" state because in this case, the crossing would be slow and the quantum yield would be temperature dependent.

The conventional explanation of the high, wavelength independent quantum yield would be a strong coupling between the excited state surfaces as shown in Figure 6.12 (note that this is only an approximation of the traditional model; less conventional alternatives will be considered later). Because the reactive curve crosses the ^{3}MLCT surface at the minimum, no wavelength dependence will occur. Changing the $(CO)_5$-group for Ph_3Sn- may also affect the location of the crossing point mainly by altering the position of the reactive $\sigma\pi^*$ (or $^3\sigma\sigma^*$) state. However, the wavelength independence of reaction indicates that the reactive curve in both complexes cannot be located too far away from the minimum of the MLCT surface. The most likely consequence of the presence of the Sn atom is an increased rate of vibrational relaxation in the excited system. The fact that only a single long lived state is observed in the picosecond spectra is in accord with this hypothesis.

The type of reactivity (i.e. temperature, wavelength independence) exhibited by the M-Re bonded complexes is not without precedent. Earlier work on the $M(CO)_6$

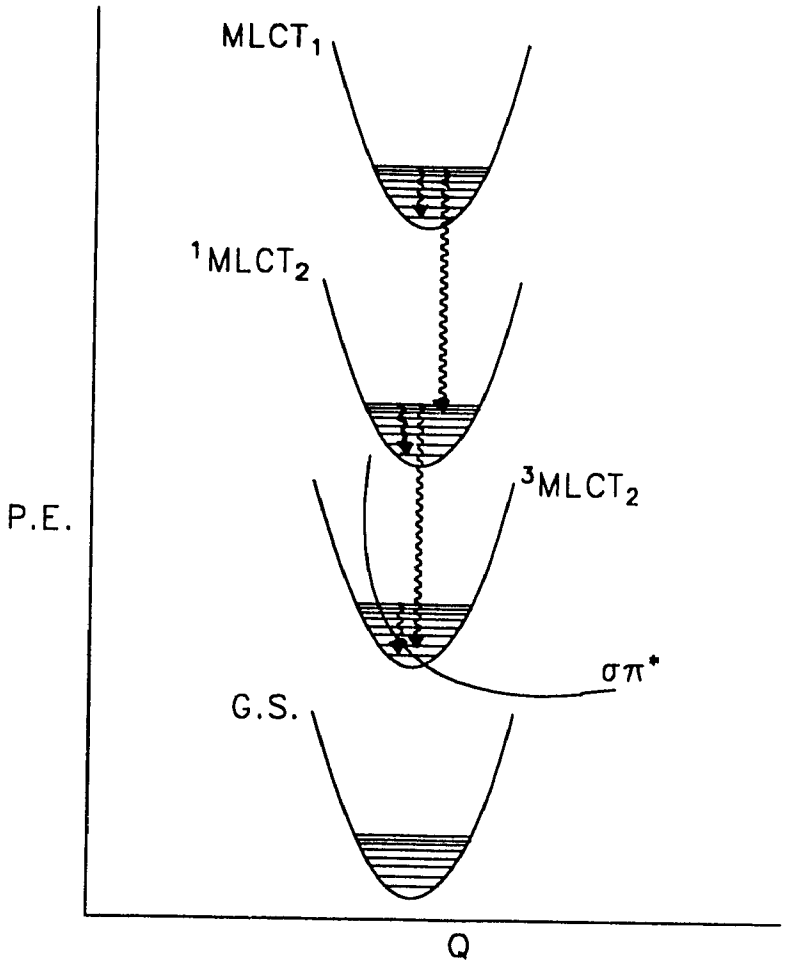

Figure 6.12. Schematic potential energy coordinate diagram showing the relationship between the ^{3}MLCT and the reactive states.

(M = Cr, W) systems[31] provides classic proof that the dissociation of a CO molecule in this complex is an ultrafast process that occurs from the lowest energy ^{3}MLCT excited state with a quantum yield less than unity. Moreover, the quantum yield for this reaction

is independent of both temperature and wavelength of excitation[31]. This system can be compared with the classical I_2 recombination as described by Harris and Harris[32]. In this system, excitation leads to the population of a dissociative excited state that is high in energy. The primary dissociation event occurs in the femtosecond time domain with a quantum yield of unity. Immediately following dissociation the system which now consists of a broken bond and excess energy, reaches a point within the state where it remains. The only ways out of this state are via relaxation processes, all which possess time constants. That is, the system undergoes vibrational equilibration *while still in the excited state*. Since the photochemistry of $Cr(CO)_6$ is similar to that of the M-Re systems (i.e. temperature and wavelength independent), it can be inferred that this reaction parallels the early time behaviour of $Cr(CO)_6$ or I_2. Thus, the photoreaction of $(CO)_5Re\text{-}Re(CO)_3(bpy')$ or $Ph_3Sn\text{-}Re(CO)_3(bpy')$ should also proceed with a quantum yield of unity until the M-Re bond is broken (i.e. until the hot photoproducts are formed). The highly excited system then undergoes vibrational relaxation on the excited state surface(s), but not on the ground state surface (since the latter process occurs at a slower rate[ref] than what we have observed in our spectra).

6.7. Conclusions

Excitation into the MLCT bands of $(CO)_5Re\text{-}Re(CO)_3(bpy')$ and $(Ph)_3Sn\text{-}Re(CO)_3(bpy')$ yields homolysis of the M-Re bond, a process which is independent of the excitation wavelength. Picosecond spectroscopy reveals that identical excited states are produced under excitation into $MLCT_1$ or $MLCT_2$. In the case of $(CO)_5Re$-

$Re(CO)_3(bpy')$, the ESA has three distinct components: a short-lived MLCT state which absorbs in the blue region and decays in < 500 ps. The decay of this state is affected by the solvent in that it is not observed in solvents such as CH_2Cl_2 which efficiently dissipate the excess energy received upon excitation. This is assigned to vibrational relaxation of the excited state which is populated directly by the excitation pulse ($MLCT_1$ and $MLCT_2$ for 355 nm and 532 nm excitation, respectively). There are also two longer lived excited states that absorb at lower energy. One has τ > 10 ns and is assigned to a ^{3}MLCT state, the other is somewhat shorter lived (it decays within 2.5 ns) and is assigned to a ^{1}MLCT state. In both cases, the ESA is attributed to $MLCT_2$. Note that the rate of ^{1}MLCT ---> ^{3}MLCT conversion (or possibly higher ^{1}MLCT ---> lower ^{3}MLCT) is not affected by the solvent to the same degree as ESA_1 and is observable in both halogenated and non-halogenated solvents. This demonstrates that the solvent plays an important role in determining the rates of ultrafast interstate transitions and does not affect those which occur on a somewhat slower timescale. Similar behaviour is observed in $(Ph)_3Sn$-$Re(CO)_3(bpy')$, although in this case, there is no ESA in the blue region and only a single ESA band in the red region. That is, excitation into $MLCT_1$ or $MLCT_2$ yields direct population of the long lived ^{3}MLCT state (τ > 10 ns). Again, the excited state is ascribed to $MLCT_2$.

In order to account for the high quantum yield and the observed wavelength independence, the reactivity of the complex is postulated to be comparable to the ultrafast photodissociation reaction of $Cr(CO)_6$. That is, the M-Re bond in L_nM-$Re(CO)_3(bpy')$ (L_nM- = Ph_3Sn- or $(CO)_5Re$-) parallels the Cr-CO bond in $Cr(CO)_6$ where femtosecond

time resolved spectroscopy on the latter species showed that the primary dissociation of the Cr-CO bond occurs in the femtosecond time domain. This reaction has a quantum yield of unity until this bond is broken. Once the bond is broken, the system remains in an excited state and undergoes vibrational relaxation analogous to what was observed in the photodissociation of I_2 (where vibrational relaxation on the excited state surface occurs faster than that on the ground state surface). Thus, the same condition (i.e. femtosecond breaking of the M-Re bond with the hot fragments sitting on a high energy surface) is attained whether $L_nM\text{-}Re(CO)_3(bpy')$ is excited with either UV or visible light. The quantum yield is defined by the events which follow (i.e. by which path the system takes to reach the reactive surface). Because these spectra are assigned to a ^{3}MLCT excited state, the system must relax into this state *prior* to reaction. Thus, the ^{3}MLCT state is a precursor to the photoproduct. Note that femtosecond spectroscopy cannot be used to test directly that 100% of the system reaches the critical point on the excited surface as this would be very difficult to quantify. Therefore, only the probability of crossing to the ^{3}MLCT state can be tested. Consequently, before any concrete conclusions can be drawn regarding the exact mechanism of relaxation in these M-Re bonded systems, the sequence of population of each excited state along the deactivation pathway must be determined.

6.8. References

1. Cotton, F.A. *Acc. Chem. Res.* **1969**, *2*, 240.

2. Cotton, F.A. *Acc. Chem. Res.* **1978**, *11*, 225.

3. Trogler, W.C.; Gray, H.B. *Acc. Chem. Res.* **1978**, *11*, 232.

4. Levenson, R.A.; Gray, H.B. *J. Am. Chem. Soc.* **1975**, *97*, 6042.

5. Cotton, F.A.; Wilkenson, G. *Advanced Inorganic Chemistry*, 4th edition, J. Wiley and Sons: New York, **1980**, pp. 1080-1112, and references therein.

6. a) van der Graaf, T.; Hofstram R.; Schilder, P.G.M.; Rijkhoff, M.; Stufkens, D.J.; van der Linden, J.G.M. *Organometallics* **1991**,

   b) Stufkens, D.J.; van der Graaf, T.; Stor, G.J.; Oskam, A. **1991**, *NATO Summer School*, France.

7. Geoffroy, G.L.; Wrighton, M.S. *Organometallic Photochemistry*, Academic Press: New York, 1979.

8. Meyer, T.J.; Caspar, J.V. *Chem. Rev.*, **1985**, *85*, 187.

9. Stufkens, D.J. in *Stereochemistry of Organometallic and Inorganic Compounds*, Vol. 3, ed. I. Bernal, Elsevier, Amsterdam, 1989, pp.226-300.

10. Wrighton, M.S.; Graff, J.L.; Luong, J.C.; Reichel, C.L.; Robbins, J.L. *Reactivity of Metal-Metal Bonds*, ACS Symposium Series, No. 155, Ed. M.H. Chisolm, 1981, p.85.

11. Wrighton, M.S.; Bredesen, D. *J. Organometal. Chem.* **1973**, *50*, C35.

12. Wrighton, M.S.; Ginley, D.S. *J. Am. Chem. Soc.* **1975**, *97*, 2065.

13. Stufkens, D.J. *Comments Inorg. Chem.* **1992**, *13*, 359.

14. Kokkes, M.W.; Snoeck, T.L.; Stufkens, D.J.; Oskam, A.; Cristopherson, M.; Stam, C.H. *J. Mol. Struct.* **1985**, *131*, 11.

15. Morse, D.L.; Wrighton, M.S. *J. Am. Chem. Soc.* **1976**, *98*, 3931.

16. Luong, J.C.; Faltynek, R.A.; Wrighton, M.S. *J. Am. Chem. Soc.* **1979**, *101*, 1597.

17. Lindsay, E.; Vlček, A., Jr.; Langford, C.H. *Inorg Chem.*, **1993**, in press.

18. Balk, R.W.; Snoeck, T.L.; Stufkens, D.J.; Oskam, A. *Inorg. Chem.* **1980**, *19*, 3015.

19. Van Dijk, H.K.; Stufkens, D.J.; Oskam, A. *J. Am. Chem. Soc.*, **1989**, *111*, 541.

20. Meyer, T.J. *Pure and Appl. Chem.* **1986**, *58*, 1193.

21. Ford, P.C.; Wink, D.; DiBenedetto, J. *Prog. Inorg. Chem.* **1983**, *30*, 213.

22. Larson, L.J.; Oskam, A.; Zink, J.I. *Inorg, Chem.* **1991**, *30*, 42.

23. Andréa, R.R.; de Lange W.G.; Stufkens, D.J.; Oskam, A. *Inorg. Chem.* **1989**, *28*, 318.

24. Andréa, R.R.; de Lange W.G.; Stufkens, D.J.; Oskam, A. *Inorg. Chim. Acta*, **1988**, *149*, 77.

25. Shin, K.S.; Clark, R.J.H.; Zink, J.I. *J. Am. Chem. Soc.* **1989**, *111*, 4244.

26. Yoo, C.S.; Zink, J.I. *Inorg. Chem.* **1983**, *22*, 2476.

27. Kobayashi, T. *Coord. Chem. Rev.*, **1985**, *64*, 1.

28. Stufkens, D.J. *Private communication.*

29. Wrighton, M.S.; Graff, J.L.; Luong, J.C.; Reichel, C.L.; Robbins J.L. ACS Symposium Series, No. 155, *Reactivity of Metal-Metal Bonds*, ed. Malcolm H. Chisholm, 1981.

30. a) Langford, C.H.; Moralejo, C.; Sharma, D.K.; *Inorg. Chim. Acta.* **1987**, *126*, L11.
    b) Joly, A.G.; Nelson, K.A. *Chemical Physics* **1991**, *152*, 69.

    c) Joly, A.G.; Nelson, K.A. *J. Phys. Chem.* **1989**, *93*, 2876.

31. Nasielski, J.; Colas, A. *J. Organomet. Chem.* **1975**, *101*, 215.

32. Harris, A.L.; Brown, J.K.; Harris, C.B. *Ann Rev. Phys. Chem.* **1988**, *39*, 341.

Concluding Remarks

Several interesting observations have been made from the experimental results obtained in this investigation of early excited state dynamics of selected transition metal complexes. The picosecond photooxidation of $[M(mnt)_2]^{2-}$ (M = Ni, Pt) is governed solely by electronic factors involving the coupling of a CTTS state with one of higher energy which is initially populated upon excitation. Factors such as vibrational relaxation and solvent reorientation do not seem to play a role. The

reaction is more efficient under 313 nm excitation than when light of 365 nm is used to excite the complex indicating that the coupling with the CTTS state is much more efficient at higher energies of excitation (probably because at higher energy, there is an increased coupling to the CTTS states).

The solvent, however, appears to be an important factor in the early time behaviour of all of the carbonyl complexes studied. In the complexes $W(CO)_5$(4-X-Py) (X = CN, Formyl), the intersystem crossing which populates the reactive ^{1}MLCT excited states is solvent dependent and follows biphasic kinetics. The dominant ultrafast component occurs on the same (or even shorter) timescale as vibrational relaxation. $W(CO)_4$(phen) exhibits different reactivity which is governed by the coupling of the states involved. MLCT excitation leads to an associative reaction, but the reactivity follows two distinct pathways under LF excitation: a major dissociative pathway accompanied by a minor associative pathway. LF and MLCT excitation in the picosecond time domain reveal two MLCT states in rapid equilibrium (τ = 1 ns), the reactive one being distorted thereby facilitating nucleophilic attack. Lastly, MLCT excitation of $(CO)_5$Re-

$Re(CO)_3(bpy')$ leads to the homolysis of the Re-Re bond, a wavelength independent process. Time resolved picosecond spectroscopy reveals an excited state absorption with three distinct components: a short lived MLCT state whose relaxation is solvent dependent. This state is probably the result of vibrational relaxation of the excited state which is populated directly by the excitation pulse. Two longer lived ESA bands are also observed. These are assigned to ^{1}MLCT and ^{3}MLCT states, respectively. The rate of conversion between these two states is not dependent on the solvent. Furthermore, it was revealed that the ^{3}MLCT state is a precursor to the photoproduct since the system must first relax into a ^{3}MLCT state prior to reaction. Ph_3Sn-$Re(CO)_3(bpy')$ exhibits only the ^{3}MLCT state, probably because it relaxes too fast for the other states to be observed in this time domain (i.e. the presence of Sn seems to increase the rate of relaxation). Thus, it can be concluded that the solvent, through electronic factors, exerts an exceptional control on processes which occur in the sub-picosecond time domain.

This work has revealed that excited state relaxation pathways are, in these compounds, selected very shortly after the electronic excitation, on timescales where the Born-Oppenheimer approximation is no longer applicable. Involvement of optically excited vibronic levels might provide the specific vibrational coupling needed for activation of particular photophysical (e.g. ISC) as well as prompt photochemical processes. These observations lead to three obvious areas for further research. Because of the ultrafast nature of the reactivity of these complexes, pulses with a width of 30 ps are too slow to adequately examine the primary events. A pulse width in the femtosecond time domain would be ideal as this would provide an excellent opportunity

to probe in detail the effects of solvent on vibrational relaxation of the Franck-Condon states an on intersystem crossing. The use of time-resolved vibrational spectroscopies such as IR and resonance Raman could yield structural information (i.e. distortions) regarding the excited states which is not available from electronic absorption spectroscopy. The second area would be to extend this study and examine both the solvent and wavelength dependence of the reactivity of other transition metal complexes. This would show whether the effects observed during the course of this research hold for a wider variety of transition metal complexes. A greater understanding of the dynamics of relaxation processes which occur prior to chemical reaction may result. Lastly, these studies have shown the need to develop a new theoretical approach to describe ultrafast processes. Alternatives could be selection rules like the octupole rule developed by Hollebone and/or methods based on time-dependent quantum mechanics.

Appendix A. Supplementary information for $[M(mnt)_2]^{2-}$ (M = Ni, Pt).

This appendix includes the extinction coefficients for $[M(mnt)_2]^{-1}$ (M = Ni, Pt) in various $CHCl_3$-CH_3CN mixtures which were obtained using a Beer-Lambert plot and the evaluation of the statistics for the normalized double reciprocal plots.

Table A.1. Extinction coefficients of $[M(mnt)_2]^-$ (M = Ni, Pt) in various $CHCl_3$-CH_3CN mixtures.

$[Ni(mnt)_2]^-$		$[Pt(mnt)_2]^-$	
$\chi(CHCl_3)$	ϵ_{818} $(M^{-1}cm^{-1})^a$	$\chi(CHCl_3)$	ϵ_{818} $(M^{-1}cm^{-1})^a$
0.0000	4700	0.0000	11 100
0.0676	4600	0.0310	11 050
0.1403	4700	0.1000	11 000
0.2186	4700	0.2000	10 850
0.3032	4300	0.3000	10 740
0.3949	4300	0.4000	10 620
0.4947	4400	0.5000	10 500
0.7231	4300	0.6000	10 380
0.8546	3900	0.7000	10 270
0.9400	3900	0.8500	10 100

a) The error is ± 10%.

Fisher's Z transformation is used to compare the correlation of two different data sets. In this case, it was used to establish that the slopes of the double reciprocal plots (Figures 3.12 and 3.13), and thus K_E, are statistically equivalent.

First, the z statistics, z_1 and z_2, are calculated using the correlation coefficients of the double reciprocal plots for 313 nm and 365 nm excitation (R^2 = 0.997 and 0.984 for the 313 nm and 365 nm data, respectively).

$$z_1 = \frac{1}{2} \ln\left(\frac{1+r_1}{1-r_1}\right) \tag{A1}$$

The z values are 2.76 and 3.63 for the 313 nm and 365 nm data, respectively. The next step is to identify the degrees of freedom in the system. This is accomplished by summing the degrees of freedom (df) in each data set (Equation A2).

$$df = (n_1-3) + (n_2-3) \tag{A2}$$

where n_1 and n_2 are the number of data points in data set 1 and 2, respectively. Since each curve has 9 data points, it is obvious that $n_1 = n_2 = 9$ and there is a total of 12 degrees of freedom. Now, a test statistic, Z, can be evaluated using Equation A3.

$$Z = \frac{z_1 - z_2}{\sqrt{\frac{1}{df_1} + \frac{1}{df_2}}} \tag{A3}$$

Thus, Z = -1.51. The absolute value of Z is then compared to the Z in the statistical tables (Reference 12 in Chapter 3) which corresponds to $Z_{0.975}$ (i.e. $Z_{1-\alpha/2}$ where α = 0.05 for a 95% confidence level). The table value is 2.179 assuming 12 degrees of freedom. Since $Z_{tab} > Z_{calc}$, the slopes (and intercepts) are statistically equivalent.

The t test was used to compare the slope calculated for the 313 nm photolysis of $[Ni(mnt)_2]^{2-}$ with that obtained from the normalized double reciprocal plot for the 365 nm photolysis of $[Ni(mnt)_2]^{2-}$ (Figure 3.14). By definition,

$$\pm t = (\bar{X} - \mu)\frac{\sqrt{N}}{s} \qquad \text{(A4)}$$

where μ is the calculated value (0.25), X is the experimental value (i.e. the slope of the 365 nm double reciprocal plot, 0.217), N the degrees of freedom (6) and s the standard deviation (0.05). Using Equation 3.4 and the above data, a t value of 1.6 is calculated. For 6 degrees of freedom, the tabular value for a 95% confidence level is 2.447 (Reference 13 in Chapter 3). Since $t_{tab} > t_{calc}$, the slopes are statistically indistinguishable.

Appendix B. Spectral changes in the continuous photolysis of $W(CO)_4$(phen)

This appendix contains data for spectral changes observed during the continuous photolysis of $W(CO)_4$(phen) at different wavelengths in various solvents. In all cases, the reactant and the photoproduct are referred to as "A" and "B", respectively.

Table B.1. Spectral data observed during the conversion of $W(CO)_4$(phen) to $W(CO)_3$(L)(phen) under visible irradiation.

Solvent	Isosbestic points (± 2 nm)	λ_{max} (± 2 nm)	
		$W(CO)_4$phen	$W(CO)_3$(L)phen
Neat pyridine	392; 514	462	596
0.33 M (n-Bu)$_3$P in CH_2Cl_2	372; 514	486	594
0.3 M (n-Bu)$_3$P in toluene	388; 544	508	638
0.3 M (n-Bu)$_3$P in C_2Cl_4[a]	432; 558	534	658

a) Solutions of $W(CO)_4$(phen) in the (n-Bu)$_3$P-C_2Cl_4 mixture also contained 8% (v/v) CH_2Cl_2.

Table B.2. Extinction coefficients[a] ($M^{-1}cm^{-1}$) for $W(CO)_4(phen)$ in various solvents.

Solvent	Wavelength (nm)			
	ϵ_{366}	ϵ_{488}	ϵ_{514}	ϵ_{610}
neat pyridine	1960	4815	3020	b
0.33 M (n-Bu)$_3$P in CH_2Cl_2	2710	5870	4620	b
0.3 M (n-Bu)$_3$P in C_2Cl_4[c]	760	2120	2510	540
0.3 M (n-Bu)$_3$P in toluene	1145	4030	4285	b

a) Extinction coefficients are ± 10%.
b) Minimal absorption was observed at 610 nm in this solvent.
c) Solutions of $W(CO)_4(phen)$ in the (n-Bu)$_3$P-C_2Cl_4 mixture also contained 8% (v/v) CH_2Cl_2.

Table B.3. Extinction coefficients[a] ($M^{-1}cm^{-1}$) for $W(CO)_3(L)(phen)$ in various solvents.

Solvent	Wavelength (nm)				
	ϵ_{366}	ϵ_{488}	ϵ_{514}	ϵ_{610}	ϵ_{700}
Neat pyridine	1960	2470	2780	4280	1950
0.33 M (n-Bu)$_3$P in CH_2Cl_2	3510	2550	3880	6170	2020
0.3 M (n-Bu)$_3$P in C_2Cl_4[b]	1410	460	825	2620	2085
0.3 M (n-Bu)$_3$P in toluene	2115	4030	1600	4660	2760

a) Extinction coefficients are ± 10%.
b) Solutions of $W(CO)_4(phen)$ in the (n-Bu)$_3$P-C_2Cl_4 mixture also contained 8% (v/v) CH_2Cl_2.

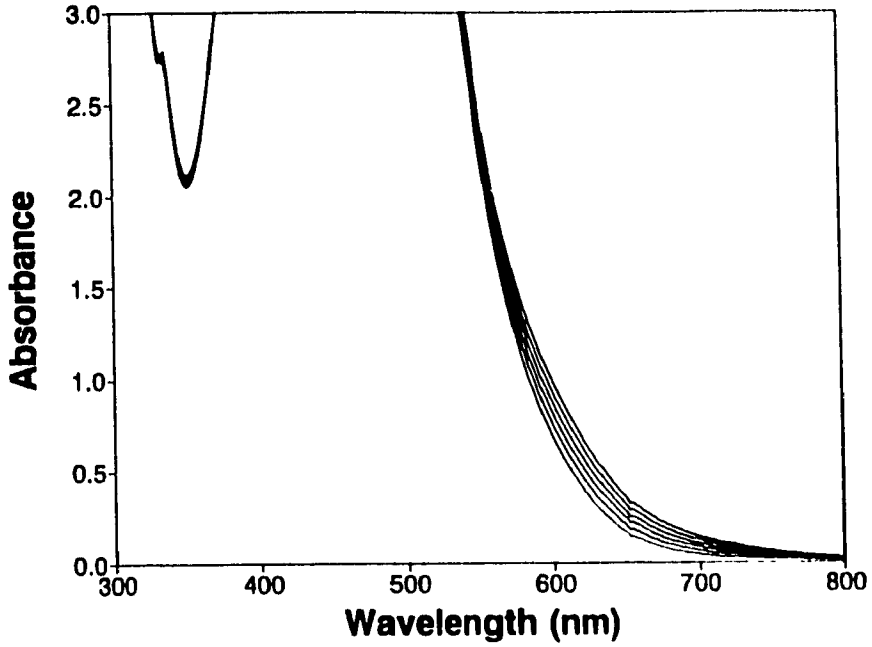

Figure B.1. Electronic spectral changes for $W(CO)_4$(phen) in 0.36 M $(n\text{-}Bu)_3P$ in CH_2Cl_2 using 365 nm excitation. The times of irradiation from reactant A to product B are: 0, 10, 20, 30, 40, and 50 minutes.

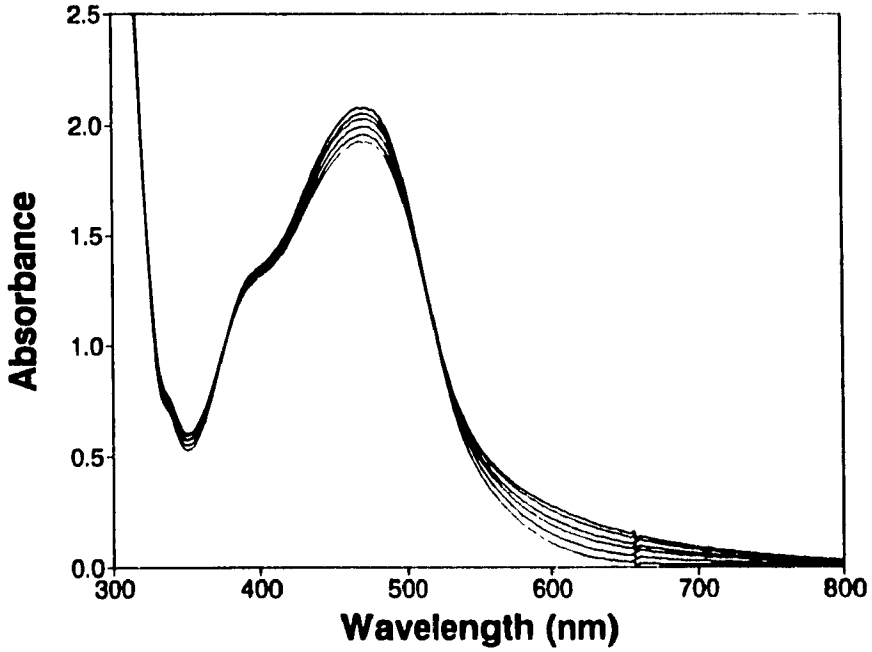

Figure B.2. Electronic spectral changes for $W(CO)_4$(phen) in neat pyridine using 488.0 nm excitation. The times of irradiation from reactant A to product B are: 0, 180, 360, 540, 758, and 903 seconds.

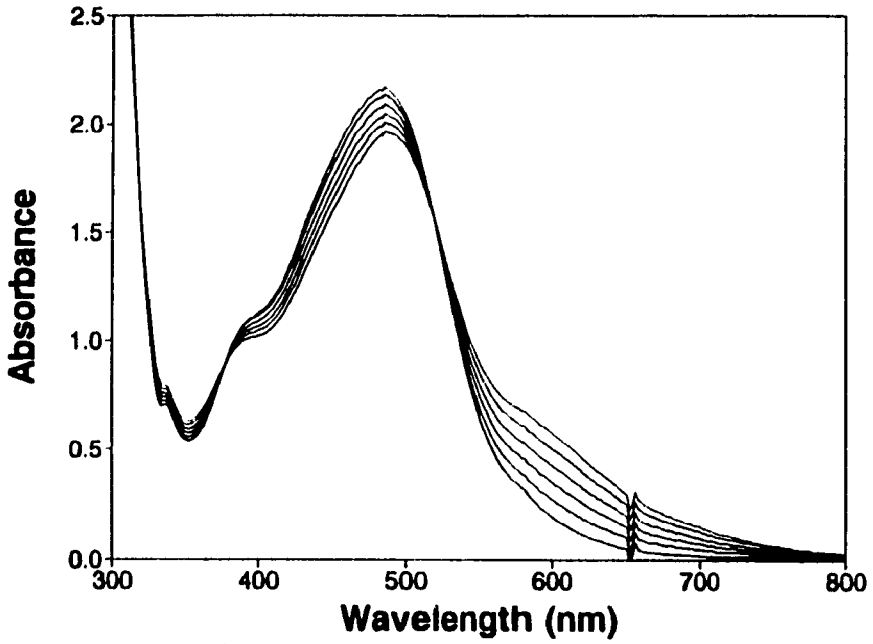

Figure B.3. Electronic spectral changes for $W(CO)_4(phen)$ in 0.3 M $(n\text{-}Bu)_3P$ in CH_2Cl_2 using 488.0 nm excitation. The times of irradiation from reactant A to product B are: 0, 180, 360, 540, 720, and 900 seconds.

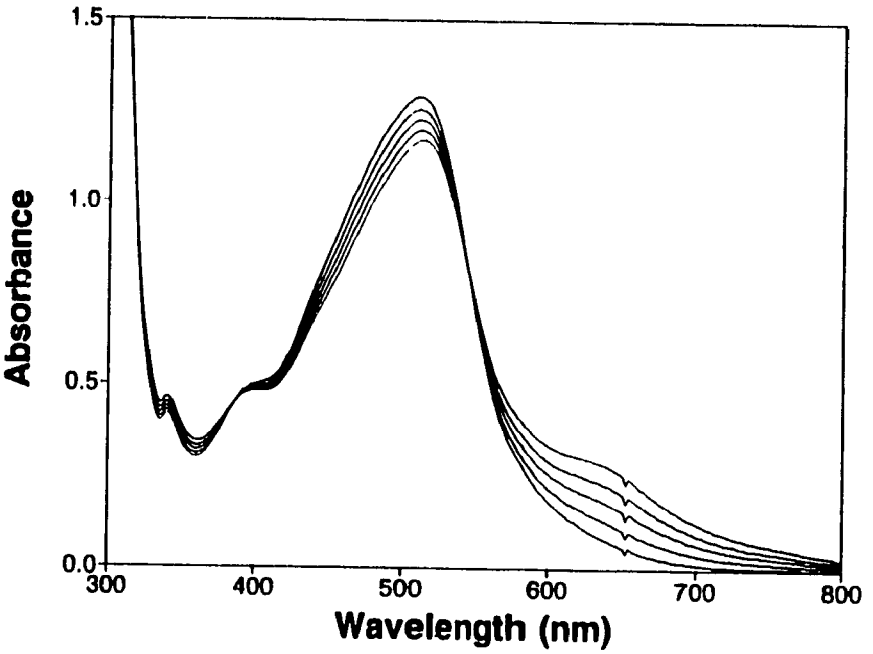

Figure B.4. Electronic spectral changes for $W(CO)_4(phen)$ in 0.3 M $(n\text{-}Bu)_3P$ in toluene using 488.0 nm excitation. The times of irradiation from reactant A to product B are: 0, 5, 10, 15,and 20 seconds.

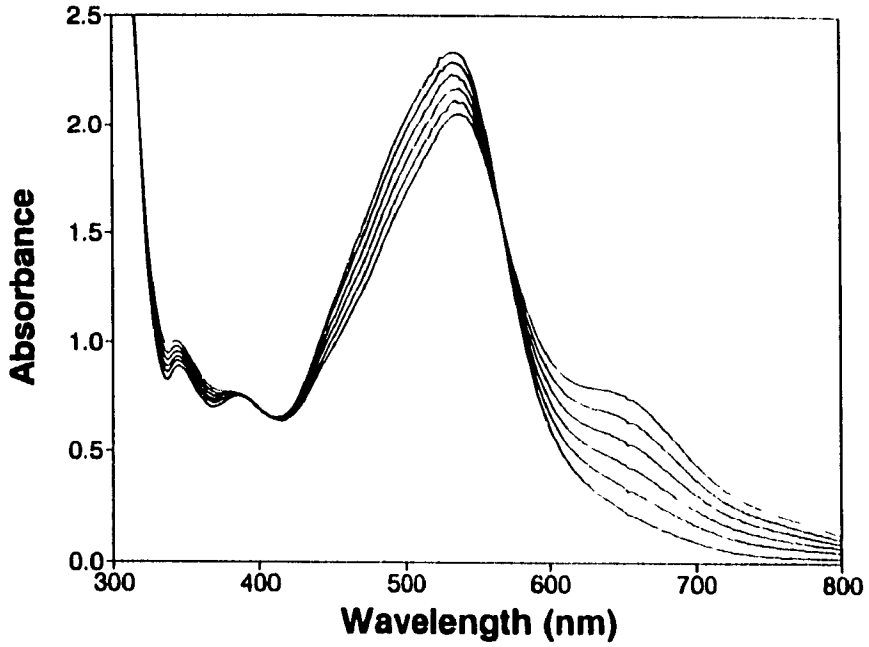

Figure B.5. Electronic spectral changes for $W(CO)_4(phen)$ in 0.3 M $(n\text{-}Bu)_3P$ in C_2Cl_4 using 488.0 nm excitation. The times of irradiation from reactant A to product B are: 0, 60, 120, 180, 240, and 301 seconds.

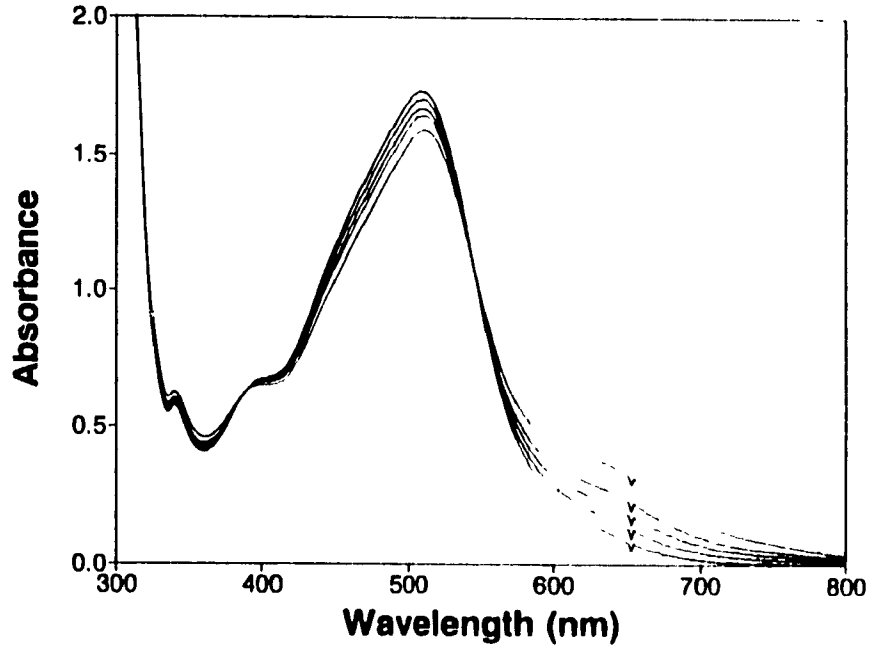

Figure B.6. Electronic spectral changes for $W(CO)_4(phen)$ in 0.3 M $(n\text{-}Bu)_3P$ in toluene using 514.5 nm excitation. The times of irradiation from reactant A to product B are: 0, 15, 30, 45, and 74 seconds.

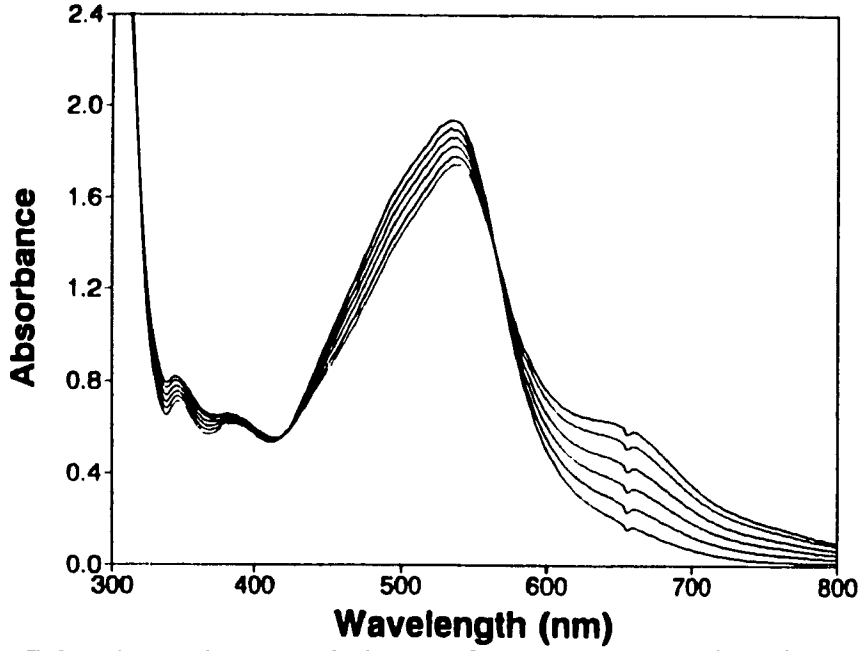

Figure B.7. Electronic spectral changes for $W(CO)_4$(phen) in 0.3 M $(n\text{-}Bu)_3P$ in C_2Cl_4 using 514.5 nm excitation. The times of irradiation from reactant A to product B are: 0, 30, 60, 91, 126, and 150 seconds.

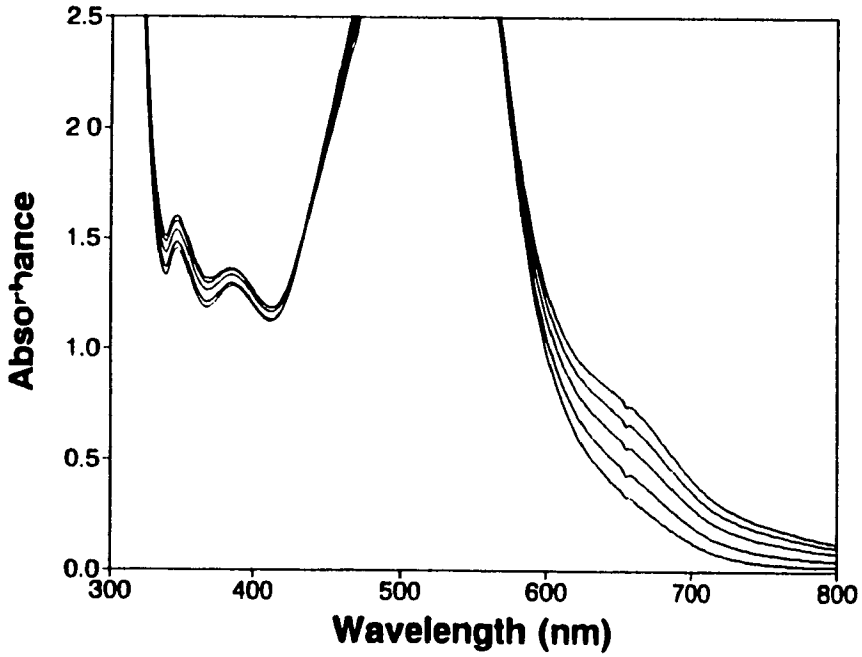

Figure B.8. Electronic spectral changes for $W(CO)_4$(phen) in 0.3 M $(n\text{-}Bu)_3P$ in C_2Cl_4 using 610.9 nm excitation. The times of irradiation from reactant A to product B are: 0, 60, 120, 180, 240 seconds.

Appendix C. Picosecond spectra of $W(CO)_4$(phen)

This appendix contains spectra recorded in picosecond flash photolysis experiments on $W(CO)_4$(phen) at 355 nm and 532 nm in various solvents.

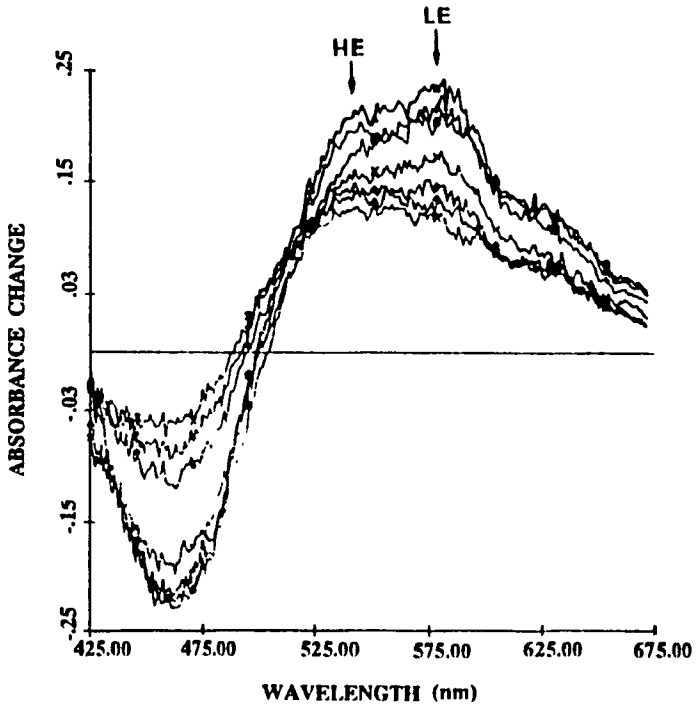

Figure C.1. Transient absorption spectra of $W(CO)_4$(phen) in acetonitrile (plus 2% (v/v) water) using 355 nm excitation recorded at probe delays of 50 and 500 ps and at 1, 2 and 5 ns in order of decreasing absorbance change.

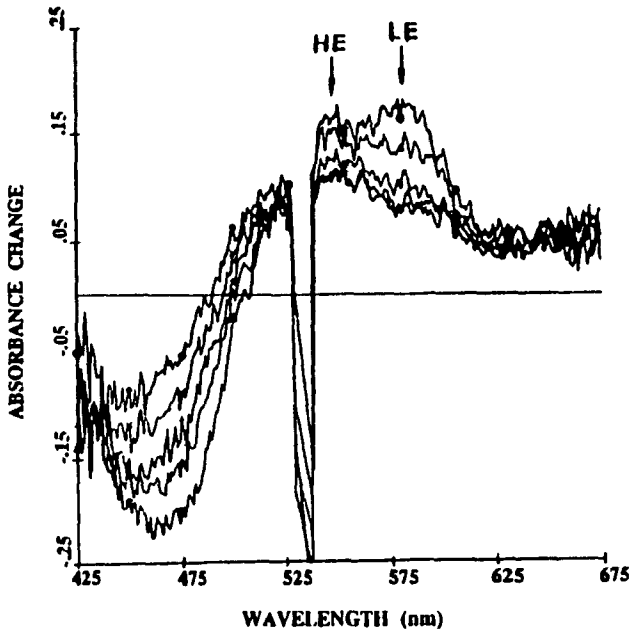

Figure C.2. Transient absorption spectra of $W(CO)_4(phen)$ in acetonitrile using 532 nm excitation recorded at probe delays of 50 and 500 ps and at 1, 2 and 5 ns in order of decreasing absorbance change.

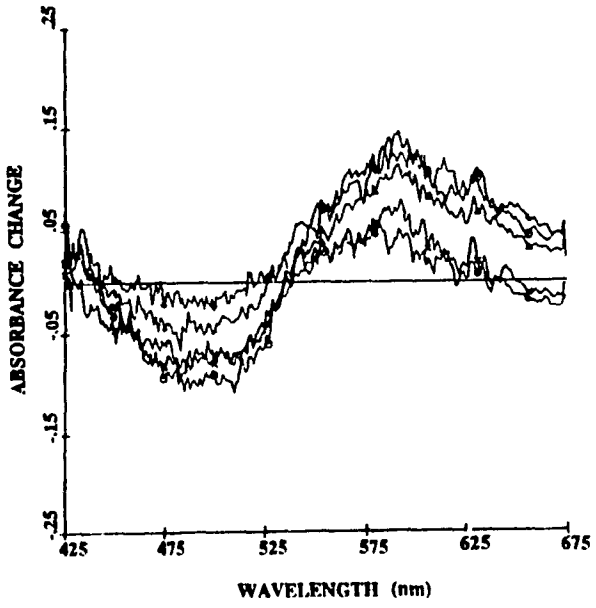

Figure C.3. Transient absorption spectra of $W(CO)_4(phen)$ in benzene (plus 2% (v/v) pyridine) using 355 nm excitation recorded at probe delays of 50 and 500 ps and at 1, 2 and 5 ns in order of decreasing absorbance change.

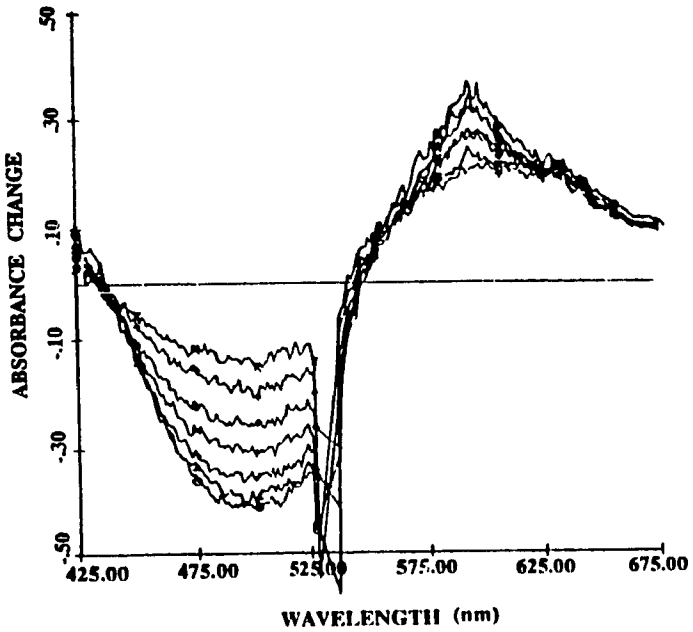

Figure C.4. Transient absorption spectra of $W(CO)_4(phen)$ in benzene using 532 nm excitation recorded at probe delays of 50 and 500 ps and at 1, 2 and 5 ns in order of decreasing absorbance change.

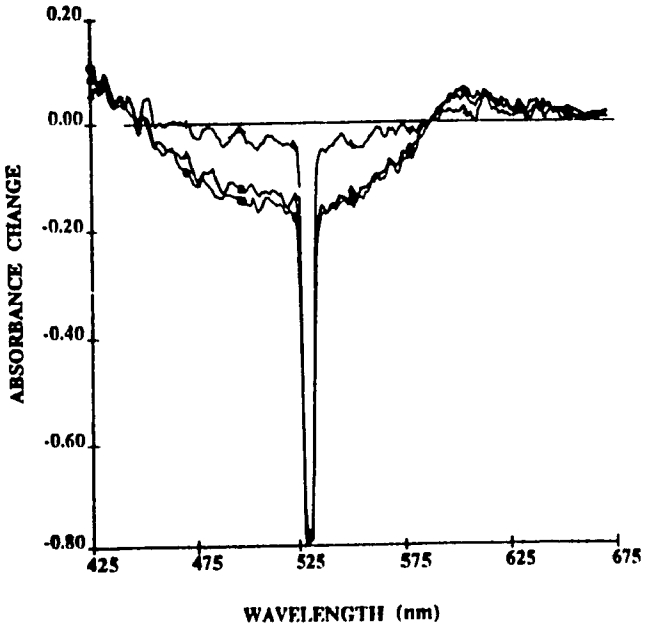

Figure C.5. Transient absorption spectra of $W(CO)_4(phen)$ in tetrachloroethylene using 532 nm excitation recorded at probe delays of 50 and 500 ps and 5 ns in order of decreasing absorbance change.

Appendix D. Quantitization of picosecond flash photolysis data

Data acquired during picosecond flash photolysis measurements can be quantitized by taking the ratio between the average absorbance change for several wavelengths accross the ESA band and the bleach maximum. The results are summarized in Tables D1 to D4.

Table D.1. Average ΔA values for various wavelengths in the ESA spectra of $W(CO)_4$(phen) recorded with 532 nm excitation.

CH_3CN	460 nm	500 nm	560 nm	586 nm	625 nm
50 ps	-0.216	-0.028	0.151	0.167	0.050
500 ps	-0.174	-0.005	0.135	0.133	0.060
5 ns	-0.082	0.053	0.105	0.082	0.049
C_5H_5N					
50 ps	-0.206	-0.172	0.254	0.286	0.214
500 ps	-0.182	-0.148	0.216	0.267	0.206
5 ns	-0.040	-0.021	0.124	0.143	0.142
C_4H_8O					
50 ps	-0.399	-0.379	0.159	0.274	0.130
500 ps	-0.342	-0.328	0.131	0.239	0.118
5 ns	-0.091	-0.079	0.048	0.070	0.075
CH_2Cl_2					
50 ps	-0.293	-0.241	0.163	0.234	0.109
500 ps	-0.230	-0.177	0.124	0.179	0.070
5 ns	-0.067	-0.023	0.059	0.057	0.024

Table D.1. (continued). Average ΔA values for various wavelengths in the ESA spectra of $W(CO)_4$(phen) recorded with 532 nm excitation.

0.3 M *n*-Bu_3P in CH_2Cl_2					
50 ps	-0.276	-0.244	0.147	0.223	0.087
500 ps	-0.223	-0.184	0.113	0.176	0.070
5 ns	-0.072	-0.033	0.045	0.033	0.011

Table D.2. Average ΔA values for various wavelengths in the ESA spectra of $W(CO)_4$(phen) recorded with 355 nm excitation.

CH_3CN	460 nm	500 nm	560 nm	586 nm	625 nm
50 ps	-0.218	-0.024	0.190	0.198	0.126
500 ps	-0.186	-0.013	0.159	0.158	0.086
5 ns	-0.062	0.040	0.126	0.104	0.076
C_5H_5N					
50 ps	-0.145	-0.093	0.161	0.207	0.137
500 ps	-0.150	-0.110	0.139	0.190	0.123
5 ns	-0.077	-0.053	0.105	0.103	0.088
C_4H_8O					
50 ps	-0.369	-0.340	0.152	0.219	0.150
500 ps	-0.300	-0.262	0.134	0.205	0.141
5 ns	-0.149	-0.128	0.151	0.176	0.166
CH_2Cl_2					
50 ps	-0.292	-0.239	0.109	0.157	0.083
500 ps	-0.261	-0.205	0.070	0.110	0.044
5 ns	-0.115	-0.072	0.011	0.055	0.029

Table D.3. Normalization (with respect to the bleach) of various areas of the ESA spectra of $W(CO)_4$(phen) recorded with 532 nm excitation.

CH_3CN	460 nm	500 nm	560 nm	586 nm	625 nm
50 ps	1	0.130	0.699	0.773	0.231
500 ps	1	0.029	0.776	0.764	0.345
5 ns	1	0.646	1.28	1.00	0.598
C_5H_5N					
50 ps	1	0.835	1.23	1.39	1.04
500 ps	1	0.813	1.19	1.47	1.13
5 ns	1	0.525	3.10	3.58	3.55
C_4H_8O					
50 ps	1	0.950	0.398	0.687	0.326
500 ps	1	0.959	0.383	0.699	0.345
5 ns	1	0.868	0.527	0.769	0.824
CH_2Cl_2					
50 ps	1	0.822	0.556	0.799	0.372
500 ps	1	0.770	0.539	0.778	0.304
5 ns	1	0.343	0.881	0.851	0.358
0.3 M *n*-Bu_3P in CH_2Cl_2					
50 ps	1	0.884	0.532	0.808	0.315
500 ps	1	0.825	0.507	0.789	0.314
5 ns	1	0.458	0.625	0.458	0.153

Table D.4. Normalization (with respect to the bleach) of various areas of the ESA spectra of $W(CO)_4$(phen) recorded with 355 nm excitation.

CH_3CN	460 nm	500 nm	560 nm	586 nm	625 nm
50 ps	1	0.110	0.872	0.908	0.578
500 ps	1	0.070	0.855	0.849	0.462
5 ns	1	0.645	2.03	1.68	1.23
C_5H_5N					
50 ps	1	0.641	1.11	1.43	0.945
500 ps	1	0.733	0.927	1.27	0.820
5 ns	1	0.688	1.36	1.34	1.14
C_4H_8O					
50 ps	1	0.921	0.412	0.593	0.407
500 ps	1	0.873	0.467	0.683	0.470
5 ns	1	0.859	1.01	1.18	1.11
CH_2Cl_2					
50 ps	1	0.818	0.373	0.538	0.284
500 ps	1	0.894	0.702	0.377	0.151
5 ns	1	0.626	0.096	0.478	0.252